N65-23738

NASA CR-54191
ADL 65958-00-04

BASIC INVESTIGATIONS OF MULTI-LAYER INSULATION SYSTEMS

prepared for

NATIONAL AERONAUTICS AND SPACE ADMINISTRATION

CONTRACT NAS 3-4181

ARTHUR D. LITTLE, INC.

Requests for copies of this report should be referred to

National Aeronautics and Space Administration
Office of Scientific and Technical Information
Attention: AFSS-A
Washington, D.C. 20546

NASA CR 54191
ADL 65958-00-04

FINAL REPORT

BASIC INVESTIGATION OF MULTI-LAYER INSULATION SYSTEMS

prepared for

NATIONAL AERONAUTICS AND SPACE ADMINISTRATION

October 30, 1964

CONTRACT NAS3-4181

Technical Management
NASA Lewis Research Center
Cleveland, Ohio
Advanced Rocket Technology Branch
James J. Kramer
James Barber

ARTHUR D. LITTLE, INC.
Acorn Park
Cambridge 40, Massachusetts

//

ACKNOWLEDGMENTS

The following personnel of Arthur D. Little, Inc., were associated with this program:

Igor A. Black	Richard B. Hinckley
Jacques M. Bonneville	Jere L. Lundholm
Paul R. Doherty	Raymond W. Moore
Alfred G. Emslie	Frank E. Ruccia
Peter E. Glaser	Peter F. Strong

Joseph P. Sullivan

We should like to acknowledge the assistance and co-operation of Messrs. James J. Kramer and James Barber of the NASA Lewis Research Center, Advanced Rocket Technology Branch, in the conduct of this work.

TABLE OF CONTENTS

PART I

INTRODUCTION

TABLE OF CONTENTS

I. INTRODUCTION

On October 30, 1963, Arthur D. Little, Inc. initiated work on "Basic Investigations of Multi-layer Insulation Systems" under Contract No. NAS3-4181 with the NASA Lewis Research Center. This effort is, in part, a continuation of previous work initiated under Contract Nos. NAS5-664 and NASw-615.

The heat leak into stored cryogenic propellants carried in space vehicles has an important effect on the quantities lost through vaporization, on the tank pressure limits, and on the utilization of the propellants. The heat leak rate to the propellants varies as the vehicle changes its environment, starting in the earth's atmosphere and ending in the vacuum of space. In all the environments, the heat leak to oxygen and, particularly, to hydrogen propellants must be limited and regulated in order to make the mission feasible and practical.

The means of limiting the heat flow in all the environments through the use of multi-layer insulations separately and in combination with other insulating media has received considerable attention.

Our studies both analytical and experimental, as reported herein, have dealt separately with the performance of the insulating media and environments.

Specifically, the present contract includes four major tasks: (1) a series of experiments to measure the efficacy of insulations with three thermal conductivity apparatus; (2) a series of tests to determine the heat leak through various insulation materials installed on either of two calorimeter tanks; (3) the design, construction and operation of an emissometer to determine the total hemispheric emittance of candidate materials for multi-layer insulations and; (4) analytical studies in support of the other three tasks.

Although each task appears as a separate item in the contract, each has provided theoretical or experimental support for the others. As a matter of expedience and ease of reference, the detailed tasks

are described in separate parts of this report; many of the interpretations and ideas were, however, derived through discussions between staff members engaged in the different areas. For easy reference, we have summarized the objectives of the four tasks in parts A through D of this section and following this, we have presented a succinct summary of the results.

A. Thermal Conductivity Measurements

To rapidly screen various, high efficiency, insulations and to determine the transient and permanent effects that occur under mechanical loads, three thermal conductivity apparatus were employed. A number of promising materials for both radiation shields and spacers were studied and evaluated. One apparatus was modified to enable accurate measurement of the applied mechanical loads ranging from 0 to 2 psig. This modified apparatus was checked for reliability and accuracy with a standard insulation which had been previously tested. Tests were also carried out with a foam-radiation shield multi-layer insulation under conditions simulating both a "vacuum-bagged" ground hold and the high vacuum of space.

A brief summary of the results obtained is presented in Part I-E and a detailed discussion is found in Part II.

B. Insulated Tank Calorimeters

The selection of promising insulations for space-borne cryogenic tanks was made from the results of the Thermal Conductivity studies. The actual fabrication and testing of such insulations on a larger scale was carried out on calorimeter tanks. In such studies, the problems of fabrication over curved surfaces were delineated and different solutions tried. Also, the deleterious effect of penetrations could be studied and experimental heat leak data analyzed and compared with theoretical predictions. The problem of the transition from a ground environment to space requires that the insulations be protected against inleak of condensible vapors and mechanical damage at atmospheric pressure, and that the insulation be readily evacuated to a high-vacuum state when the tank is carried into space.

Various solutions to this problem were studied with the calorimeter tank system. Measurement of temperature gradients within the multi-layer shields were made and compared in many cases to theoretical values.

A brief summary of the salient results and conclusions is presented in Part I-F and complete details in Part III.

C. Emissometer

A simple emissometer has been fabricated and used extensively in this program to determine the emittance of materials proposed for radiation shields in multi-layer insulations. Also, the increase in emissivity due to the surface contaminants and imperfections on the surfaces of the shields was studied. The instrument has been employed as quality control instrument for purchased multi-layer materials.

Sketches of the apparatus, methods of operation and data taken on various materials are included in Part IV of this report.

D. Supporting Calculations

During our earlier work on other NASA contracts, several theoretical studies were conducted to determine factors such as (a) gas conduction in multi-layered radiation shields, (b) radiation transfer by closely spaced shields, (c) radiative heat transfer through seams and penetrations in multi-layer insulations, (d) the thermal radiation incident on space vehicles, (e) venting of multi-layer insulation during ascent, and (f) the optimum design of thermal protection systems. Each study, generally, was the subject of a separate report and did not reflect the accuracy of the analyses as verified by experimental data. During the latest program, limited experimental data became available to permit checking and modification of previous analyses.

We have, therefore, updated, modified and summarized these previous analyses into a single topical report entitled "Design and Optimization of Space Thermal Protection for Cryogens - Analytical Techniques and Results" by Dr. Jacques M. Bonneville (NASA CR-54190). This report is being published concurrently with our final report on Contract NAS3-4181 and fulfills our contractual obligation for supporting calculations.

E. Summary of Results and Conclusions from the Thermal Conductivity Apparatus Studies

General

Several multi-layer insulations were tested and evaluated primarily on their relative heat leak, their ability to withstand mechanical loads, and their weight. No particular insulation was rated best within all of these categories. However, it became apparent that those insulations with fine netting spacers were superior in being the lightest weight and best insulators (based upon the $K\rho$ product) but were definitely inferior with respect to foam or matted fiber spacers when subjected to compressive mechanical loads. Properly orientated spacers, of foam or matted fibers, with large amounts of material removed, resulted in superior insulation systems when considering the above criterion.

Radiation Shields

Only two types of radiation shield materials were tested, sheet aluminum (to 0.5 mil) and aluminized Mylar. Insulations using the former were superior in having lower heat leaks while the latter rated better on a weight basis. Use of thinner aluminum sheets or of aluminized Mylar with emissivities closer to metallic aluminum would imporve the performance of both. It was found that the surface treatment of the aluminum (smooth or embossed) had no apparent effect on the insulating qualities.

Mechanical Loading

It was remarked above that multi-layer insulations made from fiber mat (or foam) spacers withstood mechanical loads best. With one sample of aluminum-Fiberglas insulation, application and release of a mechanical load actually improved the insulation characteristics.

With applied loads, as low as 0.01 psig, the heat flux through a typical aluminum-nylon net insulation was proportional to the 2/3 power of the applied load.

Perforations and Penetrations

Perforations on a crinkled aluminized polyester film insulation system caused the heat flux to increase by about 20%; whereas,

perforations of the same hole size and amount of open area in aluminum radiation shields combined with netting spacers caused the heat flux to increase by more than 150%.

Comparison tests on a multi-layer insulation system that had been damaged by meteoroid bumper debris caused by hypervelocity impacts and an undamaged insulation indicated that the thermal properties of the damaged sample were not significantly degraded by the bumper debris damage under the simulated impact test condition.

Tests of the effectiveness of a buffer zone in thermally decoupling a multi-layer insulation system from a penetration have confirmed the analytical prediction.

Number of Radiation Shields

With many radiation shields, the actual heat leak is larger than predicted by simple theory. This deviation is ascribed (1) to the increased weight of the insulation which causes more solid conduction and (2) to the increase in emittance of the radiation shields operating at higher temperature levels.

Purged Gas Insulations

The thermal conductivity of a purged system approaches the thermal conductivity of the purge gas and is independent of the thermal conductivity of the evacuated system.

F. Summary of Results & Conclusions from the Calorimeter Studies

General

Fifteen experimental test series were carried out on multi-layer insulations attached to calorimeter tanks containing liquid hydrogen or nitrogen. The lowest heat flux measured on any insulation was 0.38 Btu/hr-ft^2 for a 5 aluminum shield (2 mil sheet aluminum) spaced with 1/8 x 1/8-inch ash vinyl coated Fiberglas screen. This system was, unfortunately, also the highest weight insulation with a shield-spacer unit weight of 0.044 lbs/ft^2.

The lightest insulation had a shield-spacer unit weight of 0.0045 lb/ft^2. This was a five shield (aluminized polyester film, coated on both sides, 0.25 mil thick) with nylon net spacers. This

system had the poorest insulating characteristics and heat leaks of about 1.1 Btu/hr-ft^2 were measured. However, the very low density of this system gave it the lowest ($K\rho$) value of any insulation tested, i.e., a value of 0.00072 Btu-in.-lb/hr-ft^5-$^\circ$F.

These values quoted above were for liquid nitrogen in the calorimeter. For liquid hydrogen, heat fluxes increased about 5 per cent; this increase is considerably larger than the theoretically predicted increase of 0.5 to 1 per cent.

Fabrication of Multi-Layer Insulations

No unforeseen problems arose in fabrication of multi-layer insulations to the calorimeter tanks. Application of shields one-at-a-time to a tank, with extreme care to prevent thermal shorts, is a time-consuming job. Significant improvements in cutting, fabrication, and repair techniques are feasible. Two fabricated systems showed no deterioration when transported by commercial truck carriers.

Thermal contractions will cause a stress on the insulation for continuously wound shield and spacers, or may induce gaps when insulation is applied in segments. Such contraction stresses are minimized by "shingle" attachment methods.

Fiberglas-reinforced polyurethene foams (closed-cell type) were successfully bonded to calorimeter tanks and cycled from ambient to liquid hydrogen temperatures with no apparent detachment and with no cryopumping of the atmosphere.

Simulation Tests--Ground-to-Space Environment

Ground hold simulations were made with both helium and nitrogen gas purges. Both chamber purges and closed-bag purges were used. Lower net heat leaks were found with the nitrogen system during a pressure transient from atmospheric pressure to a high vacuum.

The use of a purge bag reduced the ground environment heat leak. However, partial evacuation of the bag (with atmospheric pressure outside of the bag) caused a significant increase in heat leak as the multi-layer system was sensitive to applied pressure and inleakage of condensible gases increased the solid conduction.

Penetration Tests

A penetration placed within the multi-layer insulation increased the heat leak to a greater degree than predicted from theory; measured temperature gradients were in accord with those predicted. No explanation has satisfactorily explained the heat flux discrepancy for this single test.

Gravity Effects

Heat flux values measured on the upper half of the calorimeter tank have invariably been larger than those on the lower half. This difference has been ascribed to settling of the insulation on the upper half. Such compacting simulates a mechanical load and increases the heat leak. These effects may be accentuated during a lift-off acceleration and lessened during a "no-g" orbiting state.

Aluminized Mylar Stability

Aluminum bonded to Mylar film is sensitive to mechanical abrasion and may detach. Also, water has a very deleterious effect on this reflector material.

Nylon Netting

Nylon netting, used as a spacer material, gives good performance under no-load conditions. Insulation systems with such a spacer, however, will degrade under an imposed load; even ordinary thermal contraction will increase significantly the solid conduction component.

PART II

EXPERIMENTAL PROGRAM

THERMAL CONDUCTIVITY APPARATUS

TABLE OF CONTENTS

TABLE OF CONTENTS (Cont'd)

LIST OF FIGURES

LIST OF FIGURES (Cont'd)

LIST OF TABLES

LIST OF TABLES (Cont'd)

II. EXPERIMENTAL PROGRAM

THERMAL CONDUCTIVITY MEASUREMENTS

A. SUMMARY

1. Purpose and Scope

This report summarizes the work carried out on the experimental measurements of thermal protection systems for liquid-hydrogen tanks by Arthur D. Little, Inc., at Cambridge, Massachusetts, and at the NASA Lewis Research Center, Cleveland, Ohio. This work, under Contract No. NAS3-4181, is a continuation of the theoretical and experimental program begun under Contract NAS5-664 and NASw-615.[1]

As in the previous contracts, the purpose of the work was to increase knowledge of the thermal behavior of multilayer insulations and to obtain data on the effects of variables on their performance. The major emphasis was on problems of installation and techniques for transition from ground-hold to space conditions. Less emphasis was placed on the theoretical aspects of the behavior of insulation systems.

2. Approach

Our previous work indicated that the most profound effects on multilayer insulation performance were produced by mechanical load, gas pressure and type, and thermal shorts. We, therefore, performed thermal conductivity tests to investigate:

a. the effects of compressive mechanical loads on several multilayer insulation systems;
b. the effects of purge gas within multilayer insulation systems;
c. the effects of perforations in the radiation shields;
d. the effectiveness of a buffer zone against radiation into the edge of a multilayer insulation sample;
e. new material and combinations thereof as they become available;
f. the effects of added radiation shields on heat flux; and,

g. testing insulations in support of work being done on other parts of this program.

3. Findings and Conclusions

On the basis of the results of tests on different multilayer insulation systems, we can summarize our findings and conclusions as follows:

a. The configuration of the radiation shield surface (i.e., smooth or embossed) appears to have no influence on the heat flux when the shield is used in combination with fiberglass mat or cloth spacers.

b. The application and subsequent release of mechanical loads on a sample in the test apparatus appear to improve the thermal insulating properties of a system containing aluminum radiation shields and fiberglass cloth spacers.

c. When the number of radiation shields is increased, experimental variations from the theoretical heat flux are observed, which indicate that: (1) because of the weight of the overlying material in thicker samples, the solid conduction may increase; and (2) additional radiation shields may be less efficient because their temperature may be higher and hence their emittance greater.

d. The thermal performance under mechanical load depends upon the behavior of the spacer materials. Less resilient materials (as compared to fiber mats or foam spacers), such as cloth and netting, exhibit a higher heat flux under mechanical load. The heat flux through the spacer can be lowered by reducing the load-supporting area within the range of the compressive strengths of the spacer materials.

e. Tests at mechanical loads as low as 0.01 psi have confirmed that the heat flux through a multilayer insulation of aluminum shields and nylon netting is proportional to the 2/3 power of the applied load.

f. The thermal conductivity of a purged system approaches the thermal conductivity of the purge gas and is effectively independent of the thermal conductivity of the evacuated system.

g. Tests of the effectiveness of a buffer zone to thermally decouple a multilayer insulation system from a penetration have confirmed the analytical prediction.

h. Perforations in a crinkled aluminized polyester film insulation system caused the heat flux to increase by about 20%; whereas, similar perforations (i.e., the same hole size and amount of open area) in aluminum radiation shields used in combination with netting spacers caused the heat flux to increase by more than 150%.

i. Comparison of tests on a multilayer insulation system that had been damaged by metecroid-bumper debris caused by hypervelocity impacts and on an undamaged insulation indicated that the thermal properties of the damaged sample were not significantly degraded by the bumper-debris damage.

Our work to date has shown that it is feasible to select material combinations which will minimize the effects of mechanical loads on a multilayer insulation system and that the system can be arranged so that influences of penetrations can be minimized. If the present rate of progress--both in experimentation and application--in the development of improved multilayer insulation systems' performance can be maintained, it appears very likely that by the time extended space missions are required, it will be possible to keep the boil-off rates of cryogenic fluids within a few per cent per year.

4. Recommendations

On the basis of our thermal-performance data for multilayer insulations, we recommend that NASA:

a. Continue the program to optimize materials and material combinations; in particular, to develop spacer materials with greater contact resistance and radiation shield materials with lower emittance. Determine the effect of temperature on the emittance of radiation-shield materials.

b. Develop improved thermal-insulation systems; that is, systems having a smaller product of thermal conductivity times density.

c. Continue the program to develop systems that will retain their thermal-insulation properties over a wide range of applied loads and will overcome problems encountered during application of the insulation system to a tank; that is, problems such as compressive loads caused by tension during the wrapping process.

B. INTRODUCTION

The theoretical and experimental investigations of the performance of multilayer insulation systems performed by various laboratories have brought about a greater awareness of the role such insulation systems can play in the long-term protection of cryogenic fluids in space. The results obtained in these earlier laboratory investigations are now being applied, in several programs, to systems designs that approach the scale of space-flight hardware.

The search for applications of multilayer insulation systems has shown the necessity for additional information on the behavior of these systems under conditions which approximate more closely those expected during actual use, including: (1) the mechanical pressure exerted on the insulation system, (2) the purging of systems during prelaunch and checkout, (3) the ensuring of rapid and maximum removal of gases within the

insulation system, and (4) the thermal decoupling of the insulation from penetrations. All these conditions will have important effects on the optimization--of both function and weight--of the various multilayer insulation systems.

To obtain the full effectiveness of multilayer insulation systems for future space missions, increased effort has been concentrated on the development of new insulation materials. Various companies have performed extensive development efforts to provide new and improved materials, particularly for spacers and reflecting coatings on polyester films. As soon as new insulation systems and materials have become available, we have included them in our experimental program.

The following sections discuss the portions of our work which deal with the techniques and results of measuring the thermal conductivity of multilayer insulation systems as a function of different variables.

C. INSULATION SYSTEMS

We chose the multilayer insulation systems for this program on the basis of their potential to perform effectively in both ground and space environments. We considered the following criteria of utmost importance: (1) types of material, (2) heat-transfer characteristics, (3) unit weight, (4) potential applications, and (5) specific missions under consideration. The selected systems were either supplied by the companies which had developed them or--in the case of systems which we developed--assembled from materials with desirable properties. The materials represented as wide a range of spacer and radiation-shield combinations as possible so that the data obtained would be useful in predicting the performance of similar multilayer insulation systems.

We tested 18 different insulation systems with the thermal-conductivity apparatus. Table II-1 provides details of the insulation systems tested, the supplier of each sample, and the variable investigated on each sample. It also identifies each system by number for convenient referencing in the discussion that follows.

TABLE II-1

TABLE OF INSULATION SYSTEMS TESTED

Insulation System	Radiation Shield Material	Spacer Material	Variable Investigated	Sample Number**	Sample Supplier
A. Multilayer Insulation Samples					
I	(20)* Crinkled polyester film, aluminized on one side, 0.00025 inches thick. National Research Corporation	None	Perforations Quality Purge Gas	1051, 1052, 1053 1054 3034, 2036	National Research Corporation
II	(5) Polyester film, aluminized on one side, 0.00025 inches thick. National Research Corporation	(6) Vinyl-coated glass fiber screen, 1/8 x 1/8 inch mesh and 0.02 inch thick. Owens Corning Co.	Number of Radiation Shields	2031	Arthur D. Little, Inc.
III	(10) Polyester film, aluminized on one side, 0.00025 inches thick. National Research Corporation	(11) Vinyl-coated glass fiber screen, 1/8 x 1/8 inch mesh and 0.02 inch thick. Owens Corning Co.	Number of Radiation Shields	2035	Arthur D. Little, Inc.
IV	(20) Polyester film, aluminized on one side, 0.00025 inches thick. National Research Corporation	(21) Vinyl-coated glass fiber screen, 1/8 x 1/8 inch mesh and 0.02 inch thick. Owens Corning Co.	Number of Radiation Shields	2034	Arthur D. Little, Inc.
V	(40) Polyester film, aluminized on one side, 0.00025 inches thick. National Research Corporation	(41) Vinyl-coated glass fiber screen, 1/8 x 1/8 inch mesh and 0.02 inch thick. Owens Corning Co.	Number of Radiation Shields	2032	Arthur D. Little, Inc.
VI	(10) Aluminum alloy 1145-H19, bright on both sides, 0.002 inches thick. Alcoa	(11) Vinyl-coated glass fiber screen, 1/8 x 1/8 inch mes and 0.02 inch thick. Owens Corning Co.	Buffer Zone Purge Gas Calibration	3036 2037, 3032, 3033 3030, 3031	Arthur D. Little, Inc.

* The number of layers of radiation shields and spacers is given in parenthesis.

** The first digit of the sample number refers to the apparatus in which that sample was tested.

TABLE II-1 (Cont'd)

Insulation System	Radiation Shield Material	Spacer Material	Variable Investigated	Sample Number	Sample Supplier
VII	(5) Aluminum alloy 1145-0, bright on both sides, 0.002 inches thick. Alcoa	(6) Vinyl-coated glass fiber screen, 1/8 x 1/8 inch mesh and 0.02 inch thick. Owens Corning Co.	Support of Insulated Tank Program	2030	Arthur D. Little, Inc.
			Meteoroid Bumper-Debris Damage	2041, 2042	
VIII	(10) Smooth aluminum, 0.0005 inch thick.	(11) Fiberglass mat, 0.014 inch thick.	None (Given here for reference)	2026	L'Air Liquide, Sassenage, France
IX	(10) Smooth aluminum, 0.0005 inch thick.	(11) Spacers, each consisting of three layers of 0.001 inch thick glass fiber cloth.	None (Given here for reference)	2027	L'Air Liquide, Sassenage, France
X	(10) Aluminum, 0.0005 inch thick, Embossed with wave-like pattern.	(11) Fiberglass mat, 0.014 inch thick.	Material Mechanical Load	2028	L'Air Liquide, Sassenage, France
XI	(10) Aluminum, 0.0005 inch thick, Embossed with wave-like pattern	(11) Spacers, each consisting of three layers of 0.001 inch thick glass fiber cloth.	Material Mechanical Load	2029	L'Air Liquide, Sassenage, France
XII	(10) Aluminum alloy 1145-H19, bright on both sides, 0.002 inch thick. Alcoa	(11) CT-449 material, 0.02 inch thick and 9.0 lb/ft^3 density. 11% support area. CTL Div. of Studebaker Corporation	Mechanical Load	2038	Arthur D. Little, Inc.
XIII	(10) Aluminum alloy 1145-H19, bright on both sides, 0.002 inch thick. Alcoa	(11) CT-449 material, 0.02 inch thick and 9.0 lbs/ft^3 density. CTL Div. of Studebaker Corp.	Mechanical Load	1058	Arthur D. Little, Inc.
XIV	(10) Aluminum alloy 1145-H19, bright on both sides, 0.002 inch thick. Alcoa	(11) Nylon netting 0.007 inch thick. Sears Roebuck #36G1008H	Mechanical Load	2040	Arthur D. Little, Inc.
			Small Mechanical Load	3037	
XV	(10) Polyester film, 0.00025 inch thick, double aluminized coating on both sides. National Research Corporation	(11) Nylon netting 0.007 inch thick. Sears Roebuck #36G1008H	Mechanical Load	2039	Arthur D. Little, Inc.

TABLE II-1 (Cont'd)

Insulation System	Radiation Shield Material	Spacer Material	Variable Investigated	Sample Number	Sample Supplier
XVI	(10) Polyester film, 0.00025 inch thick, double aluminized coating on both sides. National Research Corporation	(11) Polyurethane foam, Freon blown 0.02 inch thick, 2.7 lbs/ft^3 density. Goodyear Aerospace Corp.	Mechanical Loads	1064	Arthur D. Little, Inc.
XVII	(10) Polyester film, 0.00025 inch thick, double aluminized coating on both sides. National Research Corporation	(11) Polyurethane foam, Freon blown 0.02 inch thick. 11% support area. Goodyear Aerospace Corp.	Mechanical Loads	1065	Arthur D. Little, Inc.
B. Miscellaneous Insulation Samples					
XVIII	Polyether foam, Freon blown, 8 lbs/ft^3 density, 1/2 inch thick		In support of Insulated Tank Program	2033	Arthur D. Little, Inc.
XIX	Rigid One Shot Foam No. 1 with 10% chopped strand glass fiber. Foam 1/2 inch thick, foamed in place against a 1/8 inch thick 12-inch diameter aluminum plate.		In support of Insulated Tank Program	1060, 1062	Arthur D. Little, Inc.
XX	Composite insulation sample consisting of insulation systems XIX on the cold side and insulation system VII.		In support of Insulated Tank Program	1063	
XXI	A rigid phenolic laminate (FED SPEC HH-P-256-2 Grade EL)		Contact Resistance	1059, 1061	Arthur D. Little, Inc.

D. APPARATUS AND INSTRUMENTATION

1. Description

To measure the thermal conductivity of multilayer insulations and to study the effects of different variables on thermal conductivity, we have designed and built a flat-plate apparatus, shown in Figure II-1, consisting of a double-guarded cold-plate, a warm-plate, a sample chamber, and a vacuum jacket. A circulating fluid keeps the warm-plate at the desired uniform temperature. The cold-plate consists of the bottom surfaces of the measuring vessel, and the surrounding guard vessel. The enclosing bell jar permits the apparatus to be evacuated to pressures as low as 10^{-6} torr. The pressure within the sample chamber is controlled separately, so that the sample can be exposed to varying levels of gas pressure. The quantity of heat flowing through a 6-inch-diameter center section of a 12-inch-diameter (approximately) test sample is determined by the boil-off rate of the cryogenic liquid contained in the measuring vessel. The volume flow rate of the boil-off gas is used to calculate the thermal conductivity. This apparatus is described in detail elsewhere.[1]

During this program, three double-guarded cold-plate units were used to measure the thermal conductivity of various thermal insulators at liquid-hydrogen and liquid-nitrogen temperatures. Two units, No. 1 and No. 2, are located at the Lewis Research Center in Cleveland, Ohio, and a third, No. 3, is located at the Arthur D. Little, Inc., Laboratory in Cambridge, Massachusetts.

2. Improvements

a. Liquid-Hydrogen Transfer Lines

The vacuum-jacketed hydrogen-transfer lines on the units that operate with liquid hydrogen were modified so that only one 150-liter portable storage dewar is now required to supply each apparatus; whereas, previously, two were required for each apparatus. This change provides for ease and safety of operation and for more economical use of liquid hydrogen. The

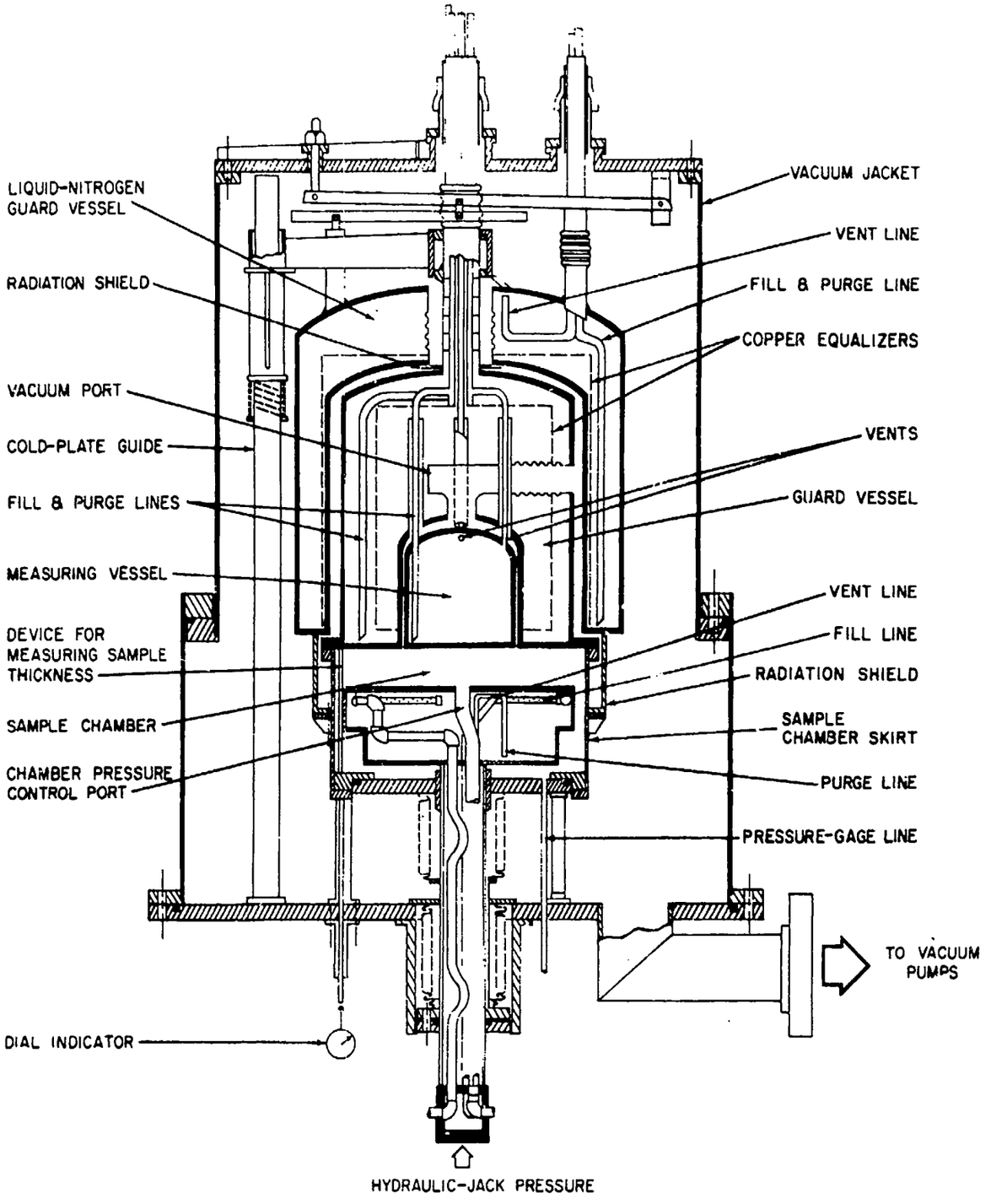

FIGURE II-1 CROSS-SECTION OF DOUBLE-GUARDED COLD-PLATE THERMAL-CONDUCTIVITY APPARATUS

valves in these transfer lines were replaced with valves suitable for use with liquid hydrogen. We replaced the soft-soldered copper fittings on the fluid lines to the warm-plate of apparatus No. 1 with a stainless steel assembly. This assembly will permit higher warm-plate temperatures to be attained during testing and will eliminate hazardous soldering operations, which formerly required shut-down of hydrogen testing on units No. 1 and No. 2.

b. Small Mechanical-Loading Device

The original thermal-conductivity apparatus is equipped with a movable warm-plate, which, when driven hydraulically, may be used to compress insulation samples against the cold-plate to determine the effect of mechanical loading on thermal properties. In our work of the past two years, this device has been used extensively to apply mechanical loading of 2-15 psi to a shaft that slides through an "O"-ring seal in the vacuum-chamber wall; frictional losses at that seal introduce uncertainty in this method and limit its reliable use to mechanical loading above 2 psi.

Although evacuated multilayer insulation applied to space-vehicle tankage may be subjected to loading of about one atmosphere during the ground-hold period, it is anticipated that, during space flight, loads considerably smaller than 2 psi may be present within the insulation system. Among the causes of such small loading may be: wrapping tension of the insulation, thermal expansion of the insulation components with respect to the tank, and compression of the system in the vicinity of tank support members.

In order to apply and measure small mechanical loads on multilayer insulation samples, we required additional instrumentation. We considered several loading methods, but excluded designs with electrical components because of their potential hazard in a possible hydrogen-in-air atmosphere. We finally constructed a device using welded bellows (shown in Figure II-2), because of its apparent advantages in accuracy, simplicity, and economy.

The device consists of the following essential components:

(1) A floating plate, to transmit the load into the sample. This plate is rigid (0.5-inch

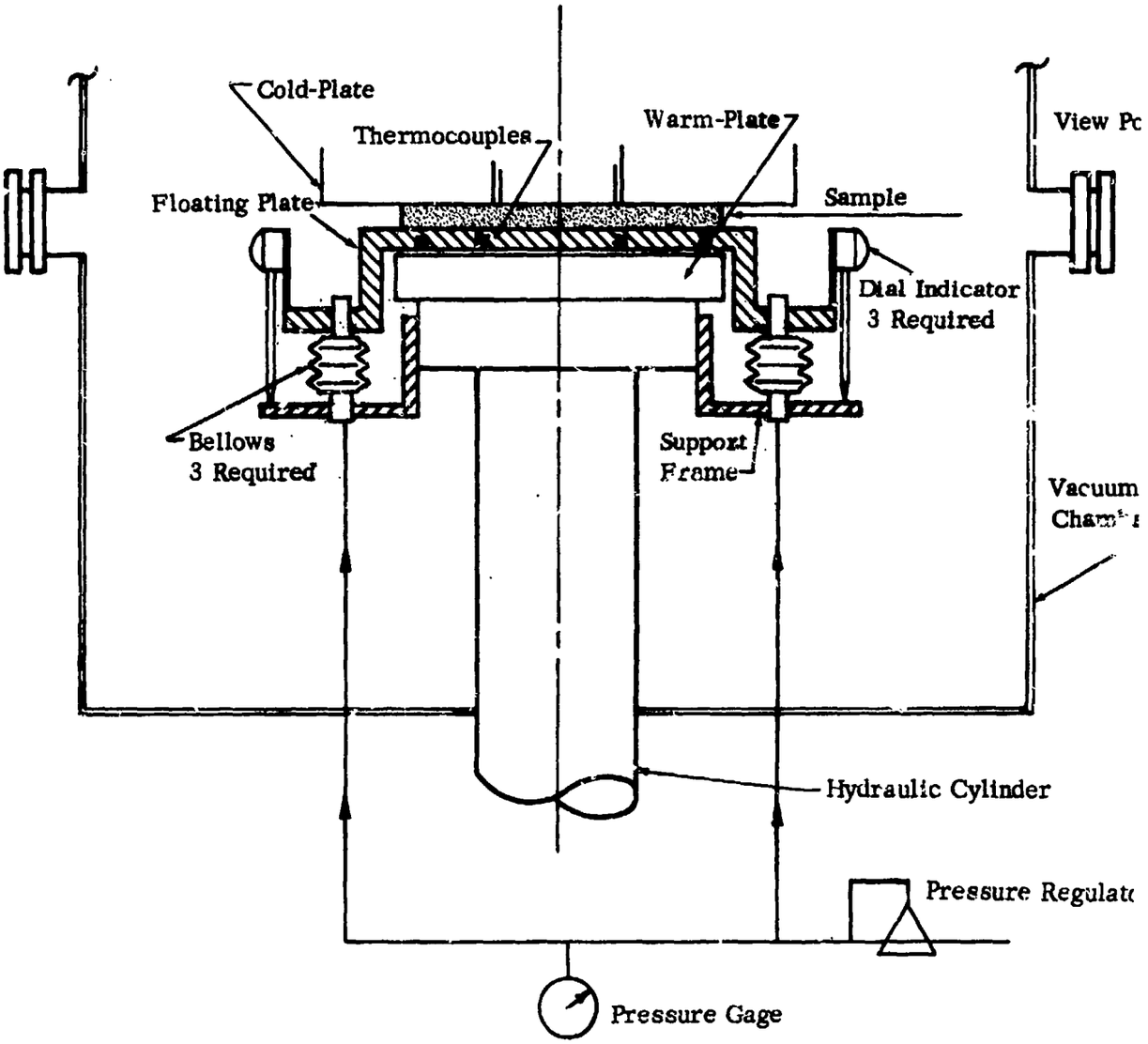

FIGURE II-2 VIEWING PORTS AND DEVICE TO MEASURE SMALL COMPRESSIVE LOAD

thick), contains several copper-constantan thermocouples, and, in this arrangement, substitutes for the warm plate.

(2) Three welded bellows assemblies, to convert pneumatic pressure into a force that is applied to the floating plate.

(3) Three dial indicator assembles, to determine the position of the floating plate.

(4) A support frame (which attaches to the warm-plate structure), to support the bellows assemblies and provide a reference surface for the dial-indicator measurements.

Two more required modifications in the thermal-conductivity apparatus were accomplished: (1) viewing ports to observe the dial indicators were installed in the vacuum-chamber wall; and, (2) the sample-chamber wall was lowered to make room for the welded bellows assembly. The dewar assembly, previously supported by the sample-chamber wall, had to be supported now by three rods.

In the operation of this device, a sample is placed on the floating plate as shown in Figure II-2, and the bellows are pressurized. The pressure extends the bellows and raises the floating plate, compressing the sample against the cold-plate. The warm-plate, to which the support frame is attached, is then raised by the external hydraulic cylinder until the dial indicators show that the bellows are returned to their unpressured height. The force acting on the sample can then be computed directly from the pressure-gauge indication. This force is independent of the spring constant of the bellows.

We installed the device in the conductivity apparatus and, after some brief preliminary measurements, conducted a test with a sample of a typical multilayer insulation system. In this test, the thermal-conductivity apparatus operated satisfactorily and measured mechanical loads as low as 0.01 psi. The pressure regulator in the pneumatic system was the limiting factor; it appears that a regulator of higher sensitivity may make the apparatus capable of measuring loads down to approximately 0.004 psi.

3. Calibration

Calibration tests were performed on two of the three operating units to determine if the performance of the apparatus was impaired by recent modifications or by normal operation over a period of nearly two years. In the calibration tests, a flat heater was attached to the measuring-vessel portion of the cold-plate. An aluminum radiation shield, attached to the measuring vessel, surrounded the heater to ensure that all of the power supplied to the heater would be transferred to the measuring vessel. The measuring, guard, and nitrogen vessels, and the warm-plate were filled with liquid nitrogen to minimize temperature differences between the surfaces of the sample chamber. In addition, a radiation shield, fastened to the guard vessel, enclosed the radiation shield and heater described above to further reduce the possibility of stray radiation reaching the measuring vessel. The same calibration method was used for all three apparatus after fabrication. Measurements showed that the power dissipated in the leads of the heater circuit was 3.9% of the total power measured at the terminals. The data were adjusted to account for this power loss.

The test was conducted at power inputs to the heater of from 0 to approximately 44 milliwatts. The results of these tests are given in Tables II-2 and II-3, where the power dissipated at the heater (input) is compared to the boil-off rate (output). The calibration data are within reasonable experimental error and, we believe, demonstrate that the performance of each of these units is satisfactory and has not been impaired by either modification or use.

E. EXPERIMENTAL RESULTS

1. Materials

a. Comparison of Radiation Shield and Spacer Materials

Tests were performed on samples of four insulation systems that were submitted by L'Air Liquide. These samples consisted of combinations of smooth- or waffled-aluminum radiation shields and fiberglass cloth or fiberglass mat. The samples are described in Table II-1, Insulation Systems VIII, IX, X, and XI. The results of the tests performed on these

TABLE II-2

HEATER CALIBRATION OF THERMAL-CONDUCTIVITY APPARATUS NO. 1

January 1964

T_{cold} = -320°F

Heater Power (input)		Boil-Off Rate (output)	Difference (output minus input)	
(BTU/hr-ft^2)	(watts x 10^{-3})	(watts x 10^{-3})	(watts x 10^{-3})	(%)
0	0	0.2	+0.2	---
0.147	9	9.0	0.0	0.0
0.336	20.5	19.6	-0.9	-4.6
0.715	43.7	43.8	+0.1	+0.2

TABLE II-3

HEATER CALIBRATION OF THERMAL-CONDUCTIVITY APPARATUS NO. 3

January 1964

T_{cold} = -320°F

Heater Power (input)		Boil-Off Rate (output)	Difference (output minus input)	
(BTU/hr-ft^2)	(watts x 10^{-3})	(watts x 10^{-3})	(watts x 10^{-3})	(%)
0.178	10.9	11.1	+0.2	+1.8
0.425	26.0	25.4	-0.6	-2.3
1.26	76.8	76.4	-0.4	-0.5

samples are given in Tables II-4 through II-7. The first two samples (Nos. 2026 and 2027) were tested and reported under the previous contract but are repeated here for reference. Figure II-3 and II-4 are plots of data taken from those tables and are presented to demonstrate the following:

(1) With the spacer materials tested and for the condition of slight, although unmeasured, mechanical loadins on the insulation samples, the embossed aluminum radiation shields appeared to produce the same heat flux through the insulation system as the smooth radiation shields. Only a limited amount of the collected data was useful for comparing the smooth-aluminum with the embossed aluminum radiation shields, because the samples containing the former were tested near their optimum density (zero load) while the samples containing the latter were tested primarily as load-bearing insulations. Figure II-3 shows heat flux plotted as a function of the number of radiation shields per inch for all four insulation systems. In Figure II-3, comparing the results of the tests on the samples that contain the same spacer materials, sample No. 2026 with 2028 and sample No. 2027 with 2029; the curves are apparently parallel and very close together. In the range where the curves overlap, the samples are under very slight, although unmeasured, mechanical loading.

(2) Applying and then releasing the mechanical load imposed on a sample in the test apparatus apparently improves the thermal insulating properties for the sample containing aluminum radiation shields and fiberglass cloth spacers.

TABLE II-4

EFFECT OF DENSITY ON THE THERMAL PROPERTIES OF A MULTILAYER INSULATION (SYSTEM VIII)

Sample Description: Ten aluminum radiation shields of smooth aluminum and eleven spacers of fiberglass mat 0.014-inch thick. (St. Gobain)

Cold Plate Emissivity: 0.9

Warm Plate Emissivity: 0.3

Sample Chamber Pressure: less than 1×10^{-5} torr

Plate Separation (in)	Number Radiation Shields Per Inch	ρ Sample Density ($\frac{lbs}{ft^3}$)	Heat Flux ($\frac{Btu}{hr\text{-}ft^2}$)	K Thermal Conductivity ($\frac{Btu\text{-}in}{hr\text{-}ft^2\text{-}F}$)	K · ρ Product of Thermal Conductivity and Density ($\frac{Btu\text{-}in}{hr\text{-}ft^2\text{-}F} \times \frac{lbs}{ft^3}$)	Warm-Plate Temperature (F)	Cold-Plate Temp. (F)	Test Date	Test Number
0.505	19.8	4.5	0.099	0.00010	0.00045	69	-423	Sept 12	2026 L
0.460	21.8	5.0	0.11	0.00010	0.00050	69	-423	Sept 11	2026 K
0.437	22.9	5.3	0.15	0.00013	0.00069	69	-423	Sept 10	2026 J
0.424	23.6	5.4	0.23	0.00020	0.0011	70	-423	Sept 9	2026 I
0.412	24.3	5.6	0.31	0.00026	0.0015	69	-423	Sept 6	2026 H
0.410	24.4	5.6	0.34	0.00028	0.0016	68	-423	Aug. 30	2026 D
0.395	25.3	5.8	0.49	0.00041	0.0024	69	-423	Sept 6	2026 G
0.369	27.1	6.3	0.85	0.00064	0.0040	69	-423	Sept 5	2026 E
0.320	31.2	7.2	1.75	0.0011	0.0079	68	-423	Sept 5	2026 F

TABLE II-5

EFFECT OF DENSITY ON THE THERMAL PROPERTIES OF A MULTILAYER INSULATION (SYSTEM IX)

Sample Description: Ten aluminum radiation shields of smooth aluminum and eleven spacers each made of 3 layers of fiberglass cloth (genin), 0.004-inch total spacer thickness.

Sample Chamber Pressure: less than 1×10^{-5} torr

Cold Plate Emissivity: 0.9

Warm Plate Emissivity: 0.3

Plate Separation (in)	Number of Radiation Shields Per Inch	ρ Sample Density ($\frac{lbs}{ft^3}$)	Heat Flux ($\frac{Btu}{hr\text{-}ft^2}$)	K Thermal Conductivity ($\frac{Btu\text{-}in}{hr\text{-}ft^2\text{-}F}$)	$K \cdot \rho$ Product of Thermal Conductivity and Density ($\frac{Btu\text{-}in}{hr\text{-}ft^2\text{-}F} \times \frac{lbs}{ft^3}$)	Warm-Plate Temperature (F)	Cold-Plate Temp. (F)	Test Date	Test Number
0.350	28.6	5.6	0.24	0.00017	0.00095	69	-423	10-16-63	2027 a
0.255	39.2	7.7	0.27	0.00014	0.0011	67	-423	10-17-63	2027 b
0.168	59.5	11.7	0.34	0.00012	0.0014	68	-423	10-18-63	2027 d
0.153	65.4	12.8	0.74	0.00022	0.0028	67	-423	10-19-63	2027 f
0.133	75.2	14.7	1.27	0.00035	0.0051	67	-423	10-20-63	2027 h
0.075	133	26.2	2.62	0.0040	0.011	68	-423	10-23-63	2027 j
0.159	63	12.4	0.27	0.00011	0.0014	63	-320	10-31-63	2027 q
0.167	60	11.8	0.31	0.00014	0.0015	62	-320	11-4-63	2027 r
0.203	49.2	9.7	0.21	0.00012	0.0012	56	-320	11-22-63	2027 s
0.142	70.4	13.8	0.46	0.00021	0.0026	54	-320	11-27-63	2027 t
0.256	39	7.7	0.20	0.00013	0.0010	54	-320	11-30-63	2027 u
0.192	52	10.2	0.20	0.00010	0.0013	55	-320	12-4-63	2027 v
0.192	52	10.2	0.21	0.000076	0.00078	54	-423	12-5-63	2027 w
0.069	145	28.5	6.3	0.00091	0.026	52	-423	12-6-63	2027 x
0.070	143	28.1	4.5	0.00065	0.018	54	-423	12-7-63	2027 y
0.066	152	29.8	14.5	0.0020	0.060	50	-423	12-9-63	2027 z
0.080	125	24.6	2.5	0.00052	0.013	[illegible]	[illegible]		

TABLE II-6

EFFECT OF MECHANICAL LOADS ON THE HEAT FLUX THROUGH A MULTILAYER INSULATION (SYSTEM X)

Sample Description: Ten radiation shields of embossed aluminum, approximately 0.0005 inch thick, and eleven spacers of 0.014 inch thick fiberglass mat (St. Gobain).

Sample Chamber Pressure: Less than 1×10^{-5} torr

Cold late Emissivity: 0.9

Warm Plate Emissivity: 0.3

Sample Thickness (in)	Mechanical Load (psi)	Number of Radiation Shields/Inch	ρ Sample Density ($\frac{lbs}{ft^3}$)	Heat Flux ($\frac{Btu}{hr\text{-}ft^2}$)	K Thermal Conductivity ($\frac{Btu\text{-}in}{hr\text{-}ft^2\text{-}F}$)	K · ρ Product of Thermal Conductivity & Density ($\frac{Btu\text{-}in}{hr\text{-}ft^2\text{-}F} \cdot \frac{lbs}{ft^3}$)	Warm Plate Temperature (F)	Test Date	Test Number
0.405	*	20.8	5.4	0.48	0.00041	0.0022	43	12-24-63	2028 a
0.330	*	30.3	6.7	1.6	0.0011	0.0074	49	12-27-63	2028 b
0.205	5	49.8	10.7	7.1	0.0031	0.033	47	12-30-63	2028 c
0.166	15	60.3	13.3	12.5	0.0044	0.058	43	12-31-63	2028 d
0.190	5	52.6	11.6	7.9	0.0032	0.037	45	1-2-64	2028 e
0.323	*	31.0	6.8	1.4	0.00097	0.0066	46	1-3-64	2028 f
0.408	*	24.5	5.4	0.27	0.00023	0.0012	46	1-4-64	2028 g

* Small and not measurable.

TABLE II-7

EFFECT OF MECHANICAL LOADS ON THE HEAT FLUX THROUGH A MULTILAYER INSULATION (SYSTEM XI)

Sample Description: Ten radiation shields of embossed aluminum, approximately 0.0005 inch thick, and eleven spacers each made of 3 layers of fiberglass cloth (genin), 0.004 inch total spacer thickness

Sample Chamber Pressure: Less than 1×10^{-6} torr

Cold Plate Emissivity: 0.9

Warm Plate Emissivity: 0.3

Sample Thickness (in)	Mechanical Load (psi)	Number of Radiation Shields/Inch	ρ Sample Density $(\frac{lbs}{ft^3})$	Heat Flux $(\frac{Btu}{hr\text{-}ft^2})$	K Thermal Conductivity $(\frac{Btu\text{-}in}{hr\text{-}ft^2\text{-}F})$	K · ρ Product of Thermal Conductivity & Density $(\frac{Btu\text{-}in}{hr\text{-}ft^2\text{-}F} \cdot \frac{lbs}{ft^3})$	Warm Plate Temperature (F)	Test Date	Test Number
0.151	*	66.3	15.5	0.72	0.00023	0.0035	48	1-8-64	2029 a
0.141	*	71.0	16.6	1.4	0.00041	0.0068	43	1-9-64	2029 b
0.076	5	132.0	30.8	115	0.018	0.55	45	1-10-64	2029 c
0.120	*	83.4	19.6	1.3	0.00034	0.0067	45	1-10-64	2029 d
0.063	15	159.0	37.2	246	0.033	1.23	43	1-15-64	2029 e
0.065	5	154.0	36.1	169	0.023	0.83	46	1-16-64	2029 f
0.113	*	88.5	20.8	0.73	0.00018	0.0037	44	1-20-64	2029 g
0.121	*	82.6	19.4	0.87	0.00023	0.0045	43	1-21-64	2029 h
0.145	*	69.0	16.2	0.28	0.000088	0.0014	44	1-23-64	2029 i

* Small and not measurable.

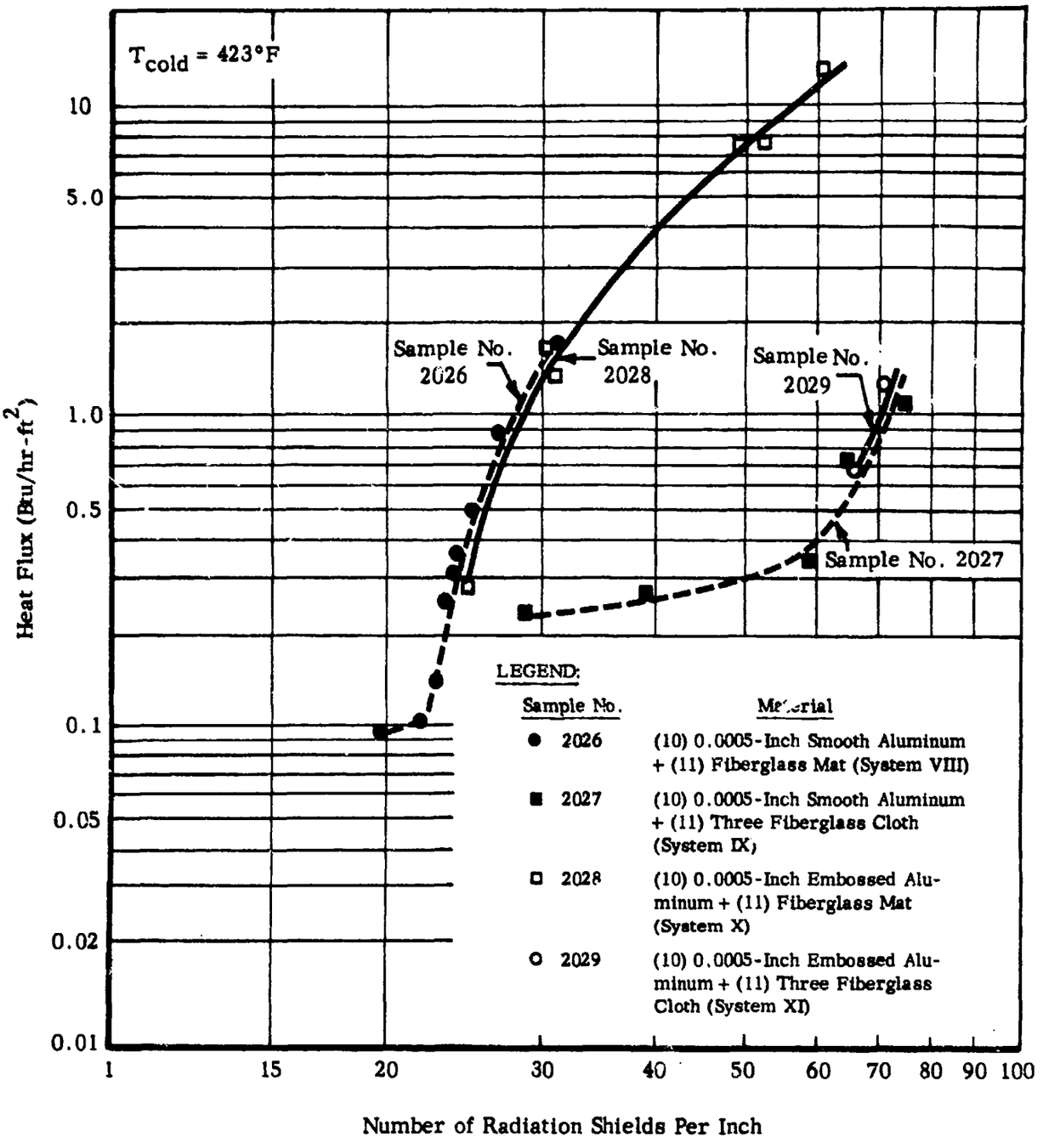

FIGURE II-3 EFFECTS OF EMBOSSED RADIATION SHIELDS AND SPACER MATERIAL ON HEAT FLUX THROUGH MULTILAYER INSULATION SYSTEMS (SYSTEMS VIII, IX, X AND XI)

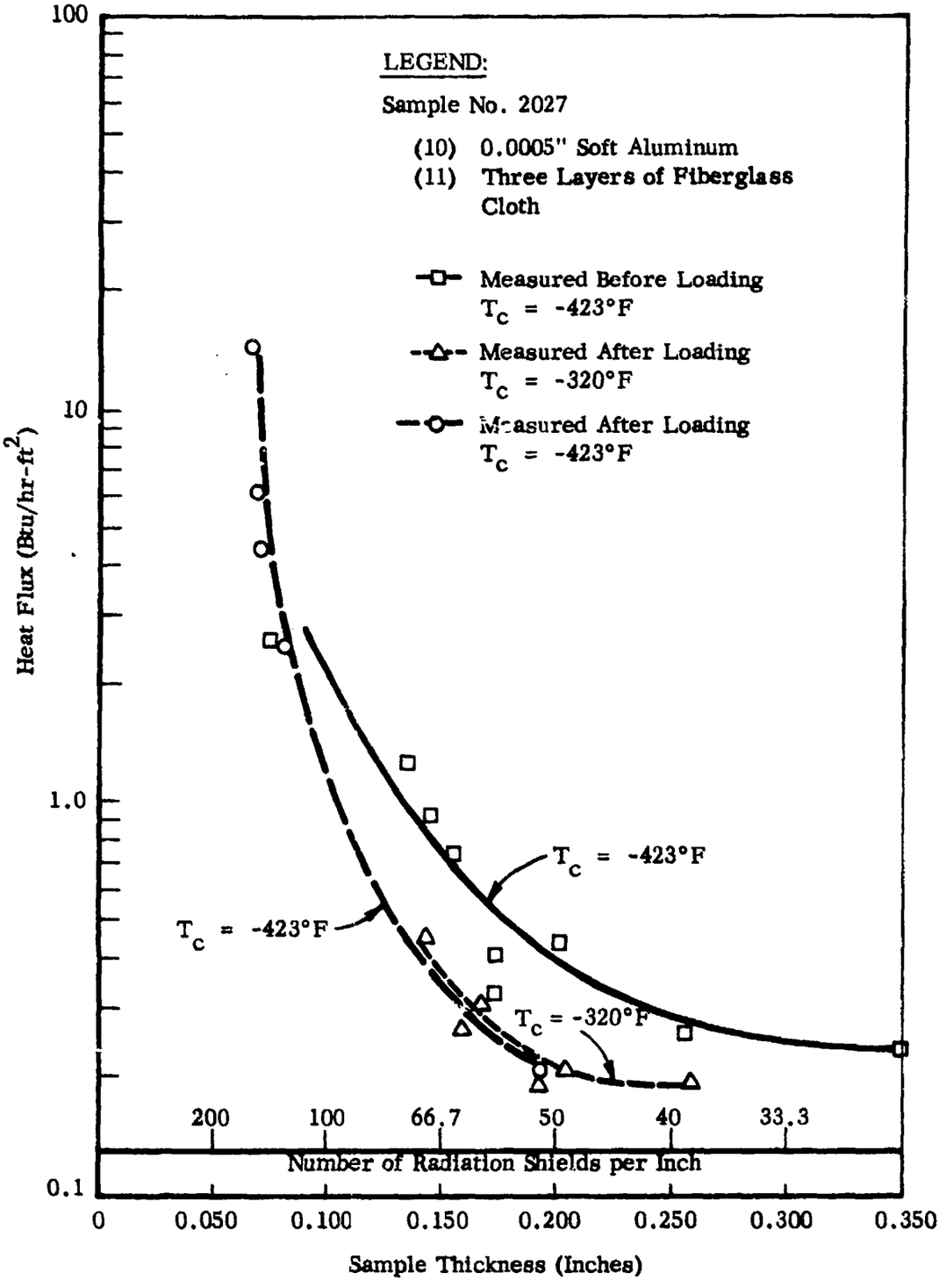

FIGURE II-4 EFFECT OF MECHANICAL LOADS ON THE HEAT FLUX THROUGH A MULTILAYER INSULATION (SYSTEM IX)

Figure II-4 shows heat flux plotted as a function of sample thickness for the system containing smooth aluminum radiation shields and fiberglass cloth spacers. The solid curve represents data taken before any appreciable mechanical loading was applied to the insulation sample. An estimated 1-psi load was applied to the sample and then released, and then tests similar to those before loading were performed. The data obtained after mechanically loading the sample are represented by the dashed curve. Although most of the data taken after release of the load were obtained with the cold-plate at -320°F--the cold-plate was at -420°F before loading--we believe that in these tests the heat flux is not affected by this change in cold-plate temperature. (Refer to pp. 61 and 62 of Report No. 65008-00-02, Contract No. NAS5-664.) The dashed curve can, therefore, be imagined to extend through the 0's and the Δ's which represent T_c of -423 and -320, respectively, and it appears that applying and releasing the mechanical load results in a more tightly packed sample and a lower heat flux through the insulation systems.

b. Quality

A sample of a multilayer insulation system consisting of 20 radiation shields of crinkled aluminized-polyester film 0.00025-inch thick was tested to determine the insulating properties at its optimum density. A sample of similar material which had been purchased more than two years earlier was tested in March 1962, but recent data (obtained from samples No. 1050, 1052, and 1053) indicated that the material quality had improved during the interim period. A conference with the manufacturer revealed that, during that time, the fabricating process had been modified to produce a more controlled and uniform aluminum coating on the polyester film.

The results of these tests appear in Table II-8. Figure II-5 shows two curves representing heat flux plotted vs. the number of layers per inch: one curve is plotted for the early data; the other, for the more recent data. At 40 radiation shields per inch, the heat flux through the sample tested this year is approximately 30% lower than for the sample tested earlier, thus indicating an improvement in the quality of this insulation.

TABLE II-8

EFFECT OF MATERIAL QUALITY ON THE THERMAL PROPERTIES OF A MULTILAYER INSULATION (SYSTEM I)

Sample Description: Twenty radiation shields of crinkled aluminized polyester film

Sample-Chamber Pressure: Less than 1×10^{-5} torr

Cold-Plate Temperature: -423° F

Cold-Plate Emissivity: 0.9

Warm-Plate Emissivity: 0.3

Sample Thickness (in.)	Number of Radiation Shields/in.	(ρ) Sample Density ($\frac{lbs}{ft^3}$)	Heat Flux ($\frac{Btu}{hr\text{-}ft^2}$)	(K) Thermal Conductivity ($\frac{Btu\text{-}in.}{hr\text{-}ft^2\text{-}F}$)	K · ρ Product of Thermal Conductivity and Density ($\frac{btu\text{-}in.}{hr\text{-}ft^2\text{-}F} \times \frac{lbs}{ft^3}$)	Warm-Plate Temp. (F)	Test Date	Test Number
0.501	39.9	1.53	0 233	.000250	.000383	40	2-4-64	1054 a
0.432	46.3	1.77	0.308	.000287	.000508	42	2-5-64	1054 b
0.403	49.6	1.90	0.227	.000197	.000374	40	2-10-64	1054 c
0.375	53.3	2.04	0.325	.000264	.000539	40	2-11-64	1054 d
0.358	55.9	2.14	0.326	.000252	.000540	40	2-12-64	1054 e
0.328	61.0	2.26	0.475	.000334	.000756	43	2-13-64	1054 f
0.278	71.9	2.75	0.710	.000427	.00117	40	2-14-64	1054 g
0.190	105	4.03	1.42	.000580	.00234	43	2-14-64	1054 h
0.400	50.0	1.91	0.260	.000224	.000428	40	2-17-64	1054 i
0.802	24.9	0.95	0.296	.000515	.000489	40	2-18-64	1054 j
1.297	15.4	0.59	0.543	.00152	.000897	40	2-19-64	1054 k
0.116	172	6.60	5.06	.00127	.00845	40	2-20-64	1054 l
0.062	323	12.3	31.4	.0042	.0517	41	2-23-64	1054 m

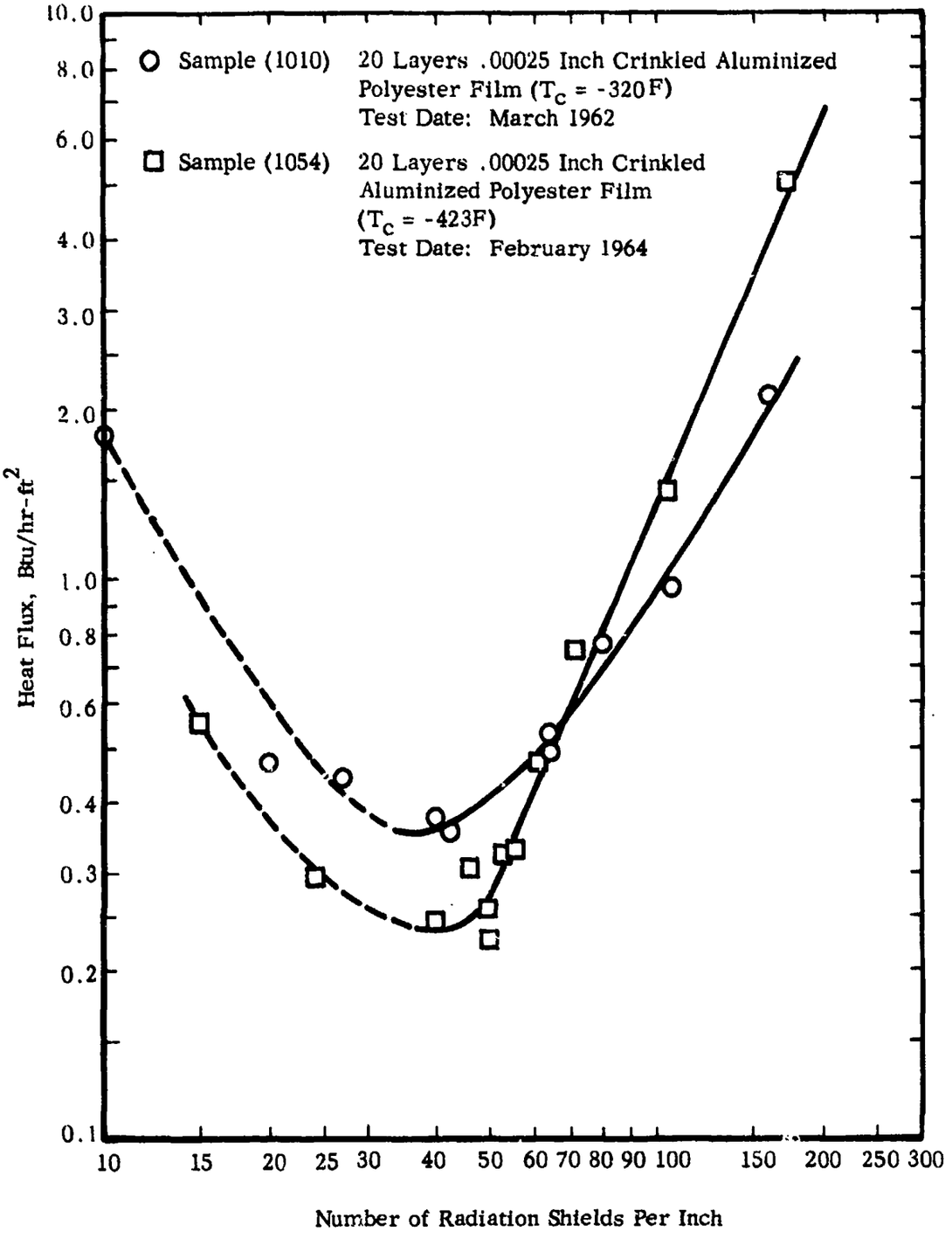

FIGURE II-5 EFFECT OF MATERIAL QUALITY UPON THE HEAT FLUX THROUGH A MULTILAYER INSULATION (SYSTEM I)

c. Emittance

A series of tests has been made to determine the total hemispherical emittance of various surfaces encountered in multilayer insulation systems. To perform these tests, we used the thermal-conductivity apparatus and a technique in which the warm-plate is covered with the material to be measured, and is allowed to radiate to the nearby cold-plate. The distance between these parallel surfaces may be made small in comparison with their diameters, so that the shape factor of either surface is 1. Knowing the temperatures of the two surfaces, the total hemispherical emittance of the cold-plate, and the heat input to the cold-plate, we can then determine the emittance of the covering applied to the warm-plate. For diffuse and gray surfaces (for which emittance is independent of wavelength) the net heat flux between the two surfaces is given by[2]:

$$\frac{q}{a} = \frac{\sigma(T_s^4 - T_c^4)}{\frac{1}{\epsilon_s} \quad \frac{1}{\epsilon_c} - 1} \qquad \text{(II-1)}$$

where:

q = Heat Flux, Btu/hr

σ = 0.174×10^{-8} Btu/hr-ft^2-$^oR^4$

T = Temperature, ^oR

a = Area, ft^2

ϵ_s = Emittance of Sample

ϵ_c = Emittance of Cold-Plate

The total hemispherical emittance of the cold-plate (ϵ_c), which was coated with a 0.002-to-0.005-inch layer of Black Velvet Coating 9564 (Minnesota Mining & Manufacturing Co.) had to be determined before any highly reflective surfaces could be tested. In order to establish this (ϵ_c), the warm-plate was also painted with the same black coating and a series of tests was conducted with the warm-plates and the cold-plates at several temperature levels. The emittance values were then calculated by using the data so obtained for the simultaneous solutions of a number of equations of the form of equation II-1.

Tests were then performed to determine the emittance (ϵ_s) of a sample of 0.002-inch thick 1145-H19 aluminum (Alcoa). The aluminum was bonded to the warm-plate with a small amount of vacuum grease to insure good thermal contact. For the low heat flux measured, the temperature drop across the foil-warm-plate interface was negligible, and the warm-plate temperature readings were taken as the sample temperature. For these tests, the cold-plate temperature was varied (-320°F and -423°F) while the warm-plate temperature was held constant (41 to 42°F), and the net heat flux between the two surfaces was measured.

The results of these measurements appear in Table II-9. The emittance of the black velvet coating was found to be 0.93 at about 40°F, and appeared to change linearly with temperature: 0.87 at -423°F, and 0.95 at 300°F. Figure II-6 shows the emittance of this coating plotted as a function of temperature. The emittance of the aluminum foil, which was at about 40°F, was found to be 0.02 for two tests: one test with the cold-plate at the normal boiling point of liquid nitrogen and the other test with the cold-plate at the normal boiling point of liquid hydrogen.

An error analysis was performed upon the computation; the results, given in Table II-10, show that uncertainties in the computed emittance of the warm surface fall in the 3-5% range, assuming the gray-body condition to be valid. Edwards and Nelson[3] have examined the gray-body assumption and have concluded that for $T_s^4 \gg T_c^4$, which in the case for these tests, errors due to nongrayness are negligible.

2. Number of Radiation Shields

Tests were performed on samples of multilayer insulations (Table II-1, Systems II-2, 3, 4 & 5) to determine the effect, if any, of the number of radiation shields on heat flux.

The test results are presented graphically in Figure II-7. The points shown are the optimum heat flux rates obtained for each sample, corrected to a warm-plate temperature of 41°F. The parallel solid lines give the computed heat flux through a multilayer insulation system assuming that the heat flow were due to radiation only. Emittance values of 0.3 and 0.9, respectively, were used for the warm and cold boundaries of the system, and a value of 0.36 was taken for the uncoated surface

TABLE II-9

EMITTANCES OF A BLACK SURFACE AND AN ALUMINUM SHEET

Measured Heat Flux (Btu/hr-ft^2)	Computed ϵ_s	Warm-Plate Temperature T_s (^oF)	Cold-Plate Temperature T_c (^oF)	ϵ_c	Test Material	Test Number
87.7	0.93	39	-423	0.87	3M Black Velvet Coating #9564 (1)	1055 a
0.50	0.88	-320	-423	0.87	"	1055 b
89.9	0.93	42	-320	0.88	"	1055 c
487	0.96	300(2)	-320	0.88	"	1056 a
466	0.94	297(3)	-423	0.87	"	1056 b
219	0.94	164(2)	-423	0.87	"	1056 c
2.10	0.02	42(4)	-320	0.88	1145-H19 Aluminum 0.002" Thick	1057 a
2.05	0.02	41(4)	-423	0.87	"	1057 b

(1) .002 - .005" coating on machined stainless steel substrate
(2) $\pm$ 3F
(3) $\pm$ 5F
(4) $\pm$ 1F

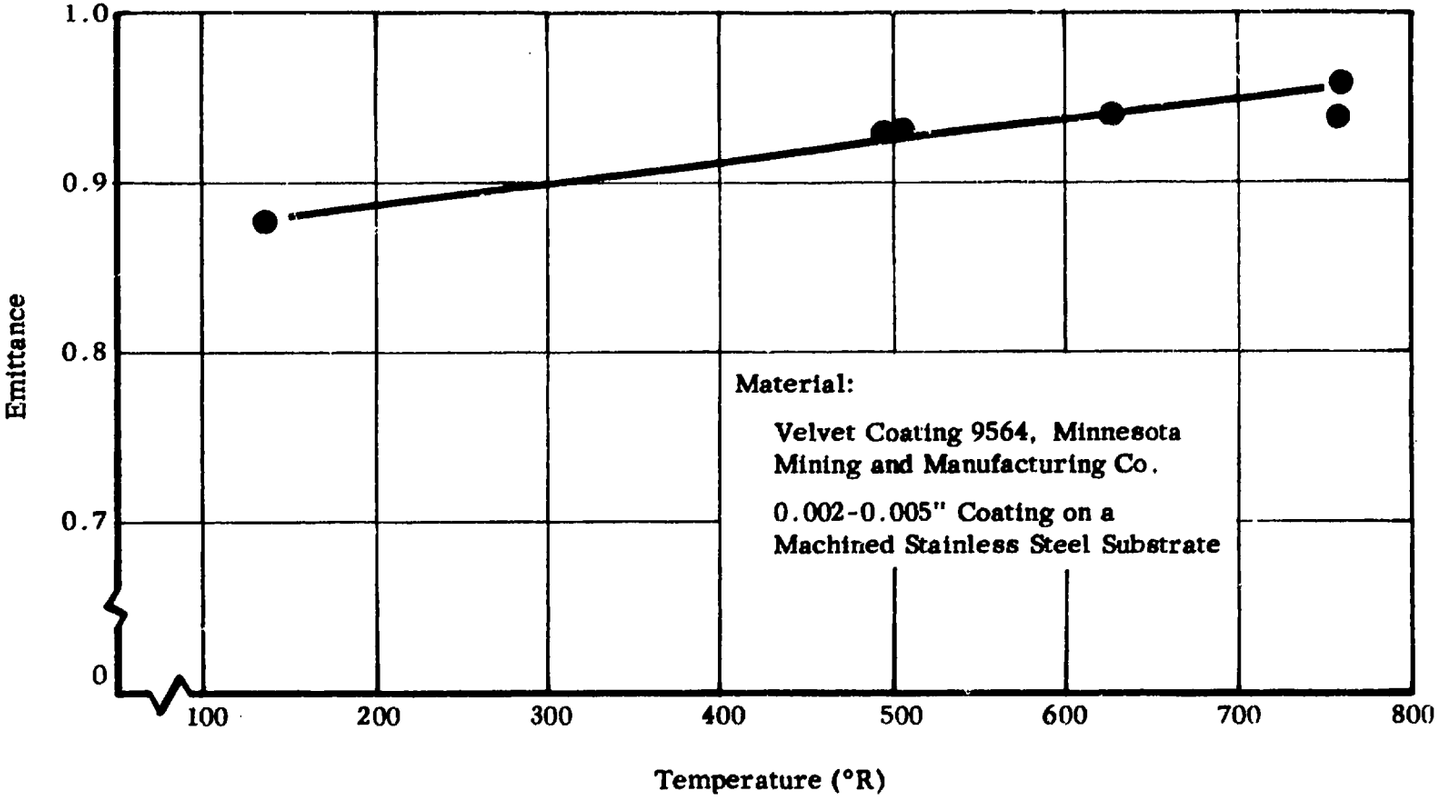

FIGURE II-6 EFFECT OF SURFACE TEMPERATURE ON THE EMITTANCE OF A BLACK COATING

TABLE II-10

UNCERTAINTIES IN THE EMITTANCE MEASUREMENTS

(1) Parameter	(2) Typical Value	(3) Uncertainty	(4) Contribution of Uncertainty of Parameter to Uncertainty of Result	(5) Value of (4) Squared
LOW ϵ SAMPLES				
A_s, measuring-vessel area	193.8 cm^2	$\pm$ 1.25 cm^2	6.45×10^{-5}	41.6×10^{-10}
q_m, measured heat flux	0.0217 watts	$\pm$ 0.00066 watts	29.0×10^{-5}	842×10^{-10}
T_s, sample temperature	211°K	$\pm$ 0.5°K	9.75×10^{-5}	95.2×10^{-10}
T_c, cold-plate temperature	77°K	$\pm$ 0.5°K	0.05×10^{-5}	----------
ϵ_s, sample emittance	0.01	--------	----------	----------
ϵ_c, cold-plate emittance	1.00	$\pm$ .03	0.03×10^{-5}	----------
			Total = 978.8×10^{-10}	
			$\sqrt{\text{Total}} = 31.2 \times 10^{-5}$	
			Error = $\frac{0.000312}{0.01} = 3.1\%$	
HIGH ϵ SAMPLES				
A_s, measuring-vessel area	193.8 cm^2	$\pm$ 1.25 cm^2	625×10^{-5}	0.4×10^{-4}
q_m, measured heat flux	6.15 watts	$\pm$ 0.18 watts	$2{,}830 \times 10^{-5}$	8.0×10^{-4}
T_s, sample temperature	279°K	$\pm$ 0.5°K	750×10^{-5}	$.56 \times 10^{-4}$
T_c, cold-plate temperature	20°K	$\pm$ 0.5°K	0.3×10^{-5}	----------
ϵ_s, sample emittance	0.97	--------	----------	----------
ϵ_c, cold-plate emittance	0.90	$\pm$ .03	$2{,}820 \times 10^{-5}$	7.95×10^{-4}
			Total = 16.91×10^{-4}	
			$\sqrt{\text{Total}} = 4.1 \times 10^{-2}$	
			Error = $\frac{.041}{.97} = 4.2\%$	

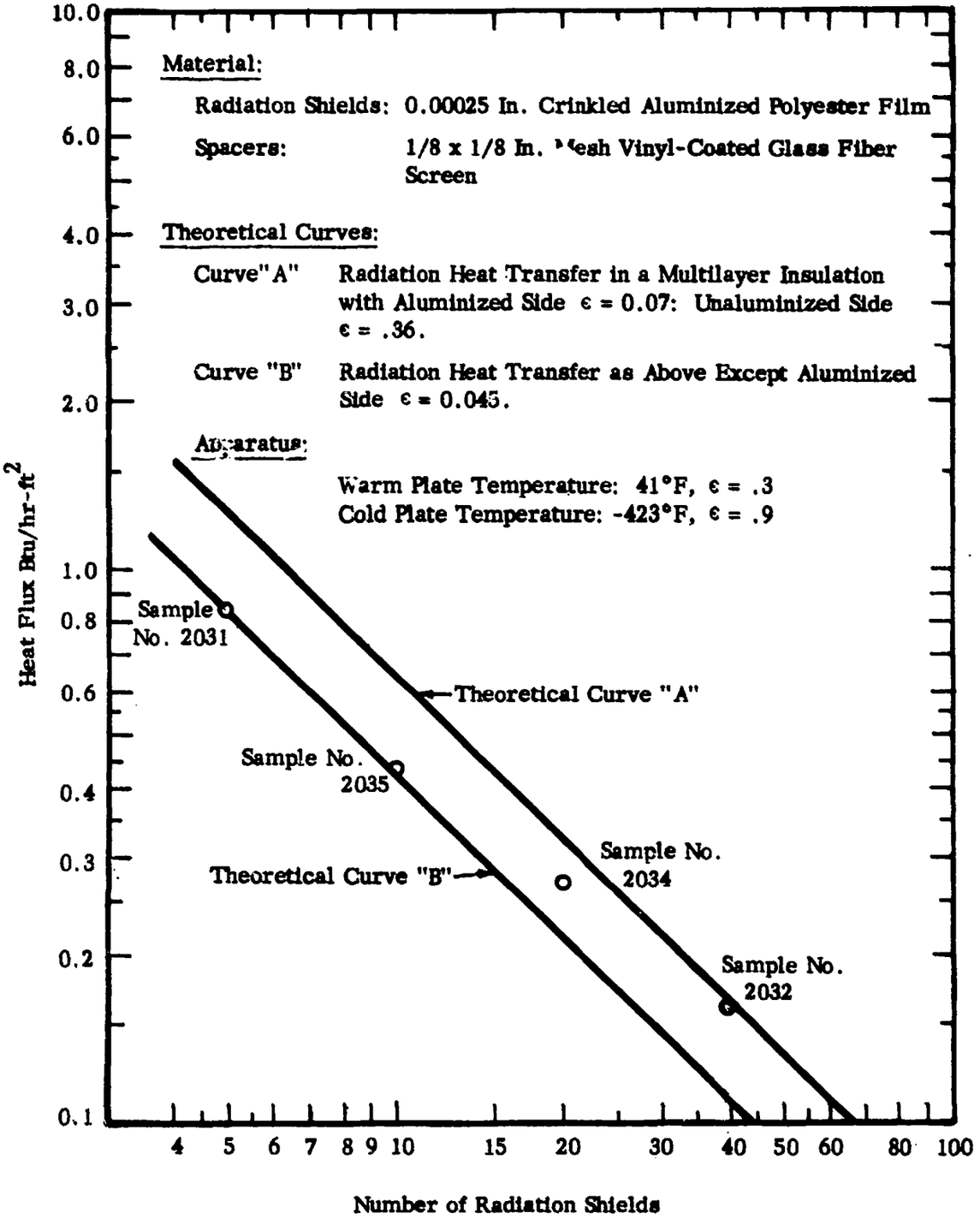

FIGURE II-7 EFFECT OF NUMBER OF RADIATION SHIELDS ON NET HEAT FLUX

of the polyester film. For curve A, an emittance value of 0.07 was taken for the aluminized surface of the polyester film; curve B was computed with an emittance value of 0.045. The heat flow rate was determined by equating the heat flux between the shields, and solving a series of equations of the form of equation II-1.

The thermal radiation data of the radiation shields were determined in tests performed in another phase of this program. See section E-1-c of this report for details of these measurements.

The rising trend of the data points with increased numbers of radiation shields, as compared with the theoretical curve for radiation heat transfer, suggests an increasing solid conduction component for the thicker samples. This could be partly due to the compression of the lower layers of the sample by the weight of the overlying material, which is appreciable for the thicker samples. A possible increase in emittance of the radiation shields at higher temperatures, resulting in a less efficient use of additional shields, may also partially account for the rising trend.

3. Mechanical Loading

Because of the adverse effect compressive loads have on multilayer insulations, we continued our investigation of various multilayer insulation systems which showed the potential to withstand mechanical compression without excessive deterioration of their thermal properties. In these tests the samples were compressed between the two rigid flat plates of the test apparatus.

We tested samples of eight insulation systems, consisting of combinations of aluminum or aluminized polyester film radiation shields with cloth, netting, mat, or foam spacers. The test samples are described in Table II-1, Systems X through XVII inclusive; the test results are provided in Tables II-11 through II-17 and Figures II-8 and II-9. Figure II-8 contains a plot of heat flux vs. mechanical load for these eight insulation systems; the data are presented as follows:

a. The points at zero mechanical load were determined by optimizing the density (see Figure II-9):
b. The darkened points are the results of tests made at incrementally increasing mechanical loads; and
c. The light points are the results of tests made at incrementally decreasing mechanical loads.

TABLE II-11

EFFECT OF MECHANICAL LOADS ON THE HEAT FLUX THROUGH A MULTILAYER INSULATION (SYSTEM XIII)

Sample Description: Ten radiation shields of 1145-H19 aluminum, 0.002-inch thick, and eleven spacers of CTL-449 material.

Cold-Plate Temperature: -423°F

Cold-Plate Emittance: 0.9

Warm-Plate Emittance: 0.3

Mechanical Load psi	(ρ) Sample Density lbs/ft^3	Heat Flux $\frac{Btu}{hr\text{-}ft^2}$	(K) Thermal Conductivity $Btu\text{-}in/hr\text{-}ft^2\text{-}F$	(K · ρ) Product $\frac{Btu\text{-}in}{hr\text{-}ft^2\text{-}F} \times \frac{lbs}{ft^3}$	Sample Thickness inches	Radiation Shields per Inch	Warm-Plate Temp. °F	Test Date	Test Number
*	9.25	0.116	.00014	.00133	.582	17	47	4-18-64	1058 a
*	10.8	0.145	.00015	.00166	.496	20	45	4-23-64	1058 b
*	11.9	0.125	.00012	.00144	.450	22	46	4-24-64	1058 c
*	12.8	0.156	.000139	.00178	.420	24	50	5-6-64	1058 d
*	14.5	0.292	.000228	.00331	.370	27	50	5-7-64	1058 e
*	16.9	0.876	.00059	.0100	.319	30	50	5-8-64	1058 f
5.8	28.4	15.6	.00625	.177	.190	53	51	5-11-64	1058 g
10	29.9	18.2	.00693	.207	.180	55	50	5-12-64	1058 h
15	32.2	22.2	.00795	.254	.167	60	50	5-12-64	1058 i
5.8	28.5	15.6	.00617	.177	.188	53	50	5-13-64	1058 j
*	16.9	0.520	.000348	.00589	.318	31	52	5-14-64	1058 k
*	14.5	0.160	.000125	.00181	.372	27	52	5-15-64	1058 l

*Load small and below the sensitivity of the measuring apparatus

TABLE II-12

EFFECT OF MECHANICAL LOADS ON THE HEAT FLUX THROUGH A MULTILAYER INSULATION (SYSTEM XVI)

Sample Description: Ten radiation shields of 0.00025-inch thick mylar double aluminum coated on both sides and eleven spacers of 2.0 lb/ft^3 Freon blown polyurethane foam 0.02 inches thick. The spacers were formed by placing two semicircles together and cementing them only near the outer edge.

Sample-Chamber Pressure: less than 5×10^{-5} torr
Cold-Plate Temperature: -423°F
Cold-Plate Emittance: 0.9
Warm-Plate Temperature: 68 ± 1F
Warm-Plate Emittance: 0.8

Mechanical Load on Sample, psi	Sample Density, lbs/ft^3	Heat Flux, $\frac{Btu}{hr\text{-}ft^2}$	Thermal Conductivity, $\frac{Btu\text{-}in}{hr\text{-}ft^2\text{-}F}$	Product of Thermal Conductivity & Density, $\frac{Btu\text{-}in}{hr\text{-}ft^2\text{-}F} \times \frac{lbs}{ft^3}$	Sample Thickness, inches	Number of Radiation Shields per Inch	Test Date	Test Number
*	1.19	0.12	0.00017	0.00020	0.685	14.6	8-13-64	1064 a
*	1.63	0.18	0.00018	0.00030	0.500	20.0	8-14-64	1064 b
*	2.12	1.7	0.0013	0.0028	0.385	26.0	8-18-64	1064 c
5	2.30	5.8	0.0042	0.0096	0.355	28.2	8-19-64	1064 d
10	2.40	10.0	0.0069	0.017	0.340	29.4	8-20-64	1064 e
15	2.52	15.4	0.010	0.026	0.324	30.9	8-24-64	1064 f
10	2.47	12.7	0.0086	0.021	0.330	30.3	8-25-64	1064 g
5	2.41	9.4	0.0065	0.016	0.339	29.5	8-26-64	1064 h
*	2.10	1.1	0.00089	0.0019	0.387	25.0	8-27-64	1064 i
*	1.63	0.16	0.00017	0.00027	0.501	20.0	8-28-64	1064 j

*Load small and below the sensitivity of the measuring device

TABLE II-13

EFFECT OF MECHANICAL LOADS ON THE HEAT FLUX THROUGH A MULTILAYER INSULATION (SYSTEM XVII)

Sample Description: Ten radiation shields of 0.00025-inch thick mylar, double aluminum coated on both sides and eleven spacers of 2.0 lb/ft^3 Freon blown polyurethane foam 0.02-inch thick. Slots were cut in the spacers and arranged as shown in the Final Report of the previous contract to produce 11% support area.(1)

Sample-Chamber Pressure: less than 5×10^{-5} torr

Warm-Plate Temperature: $69 \pm 2F$

Cold-Plate Temperature: $-423^{\circ}F$

Warm-Plate Emissivity: 0.3

Cold-Plate Emissivity: 0.9

Mechanical Load on Sample (psi)	Sample Density $\frac{lbs}{ft^3}$	Heat Flux $\frac{Btu}{hr\text{-}ft^2}$	Thermal Conductivity $\frac{Btu\text{-}in}{hr\text{-}ft^2\text{-}F}$	Thermal Conductivity x Density $\frac{Btu\text{-}in}{hr\text{-}ft^2\text{-}F} \times \frac{lbs}{ft^3}$	Sample Thickness inch	Number of Radiation Shields per inch	Test Date	Test Number
*	0.61	0.11	0.00015	0.00009	0.675	14.8	9-3-64	1065 a
*	0.83	0.082	0.00008	0.00007	0.501	20.0	9-4-64	1065 b
*	1.09	0.21	0.00016	0.00018	0.381	26.3	9-9-64	1065 c
*	1.14	0.40	0.00029	0.00033	0.361	27.7	9-10-64	1065 d
8.3	1.20	0.65	0.00046	0.00055	0.345	29.0	9-11-64	1065 e
16.7	1.32	1.7	0.0011	0.0014	0.312	32.1	9-14-64	1065 f
25	1.55	3.4	0.0018	0.0028	0.266	37.6	9-16-64	1065 g
16.7	1.49	2.9	0.0016	0.0024	0.277	36.1	9-17-64	1065 h
8.3	1.42	2.2	0.0013	0.0018	0.291	34.4	9-18-64	1065 i
*	1.14	0.22	0.00017	0.00019	0.362	27.6	9-21-64	1065 j
*	0.83	0.11	0.00011	0.00009	0.501	20.0	9-22-64	1065 k
*	0.96	0.10	0.00009	0.00008	0.431	23.2	9-23-64	1065 l

*Load small and below the sensitivity of the measuring apparatus

TABLE II-14

EFFECT OF MECHANICAL LOADS ON THE HEAT FLUX THROUGH A MULTILAYER INSULATION (SYSTEM XII)

Sample Description: Ten radiation shields of 1145-H19 aluminum, 0.002-inch thick, and eleven spacers of a matted fibrous material designated CTL-449. Slots were cut in the spacers and arranged as shown in the previous contract to produce 11% support area.(1)

Sample-Chamber Pressure: Less than 5×10^{-6} torr

Warm-Plate Temperature: 65 ± 2F

Warm-Plate Emittance: 0.3

Cold-Plate Temperature: -423° F

Cold-Plate Emittance: 0.9

Mechanical Load on Sample	Sample Density	Heat Flux	Thermal Conductivity	Product of Thermal Conductivity & Density	Sample Thickness	Radiation Shields per inch	Test Date	Test Number
psi	$\frac{lbs}{ft^3}$	$\frac{Btu}{hr\text{-}ft^2}$	$\frac{Btu\text{-}in.}{hr\text{-}ft^2\text{-}F}$	$\frac{Btu\text{-}in.}{hr\text{-}ft^2\text{-}F} \times \frac{lbs}{ft^3}$	inches			
*	9.6	0.08	0.000072	0.00069	0.437	22.9	6-30-64	2038 a
*	11.6	0.10	0.000074	0.00086	0.360	27.8	7-1-64	2038 b
*	13.9	0.43	0.00027	0.0037	0.300	33.3	7-2-64	2038 c
8.3	23.2	4.2	0.0016	0.036	0.180	55.6	7-6-64	2038 d
25	26.0	6.5	0.0021	0.056	0.161	62.2	7-7-64	2038 e
8.3	24.4	5.1	0.0018	0.044	0.171	58.5	7-8-64	2038 f
*	13.9	0.4	0.00025	0.0034	0.300	33.3	7-9-64	2038 g
*	11.4	0.1	0.000080	0.00091	0.365	28.2	7-10-64	2038 h

* Load small and below the sensitivity of the measuring apparatus

TABLE II-15

EFFECT OF MECHANICAL LOADS ON THE HEAT FLUX THROUGH A MULTILAYER INSULATION (SYSTEM XV)

Sample Description: Ten radiation shields of 0.00025-inch thick mylar, double aluminum coated on both sides and eleven spacers of nylon netting 0.007-inch thick. (Insulation System No. 6 of the Insulated Tank Program)
Sample-Chamber Pressure: less than 4×10^{-6} torr
Warm-Plate Temperature: 66 + 2F
Warm-Plate Emittance: 0.3
Cold-Plate Temperature: -423°F
Cold-Plate Emittance: 0.3

Mechanical Load on Sample psi	Sample Density $\frac{lbs}{ft^3}$	Heat Flux $\frac{Btu\text{-}in}{hr\text{-}ft^2}$	Thermal Conductivity $\frac{Btu\text{-}in}{hr\text{-}ft^2\text{-}F}$	Product of Thermal Conductivity & Density $\frac{Btu\text{-}in}{hr\text{-}ft^2\text{-}F} \times \frac{lbs}{ft^3}$	Sample Thickness inches	Number of Radiation Shields per inch	Test Date	Test Number
*	1.45	0.23	0.00019	0.00027	0.395	25.3	7-15-64	2039 a
*	1.94	0.17	0.00010	0.00019	0.295	33.9	7-16-64	2039 b
*	2.43	0.15	0.00007	0.00017	0.235	42.6	7-17-64	2039 c
*	2.93	0.14	0.000056	0.00016	0.195	51.4	7-21-64	2039 d
*	3.46	0.18	0.00006	0.00020	0.165	60.6	7-22-64	2039 e
*	4.11	0.35	0.000098	0.00039	0.139	72.0	7-22-64	2039 f
5	7.81	74.0	0.011	0.085	0.073	137	7-23-64	2039 g
10	8.53	98.0	0.013	0.11	0.067	149	7-23-64	2039 h
15	8.79	132.0	0.018	0.15	0.065	154	7-24-64	2039 j
10	8.40	111.0	0.015	0.13	0.068	147	7-24-64	2039 k
*	3.94	0.22	0.000065	0.00026	0.145	69	7-27-64	2039 l
*	3.32	0.15	0.000053	0.00018	0.172	58.2	7-28-64	2039 m
**	7.14	50.1	0.0082	0.048	0.080	125	7-28-64	2039 n
**	6.07	14.6	0.0026	0.017	0.094	106	7-29-64	2039 o
5	7.93	82.0	0.012	0.093	0.072	139	7-29-64	2039 p

*Load small and below the sensitivity of the measuring device
**Load not measured

TABLE II-16

EFFECT OF MECHANICAL LOADS ON THE HEAT FLUX THROUGH A MULTILAYER INSULATION (SAMPLE XIV)

Sample Description: Ten radiation shields of 1145-H19 aluminum, 0.002-inch thick and eleven spacers of nylon netting 0.007-inch thick.

Sample-Chamber Pressure: less than 5×10^{-6} torr
Cold-Plate Temperature: $-423^{\circ}F$
Cold-Plate Emittance: 0.9
Warm-Plate Temperature: $69 \pm 2F$
Warm-Plate Emittance: 0.3

Mechanical Load on Sample, psi	Sample Density, $\frac{lbs}{ft^3}$	Heat Flux, $\frac{Btu}{hr\text{-}ft^2}$	Thermal Conductivity, $\frac{Btu\text{-}in}{hr\text{-}ft^2\text{-}F}$	Product of Thermal Conductivity & Density, $\frac{Btu\text{-}in.}{hr\text{-}ft^2\text{-}F} \times \frac{lbs}{ft^3}$	Sample Thickness, inches	Number of Radiation Shields per inch	Test Date	Test Number
*	3.79	0.77	0.0015	0.0058	0.988	10.1	8-5-64	2040 a
*	6.06	0.32	0.00040	0.0024	0.618	16.2	8-6-64	2040 b
*	9.25	0.13	0.00011	0.0010	0.405	24.7	8-7-64	2040 c
*	10.0	0.11	0.000082	0.00082	0.375	26.7	8-11-64	2040 d
*	12.7	0.094	0.000056	0.00071	0.295	33.9	8-12-64	2040 e
*	15.1	0.086	0.000043	0.00065	0.248	40.3	8-13-64	2040 f
*	18.7	0.19	0.000077	0.0014	0.200	50.0	8-14-64	2040 g
*	25.5	1.3	0.00040	0.010	0.147	68.0	8-18-64	2040 h
5	29.0	16	0.0043	0.12	0.129	77.5	8-19-64	2040 i
9	31.0	31	0.0076	0.24	0.121	82.6	8-20-64	2040 j
13	32.2	41	0.0097	0.31	0.116	86.2	8-21-64	2040 k
15	35.0	75	0.016	0.57	0.107	93.5	8-24-64	2040 l
9	32.2	44	0.010	0.33	0.116	86.2	8-25-64	2040 m
5	32.0	34	0.0081	0.26	0.117	85.5	8-26-64	2040 n
*	25.5	0.74	0.00022	0.0060	0.147	68.0	8-27-64	2040 o
*	18.1	0.12	0.00051	0.00093	0.207	48.3	8-28-64	2040 p
*	14.7	0.11	0.000059	0.00086	0.255	39.2	8-31-64	2040 q

*Load small and below the sensitivity of the measuring device.

TABLE II-17

EFFECT OF SMALL MECHANICAL LOADS ON THE HEAT FLUX THROUGH A MULTILAYER INSULATION (SYSTEM XIV)

Sample Description: Ten radiation shields of 1145-H19 aluminum alloy, 0.002-inch thick and eleven spacers of nylon netting 0.007-inch thick.

Sample-Chamber Pressure: less than 5×10^{-5} torr

Cold-Plate Temperature: $-320^{\circ}F$

Warm-Plate Emittance: 0.3

Cold-Plate Emittance: 0.9

Mechanical Load on Sample, psi	Sample Density, $\frac{lbs}{ft^3}$	Heat Flux, $\frac{Btu}{hr\text{-}ft^2}$	Thermal Conductivity, $\frac{Btu\text{-}in}{hr\text{-}ft^2\text{-}F}$	Thermal Conductivity x Density, $\frac{Btu\text{-}in.}{hr\text{-}ft^2\text{-}F} \times \frac{lbs}{ft^3}$	Sample Thickness, inches	Warm Plate Temperature, $^{\circ}F$	Number of Radiation Shields per inch	Test Date	Test Number
0.01	22.6	0.53	0.00025	0.0056	0.166	31	60.3	10-1-64	3037 d
0.08	24.4	1.97	0.00086	0.021	0.154	32	65.0	9-29-64	3037 a
0.31	24.8	4.21	0.0017	0.042	0.151	53	66.2	9-30-64	3037 b
1.01	25.8	7.88	0.0031	0.080	0.145	45	69.0	9-30-64	3037 c
2.5	26.2	10.1	0.004	0.11	0.143	32	70.0	10-2-64	3037 e

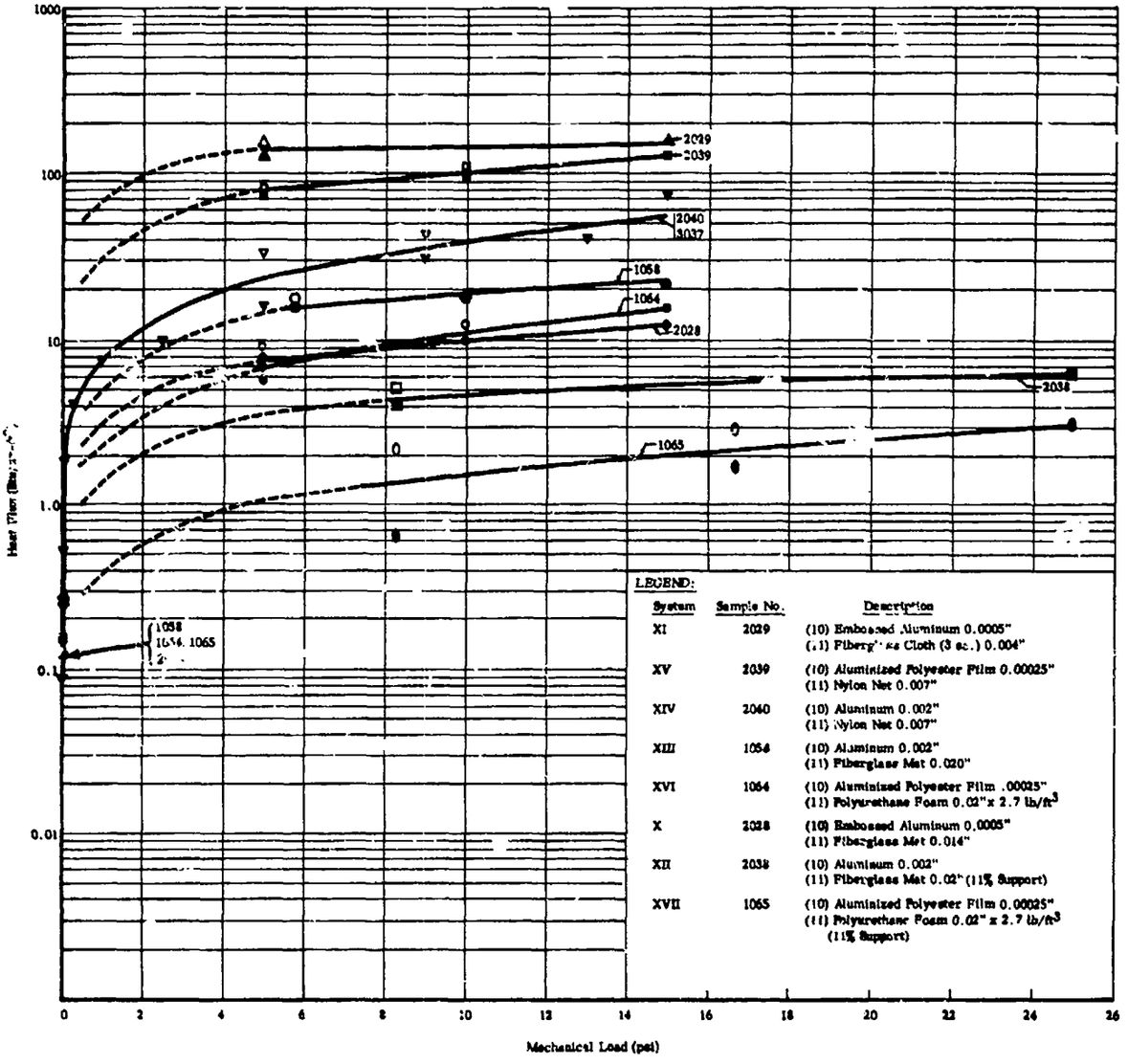

FIGURE II-8 EFFECT OF MECHANICAL LOADS ON THE HEAT FLUX THROUGH MULTILAYER INSULATIONS (SYSTEMS X TO XVII)

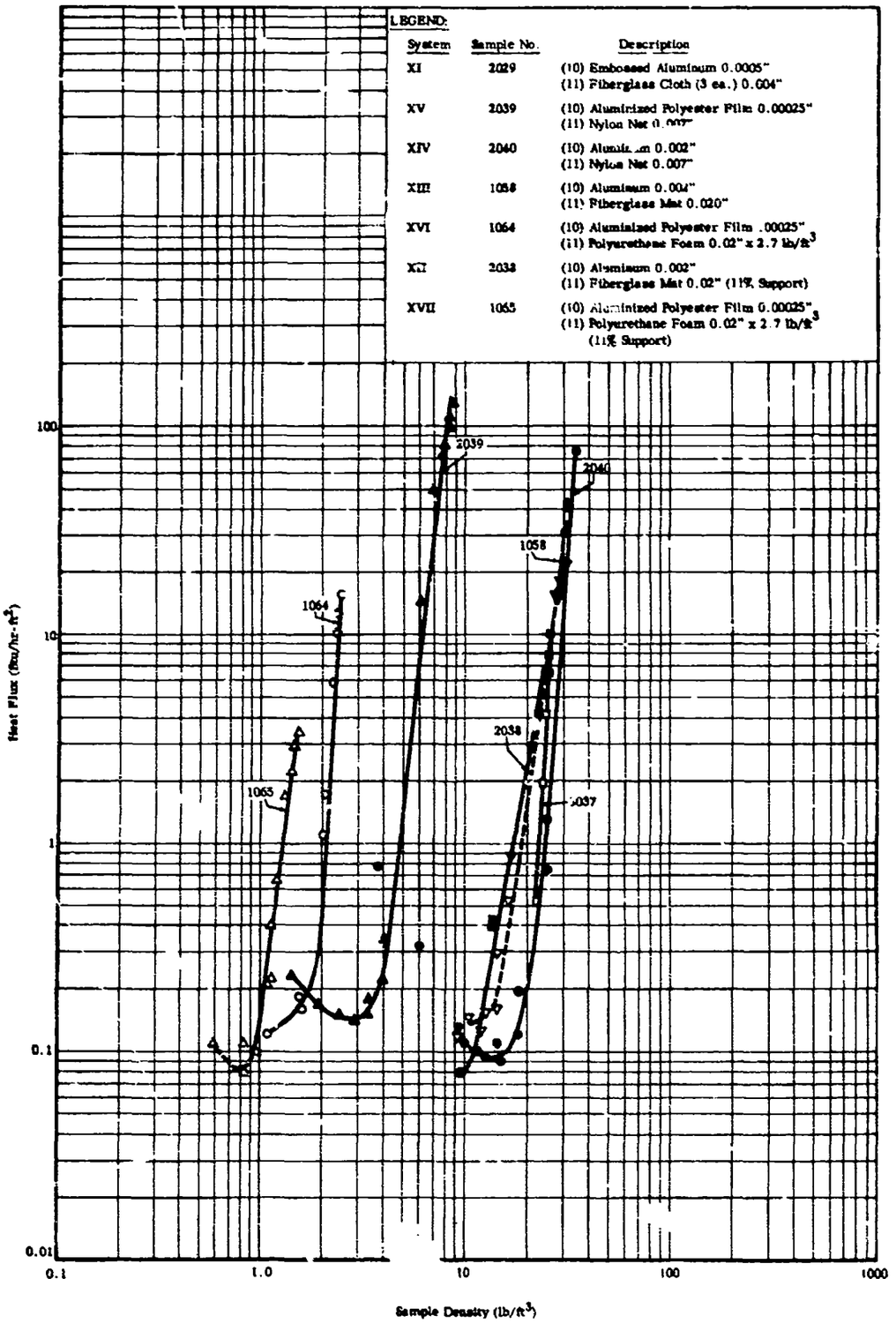

FIGURE II-9 EFFECT OF DENSITY ON THE HEAT FLUX THROUGH MULTILAYER INSULATIONS (SYSTEMS X THROUGH XV)

The curves in Figure II-8 are drawn midway between the data points obtained for increasing and decreasing loads, and except for system XIV were not continued below 1/2 psi. The results for zero load are given. The curve for system XIV is drawn through data obtained from two different samples and at two different cold-plate temperatures. The data below 2 psi, except at zero load, were obtained using one sample (number 3037) with liquid nitrogen in the cold-plate while the points at zero load and above 2 psi were obtained using another sample (number 2040) with liquid hydrogen in the cold-plate. Figure II-10 summarizes the data on system XIV. The slope of the line drawn through the data points indicates that the heat flux is proportional to the 2/3 power of the applied load.

In Figure II-8, a comparison of the curves for system X and system XI indicates that the spacer material largely determines the thermal performance of a multilayer insulation under mechanical loading. These samples contain the same radiation shield material but different spacers, resulting in heat fluxes that differ by an order of magnitude at the loads measured. For example, the insulation system containing fiberglas mat spacers (sample number 2028) appears to be one of the better load-bearing insulations that we have tested, while the system containing fiberglas cloth spacers (sample number 2029) appears to be one of the worst. Both systems contained the same embossed aluminum radiation shields.

Figure II-8 indicates that under load the thermal performance of cloth and netting spacer materials is inferior to matted and foamed spacer materials. Additional improvements may be produced by slotting the spacers to reduce the load-supporting area. Generalized descriptions of the spacer materials given in the order of improvement as thermal insulators are: cloth, net, mat, foam, mat 11% support, and foam 11% support.

For all of these systems, each test made at less than maximum load after the application of the maximum load resulted in a higher heat flux than the identical test made before application of the maximum load. Refer to Figure II-8. This may have resulted from deformation of

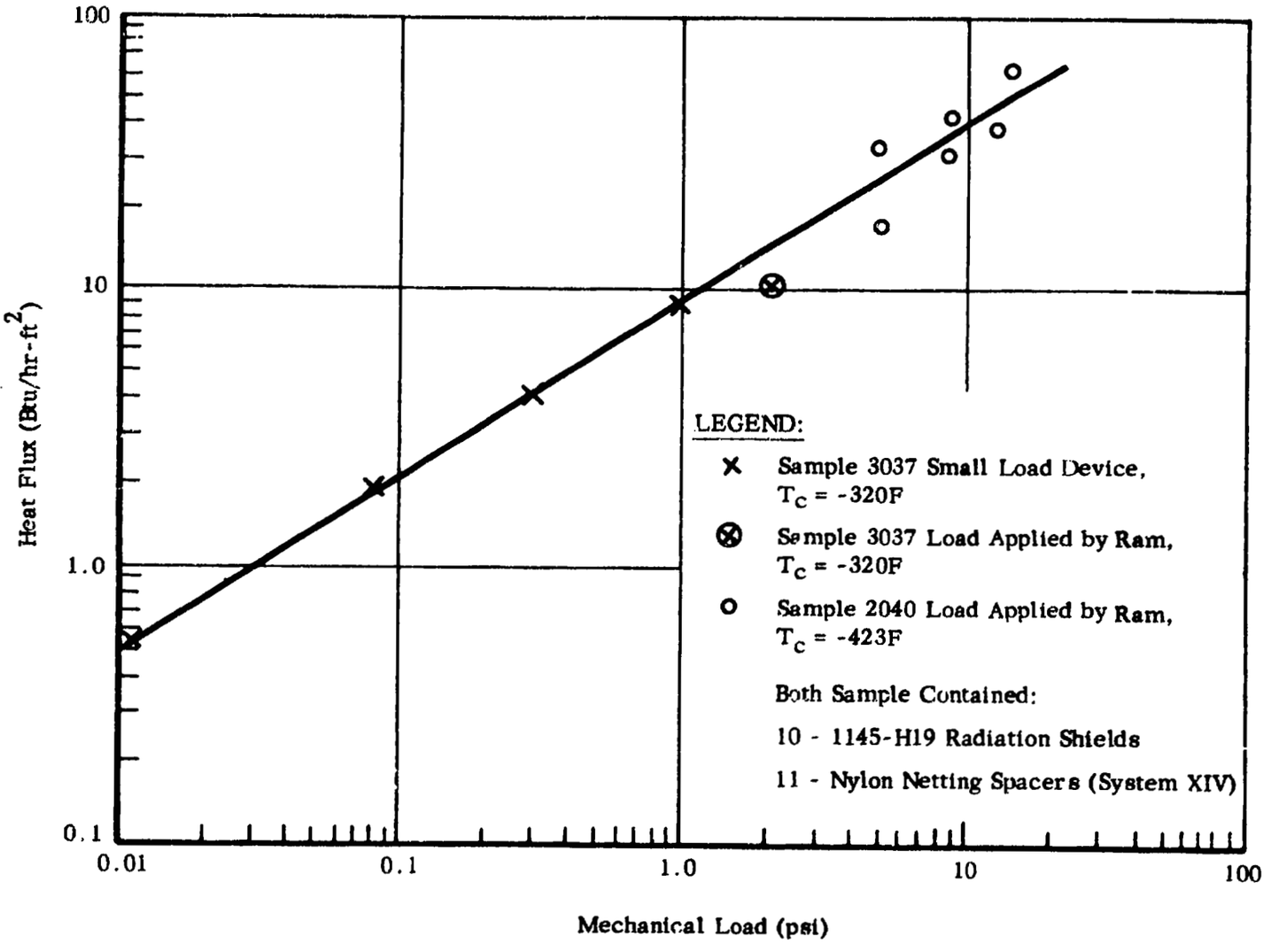

FIGURE II-10 EFFECT OF MECHANICAL LOAD ON HEAT FLUX THROUGH A MULTI-LAYER INSULATION

the insulation system by the large load and its consequent increase in density. If the system was returned to its original density, its insulation properties appeared to be slightly improved by the application of the load. Refer to Figures II-4 through II-9.

4. Purge Gas and Type of Gas

A series of tests was performed on two types of multilayer insulations to determine the qualitative effects on their thermal conductivity of various purge gases. The samples were sealed in enclosures as shown in Figure II-11 and instrumented as shown in Figure II-12. During the tests, the purging gas entered the sample-chamber through the inlet port. The sample-chamber was also filled with the purging gas and was maintained at the same pressure as the sample to prevent chamber rupture and also to minimize leakage from the sample. Purge-gas flow rates and pressures were determined with appropriate instrumentation, as shown in Figure II-12. The heat added to the system by the entering purge gas was computed to be less than 1% of the total heat flux, for all tests except test No. 3033d, and was neglected in the calculations. The heat flux measured in test No. 3033d contained about 7% additional heat that was added to the system by the condensing of the CO_2 purge gas on the cold surfaces.

The test samples were designated 3032 and 3033, each consisting of the materials of Table II-1, System VI, and sample 3034, consisting of the materials of Table II-1, System I.

The insulation samples were tested with liquid nitrogen and liquid hydrogen at the cold side; helium, nitrogen, and carbon dioxide were used for purging. The test series (initiated in Cambridge and continued in Cleveland) was interrupted because the samples were damaged during shipment and had to be repaired. After repairs were made, some tests at liquid-nitrogen temperature were repeated, with results approximately the same as those obtained earlier. One sample was evacuated and tested to determine the effect of the enclosure on the thermal performance of the insulation. In this test, the heat flux was about double that previously measured for this insulation system; such an increase could be accounted

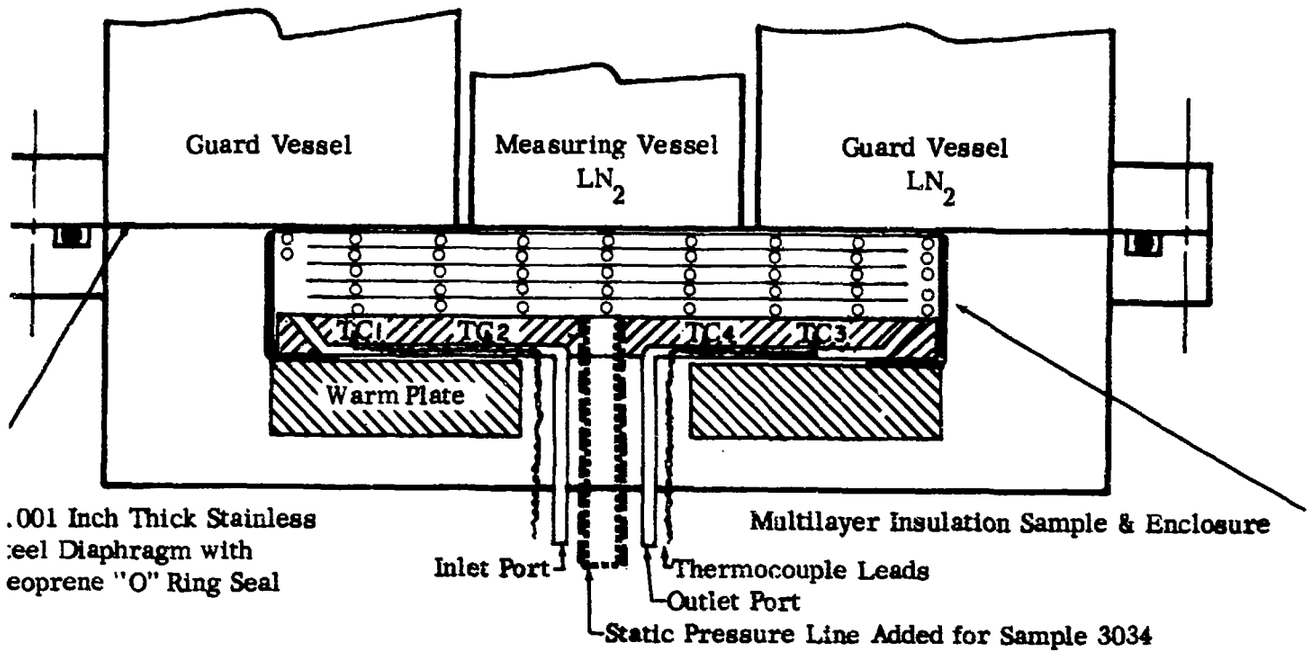

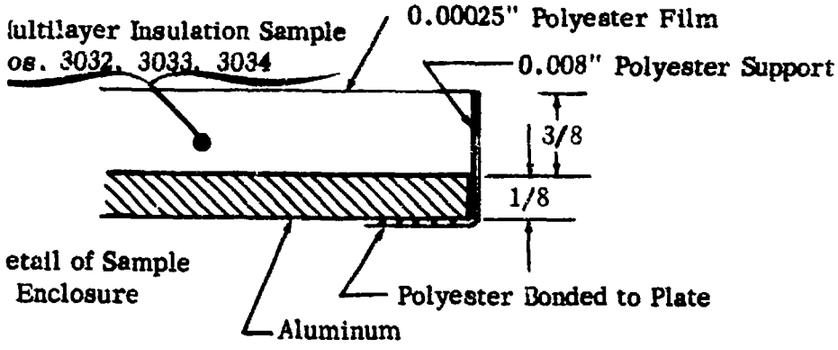

FIGURE II-11 ENCLOSURE FOR GAS PURGING SAMPLES OF MULTILAYER INSULATION SYSTEMS

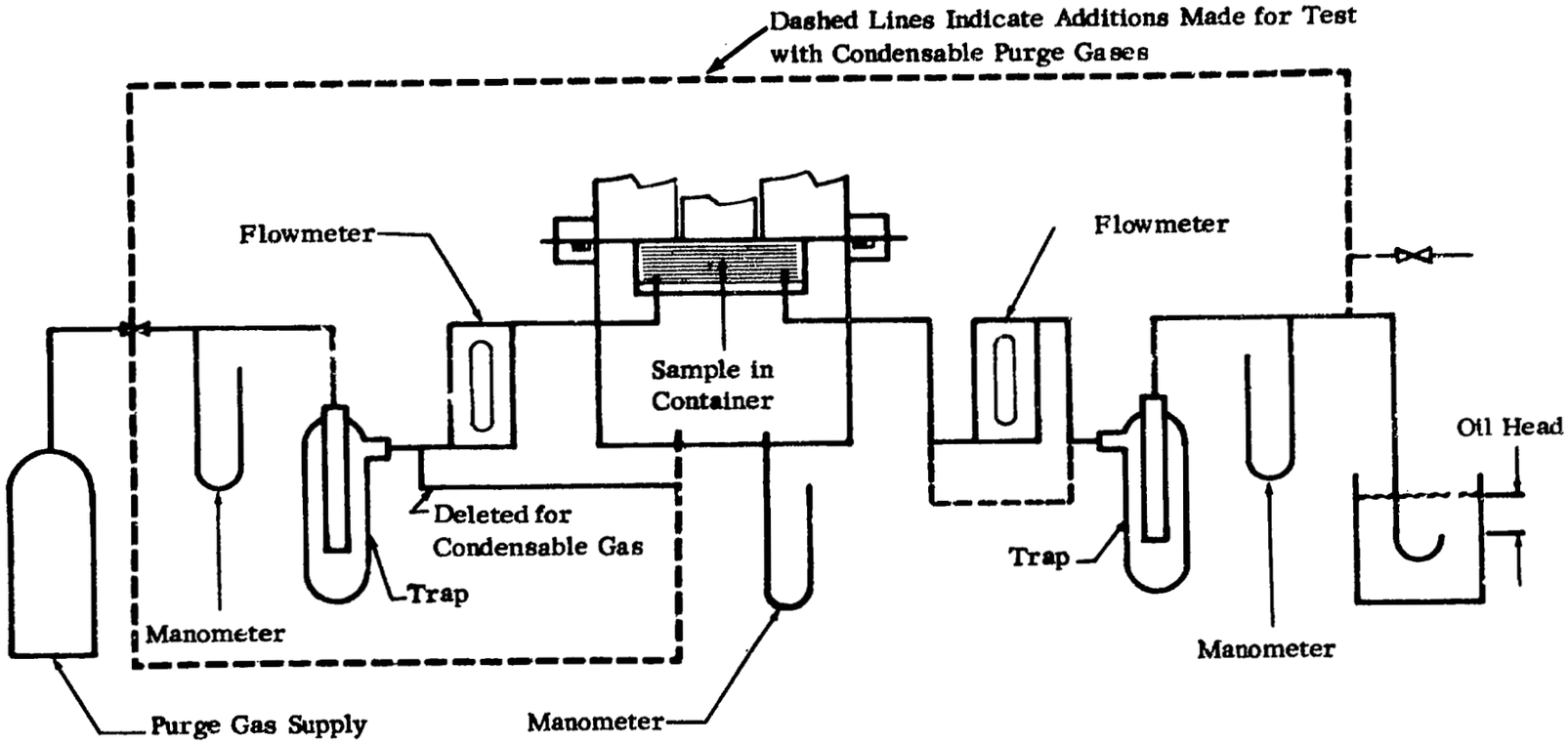

FIGURE II-12 INSTRUMENT FOR GAS PURGING SAMPLES OF MULTILAYER INSULATIONS

for by the higher pressure of the residual gas in the sample rather than by a thermally degrading effect of the enclosure.

The arrangements of the instrumentation for the tests with condensible gases was revised to allow the purge gas to enter both ports while the gas was condensing. The exhaust port was to be opened to let the purge gas through the system when condensing had subsided and the maximum amount of frost had formed within the system. However, cryopumping continued throughout the test, indicating that the formation of frost was not complete when the supply of the cryogen in the dewars was depleted. The heat flux through the purge systems was steady throughout the tests, and was apparently independent of the transient conditions within the enclosure. The results of purging with condensible gases are difficult to evaluate, because the extent of condensation in the multilayer is not easily ascertained.

For helium, nitrogen, and CO_2 purge gases, it is instructive to compare the heat flux through the insulation. When nitrogen was used as the purge gas with a cold-plate at liquid-hydrogen temperature, the heat flux was nearly eight times higher than when CO_2 was used with a cold-plate at liquid-nitrogen temperature. When helium was the purge gas, the heat flux was 4-1/2 times that of the CO_2. This would indicate that when CO_2 forms a low-density snow a lower heat flux is obtained through the insulation than when helium or condensing nitrogen is used as a purge gas. Further tests will be required to establish the thermal properties of condensing CO_2 and the time required for the purged insulation system to regain the desired low thermal conductivity after it has been exposed to a low-pressure environment (to which the CO_2 escapes).

Tables II-18 and II-19 show the results of these tests, from which the following conclusions can be drawn:

a. In every case, the thermal conductivity of the purged multilayer insulation sample was at least three orders of magnitude higher than for an evacuated sample.

b. There is a correlation between the thermal conductivity of a noncondensible purge gas and the resultant thermal conductivity of the purged sample: the

TABLE II-18

EFFECT OF PURGE GAS ON THE HEAT FLUX THROUGH A MULTILAYER INSULATION (SYSTEM VI)

Sample Description: Ten radiation shields of 1145-H19 aluminum, 0.002-inch thick, and eleven spacers of vinyl-coated glass fiber screen, 1/8 x 1/8 inch mesh and 0.020-inch thick. (The sample was enclosed in a polyester film container for purging.)

Heat Flux $\frac{Btu}{hr\text{-}ft^2}$	Thermal Conductivity $\frac{Btu\text{-}in.}{hr\text{-}ft^2\text{-}F}$	Purge Gas	Purge-Gas Flow Rate $\frac{cc}{min.}$	Cold-Plate Temperature F	Warm-Plate Temperature F	Thickness in.	Sample-Chamber Gas Pressure Atm	Test Date	Test Number
432	*	He	40	-320	*	0.35	1 He	1-27-64	3032 a
417	*	He	0	-320	*	0.35	1 He	1-28-64	3032 b
555	0.457	He	40	-423	32	0.37	1 He	6-15-64	2037 d
550	0.453	He	0	-423	32	0.37	1 He	6-15-64	2037 e
133	*	N_2	40	-320	*	0.35	1 N_2	1-29-64	3032 c
133	0.134	N_2	40	-320	27	0.35	1 N_2	2-14-64	3033 a
137	0.148	N_2	40	-320	6	0.35	1 N_2	2-18-64	3033 b
995	0.847	N_2	-	-423	18	0.37	1 N_2	6-18-64	2037 f
123**	0.115	CO_2	40	-320	69	0.36	1 CO_2	2-21-64	3033 d
0.47	0.00036	Vacuum	-	-423	64	0.37	$5X10^{-4}$ torr	6-23-64	2037 g

Note: * Warm-plate temperatures for tests 3032 a, b, and c are not available.

** Contains 7.2% additional heat added by condensing purge gas.

TABLE II-19

EFFECT OF PURGE GAS ON THE HEAT FLUX THROUGH A MULTILAYER INSULATION (SYSTEM I)

Sample Description: Twenty radiation shields of crinkled polyester film, 0.00025-inch thick aluminized on one side. (The sample was enclosed in a polyester film container for purging.)

Heat Flux $\frac{Btu}{hr\text{-}ft^2}$	Thermal Conductivity $\frac{Btu\text{-}in.}{hr\text{-}ft^2\text{-}F}$	Purge Gas	Purge-Gas Flow Rate $\frac{cc}{min.}$	Cold-Plate Temperature F	Warm-Plate Temperature F	Sample Thickness in.	Sample Chamber Gas Pressure Atm	Test Date	Test Number
533	0.53	He	50	-320	31	0.35	1 He	3-6-64	3034 a
615	0.64	He	40	-320	34	0.37	1 He	5-4-64	2036 a
603	0.66	He	40	-320	17	0.37	1 He	5-7-64	2036 e
660	0.54	He	40	-423	26	0.37	1 He	5-25-64	2036 l
498	0.52	He	0	-320	31	0.37	1 He	5-8-64	2036 f
470	0.38	He	0	-423	34	0.37	1 He	5-22-64	2036 k
96	0.095	CO_2	50	-320	50	0.35	1 CO_2	3-13-64	3034 b
108	0.12	CO_2	40	-320	10	0.37	1 CO_2	5-13-64	2036 g
115	0.12	N_2	40	-320	36	0.37	1 N_2	5-15-64	2036 i
272	0.23	N_2	40	-423	24	0.37	1 N_2	5-19-64	2036 j

conductivity of a purged sample approaches the conductivity of the purging gas and is effectively independent of the performance of the evacuated insulation sample.

c. With helium as the purge gas, the heat flux through the systems was approximately the same, independent of the cold-plate temperature.

d. The tests on each sample were repeatable even though the sample had been tested on two different apparatus and damaged and repaired between tests.

5. Buffer Zone

A number of mechanical supports, piping connections, and other structural elements must necessarily penetrate through the multilayer insulation and make direct contact with the cold-tank wall. At a given temperature gradient, the heat flow into the tank through these penetrations may be greater than through the insulation system. Because of the highly unisotropic properties of multilayer insulations (thermal conductivity along an insulation using aluminum radiation shields is 10^6 greater than across the shields), imposed temperature gradients at junctions with penetrations propagate rapidly along the insulation. It is, therefore, necessary to ensure that temperature gradients normal to the tank wall are much smaller in the insulation than those existing in the penetrating elements. This is possible if the penetration is thermally decoupled from the insulation.

The methods and requirements of decoupling vary with the specific system design. It is not possible to decouple by just leaving a gap between the penetration and the multilayer insulation, because: (a) radiation from the environment can enter the gap, and (b) radiation can be transferred through the space between the edges of the shields and the penetration.

An analysis of the magnitude of the heat flow into the insulation has indicated that the insertion of a buffer zone of a width only twice its thickness can thermally decouple penetrations from insulation edges,

even in the extreme case where the buffer zone would touch the penetration. With only radiative interchange between the buffer zone and the penetration, thermal decoupling is even more complete.[1]

In order to determine the effectiveness of a buffer zone to decouple the insulation system from the thermal environment produced by penetrations, we performed the following tests. We installed a ring-shaped heater (see Figure II-13) around the edge of a sample of multilayer insulation. The temperature at that location was varied by controlling the power supplied to the heater; the heat flux into the measuring vessel was determined by measuring the boil-off rate. The test sample was constructed of materials described in Table II-1, System XIV. An annular buffer zone of 1/8 inch width was formed by extending the spacers beyond the radiation shields. The width (x) to thickness (d) ratio for this buffer zone was 0.36. We chose this ratio because it corresponded to the configuration of most of the samples used in our previous work.

The results of these tests (see Figure II-14) indicate that the temperature change from -195 to -27°F had no effect on the heat flow pattern within the multilayer insulation sample. Even the high heater temperature of +170°F resulted in only a 23% increase in heat flux into the measuring vessel. These results indicate: (a) that a buffer zone of this material and configuration is an effective method of thermally decoupling a multilayer insulation system from penetrations; and, (b) the 0.36-ratio of width to thickness, representative of most of the samples tested previously in this program, effectively reduces edge effects.

The apparent usefulness of this concept, as indicated by these tests, points to the need for more testing in order to optimize the configuration and the material used to form a buffer zone.

6. Perforations

We continued tests on the effect of perforated radiation shields on the heat flux through samples of multilayer insulation systems. Previously[1] we had found that, for a given multilayer insulation system, the heat flux increased directly with the amount of open area and inversely with the diameter of the hole. To complete our investigation, we tested

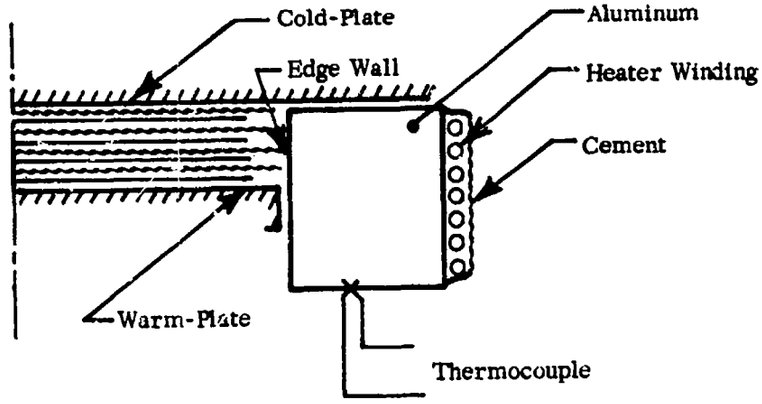

Buffer Zone Width 1/8 Inch

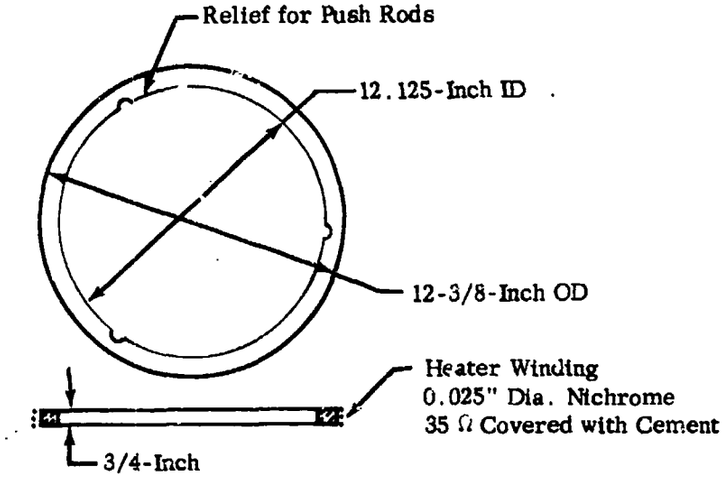

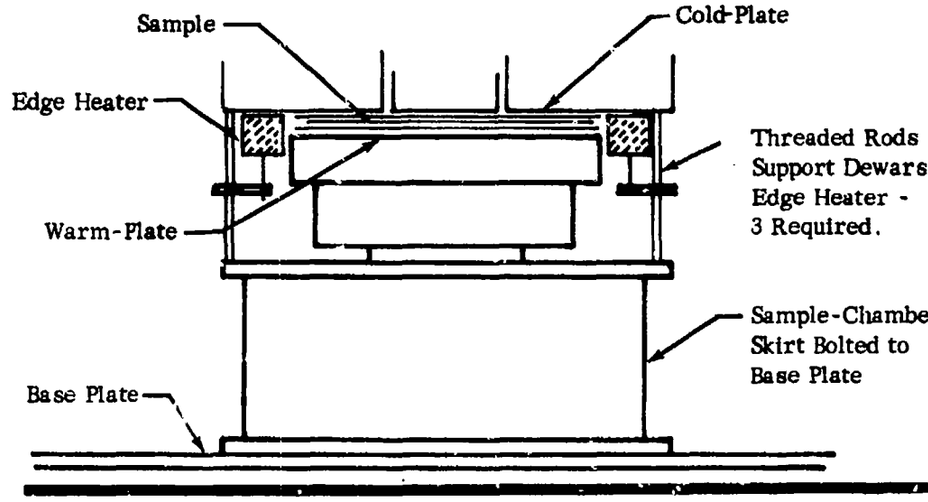

FIGURE II-13 ARRANGEMENT OF SAMPLE CHAMBER FOR TEST OF A BUFFER ZONE

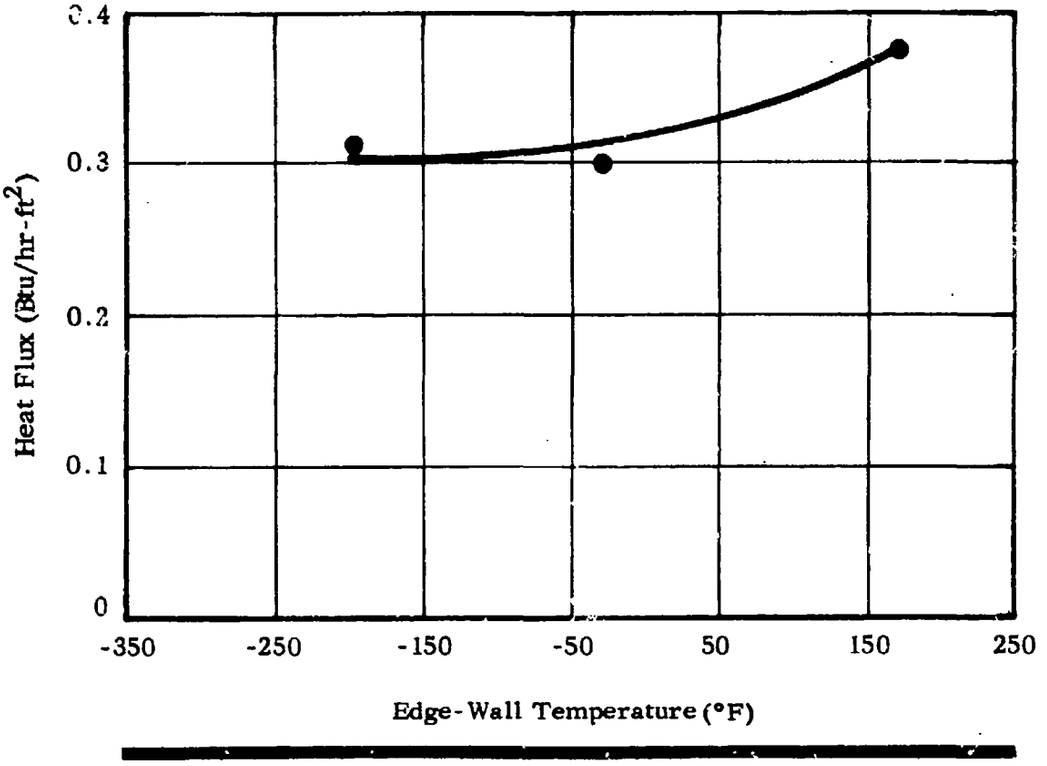

FIGURE II-14 EFFECT OF A BUFFER ZONE

multilayer insulation samples of other materials, perforated, as before, with holes of a given diameter and having different percentages of open area. We tested twenty radiation-shield samples of 0.00025-inch thick crinkled polyester film, aluminized on one side (Table II-1, System I). Each of the samples had a uniform pattern of 1/8-inch-diameter perforations, but some contained 1.23% of open area; others, 2.40%; and others, 5%. Each sample was tested at several plate separations to determine its optimum thickness; the heat flux measurements obtained for each of these thicknesses were then compared.

The results of these tests appear in Figure II-15, where heat flux is plotted as a function of amount of open area. Also shown are earlier reported data[1] for perforations of the same size in an insulation system containing 0.002-thick aluminum radiation shields. For the crinkled aluminized polyester film system, the heat flux increases directly with the amount of open area, agreeing both with theoretical predictions and with the data of the previously tested system. It appears, however, that the perforations in the samples of crinkled aluminized polyester film have a much smaller effect on the heat flux through the system than do similar perforations (i.e., the same hole size and amount of spin area) in the samples containing aluminum alloy and screening. The heat flux through the former increased by less than 20% while the heat flux through the latter increased by more than 150%. This may be a result of the more random arrangement of holes caused by crinkling of the film.

7. Insulation Tank Program Support

a. Multilayer Insulation System

A sample of an insulation system was tested in support of the Insulated Tank Program of this contract. The sample is described in Table II-1 as System VII. The results of this test, given in Table II-20, indicate an optimum spacing of about 17 radiation shields per inch; under that condition, the heat flux is approximately 0.22 Btu/hr-ft^2. This is consistent with results obtained in Test II-1-A of the Insulated

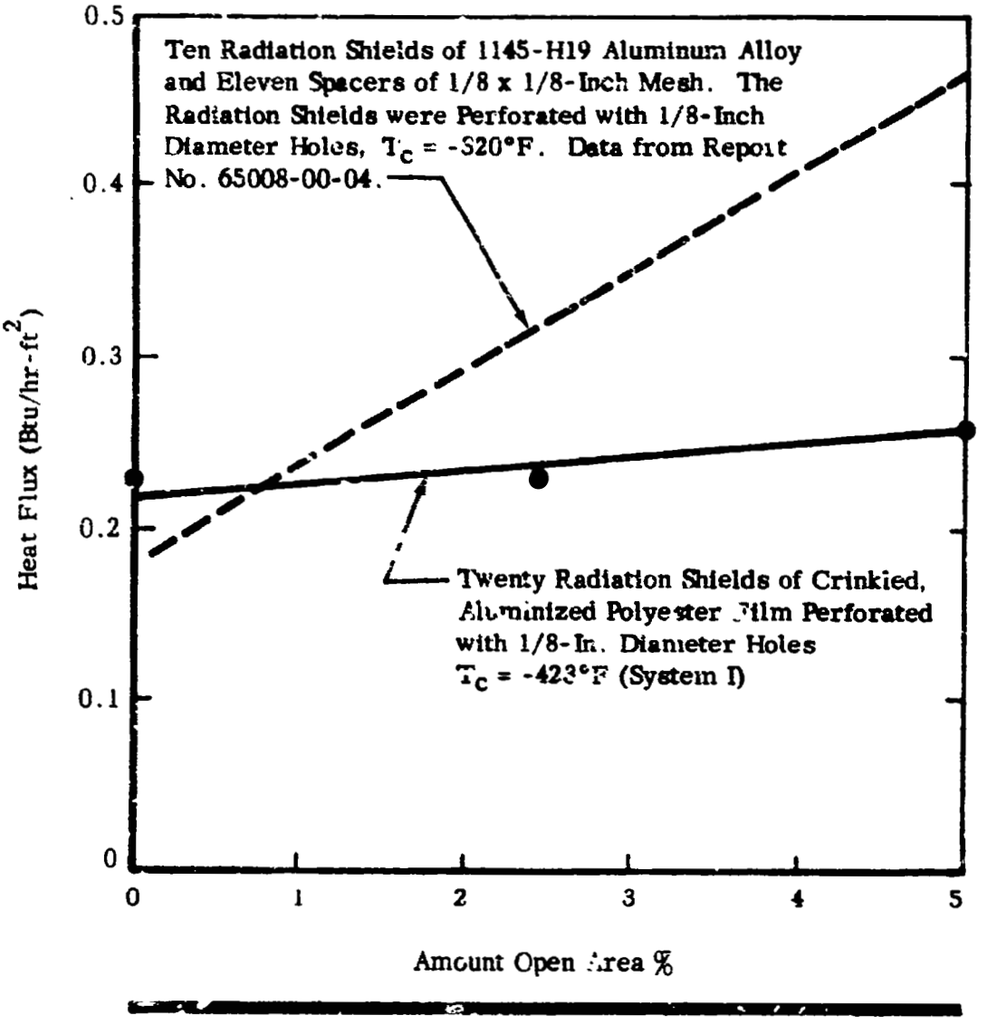

FIGURE II-15 EFFECT OF PERFORATIONS ON THE HEAT FLUX THROUGH A MULTILAYER INSULATION (SYSTEM I)

TABLE II-20

THERMAL CONDUCTIVITY OF A MULTILAYER INSULATION (SYSTEM VII)

(Tests in Support of Insulated Tank Program)

Sample Description: Five radiation shields of 1145-0 aluminum 0.002-inch thick and six spacers of 1/8 x 1/8 inch mesh vinyl-coated glass fiber screen 0.020-inch thick.

Sample-Chamber Pressure: Less than 1×10^{5} torr

Warm-Plate Emissivity: 0.3

Cold-Plate Emissivity: 0.9

Cold-Plate Temperature: -423° F

Sample Thickness in.	Number of Radiation Shields/in.	(ρ) Sample Density $\frac{lbs}{ft^3}$	Heat Flux $\frac{Btu}{hr\text{-}ft^2}$	(K) Thermal Conductivity $\frac{Btu\text{-}in.}{hr\text{-}ft^2\text{-}F}$	(K·ρ) Product $\frac{Btu\text{-}in.}{hr\text{-}ft^2\text{-}F} \times \frac{lbs}{ft^3}$	Warm-Plate Temp. F	Test Date	Test Number
0.337	14.8	8.5	0.23	0.000167	0.00142	44	2-3-64	2030 a
0.301	16.6	9.5	0.23	0.000147	0.00140	41	2-4-64	2030 b
0.265	18.9	10.7	0.19	0.000108	0.00116	42	2-5-64	2030 c
0.201	24.9	14.1	0.67	0.000288	0.00406	44	2-7-64	2030 d
0.186	26.9	15.3	1.3	0.000537	0.00822	41	2-10-64	2030 e
0.198	25.2	14.4	0.49	0.000210	0.00303	40	2-10-64	2030 f
0.194	25.8	14.7	0.66	0.000276	0.00406	40	2-11-64	2030 g
0.217	23.0	14.1	0.25	0.000118	0.00167	41	2-12-64	2030 h

Tank Program; more detail is given in the discussion of that test in Part III of this report.

b. Composite Insulation System

Tests were conducted, in support of the Insulated Tank Program, on a sample of a composite insulation system. The sample consisted of a foam and a multilayer insulation arranged as shown in Figure II-16. The foam is similar to that of test 5 performed on tank calorimeter number 1 during June and is identified as Rigid One-Shot Foam No. 1. The multilayer component of the sample consisted of five radiation shields of 0.002-inch thick 1145-H19 aluminum and 6 spacers of 0.020-inch thick vinyl-coated glass fiber screen, 1/8 x 1/8 inch mesh. In this series the foam was successively tested: (1) alone, (2) bonded to the cold-plate, and then (3) in the foam-multilayer combination. Table II-21 shows the results of these test. It also shows the results of earlier tests on a similar multilayer insulation sample. The thermal conductivity of the foam system was 0.11 Btu-in/hr-ft^2-^{o}F. The test of the composite system, however, produced inconclusive results. It is expected that the heat flux through the composite system would be less than that measured through either component taken alone. However, the results show that the heat flux through the composite system was approximately 40 times greater than the heat flux through the multilayer insulation system. This may have been a result of high gas pressure in the sample contributed by outgassing of the foam: this condition would increase the gas conduction through the multilayer insulation. We assumed that the pressure in the sample-chamber, although not measured during the test because of malfunctioning of the pressure sensor, was high because subsequent pressure measurement of the gas in the chamber containing this sample were two orders of magnitude higher than normally encountered. An increase in pressure would degrade the insulating properties of the multilayer insulation to produce the above result.

c. Foam Insulation System

Tests were conducted on a Freon-blown polyether foam insulation sample, approximately .51-inch thick and 12 inches in diameter; the faces of the sample were parallel to each other but exhibited a

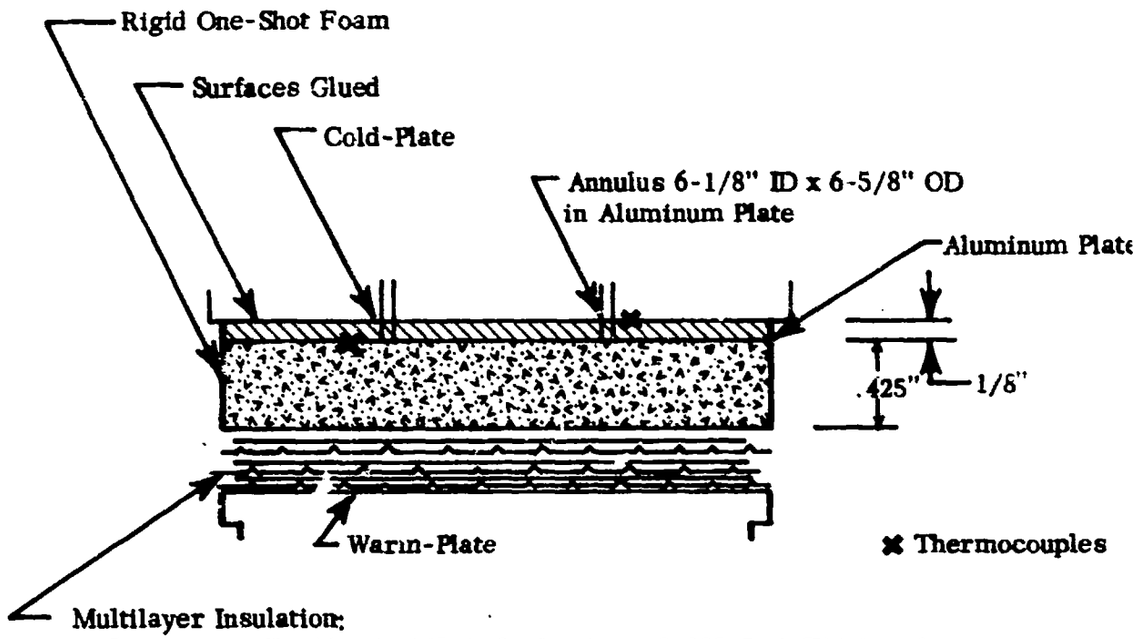

FIGURE II-16 CONFIGURATION OF A COMPOSITE SAMPLE (SYSTEM XX)

TABLE II-21

THERMAL TESTS ON A COMPOSITE INSULATION (SYSTEM XX)

Sample Description:
- Foam: Rigid One-Shot Foam No. 1
- Multilayer: Five radiation shields of 0.002-inch thick 1145-H19 aluminum and six spacers of 0.020-inch thick vinyl-coated glass screen 1/8 x 1/8 inch mesh
- Composite: Foam & Multilayer as described above combined with the foam on the cold side

Warm-Plate Temperature: 41°F for Multilayer; 65°F for others

Cold-Plate Temperature: -423°F

Sample	Heat Flux $\frac{Btu}{hr\text{-}ft^2}$	Thermal Conductivity $\frac{Btu\text{-}in.}{hr\text{-}ft^2\text{-}F}$	Sample Thickness inch	Sample-Chamber Pressure torr	Load on Sample psi	Test Date	Test Number
Foam Only	176	0.15	0.425	8×10^{-5}	15	5-29-64	1062 a
Foam Only	126	0.11	0.425	7×10^{-5}	15	6-6-64	1062 b
Foam & Gap	40	0.065	0.645	8×10^{-5}	-	6-7-64	1062 c
Multilayer	0.23	0.00015	0.301	5×10^{-6}	-	1-4-64	2030 b
Multilayer	0.19	0.00011	0.265	5×10^{-6}	-	1-5-64	2030 c
Composite	8.9	-	1.039	*	-	6-10-64	1063 a
Composite	8.2	-	0.902	*	-	6-14-64	1063 b

*Tube burned out: Subsequent pressure measurement indicated 3×10^{-4} torr in sample chamber.

slight waviness The sample was exposed to the vacuum system for more than 48 hours prior to testing The heat flux through the sample was measured under load conditions of 5, 10, 15, 20 and 25 psi. The results of these tests (see Table II-22 and Figure II-17) show that at 15, 20 and 25 psi the heat flux through the system was constant but that for smaller loads the heat flux was considerably lower. These data indicate the presence of a high contact resistance at the interfaces of the sample and the warm- and cold-plates of the apparatus; the high contact resistance decreases with loading. The measured thermal conductivity of this sample was 0.09 Btu-in/hr-ft^2-^{o}F.

8. Miscellaneous Tests

a Multilayer Insulation Sample Damaged by Meteoroid-Bumper Debris

Tests were performed on a sample (2041) of multilayer insulation that had been damaged by meteoroid-bumper debris at a hypervelocity impact range at McGill University.(1) The sample consisted of five materials described as System VII in Table II-1. The sample contained five aluminum radiation shields; two of which were perforated to a slight degree with small holes by the debris, the remaining three were not punctured. The damage to the sample is described in detail elsewhere.(4) An undamaged control sample of identical materials (sample 2042) was also tested.

The results of these tests (see Table II-23 and Figure II-18) show that there is only a small difference between the heat flux of the test sample and the control sample, indicating that the thermal properties of this insulation sample were not significantly degraded by the bumper-debris damage.

b. Tests on a Rigid Sample

Tests were performed on a sample of rigid phenolic laminate

TABLE II-22

THERMAL CONDUCTIVITY OF A FREON-BLOWN POLYETHER FOAM (SYSTEM XVIII)

Sample Description: 8 lb/ft^3 freon-blown polyether foam

Sample-Chamber Pressure: Less than 1×10^{-5} torr

Cold-Plate Temperature: -423° F

Cold-Plate Emissivity: 0.9

Warm-Plate Emissivity: 0.3

Measured Sample Density: 12.4 lb/ft^3

Mechanical Load, psi	Ram Spacing, inches	Heat Flux, $\frac{Btu}{hr\text{-}ft^2}$	Thermal Conductivity, $\frac{Btu\text{-}in.}{hr\text{-}ft^2\text{-}F}$	Warm-Plate Temperature, F	Test Date	Test Number
5	0.529	68.5	0.068	44	3-16-64	2033 a
10	0.526	74.9	0.084	47	3-16-64	2033 b
15	0.519	81.6	0.090	48	3-16-64	2033 c
20	0.515	81.1	0.089	48	3-16-64	2033 d
5	0.528	57.3	0.064	49	3-17-64	2033 e
25	0.514	83.6	0.091	49	3-17-64	2033 f

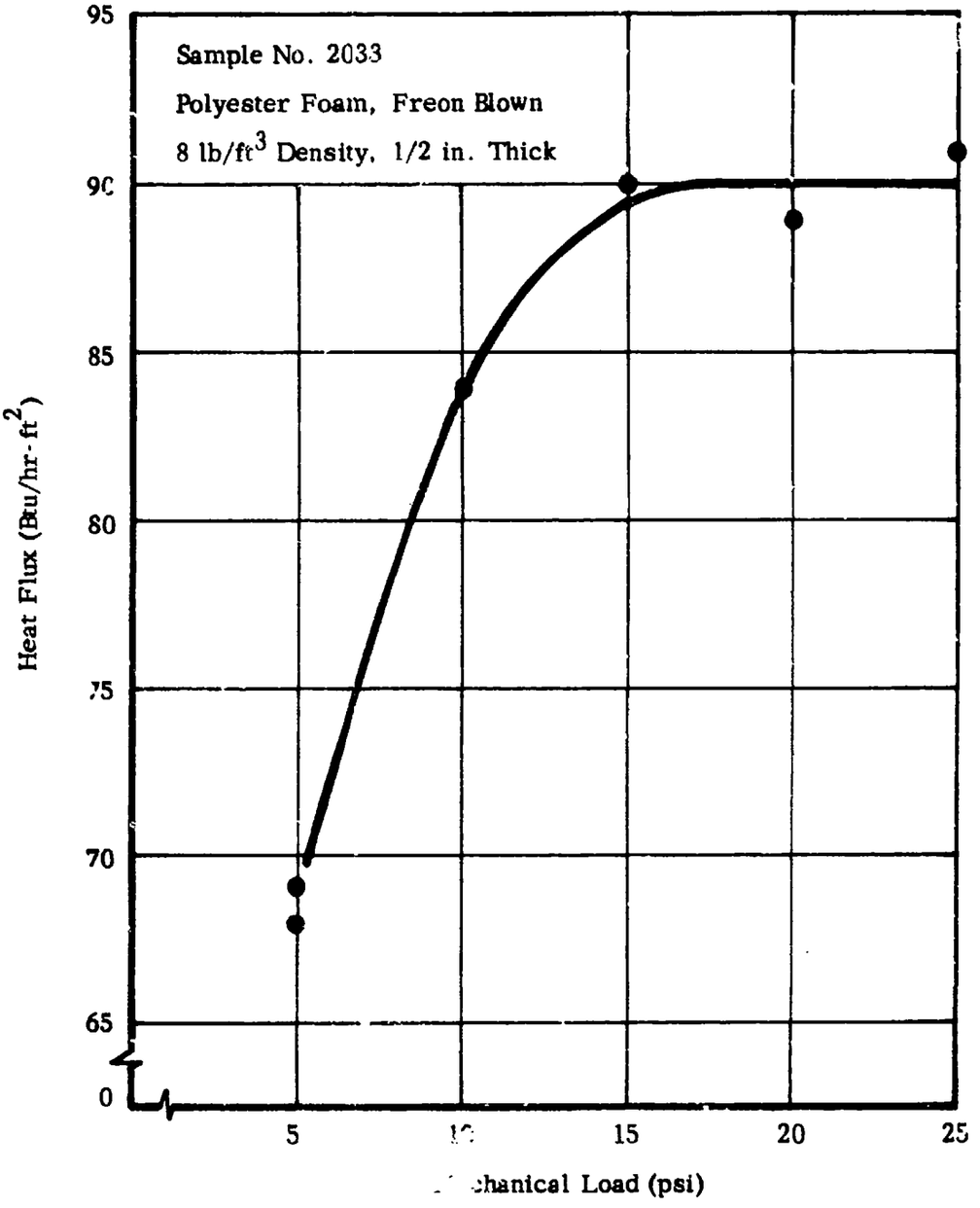

FIGURE II-17 EFFECT OF CONTACT RESISTANCE ON THE MEASURED HEAT FLUX THROUGH A FOAM INSULATION (SYSTEM XVIII)

TABLE II-23

EFFECT OF METEOROID-BUMPER DEBRIS DAMAGE ON A MULTILAYER INSULATION (SYSTEM VII)

Sample Description: Five radiation shields of 1145-0 aluminum alloy and six spacers of vinyl-coated glass fiber screen 1/8 x 1/8 inch mesh. Sample 2041 was damaged by being fired upon by hypervelocity pellets. Sample 2042 was not damaged.

Sample-Chamber Pressure: less than 7×10^{-6} torr

Warm-Plate Temperature: 68 ± 2F

Cold-Plate Temperature: -423°F

Warm-Plate Emittance: 0.3

Cold-Plate Emittance: 0.9

Sample Thickness inch	Sample Density $\frac{lbs}{ft^3}$	Heat Flux $\frac{Btu}{hr\text{-}ft^2}$	Conductivity $\frac{Btu\text{-}in.}{hr\text{-}ft^2\text{-}F}$	Thermal Conductivity x Density $\frac{Btu\text{-}in}{hr\text{-}ft^2\text{-}F} \times \frac{lbs}{ft^3}$	Number of Layers per inch	Test Date	Test Number
0.341	8.45	0.31	0.00022	0.0018	14.7	9-18-64	2041 i
0.304	9.47	0.25	0.00015	0.0014	16.5	9-22-64	2041 k
0.242	11.8	0.22	0.00011	0.0013	20.7	9-21-64	2041 j
0.216	13.3	0.24	0.00010	0.0014	23.2	9-17-64	2041 h
0.195	14.8	0.36	0.00014	0.0021	25.6	9-14-64	2041 e
0.186	15.5	0.48	0.00018	0.0028	26.9	9-16-64	2041 g
0.174	16.6	0.88	0.00031	0.0051	28.7	9-15-64	2041 f
0.303	9.5	0.18	0.00011	0.0010	16.5	9-30-64	2042 d
0.275	10.5	0.17	0.00009	0.0009	18.2	9-29-64	2042 c
0.240	12.0	0.20	0.00010	0.0012	20.8	9-28-64	2042 b
0.206	14.0	0.30	0.00013	0.0018	24.3	9-25-64	2042 a

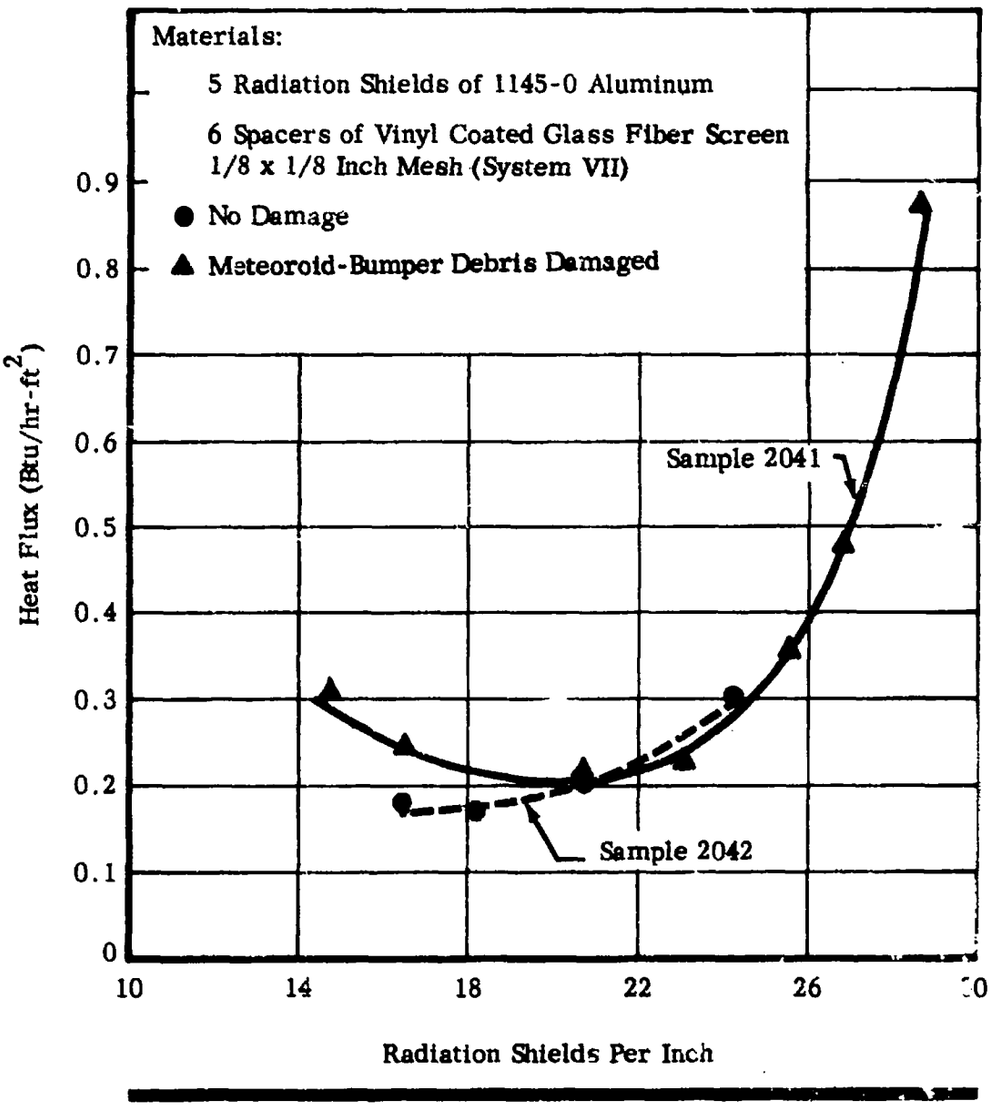

FIGURE II-18 EFFECT OF METEOROID-BUMPER DEBRIS ON HEAT FLUX THROUGH A MULTILAYER INSULATION

(FED SPEC HH-P-256-2, Grade EL). This material is a black linen Lamicoid used for instrument supports at cryogenic temperatures. Tests were performed with the cold side at -423°F and the warm side at -320°F.

Considerable difficulty was encountered in the attempt to obtain a uniform, low contact resistance between the sample and the warm- and cold-plates of the apparatus because of the rigidity of the 1-inch thick sample and possible warpage at the cold temperatures. The sample cold- and warm-plate interfaces were treated unsuccessfully with a variety of organic and silicone compounds in an attempt to reduce the contact resistance. By sandwiching the sample between layers of soft resilient materials, such as felt and sheet rubber, more reasonable results were obtained. However, none of the tests were repeatable, and the measured thermal conductivity was between 0.1 and 0.5 Btu-in/hr-ft^2-°F. The results of tests on a rigid sample are shown in Table II-24.

Because contact resistance was the controlling variable, the highest value measured would approach the actual thermal properties. A more satisfactory way to test a rigid sample of this type would be to bond the sample to the apparatus at its cold surfaces. However, to do this, an adhesive would have to be found that will bond at cryogenic temperatures, has a relatively high thermal conductivity, and will be removable after the tests without damaging the apparatus.

TABLE II-24

THERMAL TESTS ON A RIGID INSULATION (SYSTEM XXI)

Sample Description: 12-inch diameter x 0.910-inch thick disc of rigid phenolic laminate FED SPEC HH-P-256-2 Grade EL

Warm-Plate Temperature: -320° F

Cold-Plate Temperature: -423° F

Sample-Chamber Pressure: Less than 5×10^{-5} torr

Mechanical Load	Ram Spacing	Heat Flux	Thermal Conductivity	Test Date	Remarks	Test Number
psi	inches	$\frac{Btu}{hr\text{-}ft^2}$	$\frac{Btu\text{-}in.}{hr\text{-}ft^2\text{-}F}$			
20	1.015	52	0.51	6-9-64	Oiled felt pads	1061 b
20	1.020	12.4	0.12	6-11-64	Dry felt pads	1061 c
20	1.043	4.02	0.41	6-17-64	Buna N pads	1061 d

REFERENCES

(1) "Liquid Propellant Losses During Space Flight," Final Report, Report No. 65008-00-04, by Arthur D. Little, Inc., for National Aeronautics and Space Administration under Contract NASw-615. October 1963.

(2) Eckert, Ernest R. G. and Robert M. Drake. Heat and Mass Transfer. New York: McGraw-Hill Book Company, Inc. 2nd Edition, 1959.

(3) Edwards, K. D. and K. E. Nelson. "Maximum Error in Total Emissivity Measurements Due to Non-Grayness of Samples," American Rocket Society Journal, July 1964, p. 1020.

(4) "Liquid Propellant Losses During Space Flight," Addendum to Part IV of Report No. 65008-00-09, by Arthur D. Little, Inc., for National Aeronautics and Space Administration under Contract No. NASw-615, July 1964.

PART III

INSULATED TANK CALORIMETER

TABLE OF CONTENTS

LIST OF FIGURES

LIST OF FIGURES (cont'd)

LIST OF FIGURES (cont'd)

LIST OF TABLES

LIST OF TABLES (cont'd)

A. Summary

This report summarizes the work carried out by Arthur D. Little, Inc. under Contract NAS3-4181 to develop and measure the thermal performance of multi-layer insulation systems. This is a continuation of the Insulated Tank Program effort initiated in February 1963 under Contract NASw-615.

Purpose

The purpose of this study was: (1) to select insulation materials which were expected to yield improved performances of multi-layer insulation systems; (2) to design and fabricate multi-layer insulation systems, apply them to calorimeter tanks, and measure and evaluate their thermal performance using liquid hydrogen or liquid nitrogen in a simulated space environment; and (3) to develop practical methods of applying insulation to vehicle-type tanks and achieve the optimum thermal performance for the least weight of insulation.

Scope

Including two systems of the previous program, we have designed, fabricated, and tested a total of seven multi-layer insulation systems, one being a composite system consisting of a foam substrate in addition to the multi-layer concept. Each system tested is described in Table III-1. The thermal performance of each insulation system was measured in a test chamber which simulated the vacuum and a portion of the radiation spectrum found in the space environment. To simulate ground-hold conditions, tests were also made of insulation systems when contained in vacuum and helium purge environments. A group of fifteen experimental test series was conducted using the two test calorimeters and test chamber fabricated under the previous contract.

A summary of the heat fluxes measured for each insulation system under the various environmental conditions are presented in Table III-2.

Comments and Conclusions

Our comments and conclusions concerning the experimental effort conducted under this program are as follows:

1. Fifteen experimental test series were carried out on multi-layer insulations attached to calorimeter tanks containing liquid hydrogen or nitrogen. The lowest heat flux measured on any insulation was 0.38 Btu/hr-ft^2 for a 5-aluminum shield (2 mil sheet aluminum) spaced with 1/8 x 1/8-inch mesh vinyl coated Fiberglas screen. This system was also the highest weight insulation with a shield-spacer unit weight of 0.044 lbs/ft^2.

The lightest insulation had a shield-spacer unit weight of 0.0045 lbs/ft^2. This was a five shield (aluminized polyester film, coated on both sides, 0.25 mil thick) with nylon net spacers. This system had the poorest insulating characteristics and heat leaks of about 1.1 Btu/hr-ft^2 were measured. However, the very low weight of this system gave it the lowest ($K\rho$) value of any insulation tested, i.e., a value of 0.00072 Btu-in.-lb/hr-ft^5-$^\circ$F.

2. The heat fluxes obtained with the multi-layer insulations are about 5 per cent higher when using liquid hydrogen as the test fluid compared to liquid nitrogen.

The differential temperature across the insulation system in the former case is 100°F greater than in the latter case. This increase would theoretically produce a 1/2 per cent increase in the heat flux if the flux was due only to radiation heat transfer. The observed increase in flux is attributed in great part to the presence of a solid conduction brought about by physical contact of the shields and spacers.

3. Heat flux values measured on the upper half of the calorimeter tank have invariably been larger than those on the lower half. This we believe is due to the manner of support and the effect of gravity. The multi-layer insulation systems fabricated during the course of this study were essentially hung on the calorimeter tanks. That is, each layer completely enfolded the tank and received its support from the top of the tank rather than by pins, snap-ons, and other means of attachments distributed throughout the insulation. This means of support produces a mechanical load in the top of the insulation and increases the heat leak. These effects may be accentuated during a lift-off acceleration and lessened during a "no-g" orbiting state.

4. The net heat to the calorimeter tank, during simulation of the thermal transient that takes place on entering space, is greater (by more than a factor of two) for helium than for nitrogen when these gases are used previously to purge the insulation. This indicates that the nitrogen gas pressure in the multi-layer decreases more rapidly than the helium gas pressure. The probable cause of the different effects is the higher degree of nitrogen surface absorption taking place as the multi-layer cools compared to helium absorption. This effect is expected to become more pronounced as the number of shields is increased.

5. Two multi-layer insulation systems were each transported a minimum of 1000 miles by commercial truck carriers. Neither system showed any signs of mechanical failure. Measurements made prior to and at the end of 500 mile trips showed that no changes in the thermal performance of the systems had taken place during shipment.

6. If the thermal expansion coefficient for shields and spacers is large, a significant deterioration in the thermal performance of the multi-layer can occur. In the case where the shields and spacers layers are made continuous around the vessel, thermal contractions in these layers will introduce a pressure on the layers below and thus increase the solid conduction heat flux Where each layer is made up in segments, gaps may form at the joints and increase the radiation flux. In certain insulation configurations, such as the shingle method of attachment, the effect of thermal contraction in the shields and spacers can be easily minimized.

7. No unforeseen problems arose in fabrication of multi-layer insulations to the calorimeter tanks. Application of shields one-at-a-time to a tank, with extreme care to prevent thermal shorts, is a time-consuming job. Significant improvements in cutting, fabrication and repair techniques such as the application of insulation blankets appear feasible in terms of both mechanical and thermal performance of such systems.

8. A Fiberglas-reinforced, polyurethane, closed-cell, foam formed in place onto the calorimeter tank and sealed on the outside with a vapor barrier was successfully tested at liquid hydrogen and nitrogen temperatures in both space and ground environments. The 1/2 inch thick

foam gave a heat leak less that 100 Btu/hr ft^2 in typical ground conditions. The foam system was subjected to liquid nitrogen and hydrogen temperatures in a variety of ground and space simulation tests. The foam did not become detached from the tank or show any signs of cracking or cryopumping of the atmosphere. When the foam was combined with a multi-layer insulation and tested in the space environment, it produced no effect on the performance of the multi-layer insulation. The system and the application approach have a strong potential for application to space tanks.

9. A penetration placed within the multi-layer insulation increased the heat leak to a greater degree than predicted from theory; measured temperature gradients were in accord with those predicted. No explanation has satisfactorily explained the heat flux discrepancy for this single test.

10. Aluminum bonded to Mylar film is sensitive to mechanical abrasion and may detach. Also, water has a very deleterious effect on this reflector material.

Recommendations

1. The current studies performed with the emissometer and thermal conductivity apparatus indicate that shields and spacers with improved thermal and weight performance are realizable. Final experimental studies of these materials should be performed with the tank calorimeters.

2. We have currently successfully studied several techniques for controlling the heat flux in the ground environment. These have included foam substrate, helium and vacuum purged multi-layers and helium purge shroud. Techniques which appear fruitful for further investigation are those in which a purge space is provided between the multi-layer and the tank. These techniques provide a means of insulating the propellant tank in the ground environment and of bypassing around the multi-layer any gas that leaks through the propellant tank walls in the space environment.

3. The effect of perforations on the radiation heat flux has been studied analytically and experimentally with the thermal conductivity apparatus. The effect of these perforations on the heat flux, when trapped gas in the multi-layer is being vented, should be studied further in both the flat plate and tank calorimeters. In the tank studies, helium gas leaks of predetermined rates within the multi-layer and simulated pressure transients would establish the thermal performance of the insulation under simulated boost and space conditions.

4. The current insulated tank studies indicated that a nitrogen purge gas produced a lower integrated heat leak during a simulated boost transient than did helium. Additional testing with the tank calorimeter is required to confirm this effect. Other tests may be required to establish its nature.

5. The insulation on every space vehicle, cryogenic propellant tank will contain lines, supports, and wiring that will penetrate the insulation. In the current work, the studies in this area were limited and inconclusive. Greater emphasis in any future experimental studies should be placed on the practical methods of interrupting the tank surface insulation and on insulating the penetrations to minimize the net heat flow to the propellant tank.

6. Our current program has not included any studies in consideration of the permanent effects that vibration, acceleration, and accoustic environments have on the thermal performance of multi-layer insulations.

The durability and performance of any vehicle component in these environments is important to the proper functioning of any space vehicle. As space vehicle components, therefore, multi-layer insulations must be evaluated in all the possible environments. We are aware that experimental work in this area is in progress under other government contracts. Such work should be continued and augmented whenever the development of space insulations are undertaken.

7. The potential for destroying either wholly or in part, of a multi-layer insulation on a propellant tank during its history prior to launch is significant. Therefore, the time to apply, reapply, or repair any insulation system will become an important consideration in the

maintenance of schedules and the manner of handling and operating the stages at every step of the way. We believe, therefore, that strong incentives exist that warrant the development of pre-fabricated insulations which combine high thermal performance with ease and speed of application and maintenance. This approach should be emphasized in any new multi-layer insulation studies.

B. Introduction

The heat flow into the cryogenic propellants carried in space vehicles has an important effect on the quantities lost through vaporization, on the tank pressure limits, and on the utilization of the propellants. The heat flow to the propellants varies as the vehicle changes its environment, starting in the earth's atmosphere and ending in the vacua of space. In all environments, the heat flow to oxygen and, particularly, to hydrogen propellants must be limited and regulated in order to make the mission feasible and practical.

The means of limiting the heat flow in all the environments through the use of multi-layer insulations separately and in combination with other insulating media has received considerable attention and study. The studies, both analytical and experimental, have dealt separately with the performance of the insulating media and environments. It has become increasingly necessary, however, to integrate insulation performance with the wide range and changing conditions of the environments. The program described in this section has been an attempt to perform a part of this integration. We have measured and evaluated the thermal performance and suitability of several insulating media and techniques for moderating the heat flow to liquid hydrogen propellant tanks under space and ground hold conditions. This work has been performed through the use of calorimeter tanks.

C. Experimental Equipment and Procedures

1. Tank Calorimeter

The calorimeter is a vertical cylindrical vessel, 48 inches in diameter and 26 inches deep, having torispherical heads. The vessel was fabricated from 1/4-inch thick, oxygen-free, annealed copper because its

high thermal conductivity promotes isothermal-temperature conditions in the cold boundary over wide ranges of liquid bath level and insulation heat flux levels. The vessel had a maximum internal working pressure 30 psi above the external pressure and a maximum external working pressure 15 psi above the internal pressure. The tank is supported from a support flange by a 5-inch, schedule 5, type 304 stainless steel pipe that also acts as the tank vent. The 24-inch diameter support flange is mounted into the top of the vacuum chamber with bolts and O-ring seal. Additional details can be found in our final report on Contract NASw-615.

2. Cambridge Test Facilities

The Arthur D. Little, Inc., facilities located at Cambridge, Massachusetts, were used to conduct the largest portion of our test program. These facilities were limited to the use of liquid nitrogen test fluid. They consisted of a five-foot diameter vacuum chamber, 500-gallon liquid nitrogen supply tank, vacuum pumping system, cold guard and baffle supply systems, and the calorimeter vent gas measuring system.

During the space simulation tests, the calorimeter and its insulation system were installed in the five-foot vacuum chamber in the position shown in Figure III-1A. The chamber contains two interior baffles; one located in the upper half and the other in the lower half of the chamber. Each can be independently maintained at liquid nitrogen or water temperature through the use of an external supply system

The chamber and its associated systems are shown in Figure III-1B. The calorimeter is filled from a 500-gallon liquid nitrogen supply tank. This supply tank also provides the feed for the cold guard and chamber baffles when they are operated at liquid nitrogen temperatures. This is accomplished through use of a gravity tank which is elevated above the chamber. The tank support is a 4-inch column which also serves as feed line for the baffles and cold guard. The baffles vent to the gravity tank ullage space while the cold guard vents to atmosphere through a heat exchanger. The baffles can also be connected to the local water system when they are to be maintained at near room temperature.

The chamber is evacuated through use of a 4-inch oil diffusion pump and a mechanical fore pump. This system can achieve 10^{-5} mm Hg pressure with a clean and out gassed system in less than one day. A longer period of up to several days has been required to achieve this same vacuum with new insulation systems. The insulation systems were generally tested with chamber operating vacuums in the range of 10^{-5} to 10^{-6} mm Hg. Occasionally on long run tests, vacuums below 10^{-6} mm Hg were achieved.

The boil-off gases vented from the calorimeter were brought to room temperature in an air-warmed heat exchanger. The gases were measured volumetrically in dry type, positive displacement meters and vertical to the atmosphere.

3. NASA/Lewis Plum Brook Facilities

The facilities at the NASA/Lewis Research Center, at the Plum Brook Station in Sandusky, Ohio, were used to conduct the liquid hydrogen portion of the insulation tests performed under this contract. The test calorimeter was installed in the high vacuum chamber of the J-3 facility to simulate a high-altitude environmental test of the several foil insulation systems, and in the atmospheric exposure of the J-4 facility for the ground condition test of the helium purge bag and foam insulation systems. Using these facilities, which are equipped for handling liquid hydrogen and are controlled remotely from console stations, we were able to perform tests with liquid hydrogen and thereby supplement the data that was obtained using nitrogen at the ADL facilities in Cambridge.

The vacuum chamber which is a part of the J-3 facility has approximately the same dimensions as the A. D. Little, chamber. Also, the upper baffle is similar. However, there is no baffle in the lower portion of the chamber. Instead the chamber is jacketed in this area. Both the baffle and jacket can be supplied independently with either liquid nitrogen or water for temperature control of the surfaces facing the calorimeter insulations.

The J-3 and J-4 facilities are serviced by a portable liquid hydrogen dewar and a stationary liquid nitrogen dewar, each having about 7000 gallons capacity and connected to the facilities through a common

piping system that supplies the required cryogen to the calorimeter tank and cold guard coil and to the upper baffle and lower jacket on the inside of the vacuum chamber. The latter are also served with cold or heated water so that the temperature surrounding the calorimeter may be held at -320°F and from 40°F to above 100°F. The vacuum system consists of a 20" CVC diffusion pump, equipped with a liquid nitrogen cold trap controlled by a Johns & Frame LN_2 flow controller and a Model 412H Stokes mechanical forepump having 300 cfm capacity, and is capable of attaining less than 10×10^{-7} torr absolute pressure.

4. Instrumentation

The primary measurements made periodically during each test consisted of the following:

a. Calorimeter vent gas flow, temperature and pressure
b. Vacuum chamber pressure
c. Local barometer
d. Liquid level capacitance gauge
e. Temperatures in the insulation system, on the chamber baffles, at the calorimeter cold guard, of the local environment, and others as required.

At the Arthur D. Little, Inc. facility, all temperatures and the barometer data were recorded on strip charts. In addition, these and all the other data were manually recorded. Similar procedures were used at the Plum Brook facility.

5. Measured Heat Flux

We measured the shield temperature in each insulation system at select locations. Generally, the thermocouple sensors were located at the top, side, and bottom of areas of the tank which are identified as the A, B, and C locations respectively. These locations are shown in Figure III-1C. The thermocouple is identified by shield number and area location, i.e., sensor 5B is located on shield number five on the cylindrical section of the tank. Thermocouples are sometimes placed at other locations as in Insulation System No. 4. These locations are also identified by shield number and area, i.e., couple 5A3 is located on shield number five in the region between the A and B positions. Exact locations are given in additional figures presented in subsequent sections.

The thermal performance of the insulation system has been measured over intervals of approximately 24 to 100 hours. Occasionally, it was necessary to accept intervals of shorter duration because of difficulties encountered with the facility subsystems after system temperature equilibrium had been achieved. During the measurement interval, the ullage pressure of the calorimeter varied directly as the barometric pressure, i.e., the calorimeter vented to the atmosphere through a low pressure drop system and no attempt was made to control the ullage pressure.

The heat passing through the insulation is reflected as stored energy in the calorimeter system and as vaporized liquid vented from the calorimeter. When no changes in the barometric pressure occur in the measuring interval, the energy transmitted through the insulation is evidenced primarily as vaporized liquid. An almost negligible amount of energy is stored in the calorimeter ullage.

When barometric pressure changes occur during the interval, the system temperature increases or decreases directly with this pressure. An increase in system temperature results in heat storage in the calorimeter tank metal, and the liquid and gas masses. A decrease in temperature results in a heat release. Barometric changes which do work on the thermodynamic system which comprises the calorimeter and its contents are also reflected as system energies.

In Appendix A, a thermodynamic analysis of the calorimeter system is presented and the magnitude of the various energy effects are evaluated. The analysis results indicate that for the conditions under which our measurements were made, only two effects need be considered when evaluating the insulation heat flow. The first and most significant factor is the vented gas mass and the second factor is the liquid mass heat storage effect.

The total heat rate is computed from the total vaporized liquid mass vented in the data interval and the latent heat of vaporization of cryogen. The gas mass is computed from the integrated volume measurement of the calorimeter vent gas stream and its temperature and pressure at the metering point.

This measured heat flow is corrected for heat storage or heat release in the calorimeter liquid as follows: The average mass of the

liquid in the tank during the data interval is established from the liquid-level measurement, tank-volume calibration, and liquid density. The increase or decrease in the saturation temperature of the bulk liquid at the end of the data interval as compared to that at the beginning and is determined from the change in the calorimeter ullage pressure. This is a function both of the local barometric pressure and the pressure loss in the vent system. From the change in the bulk temperature and the liquid specific heat at saturation, the total heat energy stored or released during the data interval was computed and converted into an hourly rate. Any heat stored during the data interval was added to the heat flow determined from the calorimeter boil-off; a release of heat during the data interval was subtracted.

6. Test Program

We conducted fifteen test series with seven insulation systems; each series consisted of a group of tests performed with one system to measure the thermal performance in one or more environments. The principal test environments are as follows:

a. Space vacuum and 300°K radiation in all directions
b. Space vacuum, 300°K radiation on one half of the calorimeter and 77°K radiation on the other half
c. Natural atmospheric environment
d. Natural atmospheric environment with liquid nitrogen sprays on the outside of the insulation

Liquid nitrogen was the principal test fluid used in the calorimeter. Tests with this fluid were performed both at Cambridge and Plum Brook facilities. All work with liquid hydrogen was performed at Plum Brook.

Of the seven insulation systems tested, two had been fabricated under a previous contract (NASw-615). All systems except one contained five radiation shields. The principal characteristics of these systems are summarized in Table III-1.

The conditions under which each system was tested and the performance results obtained are grouped and summarized in Table III-2.

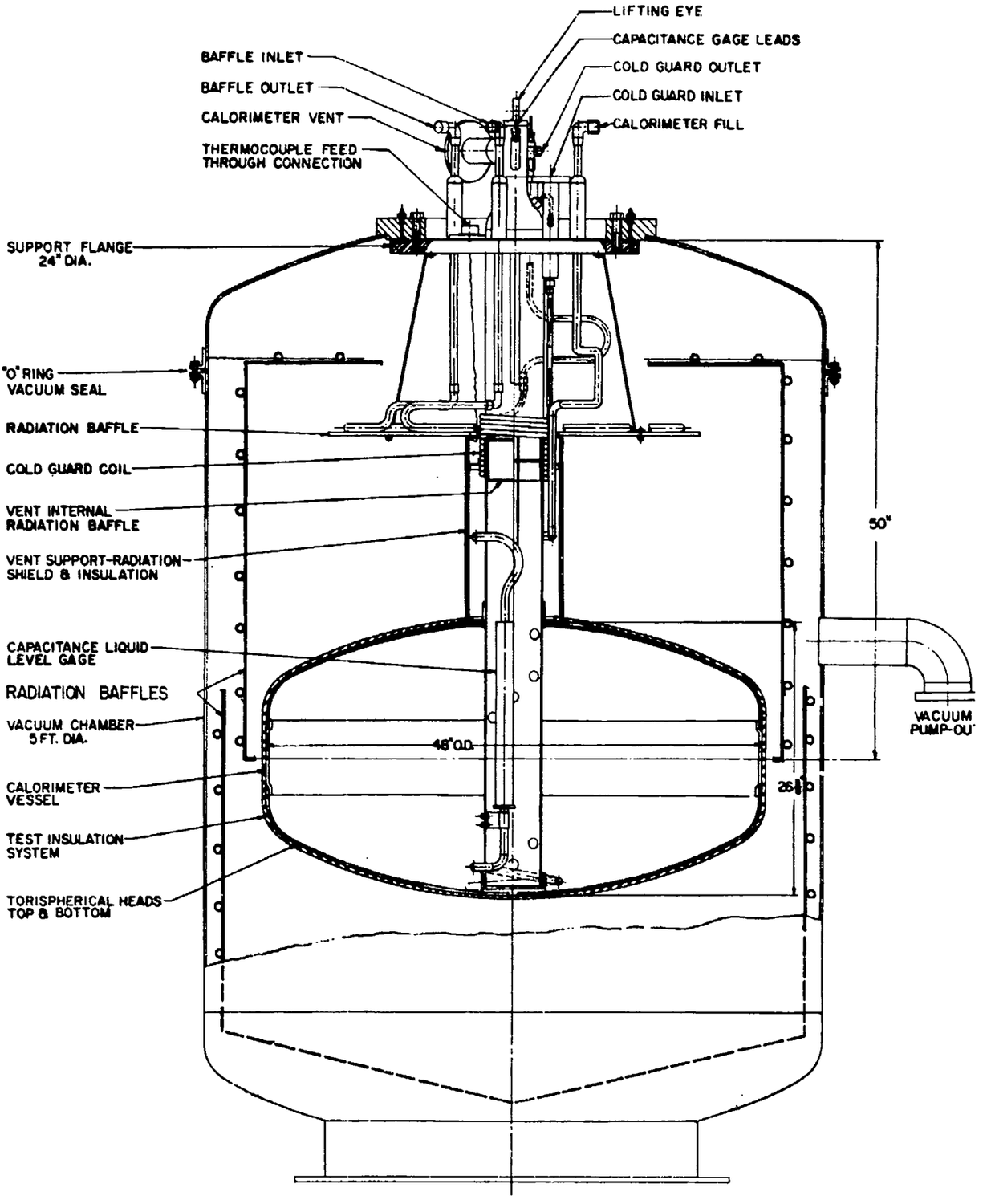

FIGURE III-1A CHAMBER AND CALORIMETER ASSEMBLY

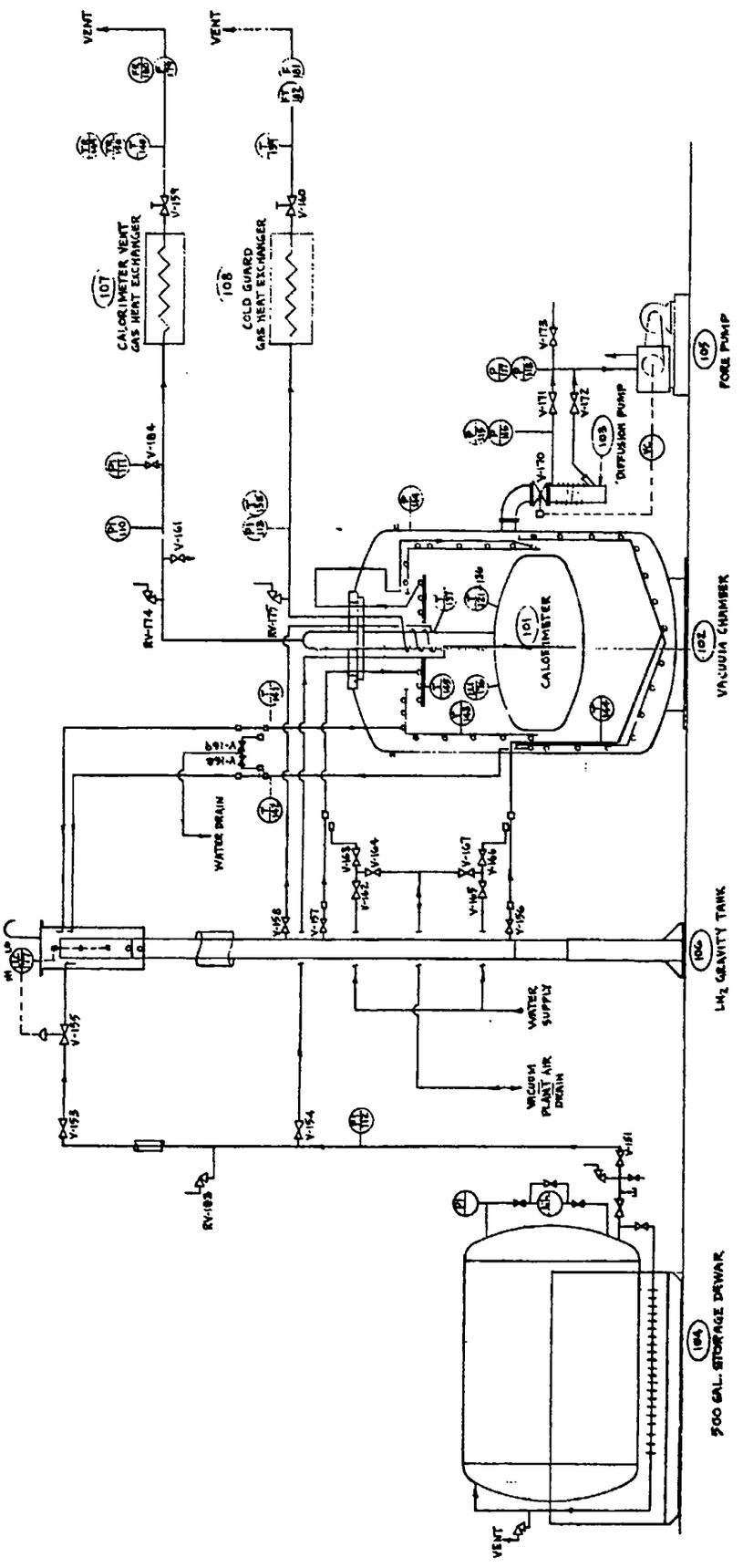

FIGURE III-1B FLOW SCHEMATIC, TANK INSULATION TEST FACILITY

III-13

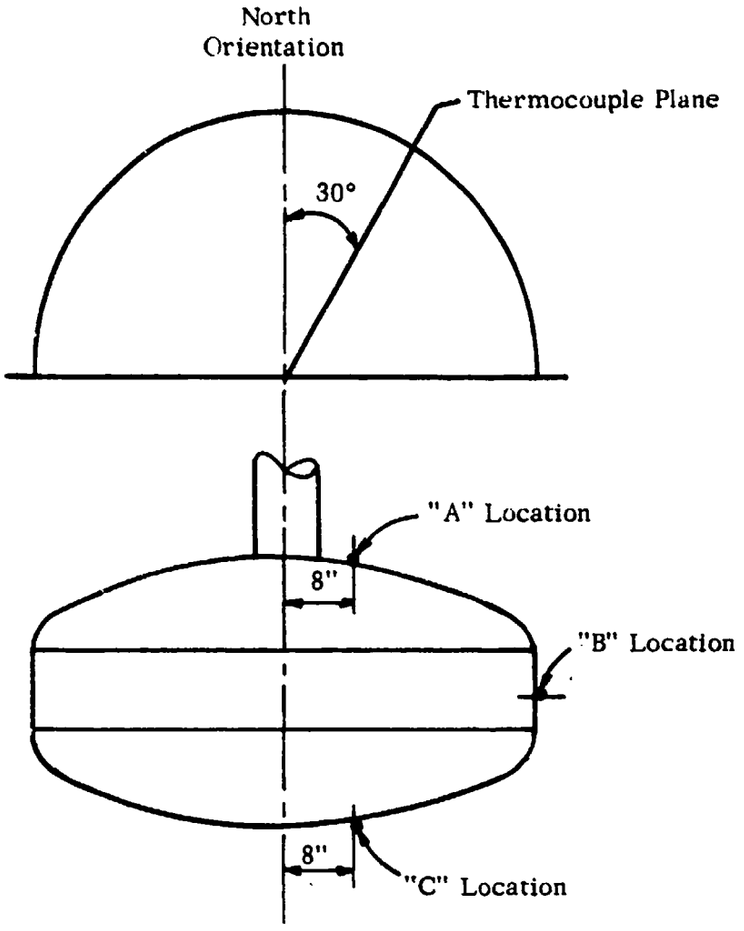

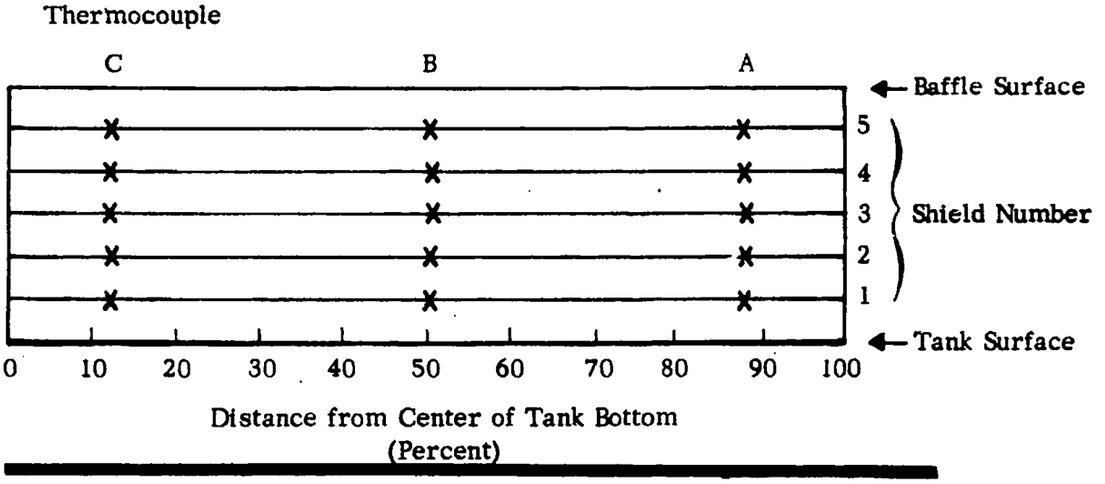

FIGURE III-1C INSULATION SYSTEM, THERMOCOUPLE LOCATIONS

SUMMARY - PROPERTIES OF INSULATION SYSTEMS AND SYSTEM COMPONENTS

Description	Insulation System No.1	Insulation System No.2	Insulation System No.3	Insulation System No.4	Insulation System No.5	Insulation System No.6	Insulation System No.7
	5 shields of aluminum and 6 spacers of vinyl coated Fiberglas applied to Calorimeter No. 1	5 shields of polyester film coated on one side with aluminum and 6 spacers of vinyl coated Fiberglas screen applied to Calorimeter No.2	Same as System No.2 with strong short (copper penetration) added to system. Applied Calorimeter No. 2.	5 shields of aluminum and 6 spacers of vinyl coated Fiberglas screen applied to Calorimeter No. 2.	Composite System with ½-in. foam substrate, vapor barrier, 5 shields of polyester film coated with aluminum on 2 sides and 6 spacers of vinyl coated Fiberglas on Calorimeter No.1.	5 shields of polyester films coated on both sides with aluminum and 6 nylon netting spacers applied to Calorimeter No.2.	System No.6 to which is added a blanket of five shields of polyester film coated on both sides with aluminum and 5 nylon netting spacers. Applied to Calorimeter No. 2.
SHIELDS							
Side Material	1145-H19 Aluminum	Polyester film coated one side with aluminum to a thickness of 300°A	Same as System No.2	1100-0 Aluminum	Polyester film coated both sides with aluminum to a thickness of 375°A	Same as System No.5	Same as System No.5
Head Material	1100-0 Aluminum	Same as System No.2	Same as System No.2	1100-0 Aluminum	Same as System No.5	Same as System No.5	Same as System No.5
Thickness (in.)	.002	.00025	Same as System No.2	.0005	.00025	Same as System No.5	Same as System No.5
Weight (lb/ft^2)	.028	.00176	Same as System No.2	.007	.00176	Same as System No.5	Same as System No.5
Emissivity	.035	.047	Same as System No.2	.035	.035	Same as System No.5	Same as System No.5
Side Geometry	Gored	Gored	Same as System No.2	Gored	Gored	Same as System No.5	Same as System No.5
Head Geometry	Spherical segments	Slit circles	Same as System No.2	Spherical segments	Slit circles	Same as System No.5	Same as System No.5
Joint Type	Butt gores; all others overlapped	Butt gores; all others overlapped	Same as System No.2	Butt gores; all others overlapped	Butt gores; all others overlapped	Same as System No.5	Same as System No.5
SPACER							
Material	¼ x ¼ in. vinyl coated Fiberglas screen	Same as System No.1	Same as System No.1	Same as System No.1	Same as System No.1	Nylon netting	Same as System No.6
Thickness (in.)	.020	Same as System No.1	Same as System No.1	Same as System No.1	Same as System No.1	.007	Same as System No.6
Weight (lb/ft^2)	.016	Same as System No.1	Same as System No.1	Same as System No.1	Same as System No.1	.00271	Same as System No.6
Fiber Diameter (in.)	.0125	Same as System No.1	Same as System No.1	Same as System No.1	Same as System No.1	.002	Same as System No.6
Open Area (percent)	81	Same as System No.1	Same as System No.1	Same as System No.1	Same as System No.1	80	Same as System No.6
Side Geometry	Gored	Same as System No.1	Same as System No.1	Same as System No.1	Same as System No.1	Gored	Same as System No.6
Head Geometry	Spherical segments	Same as System No.1	Same as System No.1	Same as System No.1	Same as System No.1	Spherical segments	Slit circles
Joint Type	Butt	Same as System No.1	Same as System No.1	Same as System No.1	Same as System No.1	Butt	Butt
SUBSTRATE	None	None	None	None		None	None
Material					Urethane foam and 10% by weight chopped Fiberglas strands		
Thickness (in.)					.5		
Weight (lb/ft^2)					.21		
Density (lb/ft^3)					5.0		
VAPOR BARRIER	None	None	None	None		None	None
Material					Laminate of aluminum and polyester film		
Thickness (in.)					.002		
Weight (lb/ft^2)					.0208		
BOUNDARY EMISSIVITY							
Calorimeter Tank	.88	.88	.88	.88	.88	.88	.88
Chamber Baffles	.93	.93	.93	.93	.93	.93	.93
PENETRATIONS							
Number	5	None	1	None	None	None	None
Diameter (in.)	.030	-	3.0	-	-	-	-
Material	S/S and Teflon sheath	-	Copper	-	-	-	-
SYSTEM PROPERTIES							
Surface Area (ft^2)	38.14	39.5	Same as System No.2	39.5	39.80[1]	39.5	39.5
Weight[2] (lb/ft^2)	.236	.104	Same as System No.2	.131	.354 (Foam Included)	.025	.047
Thickness[2] (in.)	.130	.121	Same as System No.2	.123	.625	.0432	.0795
Weight Density[3] (lb/ft^3)	24.0	10.5	Same as System No.2	13.5	6.8	7.4	7.4
Shield Density[3] (shields/in.)	45.5	49.3	Same as System No.2	48.8	-	138	134
Thermal Performance Tests	I-1, 3, 6 and 7 Series	I-2 and 4 Series	I-5 Series	II-1, 2, 3 and 4 Series	II-5, 6, 9 and 10 Series	II-7 Series	II-8 Series

Notes

1. Surface area of the vapor barrier applied over the foam substrate. All other surface areas refer to calorimeter tank surface.
2. Weight and thickness of the systems as applied to the calorimeters.
3. Weight and shield densities are based on the measured thickness and weight of a single layer which includes one shield and one spacer.

TABLE III-2

TANK PROGRAM

MULTI-LAYER INSULATION PERFORMANCE SUMMARY

	Test	Date	Location	Tank Fluid	Environment	Average Boundary Temperatures (°F) Warm	Cold	Measured Flux (Btu/hr-ft^2)	Adjusted[4] Flux (Btu/hr-ft^2)	$\frac{K\rho}{\text{Product}^2}$ $\left(\frac{\text{Btu-in-lb}}{\text{hr-ft}^5\text{-}^\circ\text{R}}\right)$	Remarks
SYSTEM NO. 1	I-1B, F, G, H[1]	Jun 63	ADL	LN_2	Vacuum	87	-320	0.38	0.37	.00255	
	I-3A, B	Dec 63	J-3	LH_2	Vacuum	48	-423	0.516	0 65	.0029	
	I-3N	Jan 64	J-3	LN_2	Vacuum	80	-320	0.612	0.62	.0041	
	I-3D2, 3	Feb 64	J-3	LH_2	Vacuum	79	-423	0.66	0.66	.0035	
	I-6	Mar 64	ADL	LN_2	Vacuum	38	-320	0.44	0.62	.0033	
	I-7	Mar 64	ADL	LN_2	Vacuum	40	-320	0.44	0.60	.0032	
SYSTEM NO. 2	I-2A, B[1]	Sep 63	ADL	LN_2	Vacuum	68	-320	1.02	1.10	.0028	
	I-4A, B, C, D	Dec 63	ADL	LN_2	Vacuum	48	-320	0.80	1.02	.0023	
	I-4E	Dec 63	ADL	LN_2	Vacuum	47	-320	0.84	1.10	.0024	Warm Lowe half
	I-4F	Jan 64	ADL	LN_2	Vacuum	-	-	Aborted	-	-	Warm Uppe half
SYSTEM NO. 3	I-5A, B, C, D	Feb 64	ADL	LN_2	Vacuum	41	-320	(46.1)[3]	-	-	
	I-5E	Feb 64	ADL	LN_2	Vacuum	38	-320	1.06	1.47	.0031	Warm uppe half
	I-5F	Feb 64	ADL	LN_2	Vacuum	38	-320	(29.3)[3]	-	-	Warm lowe half

TABLE III-2 (cont'd)

Test	Date	Location	Tank Fluid	Environment	Average Boundary Temperatures (°F) Warm	Cold	Measured Flux (Btu/hr-ft²)	Adjusted[4] Flux (Btu/hr-ft²)	$K\rho$ Product[2] $\left(\frac{\text{Btu-in-lb}}{\text{hr-ft}^5\text{-}^\circ\text{R}}\right)$	Remarks
II-1A	Apr 64	ADL	LN_2	Vacuum	48	-320	0.37	0.47	.014	
II-1B	Apr 63	ADL	LN_2	Vacuum	49	-320	0.40	0.51	.0015	Warm Lowe half
II-1C	Apr 64	ADL	LN_2	Vacuum	55	-320	0.57	0.69	.0021	Warm uppe half
II-2	Apr 64	ADL	LN_2	Helium Shroud	50	-320	290	-	-	
II-3A	May 64	ADL	LN_2	Helium Purge Bag, Ground Atmos.	72	-320	165	-	-	
II-3B	May 64	ADL	LN_2	Vacuum Purge Bag, Ground Atmos.	67	-320	234	-	-	
II-3C	Jun 64	ADL	LN_2	Vacuum (Bag installed)	66	-320	1.40	1.56	.0050	
II-4A	Jun 64	ADL	LN_2	Vacuum (Bag removed)	69	-320	0.83	0.91	.0029	
II-4B	Jun 64	ADL	None	Decompression	-	-	None	-	-	
II-5A	Jun 64	J-4	LN_2	Ground Environment	89	-320	97	-	-	Foam only
II-5B1	Jun 64	J-4	LH_2	Ground Environment	76	-423	93.0	-	-	Foam only
II-5B2	Jun 64	J-4	LH_2	Ground Environment	88	-423	93.3	-	-	Foam only

SYSTEM NO. 4

SYSTEM NO. 5

TABLE III-2 (cont'd)

SYSTEM NO. 2 (cont'd)

Test	Date	Location	Tank Fluid	Environment	Average Boundary Temperatures (°F) Warm	Cold	Measured Flux ($Btu/hr\text{-}ft^2$)	Adjusted[4] Flux ($Btu/hr\text{-}ft^2$)	$\left(\frac{K\rho \text{ Product}^2}{\frac{Btu\text{-}in\text{-}lb}{hr\text{-}ft^5\text{-}^\circ R}}\right)$	Remarks
II-5C	Jun 64	J-4	LN_2	Ground Environment	-320	-320	None	-	-	Foam only
II-5D	Jun 64	J-4	LH_2	Ground Environment LN_2 Spray for Cold Shock	-320	-423	None	-	-	Foam only
II-5E	Jun 64	ADL	LN_2	Vacuum, 50°F and -320°F Baffles	50 -320	-320	None	-	-	Foam only
II-6A1	Jun 64	J-3	LN_2	Vacuum	82	-320	1.56	1.54	.0165[5]	
II-6A2	Jul 64	J-3	LN_2	Vacuum	79	-320	.85	.85	.0091	
II-6B	Jul 64	J-3	LH_2	Vacuum	80	-320	.91	.91	.0077	
II-6C	Jul 64	J-3	LN_2	Vacuum	79	-320	.71	.72	.0076	Warm lower half
II-6D	Sep 64	J-3	LN_2	1 Atmos. Helium	30	-320	69.1	-	-	
II-9A	Sep 64	ADL	LN_2	Vacuum	67	-320	.71	.78	.0078	
II-9B	Sep 64	ADL	LN_2	1 Atmos. Helium Shroud	66	-320	85.6	-	-	
II-9C2	Sep 64	ADL	LN_2	Vacuum	71	-320	.60	.65	.0065	Warm lower half
II-9D	Oct 64	ADL	LN_2	Vacuum	66	-320	.93	1.03	.0102	Warm upper half
II-10	Oct 64	ADL	LN_2	Ground Environment Helium Purge	72	-320	92.2	-	-	

TABLE III-2 (cont'd)

	Test	Date	Location	Tank Fluid	Environment	Average Boundary Temperatures (°F) Warm	Cold	Measured Flux ($Btu/hr\text{-}ft^2$)	Adjusted[4] Flux ($Btu/hr\text{-}ft^2$)	$K\rho$ Product[2] $\left(\frac{Btu\text{-}in\text{-}lb}{hr\text{-}ft^2\text{-}^\circ R}\right)$	Remarks
SYSTEM No. 6	II-7	Aug 64	ADL	LN_2	Vacuum	74	-320	1.04	1.11	.00072	
SYSTEM No. 7	II-8	Sep 64	ADL	LN_2	Vacuum	72	-320	0.78	0.83	.0011	

Notes:

1. Test performed under Contract NASw-615, added here for completeness.
2. $K\rho$ product based on measured heat flux. See Appendix III-E-3 for method of completion.
3. This is a net heat rate to the calorimeter and not a flux. The flux cannot be computed because of the presence of a penetration in the system.
4. Measured flux adjusted to standard boundary conditions. Standard warm boundary is 80°F and standard cold boundary is -320°F.
5. The computed $K\rho$ product for all space simulation tests II-6A1 through II-9D include the weight of foam system.

D. Experimental Results

Insulation System No. 1

a. Introduction

In the previous contract period (NASW-615), we applied the first multi-layer insulation to one of the tank calorimeters. The insulation consisted of five shields of 2 mil thick aluminum and six spacers of 1/8 x 1/8-inch mesh vinyl coated Fiberglas screen. The consistant thermal performance of this insulation in the flat plate calorimeter led to its selection as the calibrating standard for the three flat plate calorimeters operated by Arthur D. Little, Inc. For the same reasons this shield-spacer combination was considered the best choice for evaluating the factors influencing the system thermal performance when the insulation geometry is radically altered from a flat plate to a tank configuration.

b. Insulation System

The construction details of this insulation system have been previously reported.(1) The principal characteristics of the system have been summarized in Table III-1. The partially completed system is shown in Figure III-2.

c. Test Condition

Tests I-3 Series (Space Simulation LH_2 and LN_2)

Tests were performed with both liquid hydrogen and liquid nitrogen test fluids at the NASA/Plum Brook Station J-3 facility. The purpose of these tests was to measure the thermal flux produced in the insulations by each of the two cryogens when used in the calorimeter tank. A further purpose of these tests was to obtain a relative calibration between the J-3 facility and the A. D. Little facilities at Cambridge through use of a single insulation system. Nine tests were performed in the chamber at J-3 with simulated space pressure and room temperature radiation source. These tests are identified as the I-3 test series and the obtained data are presented in Table III-3.

Test I-6 Series (Space Simulation LN_2)

This test series was performed at the A. D. Little facilities at Cambridge. The tank calorimeter was placed in the vacuum chamber where space pressure and radiation source were simulated. The purpose of these tests was to obtain heat flux measurements for comparison with those obtained at J-3. The data are presented in Table III-4.

Test Series I-7 (Launch and Space Simulation)

The I-7 series of tests were performed at the Cambridge test facility using liquid nitrogen as the test fluid. Their objective was to determine the effect of helium and nitrogen purge atmospheres on the thermal performance of multi-layer insulations immediately after reaching the space environment.

To provide a basis of comparison between the two purge environments, the chamber pressure and calorimeter conditions were programmed in each test as follows:

(a) Hold calorimeter in selected gas environment at one atmosphere for about three days.

(b) Pump-down chamber from 30 to 0.1 inches Hg in one hour.

(c) Vacuum pump chamber with fore pump to 25 micron pressure level.

(d) Vacuum pump chamber with diffusion pump to one micron pressure level.

(e) Admit liquid nitrogen to cold guard and achieve cold guard temperature equilibrium.

(f) Fill calorimeter with liquid nitrogen over one-hour period.

(g) Monitor shield temperature, chamber pressure, and calorimeter vent gas rate until pressure and heat flux equilibrium is achieved.

This test series consisted of two tests. Test I-7A was performed after the insulation had been purged with helium gas. Test I-7B followed the nitrogen gas purge. The resulting data are presented in Tables III-5 and 6 respectively. The time variation of the chamber

pressure and the resulting insulation heat flux are presented in Figure III-4.

d. Results and Discussion

(1) Tests

In Table III-3, the principal data obtained with this insulation system have been summarized. The typical temperature distribution within the multi-layer obtained for each test series is presented in Figure III-3. The results obtained in December with liquid hydrogen and liquid nitrogen test fluids at the J-3 facility were approximately twice that obtained in Test I-1 performed at Arthur D. Little, Inc., facilities at Cambridge.

If one assumes that the mode of heat transfer in the multi-layer insulation system is entirely by radiation, then the heat flux is directly dependent upon the shield emissivity and on the boundary temperatures. Sopp et. al.[2] reports the total hemispheric emissivity of 1145-H19 and 1100 aluminum at between .03 and .05. For sink and source temperature of -320 and 80° respectively, a heat flux of .435 Btu/hr-ft^2 is calculated for a five shield system using the lower emissivity value. In this calculation, the improvement in emissivity as shield temperature is decreased is not taken into account. Thus, the values obtained experimentally in June, 1963, compared very well with the experimental value (0.38 Btu/hr/ft^2).

The tests performed in December, 1963, at the J-3 facility resulted in heat flux measurements that were generally twice those measured previously at ADL's facility. For example, tests I-3A and I-3B performed with liquid hydrogen resulted in adjusted heat fluxes of .65 and .66 respectively. These high values (compared to .38 Btu/hr ft^2) were at first thought to result from the erratic operation of the liquid hydrogen cold guard circuit. Test I-3C was performed subsequently with liquid nitrogen in the cold guard which resulted in an adjusted flux of .74 Btu/hr/ft^2.

The presence of line connections between the high pressure helium purge system and the calorimeter vent measuring system raised the question that a leak between the two could produce an apparently high boil-off rate from which a high heat flux would be calculated. A number of these connections were removed and modified. Subsequently, tests I-3N1 and I-3N2 were performed with liquid nitrogen in the tank and cold guard. This resulted in fluxes of .61 and .63 respectively.

The next test, I-3D-1, was performed with liquid hydrogen in the tank and guard. This resulted in a flux of .72 Btu/hr/ft^2. In view of the previous smaller results obtained with hydrogen, the vent measuring circuit was inspected and found to contain a high pressure gas tie. This was removed and tests I-3D-2 and I-3D-3 were performed under the same conditions which gave adjusted heat fluxes of .65 and .66 Btu/hr/ft^2. These values were identical to those obtained in tests I-3A and I-3B.

Test I-3D-4 was performed with liquid hydrogen in the tank and liquid nitrogen in the cold guard circuit to confirm the results obtained in test I-3C under similar conditions. An adjusted heat flux of .67 was obtained. This value is also consistent with the previous four tests (I-3A, 3B, 3D-2 and 3D-3) performed with liquid hydrogen in the tank and cold guard.

It was quite evident that additional checks were required with the ADL facility. Thus, the calorimeter with the insulation system was returned to Arthur D. Little, Inc., in Cambridge and tests I-6 and I-7 were performed giving results consistent with those obtained at the J-3 facility at Plum Brook station. All the calibration heat flux results obtained with Insulation System No. 1 are summarized in Table III-7. As can be seen from this table, the first experimental value obtained is in question. Therefore, the insulation system was carefully dismantled to discover what, if any, degradation had taken place during transportation and the long storage period at Plum Brook. The dismantled insulation indicated that, indeed, degradation had taken place, resulting mainly from the accumulation of water on the inside of the first shield system at the bottom

which had caused corrosion of the aluminum foil and subsequent degradation of the emissivity with resulting loss in thermal performance of the system.

An important purpose of the test performed at the J-3 facility was to determine the effect of the test fluid on the insulation performance. In an evacuated multi-layer insulation, conduction and radiation are the two principal modes by which heat is transferred through the system in the direction perpendicular to the shields. The mode of transfer can be ascertained in two ways, i.e., (1) by measuring the temperature distribution in the shields and, (2) by comparing the heat flux obtained in tests performed both with liquid nitrogen and liquid hydrogen. If heat transfer is solely by radiation, then the shields will assume temperatures which are linear in T^4. Departure in the temperature from the theoretical temperature distribution is an indication of the effects both of conduction and varying shield emissivity. Considering the second method, it may be possible to alter the boundary temperatures without altering the radiative heat flux. For example, by lowering the tank temperature from -320°, when liquid nitrogen is used as the test fluid, to -420°, which is typical for liquid hydrogen, the radiative heat flux is increased theoretically by approximately one-half per cent (warm boundary temperature of $540^{\circ}R$). However, as the conductive heat leak is nearly linear with temperature, lowering the tank temperature by about $100^{\circ}F$ should increase any conductive heat leak by approximately 25 per cent. This prompted our performing tests at both liquid nitrogen and liquid hydrogen temperatures. It can be shown very readily that, if the heat leak increased from .62 to .66 Btu/hr/ft^2 in going from liquid nitrogen temperatures to liquid hydrogen test fluids, that the calculated conductive heat leak is about 22 per cent of the total heat leak, provided that all things remain equal except the two sink temperatures. However, this step must be taken cautiously as the difference in the two values is only about 5 per cent of the absolute heat flux measured and is, therefore, quite probably within experimental accuracy.

(2) Shield Deterioration

Upon completion of test I-7B, we dismantled the insulation system of Calorimeter No. 1. In the process, we inspected each foil for possible causes of the rise in heat flux that we initially experienced between the Cambridge and Plum Brook test. We first checked for electrical continuity between the tank shields and between the neck shields and found that none existed. The outermost shield, No. 5, of the neck and tank contained a light film of oil on the outside surface; presumably this was vacuum oil. A very light oil film was also detected on shield No. 4 of the neck; however, there was no oil detected on the No. 4 tank shield or on any of the other three inner shields of the neck and tank.

The most prominent defect found was a corroded area on the inside bottom of the No. 5 shield (outermost). The corroded shield is shown in Figure III-6. The affected portion is an annular consisting of an area of 12 inch and 24 inch inner and outer diameters respectively. Vertical streak marks were evident on the exterior of the No. 5 side foil (Figure III-5) and it appeared that the water entered the foil system by running down the side of the No. 5 shield to the botton interior, forming a pool 24 inches in diameter on the bottom. We believe that water partially evaporated while standing idle, leaving a pool 12 inches in diameter which was evaporated when the chamber was pumped to vacuum pressures.

The corrosion products formed a white substance between the foils as is evidenced on the separator netting between the No. 4 and No. 5 foils (Figure III-7) and corrosion was evident also on the outer side of No. 4 foil showing that a conductance path could have been provided between the foils. The corrosion was not apparent from the outside of No. 5 foil; however, it did work through one small area of the No. 4 foil, but not onto foil No. 3. The remaining areas of No. 4 and No. 5 foils and the complete areas of No. 3, No. 2, and No. 1 foils were comparable with the initial installation. There was one small area (approx. 1" square) where the multi-layer system had been indented (Figure III-5). Shield No. 1, 2, and 3 were in excellent condition.

The emissivity values of the multi-layer system were measured in select areas to determine the extent and degree to which the shield emissivities were deteriorated. The values obtained with the emissometer are presented in Table III-8. Also included are a number of measurements made on the original aluminum foil still available from the stored rolls. In addition, comparison must be made with a number of other measurements made on aluminum foil which gave emissivity results that ranged from .023 to .103 with 50 per cent of the data in a smaller range of .035 $\pm$ .0035.

These data indicate that the shields of the multi-layer were not deteriorated during storage except in those areas where corrosion and water staining were evident. A value of .860 at the corroded area on shield No. 5 was the highest obtained. However, it is not possible to account for the higher heat fluxes based alone on the area and emissivity of the corroded area. To degrade the insulation system from a heat flux value of .38 Btu/hr-ft^2 to .62 Btu/hr-ft^2 is the equivalent of removing about 1½ shields. The damage to the emissivities of the shield surfaces did not appear extensive as this equivalent effect would indicate. Also, there was no significant alteration in the temperature distribution in the multi-layer between test I-4 and all subsequent tests (see Figure III-3) that would indicate significant alteration in the shield surface properties or indicate the presence of thermal shorts among the shields.

In Part IV of this report, the emissivity values for a wide variety of materials obtained with the emissometer have been presented. Out of the approximately 170 emissometer tests performed, 28 were performed with aluminum foil or thin sheets. The results obtained vary from emissivity values of .023 to as high as .103. (These values were obtained at between room temperature and 93°F.) Approximately 50 per cent of the test values are in a range of emissivity values of .030 to .040. The remainder appear scattered over the range previously given. Thus, there is general agreement between the results obtained with the emissometer and those reported by Sopp.[2] Based on

these emissivity values, a five-shield aluminum foil system would have a radiation heat flux of about .50 Btu/hr-ft^2 with an 80°F source temperature and a liquid nitrogen sink temperature. This does not take into account any variation of shield emissivity with temperature.

Some of the emissivity values more directly related to this first insulation system are presented in Table III-8. The emissivity of the corroded section in shield No. 5 is .860.

The corroded portion of shield No. 5 interior is restricted to an area of approximately 2.5 square feet. If the deterioration in the insulation system is based on the average computed emissivity in Test I-1, then two entire shields have to become completely deteriorated or their equivalent. They would be removed from the system and the resultant heat flux would be approximately .63 Btu/hr-ft^2. If the average emissivity is taken as that determined from the emissometer measurements, then the two surfaces of one shield have to be completely blackened or their equivalent, one shield removed (in order to obtain that same heat leak.) Since the emissometer measurements and visual inspections indicated that only a small portion of the shield was seriously deteriorated, other causes which we have not been able to identify must have also contributed to the loss in insulation performance.

(3) Purge Gas Effect On Transient Heat Flux

The results obtained in tests 7A and B are unusual in two respects. In the first place, the theoretical pumping rate of the interstitial gas from the multi-layer will be greater for helium than for nitrogen by a factor estimated to be about 7 to 1. This is a consequence of the fact that the volume pumping rate from a perforated multi-layer in a space environment is inversely proportional to the molecular weight of the gas[1]. In the second place, the heat flux due to the presence of residual gas may be greater for nitrogen

than for helium, given the same conditions of pressure and boundary temperatures, by a factor estimated to be greater than 2. This relative effect is obtained from the Knudsen equation[3] through use of the appropriate gas properties and accommodation coefficients (helium has much lower accommodation coefficients than nitrogen.) Thus, if the helium residual gas is more rapidly pumped by the space environment and the effect of any residual helium gas on the heat flux is less than the effect of nitrogen gas, then the integrated flux during the transient period is expected to be smaller for helium than for nitrogen. The measured heat fluxes show that the opposite effect has taken place.

The observed difference would indicate that the pressure of the contained gas in the multi-layer is significantly greater over a longer period of time for helium, compared to nitrogen. This condition can occur in two ways: a.) helium gas is being desorbed at the surfaces and b.) nitrogen gas is being absorbed by the surfaces. Of the two, the latter occurrence is more probable. At a pressure of 1 micron there are about 5.4×10^{13} molecules in the multi-layer space per square cm. of tank surface. The tank alone has a mono molecular surface capacity of 8.10×10^{14} molecules $/cm^2$. There is some nitrogen pumping potential always present in the system, particularly on the shield and spacer surfaces, as their temperatures are lowered while they are approaching their steady state distribution. These tests were performed with a five shield multi-layer system. We expect that the magnitude of observed effects are dependent upon the number of shields; it will probably become more pronounced as the number of shields increases.

The measured effect of purge gas on the transient performance of multi-layer insulations has produced interesting results. We believe that tests to obtain additional data are warranted. The present results should be confirmed in tests performed in a manner similar to I-7A and B. These can and should be accomplished in

conjunction with other steady state insulation performance measurements. At a later date, these tests can be augmented, if necessary, with smaller more specialized tests to determine the absorption--desorption characteristics of select shield and spacer materials.

(4) Summary

Insulation System No. 1 gave a heat flux of .62 Btu/hr-ft^2 with liquid nitrogen and .66 Btu/hr-ft^2 with liquid hydrogen. Our interpretations of this data indicate that the radiation component of heat flux is approximately .46 Btu/hr-ft^2 and the conduction component is about .16 Btu/hr-ft^2. The estimated radiation component alone is greater than the total flux (0.38 Btu/hr-ft^2) measured under the previous contract. Some degradation of the multi-layer properties is known to have taken place prior to all the current measurements which accounts, at least in part, for the higher current values of heat flux.

The integrated heat flux of the multi-layer obtained during a simulation entry into space was greater for helium gas purge than for a nitrogen gas purge. This is contrary to the expected result and should be investigated further in other multi-layer systems.

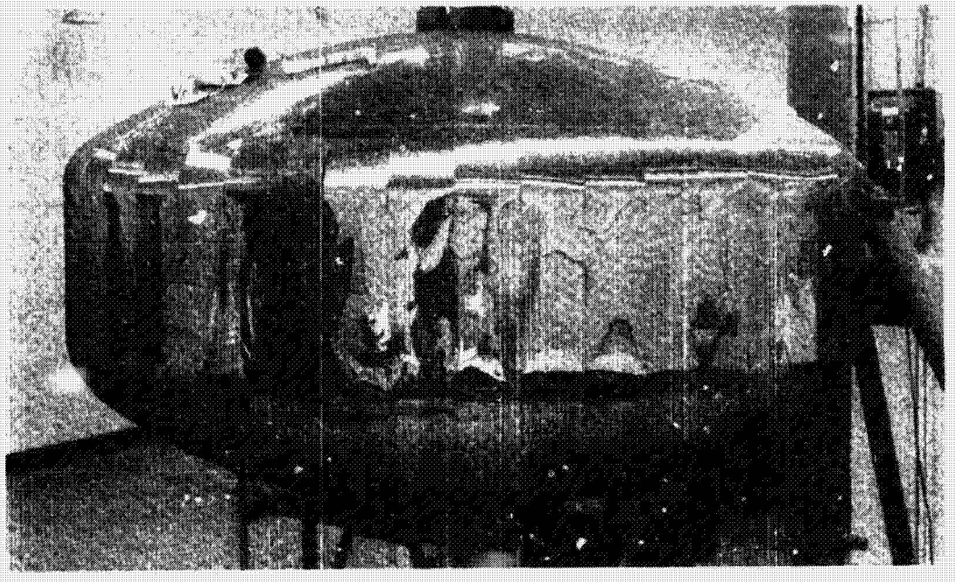

(a) Calorimeter Side

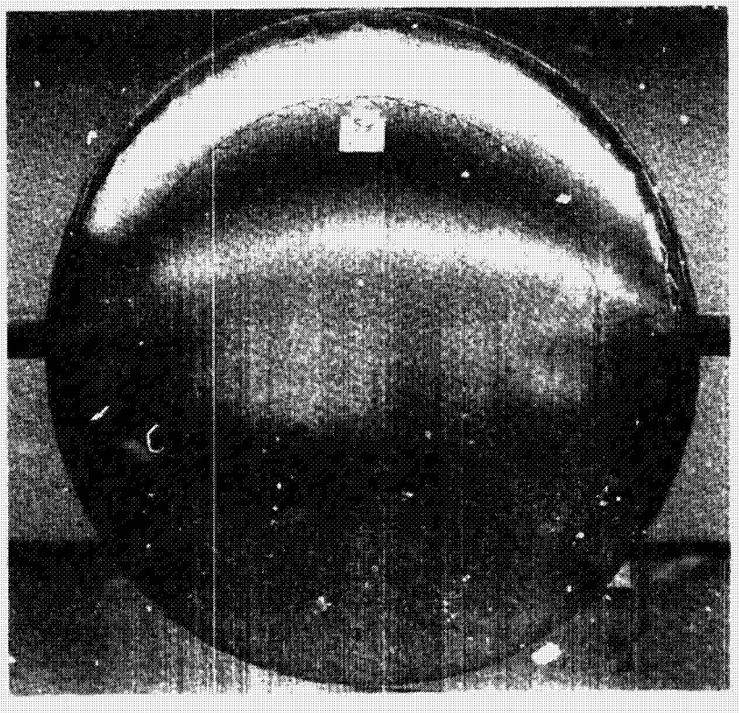

(b) Calorimeter Bottom

FIGURE III-2 NO. 4 ALUMINUM FOIL AND NO. 5 SPACER NETTING

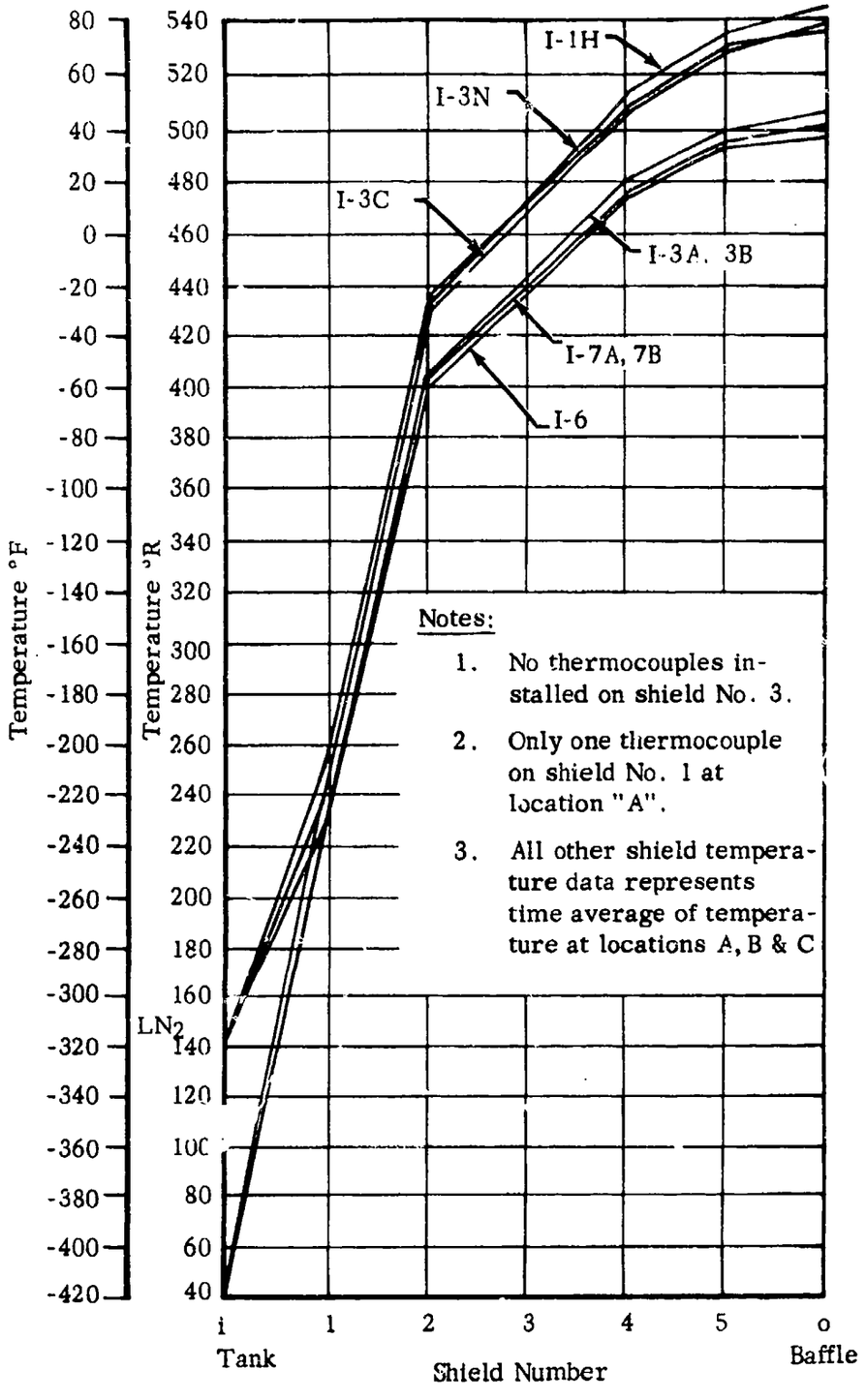

FIGURE III-3 INSULATION SYSTEM NO. 1, TYPICAL MULTI-LAYER TEMPERATURE DISTRIBUTION

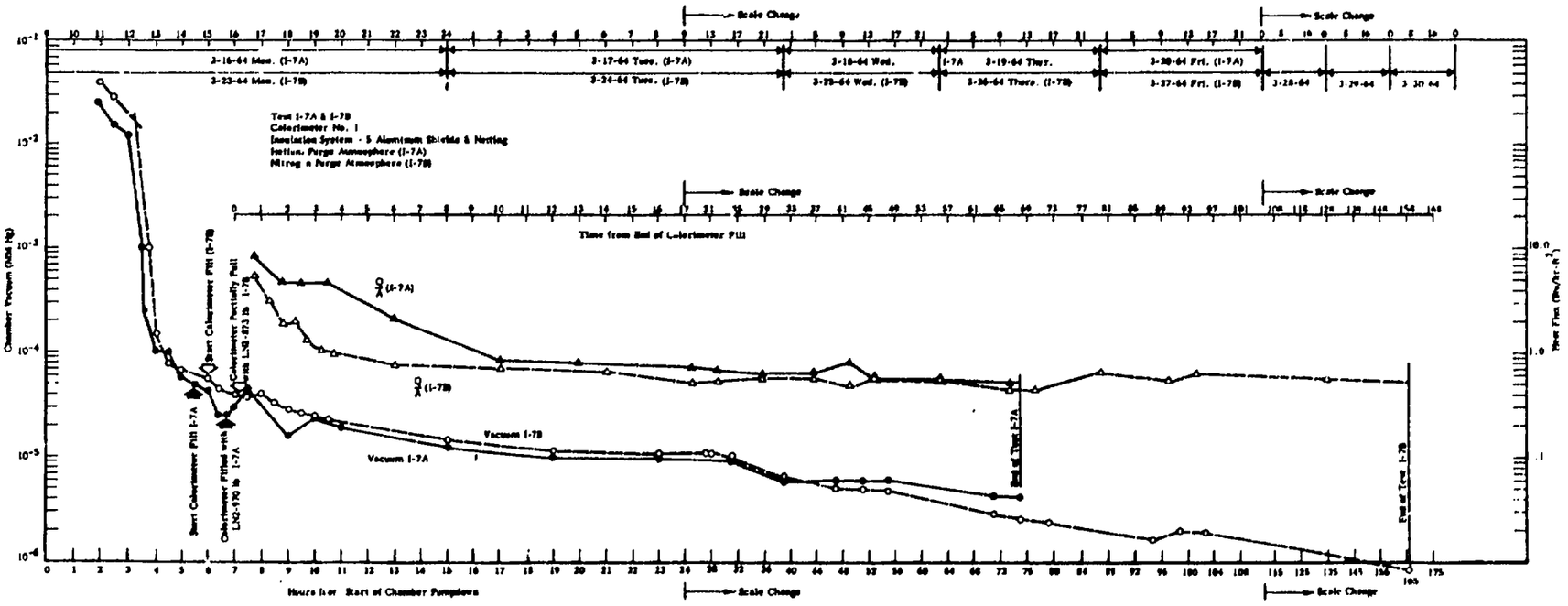

FIGURE III-4 INSULATION SYSTEM NO. 1-VACUUM AND HEAT FLUX DATA ON FIVE ALUMINUM SHIELDS, TEST 1-7A HELIUM PURGE ATMOSPHERE-TEST 1-7B NITROGEN PURGE ATMOSPHERE

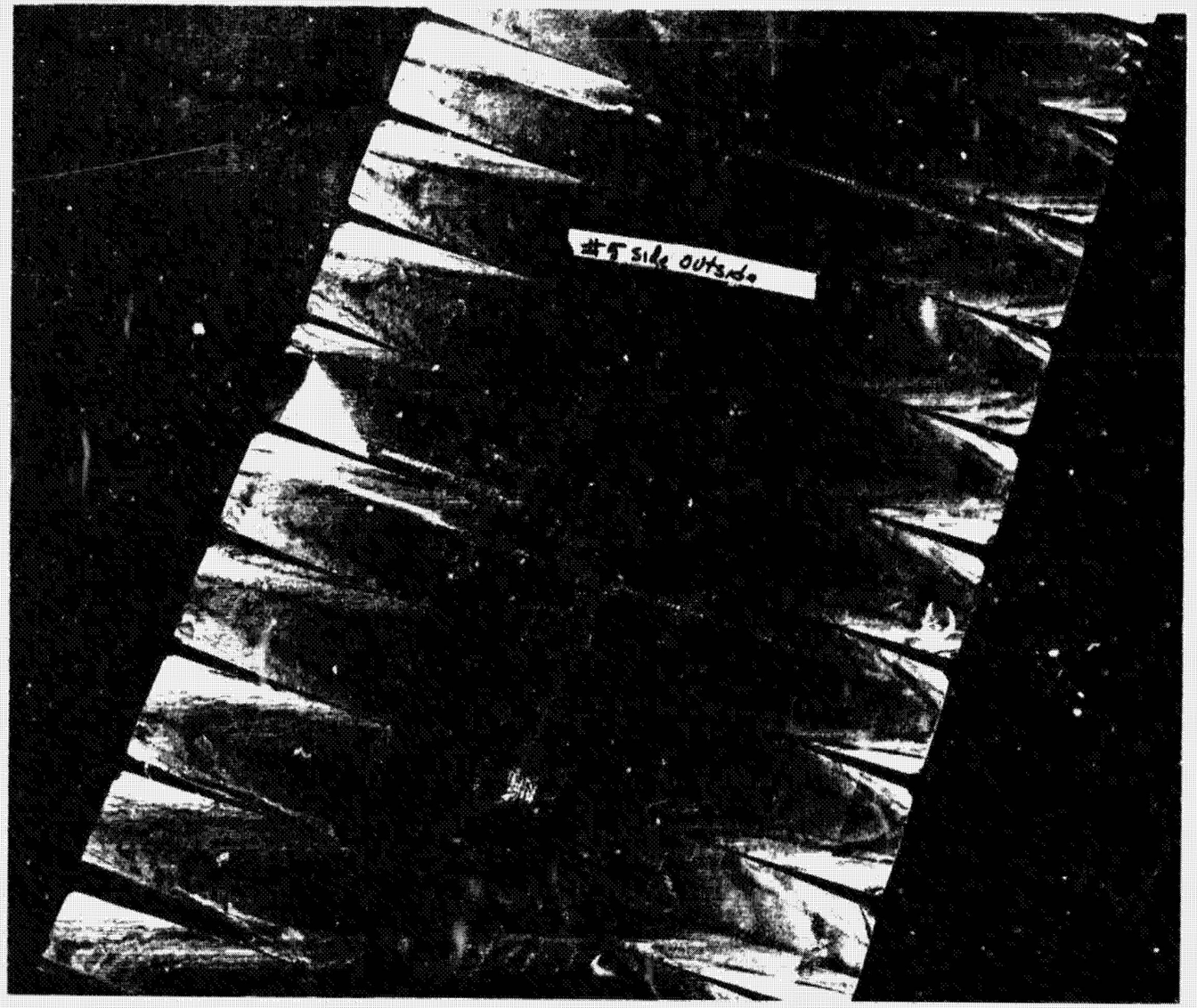

FIGURE III-5 INSULATION SYSTEM NO. 1 - NO. 5 SIDE SHIELD, OUTSIDE

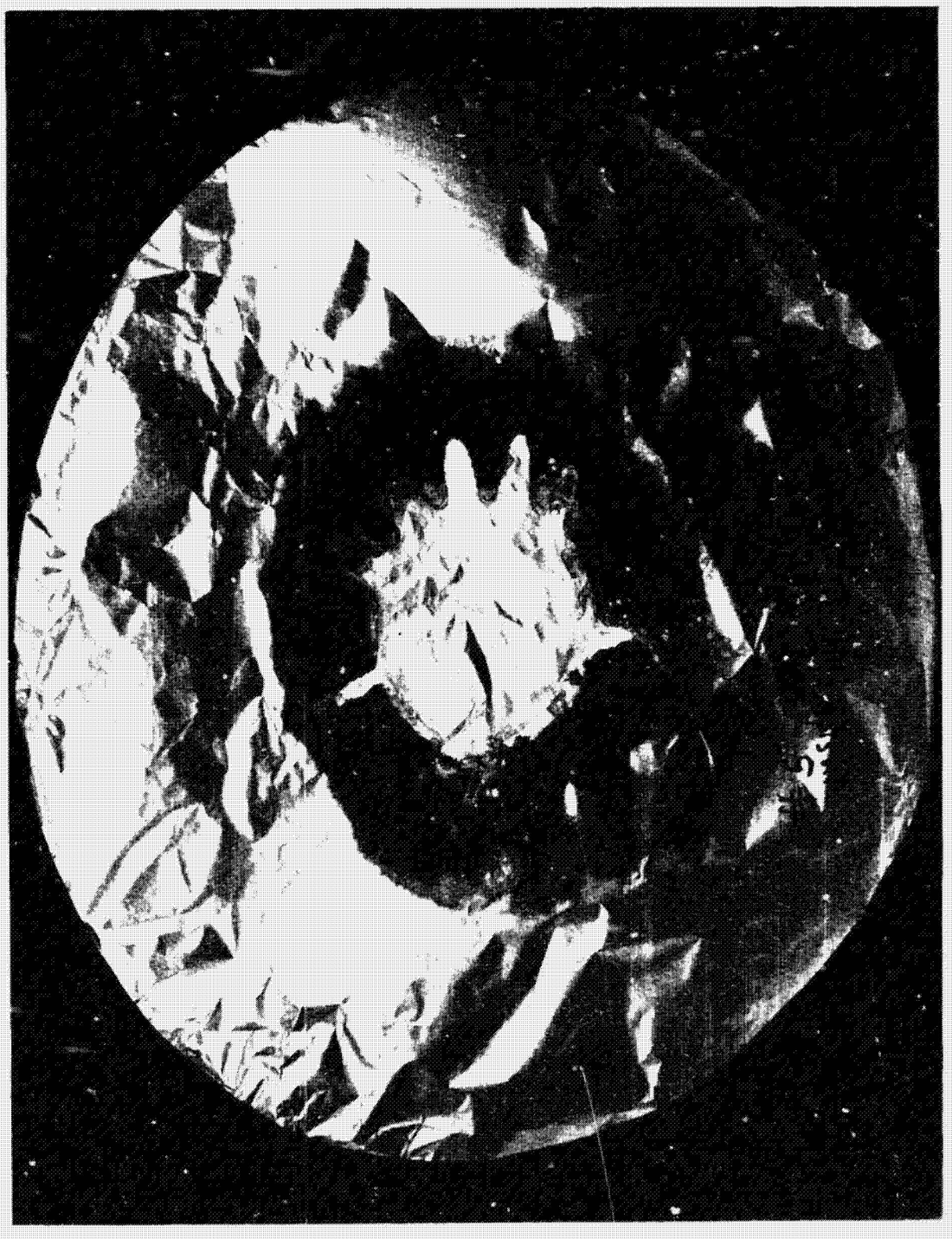

FIGURE III-7 INSULATION SYSTEM NO. 1 - NETTING BETWEEN NOS. 5 AND 4 SHIELD

TABLE III- 3

TANK INSULATION PROGRAM

TEST SUMMARY - INSULATION SYSTEM NO. 1 - CALORIMETER NO. 1 - TEST I-3

Insulation System: Five aluminum radiation shields, .002 inch thick spaced with six 1/8 x 1/8-inch mesh, vinyl coated, fiberglas screen .020 inch thick.

Test Facility: Lewis Research Center/Plum Brook Station, J-3 Facility.

Penetration and/or gaps: None

Boundary Condition: Cold boundary and warm boundary are variable as shown below.

Emissivity: Cold boundary .88 - warm boundary .93

Tank Surface Area: 38.14 ft^2

Test	Tank Liquid	Data Period Date&Time	to Date&Time	Test Duration (hrs)	Av. Vac. (mmHg)	Guard Liq/Temp (^oF)	Total Heat Flow (BTU/hr)	Measured Av. Heat Flux (BTU/hr ft^2)	Av. Baffle Temp (^oF) Upper	Lower	Adjusted[1] Heat Flux (BTU/hr ft^2)
I-3A	LH_2	12-21/2305	12-22/0907	10.03	$1.0x10^{-6}$	LH_2/-419	19.59	0.514	48	48	0.65
I-3B	LH_2	12-22/1700	12-23/0800	15.00	$1.0x10^{-6}$	LH_2/-419	19.78	0.518	47	47	0.66
I-3C	LH_2	1-20/2200	1-22/1000	36.00	$2.0x10^{-6}$	LN_2/-308	28.59[3]	0.749	81	81	0.74
I-3N-1	LN_2	1-23/1800	1-25/0800	38.00	$1.0x10^{-6}$	LN_2/-308	23.10	0.606	79	79	0.61
I-3N-2	LN_2	1-27/1600	1-28/0800	16.00	$6.0x10^{-7}$	LN_2/-308	24.17	0.633	80	80	0.63
I-3D-1	LH_2	1-30/2300	1-31/1000	11.00	$5.0x10^{-7}$	LH_2/-418	27.30	0.715	78	78	0.72[2]
I-3D-2	LH_2	1-31/1100	1-31/2400	13.00	$5.5x10^{-7}$	LH_2/-418	25.10	0.658	78	78	0.65
I-3D-3	LH_2	2-1/1100	2-2/0300	16.00	$4.5x10^{-7}$	LH_2/-418	25.28	0.664	79	79	0.66
I-3D-4	LH_2	2-2/1600	2-3/0800	16.00	$2.5x10^{-7}$	LN_2/-308	25.67[3]	0.675	79	79	0.67

NOTES:

1. Measured heat flux adjusted to standard conditions for 80°F warm boundary and -320°F cold boundary.

2. Calorimeter fill line not disconnected during this period - very likely to be erroneous indication.

3. Neck heat leak due to operation of cold guard at liquid nitrogen temperatures, was estimated at 1.68 Btu/hr and deducted from total heat leak to give this value. This value includes both the effect of heat condition from the cold guard to the tank and the effect of heat transfer from the neck to the boil-off gases.

TANK INSULATION PROGRAM

TEST SUMMARY - INSULATION SYSTEM NO. 1 - CALORIMETER NO. 1 - TEST NO. I-6

Insulation System: Five aluminum radiation shields, .002 inch thick spaced with six 1/8 x 1/8-inch mesh, vinyl coated Fiberglas screen .020 inch thick.

Test Facility: ADL/Cambridge Test Facility

Penetration and/or gaps: None

Boundary Condition: Cold boundary and warm boundary are variable as shown below.

Emissivity: Cold boundary .88 - warm boundary .93

Tank Surface Area: 38.14 ft^2

Test Period No.	Tank Liquid	Data Period		Test Duration (hrs)	Av. Vac. (mmHg)	Guard Liq/Temp (^oF)	Total Heat Flow (BTU/hr)	Measured Av. Heat Flux[2] (BTU/hr ft^2)	Av. Baffle Temp (^oF)		Adjusted[1] Heat Flux (BTU/hr ft^2)
		Date&Time	to Date&Time						Upper	Lower	
1[2]	LN_2	3-7/0830	2-9/0830	48.0	1.2×10^{-6}	-311	16.1	0.422	37	37	0.590
2	LN_2	3-9/0830	3-10/0830	24.0	1.7×10^{-6}	-311	17.9	0.472	38	38	0.653
3	LN_2	3-10/0830	3-11/0830	24.0	1.5×10^{-6}	-311	17.7	0.465	38	38	0.643
4	LN_2	3-11/0830	3-12/0830	24.0	1.7×10^{-6}	-311	16.7	0.440	38	38	0.608

Time weighted average heat flow = 16.9 BTU/hr

Time weighted average adjusted heat flux = 0.615 BTU/hr ft^2

NOTES:

1. Measured heat flux adjusted to standard conditions for 80°F warm boundary and -320°F cold boundary.
2. Calculations were made starting at period no. 1 which was approximately 20 hours after filling the calorimeter.

TABLE III - 5

TANK INSULATION PROGRAM

TEST SUMMARY - INSULATION SYSTEM NO. 1 - CALORIMETER NO. 1 - TEST NO. I-7A

Insulation System: Five aluminum radiation shields, .002 inch thick spaced with six 1/8 x 1/8-inch mesh, vinyl coated, Fiberglas screen .020 inch thick.

Test Facility: ADL/Cambridge Test Facility

Purging Medium: Helium gas

Penetration and/or gaps: None

Boundary Condition: Cold boundary and warm boundary are variable as shown below:

Emissivity: Cold boundary .88 - warm boundary .93

Tank Surface Area: 38.14 ft^2

Test Period No.	Tank Liquid	Data Period Date&Time	to Date&Time	Test Duration (hrs)	Av. Vac. (mmHg)	Guard Liq/Temp (^oF)	Total Heat Flow (BTU/hr)	Measured Heat Flux ($BTU/hr\ ft^2$)	Av. Baffle Temp (^oF) Upper	Lower	Adjusted[1] Heat Flux ($BTU/hr\ ft^2$)
1	LN_2	3-16/1600	3-16/1730	1.50	$5.5x10^{-6}$	-311	227.0	5.970	39	39	8.200
2	LN_2	3-16/1730	3-16/1810	0.66	$5.0x10^{-6}$	-311	131.2	3.450	39	39	4.740
3	LN_2	3-16/1810	3-16/1900	0.83	$5.0x10^{-6}$	-311	126.8	3.340	39	39	4.580
4	LN_2	3-16/1900	3-16/2000	1.00	$4.5x10^{-6}$	-311	129.4	3.410	39	39	4.680
5	LN_2	3-16/2000	3-16/2400	4.00	$3.5x10^{-6}$	-311	55.9	1.580	39	39	2.170
6	LN_2	3-16/2400	3-17/0400	4.00	$2.0x10^{-6}$	-311	24.3	0.637	40	40	0.868
7	LN_2	3-17/0400	3-17/0800	4.00	$2.0x10^{-6}$	-310	22.4	0.587	40	40	0.800
8	LN_2	3-17/0800	3-17/1200	4.00	$2.0x10^{-6}$	-310	20.0	0.525	40	40	0.715

(cont'd)

TABLE III - 5 ' (cont'd)

TANK INSULATION PROGRAM

TEST SUMMARY - INSULATION SYSTEM NO. 1 - CALORIMETER NO. 1 - TEST NO. 1-7A

Test Period No.	Tank Liquid	Date&Time	to Date&Time	Test Duration (hrs)	Av. Vac. (mmHg)	Guard Liq/Temp (^{o}F)	Total Heat Flow (BTU/hr)	Measured Heat Flux (BTU/hr ft^2)	Av. Baffle Temp (^{o}F) Upper	Lower	Adjusted[1] Heat Flux (BTU/hr ft^2)
9	LN_2	3-17/1200	3-17/1600	4.00	2.0×10^{-6}	-310	19.0	0.498	40	40	0.678
10	LN_2	3-17/1600	3-17/2400	8.00	1.5×10^{-6}	-310	17.6	0.461	40	40	0.628
11	LN_2	3-17/2400	3-18/0830	8.50	1.0×10^{-6}	-310	17.9	0.469	40	40	0.639
12	LN_2	3-18/0830	3-18/1200	3.50	1.0×10^{-6}	-310	22.7	0.597	40	40	0.815[3]
13	LN_2	3-18/1200	3-18/1600	4.00	1.0×10^{-6}	-310	15.7	0.412	40	40	0.560
14	LN_2	3-18/1600	3-19/0800	16.00	1.0×10^{-6}	-310	15.4	0.405	40	40	0.552
15	LN_2	3-19-0800	3-19-1200	4.00	8.5×10^{-7}	-310	14.6	0.384	40	40	0.522

Time weighted average heat flow for periods 9 thru 15[2] = 17.0 BTU/hr.

Time weighted average adjusted heat flux for periods 9 thru 15[2] = 0.607 BTU/hr ft^2.

NOTES:

1. Measured heat flux adjusted to standard conditions for 80^{o}F warm boundary and -320^{o}F cold boundary
2. Average taken on the periods following the stabilization period (approximately 20 hrs. after filling the calorimeter)
3. During this period a rapid rise in barometric pressure occurred; otherwise the marked difference in heat flux is unaccountable at this time.

TABLE III - 6

TANK INSULATION PROGRAM

TEST SUMMARY - INSULATION SYSTEM NO. 1 - CALORIMETER NO. 1 - TEST NO. I-7B

Insulation System: Five aluminum radiation shields, .002 inch thick spaced with six 1/8 x 1/8-inch mesh, vinyl coated, Fiberglas screen .020 inch thick.

Test Facility: ADL/Cambridge Test Facility

Purging Medium: Nitrogen Gas

Penetration and/or gaps: None

Boundary Condition: Cold boundary and warm boundary are variable as shown below.

Emissivity: Cold boundary .88 - warm boundary .93

Tank Surface Area: 38.14 ft^2

Test Period No.	Tank Liquid	Data Period Date&Time	to	Date&Time	Test Duration (hrs)	Av. Vac. (mmHg)	Guard Liq/Temp (^oF)	Total Heat Flow (BTU/hr)	Measured Av. Heat Flux ($BTU/hr\ ft^2$)	Av. Baffle Temp (^oF) Upper	Lower	Adjusted[1] Heat Flux ($BTU/hr\ ft^2$)
1	LN_2	3-23/1630		3-23/1700	0.50	$4.0x10^{-5}$	-309	158.0	4.140	43	43	5.500
2	LN_2	3-23/1700		3-23/1730	0.50	$4.0x10^{-5}$	-309	90.0	2.360	44	44	3.120
3	LN_2	3-23/1730		3-23/1800	0.50	$3.0x10^{-5}$	-309	54.1	1.420	43	43	1.890
4	LN_2	3-23/1800		3-23/1830	0.50	$3.0x10^{-5}$	-309	56.2	1.470	42	42	1.970
5	LN_2	3-23/1830		3-23/1900	0.50	$2.5x10^{-5}$	-309	39.3	1.030	42	42	1.380
6	LN_2	3-23/1900		3-23/1930	0.50	$2.5x10^{-5}$	-309	30.8	0.806	42	42	1.080
7	LN_2	3-23/1930		3-23/2000	0.50	$2.5x10^{-5}$	-310	28.5	0.747	42	42	1.000
8	LN_2	3-23/2000		3-23/2400	4.00	$2.0x10^{-5}$	-311	21.8	0.572	41	41	0.773
9	LN_2	3-23/2400		3-24/0400	4.00	$1.5x10^{-5}$	-312	20.0	0.524	40	40	0.714
10	LN_2	3-24/0400		3-24/0800	4.00	$1.0x10^{-5}$	-313	17.6	0.461	40	40	0.628
11	LN_2	3-24/0800		3-24/1200	4.00	$1.0x10^{-5}$	-314	14.3	0.374	41	41	0.506

(cont'd)

TABLE III - 6 (cont'd)

TANK INSULATION PROGRAM

TEST SUMMARY - INSULATION SYSTEM NO. 1 - CALORIMETER NO. 1 - TEST I-7B

Test Period No.	Tank Liquid	Data Period Date&Time	to Date&Time	Test Duration (hrs)	Av. Vac. (mmHg)	Guard Liq/Temp (^{o}F)	Total Heat Flow (BTU/hr)	Measured Av. Heat Flux[2] (BTU/hr ft^2)	Av. Baffle Temp (^{o}F) Upper	Lower	Adjusted[1] Heat Flux[2] (BTU/hr ft^2)
12	LN_2	3-24/1200	3-24/1600	4.00	1.0×10^{-5}	-311	15.1	0.395	42	42	0.530
13	LN_2	3-24/1600	3-24/2400	8.00	1.0×10^{-5}	-307	16.5	0.433	42	42	0.581
14	LN_2	3-24/2400	3-25/0800	8.00	5.0×10^{-6}	-305	15.8	0.415	42	42	0.567
15	LN_2	3-25/0800	3-25/1200	4.00	5.0×10^{-6}	-306	5.9	0.367	43	43	0.488
16	LN_2	3-25/1200	3-25/1600	4.00	5.0×10^{-6}	-309	18.0	0.470	44	44	0.620
17	LN_2	3-25/1600	3-26/0800	16.00	4.0×10^{-6}	-310	16.5	0.432	44	44	0.570
18	LN_2	3-26/0800	3-26/1200	4.00	3.0×10^{-6}	-311	13.2	0.346	44	44	0.457
19	LN_2	3-26/1200	3-26/1600	4.00	2.5×10^{-6}	-311	13.0	0.341	44	44	0.450
20	LN_2	3-26/1600	3-27/0800	16.00	2.0×10^{-6}	-310	18.8	0.492	44	44	0.650
21	LN_2	3-27/0800	3-27/1200	4.00	2.0×10^{-6}	-309	17.2	0.451	44	44	0.595
22	LN_2	3-27/1200	3-27/1600	4.00	2.0×10^{-6}	-309	18.9	0.497	44	44	0.656
23	LN_2	3-27/1600	3-30/0800	64.00	1.0×10^{-6}	-309	17.5	0.460	44	44	0.607

Time weighted average heat flow for periods 12 thru 23[2] = 16.7 Btu/hr.
Time weighted average adjusted heat flux for periods 12 thru 23[2] = 0.592 BTU/hr ft^2.

NOTES:

1. Measured heat flux adjusted to standard conditions for 80^{o}F warm boundary and -320^{o}F cold boundary.
2. Average taken on the periods following the stabilization period (approximately 20 hours after filling the calorimeter)

TABLE III-7

SUMMARY - FACILITY CALIBRATION HEAT FLUX

Test No.	Test Location	Test Duration (hrs)	Test Fluid	Adjusted Heat Flux BTU/hr ft^2
I-1[1]	ADL	36	Nitrogen	.33
I-3A	J-3	10	Hydrogen	.65
I-3B	"	15	"	.66
I-3D-2	"	13	"	.65
I-3D-3	"	16	"	.66
I-3N-1	"	38	Nitrogen	.61
I-3N-2	"	16	"	.63
I-6	ADL	120	"	.62
I-7A	"	48	"	.61
I-7B	"	140	"	.59

1. Test I-1 performed under Contract NASw-615.

TABLE III-8

SUMMARY EMISSIVITY DATA

INSULATION SYSTEM NO. 1 SHIELD

Sample	Side Measured	Date	Emissivity
Corroded foil from shield of	Non-corroded	2 June 1964	0.0470
Insulation System No. 1	Non-corroded	1 May 1964	0.0501
2 mil 1100-0 grade aluminum	Corroded	12 May 1964	0.860
Foil from calorimeter shield #1	Shiny	4 May 1964	0.0459
This sheet is not corroded 2 mil	Shiny	1 June 1964	0.0379
1100-0 grade aluminum			
Non-corroded foil from shield #5	Dull	12 May 1964	0.0355
This sample was taken from an	Dull	29 May 1964	0.0349
area immediately adjacent to a			
corroded area. (Note: the foil			
has a dull and a shiny side. The			
corrosion was on the dull side.)			
2 mil 1100-0 grade aluminum.			
Hard aluminum foil. (both sides	A	28 May 1964	0.0346
are shiny) Sample was taken from a	B	29 May 1964	0.0338
roll of new foil. 2 mil			
1145-H19 aluminum			
Aluminum foil 0.0005 in. thick,	Shiny	28 May 1964	0.0348
1100-0 grade (had a shiny and a			
dull side)			
Same type as used on shields	Shiny	29 May 1964	0.0362
Nos. 1 & 5. However, the sample	Dull	2 June 1964	0.0334
was taken from the middle of an			
unused roll. 2 mil 1100-0 grade			
aluminum			

Insulatic System No. 2

a. Introduction

Insulation System No. 2 consisted of five shields of polyester film, ¼ mil thick, coated with aluminum on the outside, and six spacers of 1/8 x 1/8-inch mesh vinyl-coated Fiberglas screen. It was fabricated onto No. 2 Calorimeter in July, 1963, under contract NASw-615. The thermal performance of the insulation was measured both under contract NASw-615 and the current contract.

The objective in testing this system was to establish the performance of the lighter weight coated film materials. Although System No. 1 was constructed using 2 mil aluminum foil, multi-layer systems used in ground based dewars have been successfully fabricated using 1/4 mil aluminum . However, 1/4 mil value represents about the lower limit in thickness with regards to the manufacture and handling of these foils. By comparison, 1/4 mil polyester film is about one-half the weight of aluminum in comparable thickness and, further, it is stronger and tears less easily than aluminum foil. In addition, lighter gauges of polyester film are available for use in multi-layer insulations.

Coated polyester films have a low thermal conductivity in a direction parallel to the film. This is a consequence of the fact that aluminum, the highly thermal conducting member of the coated films, is extremely thin (approximately 275 Å). The small metal cross section limits the heat flow in the coating. A lower conductance gives better system performance when penetrations must be placed into the multi-layer system.

b. Insulation System Description

As previously indicated, this insulation system was fabricated onto Calorimeter No. 2 under contract NASw-615. Details of its construction have, therefore, been previously reported[1]. The principal characteristics of the system are summarized here in Table III-1 and views of the side and bottom of the insulation are presented in Figure III-8.

c. Test Conditions

The heat flux measurements performed with Insulation System No. 2 are presented in Table III-9. In tests I-4A thru 4D an average adjusted value of heat flux for the entire insulation of 1.02 Btu/hr-ft^2 was measured. In test I-4E a flux value of 1.07 Btu/hr-ft^2 was obtained for the lower-half of the insulation system. These values compare with a value of 1.10 Btu/hr-ft^2 obtained in a similar measurement made in Test I-2 with the same system during the previous contract period.

Typical values of the measured temperature distribution in the insulation are presented in Figure III-9. The values shown are the average of three temperatures measured at the A, B, and C locations (see Figure III-1C) on each shield.

d. Results and Discussion

The results obtained with No. 2 insulation system indicate that, with a comparable number of shields and spacers, the aluminum-coated polyester film is less effective than the aluminum shields by a factor of 1 to 2.5 based on the measured heat flux. The higher flux could be due to a large amount of conduction taking place between the shield and spacers, or to poor shield surface emissivities or both. We, therefore, undertook to evaluate the data by making subsequest measurements of the shield properties using the Emissometer and infrared spectrophotometer instruments. In addition, we made use of the experimental temperature distribution in the shields to estimate surface emittance.

Based on the boundary temperatures of the insulation system and on the average heat flux obtained in tests I-4A thru 4D we computed a value of .087 for the average emissivity of each surface of each shield of the multi-layer system. In this computation we assumed that the aluminized and unaluminized surfaces of each shield were of the same value. Further we assumed that the emissivity was independent of shield temperature.

Through use of the ADL Emissometer we measured the emittance of the aluminized and unaluminized surface of the polyester film at

a temperature of about 93°F. The uncoated side gave an emittance value g 0.36. The opposite side, coated with aluminum to a thickness of about 275 Å, resulted in an emittance value of .047 (see Emissometer, Section IV, for tests performed 5-5-64.) A comparison of these values indicate that each shield has a single high performance (low emittance value) surface.

Using these measured emittance values for the appropriate surfaces of each shield, we computed a pure radiation heat flux of .97 Btu/hr-ft^2 for the insulation with the boundary temperature conditions prevailing in test I-4A-D. This result is greater than the measured (not adjusted) flux of 0.80 Btu/hr-ft^2 by about 20 per cent. The significance of this result is that the emittances of the insulation No. 2 shields are probably lower than those measured with the ADL emissometer.

The experimental shield temperatures shown in the Figure III-9 are compared with computed values. These computed temperatures have been determined after the manner illustrated in Appendix 2 using the two emissometer values of shield emittance. From this comparison, it is evident that there is fair argument between experimental and computed temperatures in the outer four shields. However, the experimental temperature of shield No. 1 is about 65°F greater than the computed value. This would indicate that the true emittance of the surface on shield No. 1 facing the tank is less than the value of 0.36 used in the computed temperature; i.e., less than the value measured with the emissometer at 93°F.

Emittance measurements cannot be made with the emissometer at the 180°R temperature level. It was necessary, however, to obtain qualitative information on the low temperature emittance of polyester film to corroborate the temperature data. This was accomplished through the use of an infrared spectrophotometer. There are several significant differences between these two measurement methods that should be mentioned. The emissometer measures the total hemispherical emittance integrated with respect to radiation wavelength. The spectrophotometer measures the specular transmission as a function of radiation

wavelength. This latter measurement is related to the absorptance in accordance with the equation $\alpha + \rho + \tau = 1$ and to the emissivity by the identity $\alpha = \varepsilon$ where α = absorptivity

ρ = reflectivity

τ = transmissvity

ε = emissivity

The measured transmittance of ¼ mil polyester film is shown in Figure III-10. The range of wavelengths covered are from 2.5 to 40 microns. The ordinate represents the ratio of the transmitted to insident radiation on the sample. The values of this ratio versus wavelength are summarized from the actual experimental data to produce a "block" presentation. Superimposed on this data is the block body radiation intensity spectra at 540 and 180°R. The ordinate for these data is ratio of the block body radiation at any wavelength to the peak block body radiation at the indicated temperature.

Based upon the information presented in Figure III-10, it is evident that the polyester film has several low transmission bands in regions where 540°R block body radiation intensity is large. These low transmission bands are also equated to high absorptivity and high emissivity bands. In the range of wavelengths where the 180°R block body radiation is greatest there are no similarly intense emissivity bands present. Except for the bands in the 5 to 14 micron range, the transmission averages about 0.8 in all other regions.

From the above, it is concluded that the emittance of the uncoated surface of shield No. 1 is very probably lower at the 180°R temperature level than at the 540 or temperature level. Based upon the temperature and heat flux data obtained in Tests I-4A-D, a value of emissivity of .08 is inferred for this surface. This value is considerably less than the emissometer value of 0.36 and, therefore, should be confirmed further in other experiments.

e. Summary

1. For the aluminum-coated polyester films used on the tank system, the coated side has an emissivity value in the range .04-.05.

The uncoated side has a value of approximately .36 at near room temperature and a smaller value at temperatures less than about 300°F.

2. The experimental heat flux was slightly lower than a theoretical flux based on experimental shield surface emittances obtained with the emissometer. In view of the uncertainties such as solid conduction and the variation of shield emissivity with temperature, the agreement between the two is, however, good.

(a) Calorimeter Side

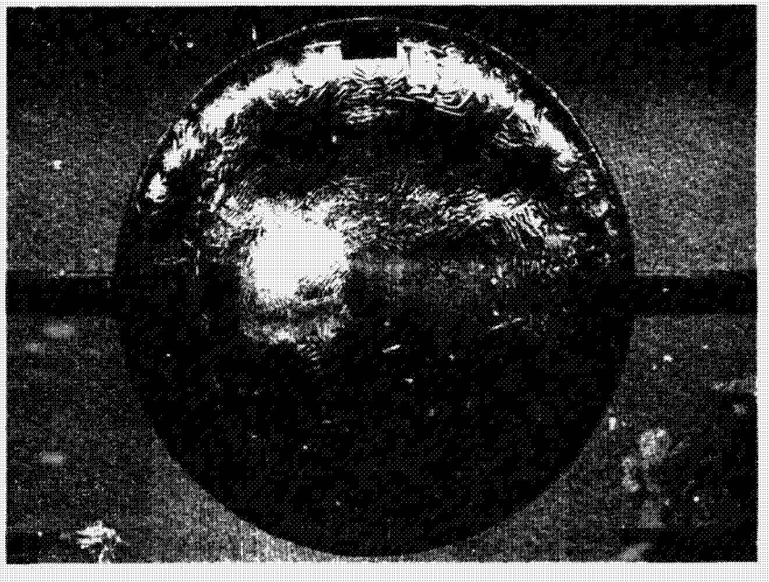

(b) Calorimeter Bottom

FIGURE III-8 ALUMINIZED-POLYESTER FILM NO. 5 FOIL AND NO. 6 SPACER NETTING

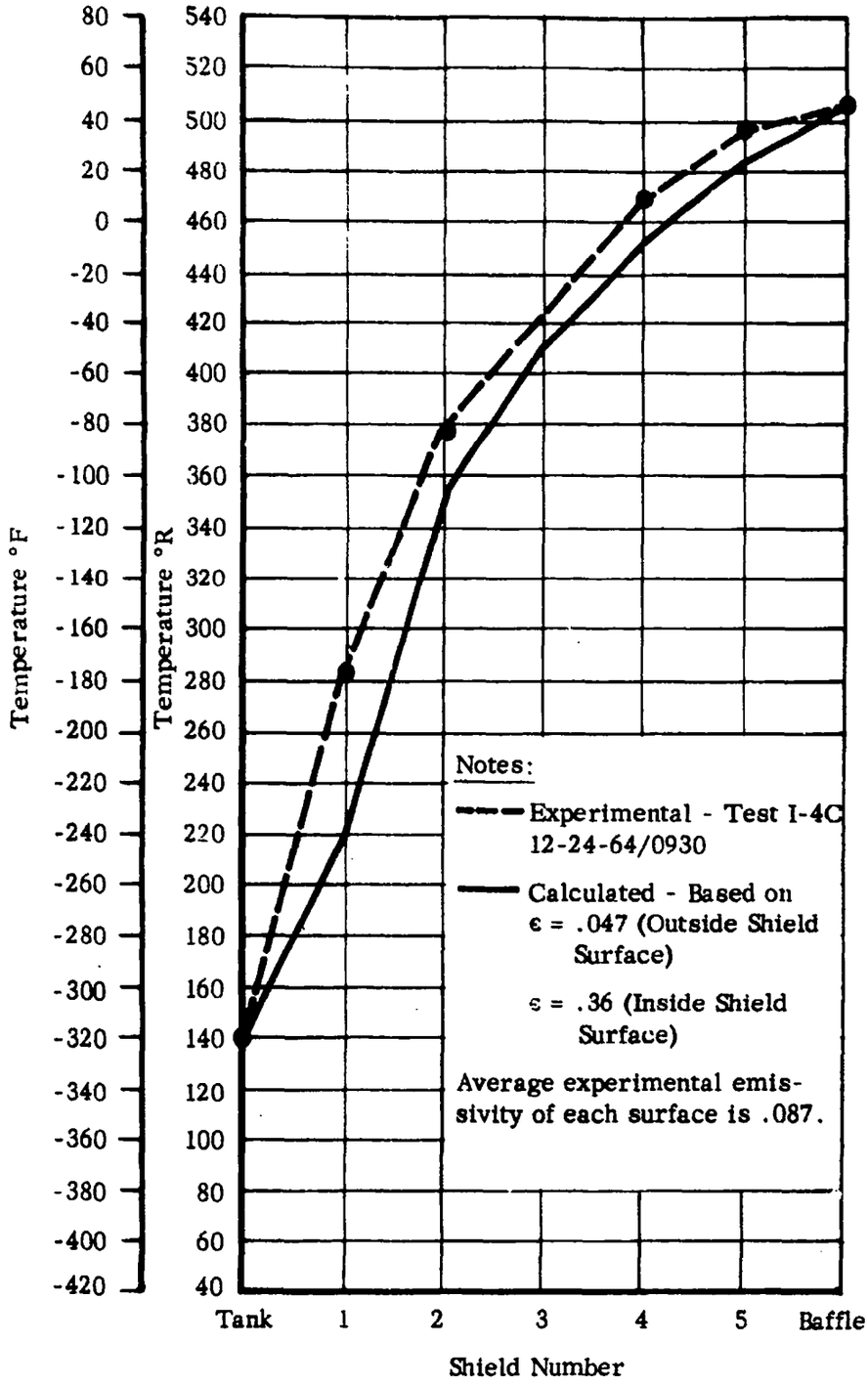

FIGURE III-9 INSULATION SYSTEM NO. 2, TYPICAL MULTI-LAYER TEMPERATURE DISTRIBUTION

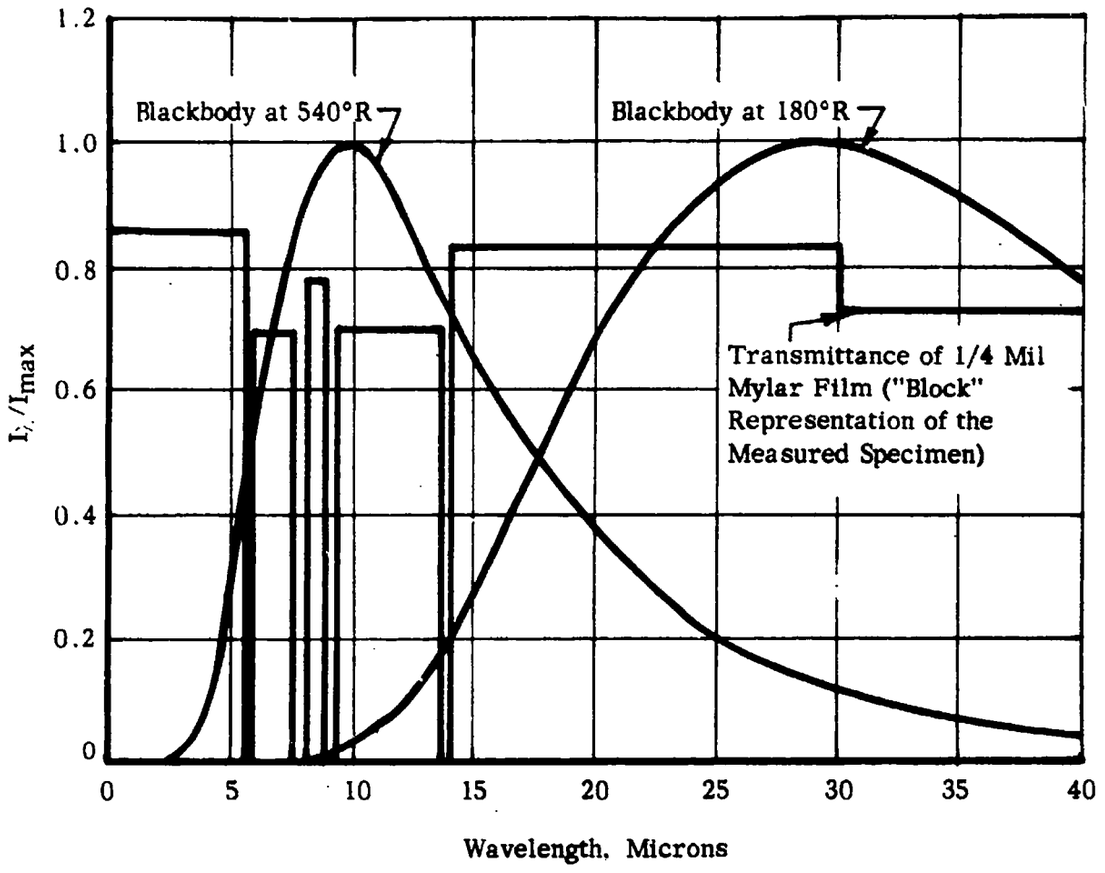

FIGURE III-10 TRANSMISSION CHARACTERISTICS OF 1/4 MIL POLYESTER FILM, 0-40 MICRONS

TABLE III-9

TANK INSULATION PROGRAM

TEST SUMMARY - INSULATION SYSTEM NO. 2

Insulation System:	Five aluminized polyester film (NRC) radiation shields, .00025 inches thick spaced with six 1/8 x 1/8-inch mesh, vinyl coated, Fiberglas screen .020 inches thick. Uncrinkled polyester film placed on tank with aluminized surface facing warm boundary.
Test Facility:	Arthur D. Little, Inc., Cambridge, Massachusetts
Penetrations and/or Gaps:	None.

Boundary Conditions:	Cold Boundary	Warm Boundary
Temperature (ave)	-320F	48 and -.88F
Emissivity	.88	.93

Tank Surface Area: 39.45 ft^2

Test	Data Period Date&Time	to Date&Time	Test Duration (hrs)	Average Vac(mmHg)	Guard Temp(^oF)	Total Heat Flow(BTU/hr)	Measured Heat Flux (BTU/hr ft^2)	Av. Baffle Temp.(^oF) Upper	Lower	Adjusted[2] Heat Flux (BTU/hr ft^2)
I-4A	12-20/1015	12-23/0830	70.25	$.3 \times 10^{-5}$	-315	32.1	.811	48	48	1.03
I-4B	12-23/0830	12-24/0930	25.00	$.4 \times 10^{-5}$	-315	31.9	.809	48	48	1.03
I-4C	12-24/0930	12-26/0830	47.00	$.4 \times 10^{-5}$	-315	31.24	.792	48	48	1.01
I-4D	12-26/0830	12-27/0900	24.50	$.35 \times 10^{-5}$	-315	31.22	.792	48	48	1.01
I-4E	12-30/1630	12-31/1430	22.00	$.13 \times 10^{-5}$	-315	16.45	.84[1]	-320	47	1.07[1]

NOTES:

1. Total heat flow into calorimeter assumed to pass through one-half surface area of insulation.
2. Measured heat flow adjusted to standard conditions for warm boundary temperature of 80°F.

Insulation System No. 3

a. Introduction

A copper penetration was placed on the bottom head of Calorimeter No. 2 along the tank axis, into the existing No. 2 Insulation System. It consisted of copper washers and a washer clamp and formed a penetration 3 inches in diameter which was placed in good thermal contact with the tank. (4) With this modification, the new system became identified as Insulation System No. 3.

The copper penetration was designed to introduce a strong thermal short into the multi-layer system that could be evaluated analytically and experimentally. The increase in the heat rate to the calorimeter produced by the penetration, coupled with the shield temperature gradients, could then be used to test and verify analytical techniques for similar type penetrations. (4)

b. Copper Penetration

The copper penetration was placed in the insulation system at the center of the bottom head of the No. 2 Calorimeter. This was accomplished through the use of copper washers 0.035 inches thick which are used to clamp each shield individually. As shown in Figure III-11, the washers are clamped at the center on a stud welded to the tank so that each washer becomes thermally shorted to the tank. The shields are separately clamped with a brass slug, to assure that they are in thermal contact with the copper washers along the 3 inch periphery. Copper used in the penetration because of its high thermal conductivity. The entire penetration is then maintained at the tank, thus establishing the boundary temperature of the shields at the periphery of the penetration.

The penetration was installed into the existing insulation system by cutting away portions of the shields and netting as shown in Figure III-12. As the washers were installed, a portion of the shield material was lapped over the copper washer as shown in Figure III-13. Figure III-14 shows the completed installation, and additional details are shown in Figure III-11.

To assess properly the performance of the penetration, we required the temperature distribution in the outer foil at the vicinity of the penetration. This data was obtained with thermocouples located as shown in Figure III-15.

Additional thermocouples were also installed on the outer shield of the insulation system at the side of the calorimeter in the vicinity of existing thermocouple 5B. Their locations relative to this thermocouple are shown in Figure III-16. The purpose of this added thermometry was to establish the temperature gradient in the outer shield in a region where the source temperature undergoes a step change. This change was accomplished with the vacuum chamber baffles by setting them at different temperatures.

c. Test Conditions

The tests performed in the I-4 series provided data representative of the insulation system without any penetration. The I-5 series were conducted under comparable conditions but with the penetration described above. The difference in total heat flow measured in the two series would then be representative of heat flow due to the penetration.

The I-5 series were carried out at the A. D. Little, Inc., facilities in Cambridge with liquid nitrogen. The first four tests, I-5A through I-5D were performed with all the chamber baffles operating at a temperature of about 41°F. More than 100 hours of data under steady state conditions were obtained in this manner. An average heat rate of 46.2 Btu/hr over the four test periods was obtained. (The average flux value is not meaningful because of the presence of the penetration.)

Tests I-5E and I-5F were performed with the upper and lower chamber baffles at different temperatures. In the former, the upper baffle was maintained at 38°F and the lower baffle was maintained at about -310°F through use of liquid nitrogen. In test 5F, the temperature level of the baffles were reversed. The operating conditions of this test, incidentally, are comparable to those of test I-4F. Average measured heat flow values of 20.8 and 29.3 Btu/hr were obtained in tests I-5E and I-5F respectively. All the heat rate results for this series are tabulated in Table III-10. Additional tests were in progress with this system when a failure of the baffle system resulted in flooding the chamber with water. The insulation system was completely immersed and upon subsequent inspection, the aluminumized polyester shields had deteriorated.

d. Test Results and Discussion

(1) Penetration Heat Rate

The analytical procedures used for calculating the heat rate through the copper penetration are presented in another report.[4] The added heat leak, due to the presence of the penetration in the insulation was estimated to be 7.5 Btu/hr for the condition in which the radiant heat flux to the tank is due to chamber baffles maintained at 80°F. In the experiments, the actual baffle temperature was more in the order of 40°F, which reduces the theoretical penetration heat rate to about 5.2 Btu/hr.

In comparison to this theoretical value, a measured heat rate of 16.6 Btu/hr was obtained for the penetration. This value was determined from tests I-4A, B, C, and D which were performed without any penetration in the insulation and from tests I-5A, B, C, and D, which were performed with the penetration. The heat rate data obtained in the former of these tests resulted in an average value of 31.7 Btu/hr. This value could not be compared directly to the heat

rate obtained with the latter tests, because baffle temperatures between the two groups of tests differed by about 7°F on the average. Thus, the heat rate on the I-4 tests was adjusted to a 41°F warm boundary temperature. This adjustment was made on the basis that the predominant heat flow is by radiation and as a result it varies as the 4th power of the outer boundary temperature. Thus, an adjusted heat rate of 29.6 Btu/hr is obtained. The average heat rate measured in I-5A, B, C, and D tests is 46.2 Btu/hr. The difference in these two values is 16.6 Btu/hr and represents the measured penetration heat rate. This result is a factor of three more than the expected value.

A heat rate value of 13.7 Btu/hr was obtained from a comparison of tests I-4E and I-5F. It will be recalled that both these tests were performed with the upper baffle at a temperature at about -320°F and the lower baffle at near room temperature. Test I-4E (see Table III-9) yielded a heat rate of 16.5 Btu with a warm baffle temperature 47°F. This rate was adjusted downward to an equivalent warm baffle temperature of 38°F corresponding to that used in Test I-5F. This resulted in a value of 15.1 Btu/hr. The average measured heat rate in Test I-5F is 29.3 Btu/hr. The difference between the latter two values, 14.2 Btu/hr, represents a second estimate of the penetration heat leak. Again the experimental result is greater than expected.

In Figure III-17, the computed and experimental temperatures of the outer shield in the vicinity of the penetration are presented. The agreement between the two is quite good. It is possible to use the experimental temperature distribution to compute the penetration heat rate. A value of 5.12 Btu/hr was obtained. This represents the integrated heat flow over an insulation area 10 inches in diameter which includes the end of penetration and its side. The measured surface temperatures and the surface emissivities were used to determine the heat flow. The result of the computation is summarized in Table III-11.

It is evident from this summary that almost 90 per cent of the estimated heat flow is to the end of the penetration. Further, the added heat flow due to the penetration would increase by not more than 2 Btu/hr if it is assumed that the surface temperature of the outer shield were -320°F instead of the values actually measured. Thus it is difficult to conceive that the total experimental heat flux resulting from the penetration would exceed 7.2 Btu/hr under the experimental conditions.

One further comparison is necessary to complete the discussion of the data; Test I-4A thru D yielded over-all heat fluxes of about .74 Btu/hr-ft^2 and Test I-4E yielded a heat flux of .77 for the lower half of the tank insulation adjusted to a warm boundary temperature of 38°F. These values are nearly equal and would indicate, therefore, that the flux for the upper and lower halves have nearly the same value. However, the result obtained in Test I-5E indicates that the measured heat flux into the upper half of the calorimeter at a warm baffle temperature of 38°F had a value of 1.06 Btu/hr-ft^2. The fluxes obtained in Tests I-4F and I-5E are not consistant with the over-all flux measured in Test I-4A, B, C, and D. There is the distinct indication, therefore, of some extraneous heat source into the insulation in addition to that caused by the penetration. The investigation of the existance of this source was precluded when the chamber became flooded.

The result of this set of experiments may be summarized as follows. The measured heat rate for the penetration is approximately 2-3 times greater than the computed value and the value estimated from temperature measured in the vicinity of the penetration. There are also inconsistencies in the data that indicate the heat rate measurements made in the I-5 test series are larger than can be reasonably expected. The larger values indicate that some extraneous heat source may have been present in the insulation system or calorimeter tank. This question could not be resolved because of the subsequent damage inflicted upon the insulation due to flooding. For the time being,

we consider the analytical techniques to be valid.

Temperature Distribution at Baffle Split

Through the use of thermocouples on the outer shield of the tank multi-layer, additional information was obtained to verify the analytical procedures. This was accomplished by setting the two baffles in the chamber at different temperatures. The baffle configuration is shown in Figure III-1. By maintaining one baffle at near room temperature and the other at liquid nitrogen temperature, a 400°F step can be obtained. Figure III-18 shows the temperature distribution and symmetry obtained for two sets of conditions.

In Part VI, these experimental results are fully discussed and compared with the analytical predictions.(4) The agreement between the two is excellent.

Aluminized Polyester Film Immersion Results

Calorimeter No. 2 and its aluminized polyester film insulation system became immersed in water when the water-filled passages of the chamber baffle ruptured. On close inspection, we discovered that significant portions of the outer aluminized polyester film no longer contained an aluminum layer. Subsequently, we removed all the foil layers and found those close to the tank to be similarly deteriorated.

We speculated that the loss of aluminum from the polyester film was due to acid etching of the aluminum and/or to migration of moisture to the aluminum-polyester film interface. We believe that the water in the tank was slightly acid because we found evidence of soldering flux in the area where the circulating coils were soft soldered to the baffle plate.

An acid etching effect was obtained when swatches of aluminized polyester film taken from stock supplies were immersed in water to which a small quantity of soldering flux had been added. A similar immersion test in pure water also produced loss of the aluminum surfacing but by operation it was noted that a smaller quantity of aluminum was removed than in the immersion tests involving the soldering flux.

We found further indication of a very weak bond between the aluminum and polyester film. During removal of the shields, we found that where the two sections of a shield had been overlapped the immersion in water adhered them together. When the two sections were pulled apart, a significant portion of the deposited aluminum on one section became adhered to and remained on the polyester surface of the second section.

The deleterious effects of the water immersion of the aluminized polyester film corroborate information obtained from other sources. From our experience, it is evident that the bond between the aluminum and polyester film is very weak and immersion in water can cause a separation of the aluminum and polyester film. We may also speculate that moisture and slight abrasive effects can cause separation of the two films. Thus, it appears that some protection is necessary for an aluminized-Mylar multi-layer insulation applied on a space vehicle propellant tank to prevent the moisture in the natural environment from accumulating in the system.

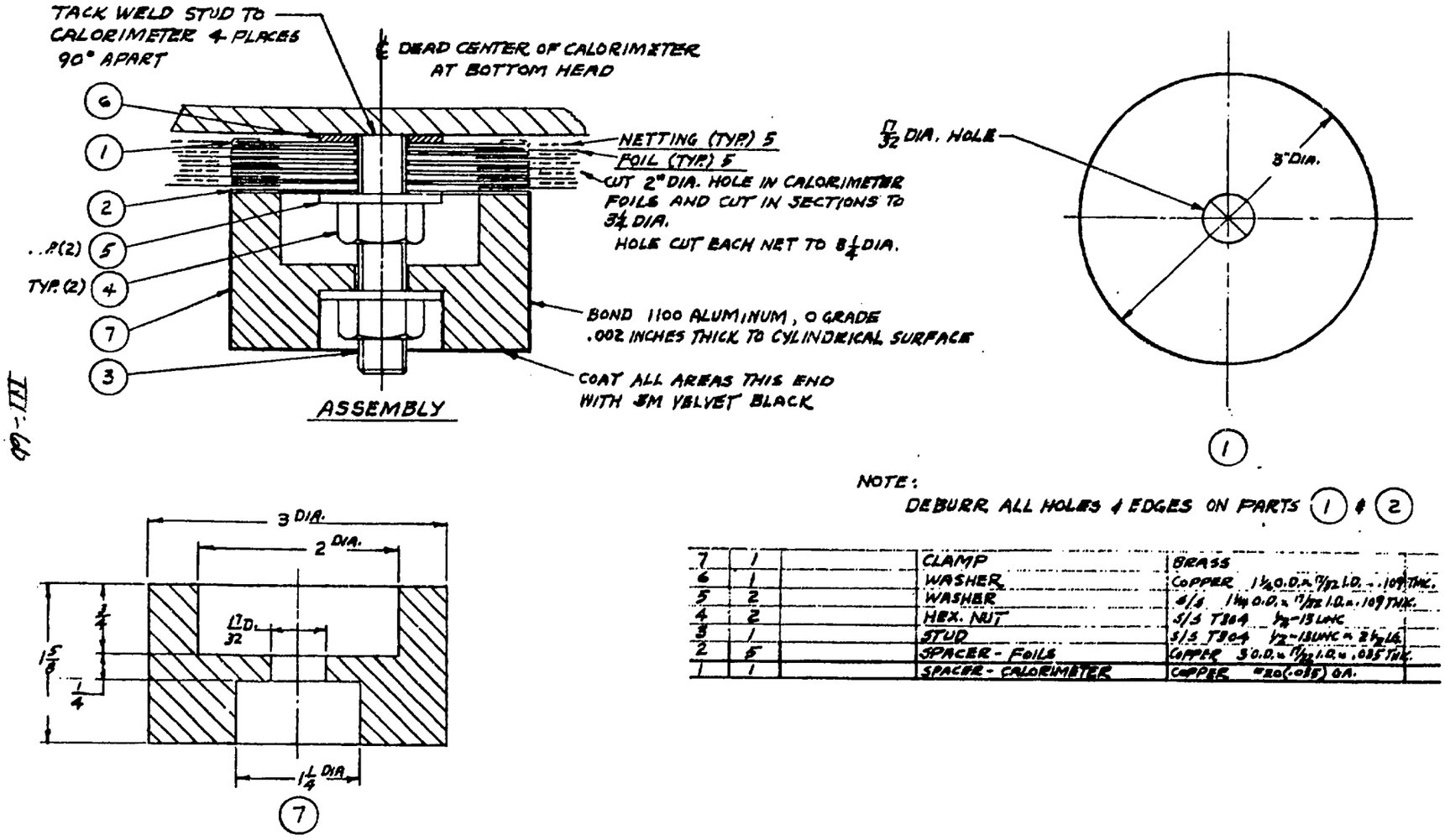

7	1		CLAMP	BRASS
6	1		WASHER	COPPER 1½ O.D. × 11/32 I.D. × .109 THK.
5	2		WASHER	S/S 1¼ O.D. × 11/32 I.D. × .109 THK.
4	2		HEX. NUT	S/S T304 ⅜-13 UNC
3	1		STUD	S/S T304 ⅜-13 UNC × 2½ LG.
2	5		SPACER - FOILS	COPPER 3 O.D. × 11/32 I.D. × .035 THK.
1	1		SPACER - CALORIMETER	COPPER ≈20 (.035) GA.

FIGURE III-11 ALUMINIZED POLYESTER FILM SYSTEM - COPPER PENETRATION DETAILS

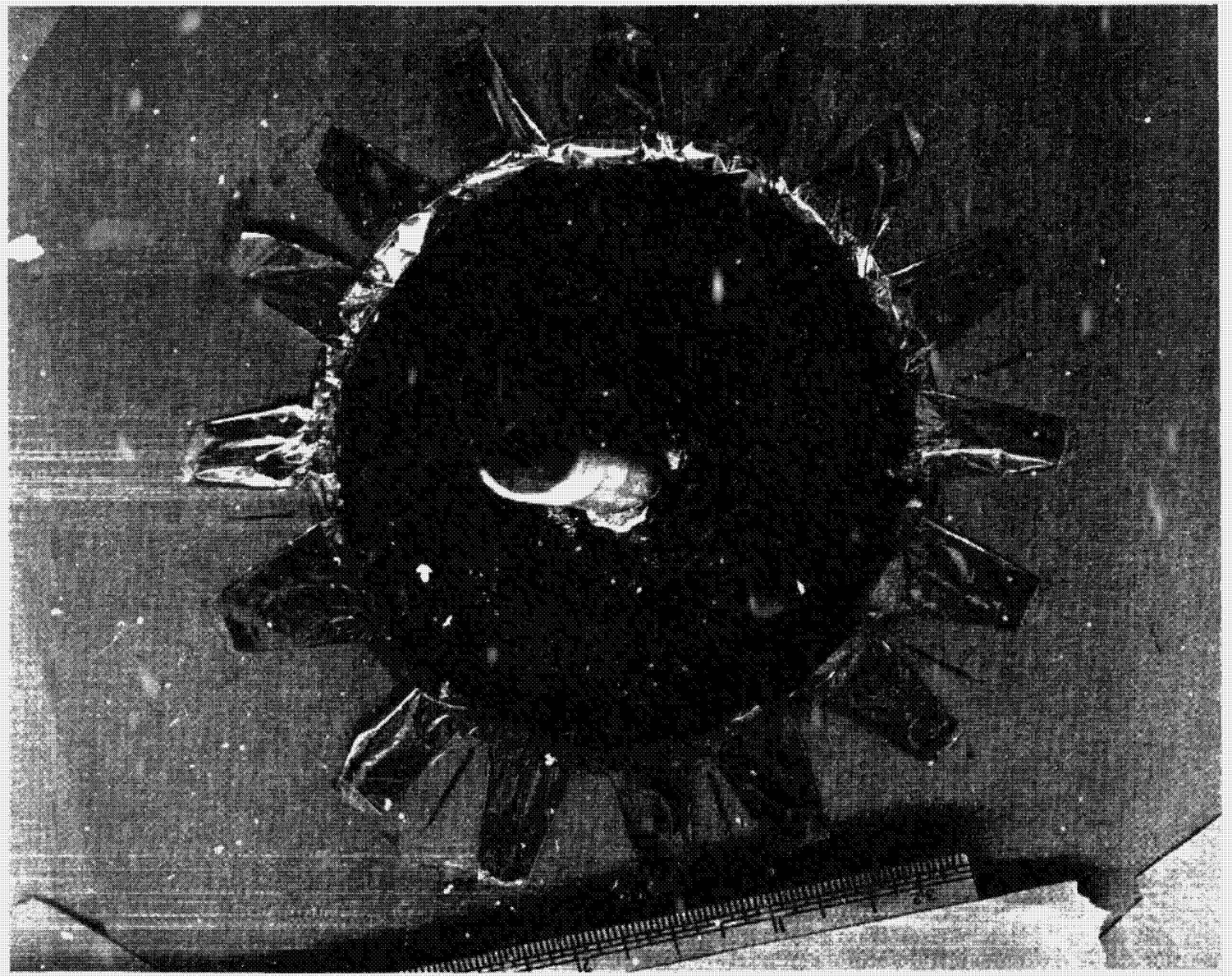

FIGURE III-12 COPPER PENETRATION - INSULATION SYSTEM CUTOUT AND STUD

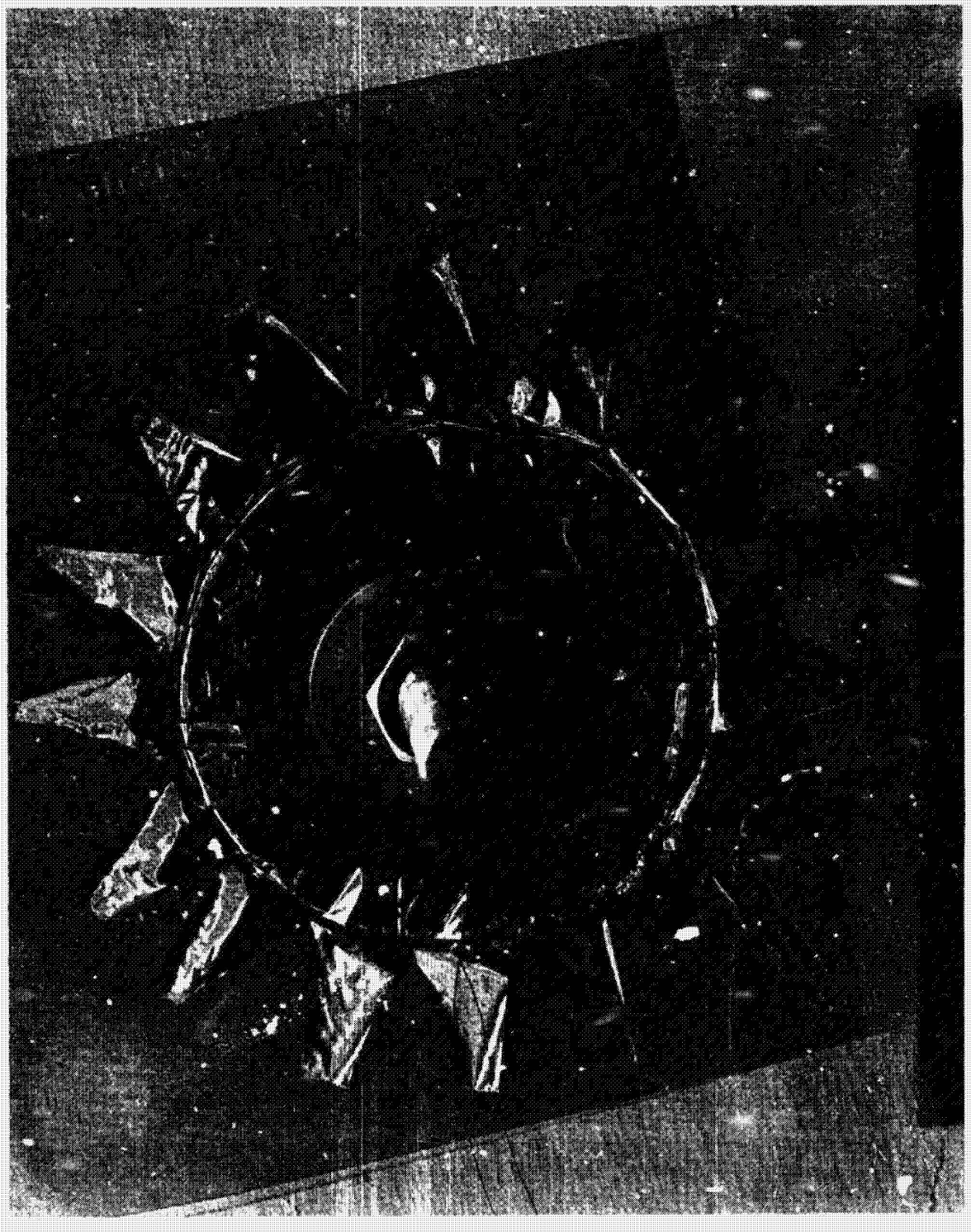

FIGURE II:-14 COPPER PENETRATION - COMPLETED ASSEMBLY

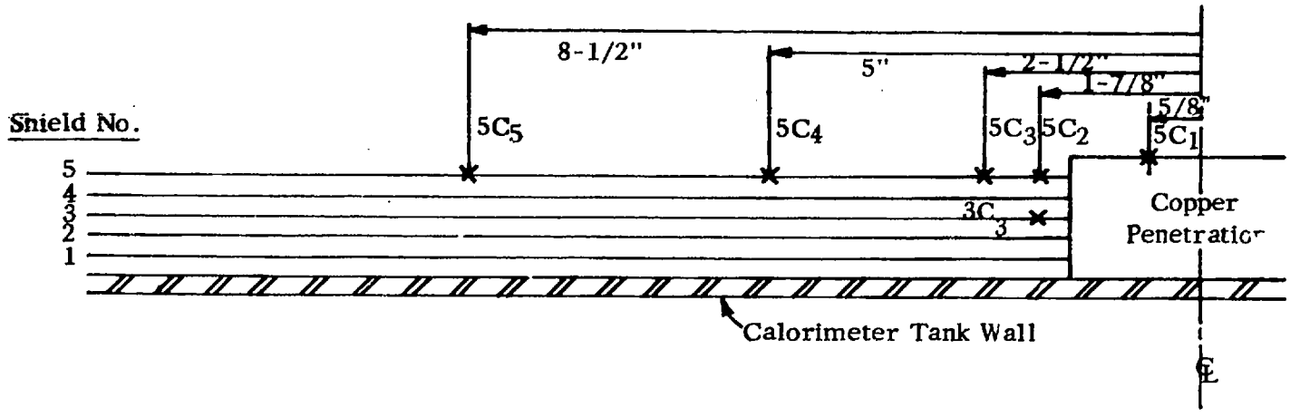

FIGURE III-15 THERMOCOUPLE LOCATIONS - COPPER PENETRATION

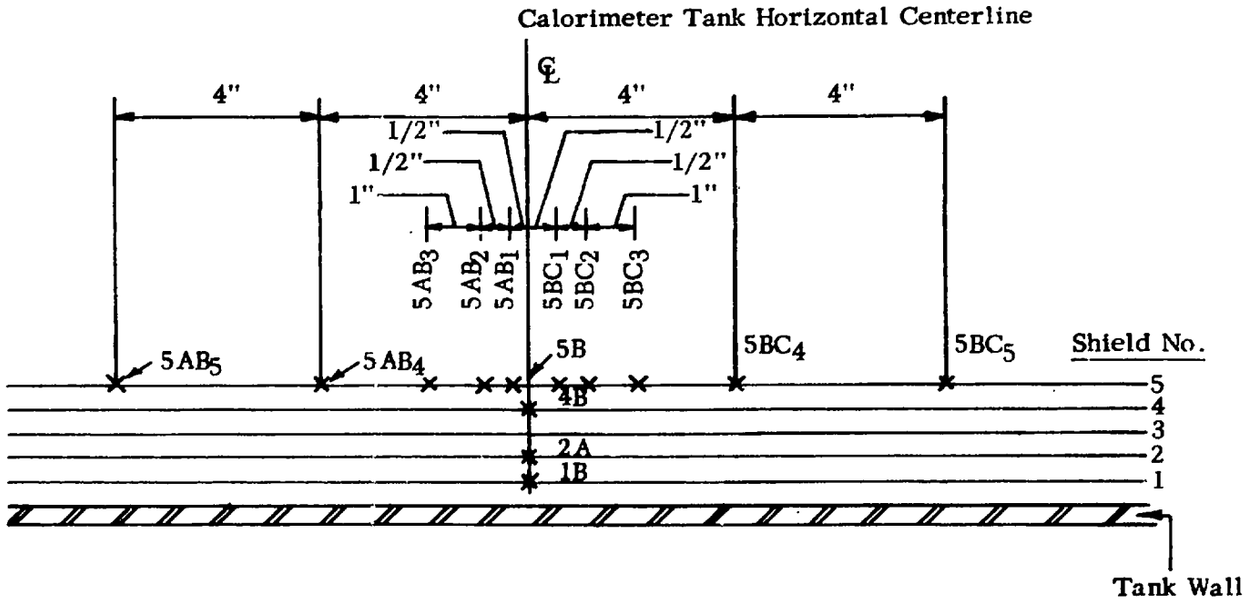

FIGURE III-16 THERMOCOUPLE LOCATIONS - TANK SIDE

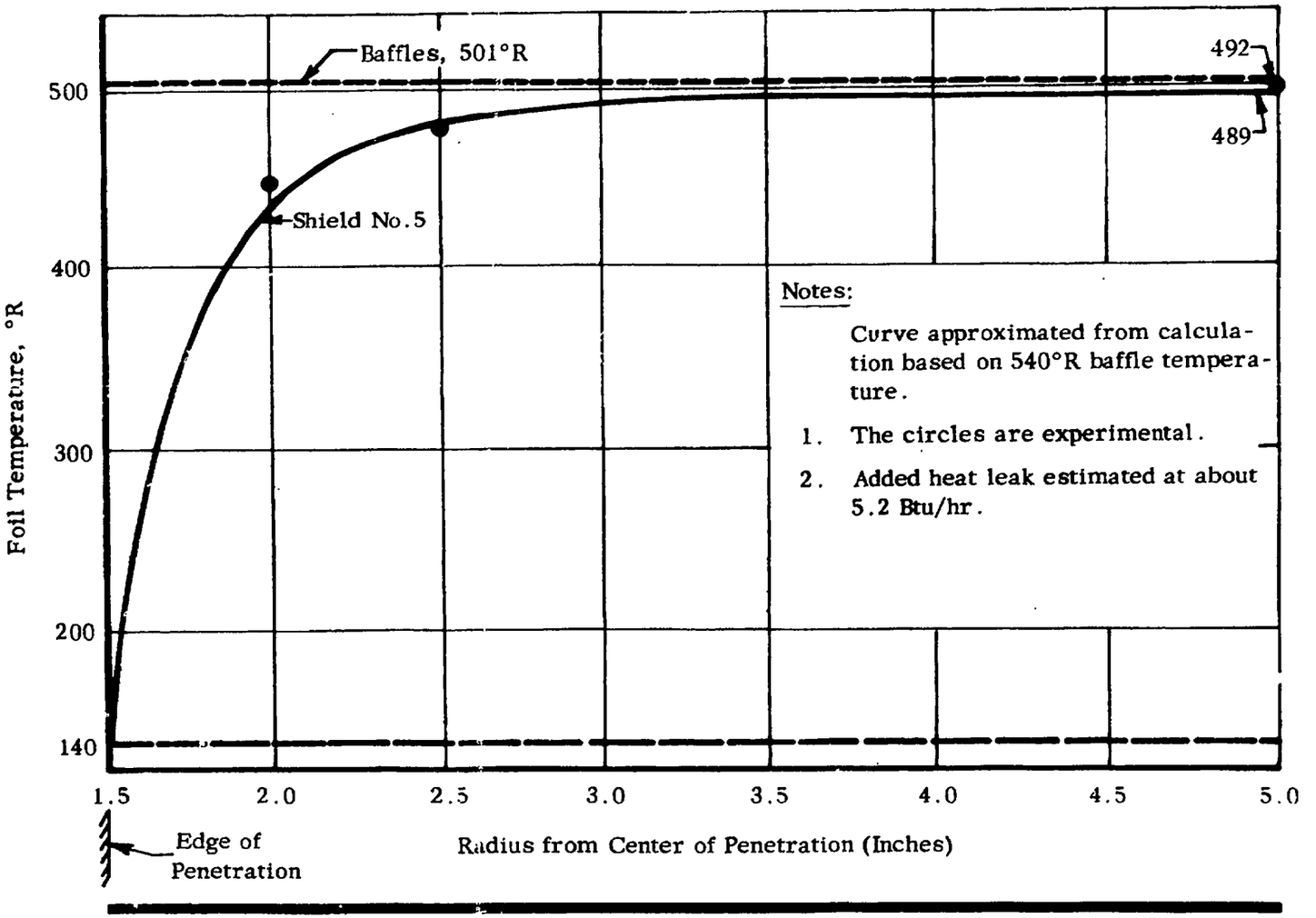

FIGURE III-17 INSULATION SYSTEM NO. 3. RADIAL TEMPERATURE DISTRIBUTION AT COPPER PENETRATION

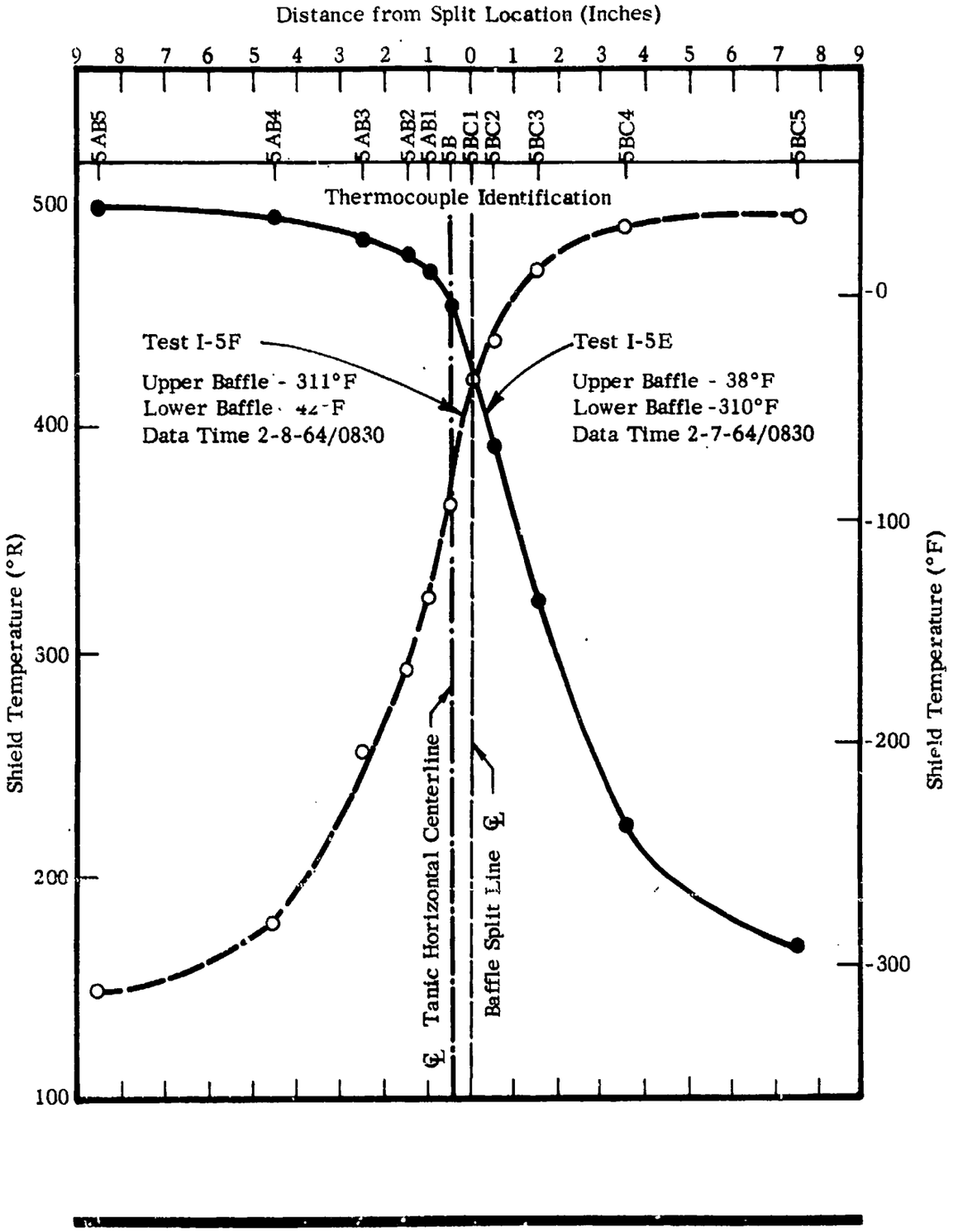

FIGURE III-18 TEMPERATURE DISTRIBUTION - OUTER SHIELD AT SPLIT BETWEEN UPPER AND LOWER BAFFLES - TEST NO. I-5E & I-5F CALORIMETER NO. 2

TABLE III-10

TANK INSULATION PROGRAM

TEST SUMMARY - INSULATION SYSTEM NO. 3 - CALORIMETER NO. 2

Insulation System	Five aluminized polyester film (NRC) radiation shields, .00025 inches thick, spaced with six 1/8 x 1/8-inch mesh, vinyl-coated, Fiberglas screens .020 inches thick. Uncrinkled polyester film placed on tank with aluminized surface facing warm boundary.
Test Facility:	Arthur D. Little, Inc., Cambridge, Mass.
Penetration and/or Gaps:	3-inch diameter copper penetration at bottom center of Calorimeter tank.
Boundary Conditions:	Cold boundary -320°F; warm boundary variable as shown below.
Emissivity:	Cold boundary .88; warm boundary .93.
Tank Surface Area:	39.45 ft^2.

Test	Tank Liquid	Data Period Date&Time	to Date&Time	Test Duration (hrs)	Ave. Vac (mmHg)	Guard Liq/Temp (°F)	Total Heat Flow (BTU/hr)	Measured Ave. Heat Flux (BTU/hr ft^2)	Ave. Baffle Temp.(F) Upper	Lower	Adjusted[4] Heat Flux (BTU/hrft^2)
I-5A	LN_2	2/1/64/1230	2/3/64/0830	44.0	$7x10^{-6}$	LN_2/-310	45.8	____[3]	41	41	____[3]
I-5B	LN_2	2/3/64/0830	2/4/64/0830	24.0[1]	$6x10^{-4}$	LN_2/-316	44.8	____[3]	41	41	____[3]
I-5C	LN_2	2/4/64/0830	2/4/64/1630	8.0[2]	____	LN_2/-316	47.6	____[3]	41	41	____[3]
I-5D	LN_2	2/5/64/0845	2/6/64/0845	24.0	$3x10^{-6}$	LN_2/-316	47.3	____[3]	40	40	____[3]
I-5E	LN_2	2/6/64/2030	2/7/64/0830	12.0	$1x10^{-6}$	LN_2/-317	20.8	1.06	38	-310	1.47[3]
I-5F	LN_2	2/7/64/1830	2/8/64/0830	14.0	$6x10^{-7}$	LN_2/-315	29.3	____[3]	-311	38	____[3]

Notes:

1. During first 8 hours of this period chamber vacuum was reading high. When vacuum system returned to operation ion gauge tube burned out and could not be replaced.
2. Ion gauge tube not reading during this period.
3. Not applicable because of penetration in insulation system.
4. Measured heat flow adjusted to standard conditions for warm boundary temperature of 80°F.

TABLE III-11

PENETRATION HEAT LEAK SUMMARY

Surface	Surface Emissivity	Surface Area Ft^2	Average Experimental Surface Temp. ^oF	Radiation Heat Flow Btu/hr
Penetration End	.94	.049	145	4.84
Penetration Cylinder	.035	.106	145	0.39
Shields around Penetration Annular Segment				
3 to 4 inches	.047	.038	145	0.19
4 to 5 inches	.047	.050	460	0.07
5 to 6 inches	.047	.060	476	0.04
6 to 7 inches	.047	.071	483	0.05
7 to 8 inches	.047	.083	488	0.03
8 to 9 inches	.047	.092	490	0.03
9 to 10 inches	.047	.103	492	0.03
Total Heat Rate				5.67 Btu/hr
Heat Rate through Area With No Penetration	.047	.546	492	-.55
Penetration Heat Leak				5.12 Btu/hr or 1.51 watt

Insulation System No. 4

a. Introduction

Insulation System No. 4 consisted of five shields of 1/2 mil aluminum foils separated by 1/8 x 1/8-inch mesh vinyl-coated Fiberglas netting spacers. Our main objective in selecting this system for test was to improve on the K P performance obtained with insulation System No. 1. In addition, it was considered of great importance to evaluate some of the handling factors associated with the fabrication of multilayer systems using light gauge aluminum foils.

This system was also used to fulfill other test objectives associated with the measurement of the ground performance of multi-layer insulations. Helium purge systems using shrouds and close-fitting bags and vacuum purge systems were investigated with the No. 4 Insulation System.

b. Insulation System Description

The shields and netting were formed and cut in a manner identical to those fabricated for the No. 1 Insulation System with one exception. Because of the thin gauge of the aluminum foil, the full spherical curvature on the end shields could not be achieved through pressure forming alone. The partially formed shields were slit along eight equidistant radii for a distance of about 12 inches from the edge. The completed insulation system is shown in Figures III-19 and 20, and additional details are provided in Table III-1.

The bag placed around the insulation system after Tests II-1 and II-2 were performed, was fabricated from a 2 mil polyester film aluminum foil laminate. The side sheet was cut and gored in a manner similar to the side sheet of the multi-layer. The ends were pressure formed also like the aluminum shields at the tank end. The bag was assembled over a die of the same size and shape as the calorimeter tanks. The die was built up so that when the bag was installed on the tank, sufficient free space was available so as not to restrain or place pressure on the multilayer insulation. The edges of all joints in the bag were butted and sealed with the laminated material containing a pressure sensitive adhesive on one side. The

bag contained tube connections at the top and bottom for purging and evacuating the bag. Another connection was provided for the thermocouple lead wires.

When the bag was installed on the tank, a seal was made at the support column through the use of a urethane foam. The completed bag is shown in Figure III-21 being purged with dry gas. In Figure III-22, the bag is shown in the evacuated condition. With a limited effort, the best vacuum achieved in the bag was about 125 mm of mercury.

c. Test Conditions

The heat flux to Insulation System No. 4 was measured under a variety of test conditions including both space and ground environments. Nine major tests were performed at the ADL test facilities in Cambridge. The test conditions and experimental results that were obtained are identified below.

Test I: (Space Environment - Entire Insulation Active)

This was the first test performed after application of the insulation system. The flux to the calorimeter was measured with full vacuum in the ADL chamber and all baffles operated at near room temperature.

Test II-1B and II-1C (Space Environment - Half Insulation Active)

These are complementary tests performed in the chamber with full vacuum to determine the heat leak through the upper and lower half of the insulation separately. In test II-1B, the lower baffle was temperature controlled with water while the upper baffle temperature was controlled with liquid nitrogen.

In test II-1C, the baffle conditions were reversed.

Test II-2 (Chamber Purged with 1 Atmosphere of Helium Gas)

This test was performed with the calorimeter installed in the chamber to simulate a shrouded tank configuration. The chamber space was continually purged with helium at a pressure of one atmosphere. The chamber baffles were temperature controlled with water and used to simulate the space vehicle shroud. Because of the high venting rate of the calorimeter, no liquid coolant was supplied to the cold guard on the vent support.

Test II-3A (Ground Atmosphere - Helium Purged Bag)

This test was performed in the prevailing natural ground environment while a bag purged with helium surrounded the insulation. The calorimeter was suspended from a hoist scale to measure the liquid nitrogen boil off rate. In addition, the gas volume rate was measured in the vent system. The calorimeter was filled with liquid nitrogen at the start of the test.

Test II-3B (Ground Atmosphere - Vacuum Purged Bag)

Like test II-3A, this test was also performed in the prevailing natural environment. We evacuated the bag that had been previously used with a helium purge. Because of leaks in the system, we could not achieve a vacuum less than 125 mm Hg. Thus, we expect that gas conduction was as important as solid conduction in establishing heat transfer within the bag. When the bag was evacuated, the netting imprints in the bag became clearly visible as can be seen in Figure III-26. Also, the insulation gave a clear metallic sound when struck with the hand. When liquid nitrogen was placed into the calorimeter, frost formed on the bag as shown in Figure III-25.

Test II-3C (Space Environment)

Because of the pressure exerted on the evacuated multi-layer during test II-3B, we expected that the insulation thermal performance might have become permanently degraded. The system was, therefore, returned to the chamber for space simulation tests with the bag still in place. The one inch vacuum connection in the bag opened to the chamber space.

Test II-4A (Space Environment)

This test was a repeat of test II-3C except that the vacuum bag was removed to permit more effective evacuation of the insulation. (Figure III-27)

Test II-4B (Depressurization)

We obtained qualitative information of the effect of rapid depressurization of a multi-layer insulation on the mechanical integrity of shield and spacer. Insulation System No. 4 was used for

this purpose after test II-4A was completed. Calorimeter No. 2 was placed into the ADL chamber and the chamber evacuated at three different rates in successive tests. The time-pressure transient of the chamber for each test is shown in Figure III-28.

d. Test Results and Discussion

Tests II-1A, -3C and -4A

The data obtained with Insulation System No. 4 under simulated space conditions are summarized below.

Test	Measured Flux Btu/hrft^2	Adjusted Flux Btu/hrft^2	Test Facility	Tank Liquid
II-1A	.37	.47	ADL	LN_2
II-3C	1.4	1.56	ADL	LN_2
II-4A	.83	.91	ADL	LN_2

Under the conditions of test II-1A, the heat leak performance of Insulation System No. 4 should have had a value between 0.22 and 0.40 Btu/hr-ft^2. The former value is based upon the experimental results obtained with the thermal conductivity apparatus in Test 2030 and includes the effects of solid conduction and the variation of shield emissivity with temperature. The latter value is computed from results obtained with the Emissometer, reported herein in Part IV, which yield average emissivity for aluminum of 0.035. In this computed flux, no account is taken of any solid conduction nor of any dependence of shield emissivity on shield temperature.

The value of heat flux measured in test II-1A is 0.38 Btu/hr is in the prescribed range. Further, the theoretical temperature distribution compares very closely with the experimental values as indicated in Figure III-23. However, during application of the insulation, electrical shorts were measured between shields and, therefore, some solid conduction paths were known to exist. We believe, therefore, while the results obtained indicate good agreement, both

with the computed and thermal conductivity apparatus values, the system is still capable of improvement.

The heat fluxes measured in tests II-3C and II-4A are 1.4 and 0.83 Btu/hr-ft^2 respectively. As can be seen, these fluxes are greater than that measured in test II-1A. The insulation was definitely degraded when the bag was evacuated prior to these tests. The high heat flux obtained in test II-3C compared to test II-4A is attributed to the presence of the bag around the insulation which probably retarded the pump down of the insulation and an added heat leak was thereby contributed by gas conduction. The weight of the bag acting on the insulation may have also increased the solid conduction heat flux.

The multi-layer temperatures measured in tests II-3C and II-4A are shown in Figure III-23. The results for both tests are similar. The gradients in the outer four shields are smaller and more linear than expected. Shield No. 2 in both cases is about 60°F higher than that shown for test II-1A. Further, the gradients between the tank and shield No. 2 are greater than expected. From the experimental data of test II-3C, we computed the radiation component and by difference the solid conduction components of heat flux. These are summarized below.

Shield No.	Shield Temp. (°R)	(Q/A) Radiation, (Btu/hr-ft^2)	(Q/A) Conduction (Btu/hr-ft^2)	(Q/A) Total (Btu/hr-ft^2)
Tank Wall	140			
		.71	0.69	1.4
1	Not avail.			
2	431			
		.228	1.172	1.4
3	453			
		.165	1.235	1.4
4	467			
		.345	1.055	1.4
5	493			
		1.1	0.3	1.4
Baffle	526			

These results would indicate that solid conduction heat transfer dominates in the outer four shields while the radiation and conduction components are nearly equal in the space between the tank wall and shield No. 2.

In the case of test II-4A, the computed radiation heat fluxes as tabulated below are similar to those of test II-3C because the temperature gradients are similar. The solid conduction component

Shield No.	Shield Temp. (°R)	(Q/A) Total Measured (Btu/hr-ft^2)	(Q/A) Radiation (Btu/hr-ft^2)	(Q/A) Conduction (Btu/hr-ft^2)
Tank Wall	140			
		.83	.76	.07
1	-			
2	440			
		.83	.27	.56
3	464			
		.83	.20	.63
4	480			
		.83	.36	.47
5	505			
		.83	.80	.03
Baffle	529			

is smaller, however, because the measured heat flow was reduced when the bag was removed.

The large amount of solid conduction in the outer layers of the insulation is explained as follows: The insulation was compressed by the vacuum bag and the shields and spacers became "packed" or compressed. However, when the system was cooled in the evacuated chamber and the effect of atmospheric pressure was removed, the layers of insulation near the tank were lowered in temperature to a greater degree than any of the others. The lower temperatures may have created a sufficient contraction in the affected shields and spacers to cause their separation from the pack. Thus, they acted more nearly like floating shields and spacers free of contacts than the outer layers.

The data obtained in these tests can also be used to demonstrate the presence of gas in the multi-layer during test II-3C. The computed conduction component between the tank wall and shield No. 2 is .69 Btu/hr ft^2 for test II-3C and .09 Btu/hr ft^2 for test II-4A. If the former were assumed to be due to solid conduction, the decrease experienced in test II-4A could not have occurred. Since in test II-4A, we are able to account for the heat flux between the tank and shield No. 2 both from the shield temperatures and shield emissivities, there is probably little conduction of any kind in this region. Therefore, the conduction present in this region during test II-3C was due very likely to the presence of gas in the multi-layer.

Test II-1B and 1C

The use of the split baffle in the chamber to create a step change in the radiation environment is a useful method for isolating the upper and lower tank areas to study penetration, gravity and other insulation effects. Tests II-1B and II-1C were performed to increase our experience with the use of this method.

The analytical results [4] indicate that the integrated heat flux in the area of the baffle split (boundary between the upper and lower baffle) for a warm upper and cold lower are the same as when the temperatures are reversed. Thus, the complete isolation of a tank section and symmetry of the heat flux at the split should result in a total heat flow, as from two tests such as: II-1B and II-1C, that is equal to the heat flow obtained when the both baffles are at the warmer temperature, i.e., test II-1A.

The sum of the heat flux obtained in test II-1B and IC is 19.2 Btu/hr. This is compared to the heat rate obtained in test II-1A which averages 14.6 Btu/hr. The difference between the two heat rates is 4.6 Btu/hr, which is a very significant percentage of the total. is to be noted that a similar result was obtained when tests performed with No. 3 Insulation System were compared, i.e. (tests I-5A, B, C, and D compared to I-5E and F).

It is possible that the surface emissivities of the actual baffles vary significantly from those used in the theoretical computation. This could result in an unsymmetrical distribution of heat flux at the insulation surface in the vicinity of the split location. This contention is contradicted by the symmetrical temperature patterns measured at the insulation surface in tests I-5E and F at the split location. Every effort should be made in future tests to obtain added experimental information to explain the effects noted in this discussion because the split baffle arrangement can be used in an important way to study multi-layer insulation performance.

Test II-2

This test simulates the configuration and conditions of a cryogenic propellant tank within a helium purged airframe shroud. It is an important test because it verifies the expected heat transfer modes and makes available useful experimental heat flux data.

In the analytical model, the calorimeter tank and chamber baffles are assumed to be cylindrical with flat ends. The diameters and surface areas are to be the same as the test counterparts. The tank and baffle temperatures used in the computation are taken as the experimental values. The multi-layer insulation was assumed to have an average thickness of 0.25 inches. Helium was chosen as the purge space gas. The computed heat flow and insulation temperatures are presented in Figure III-30a.

In the calculations, a bulk temperature was assumed for the gas in the space between the tank and baffles. The free convection coefficients were next computed for each of the three surfaces on the tank and baffle, i.e., vertical surfaces, horizontal surfaces facing up and horizontal surfaces facing down. The heat flow to or from each surface was computed using the surface areas and the temperature difference between the surface and bulk gas. The total heat flow to the tank and from the baffles were equated. If the two were not nearly equal, a new bulk temperature was chosen and new heat rates

The principal assumptions used in the calculation were: (1) that the gas bulk was uniform throughout the gas space, and (2) that the tank and baffles transferred heat with the bulk independent of one another, except for the fact that the integrated heat rates to each boundary are equal to one another. We also assumed that heat transfer through the multi-layer took place by gas conduction. Two of the pertinent experimental and computed values are compared below.

	Measured Values Test II-2A	Computed Values
Calorimeter Heat Rate (Btu/hr)	11400	11600*
Outside Multi-layer Temperature at Side of Tank	283°R	275°R

The experimentally measured distribution of temperatures with the insulation system are presented in Figure III-23. The gradient in the multi-layer is almost linear. The measured heat flux obtained with the five shield multi-layer was 290 Btu/hr-ft^2. Past experience indicates that this approaches acceptable values of allowable heat leaks for cryogenic propellant tanks in a ground environment. The heat leak to hydrogen filled tanks will be increased over measured values by approximately 20 per cent, because of the enlarged differential temperature. An increase in the thickness of the multi-layer would result in a reduction of the heat flux under the conditions being considered because an added thickness of gas in the layers increases the thermal resistance of the system.

Test II-3A

Use of a helium purge gas around a cryogenic propellant tank to control the ground environment is an alternate method to a helium purged airframe shroud. This technique can be applied when there is no airframe shroud available, when the propellant tank volume is small compared to the shrouded volume, or for other reasons which dictate the use of a bag.

---

*Average of tank value (12,420 Btu/hr) and baffle value (10,718 Btu/hr)

Test II-3A is a simulation of the helium purge bag technique. Time at the J-4 facility to perform these tests with hydrogen was not available. The results obtained with nitrogen at the ADL facilities in Cambridge, however, can be suitably interpreted to indicate the typical hydrogen performance.

For the analytical model, we assumed the calorimeter to be a cylindrical vessel, 48 inches in diameter and 14.3 inches deep having the same area as the test tank. The bag spaced away from the tank surface a distance of from .4 to 1.0 inches depending upon location. The multi-layer insulation was contained in this space. The properties of helium gas were used for computing the conductivity of the purge space and air properties were used in evaluating convection coefficients outside of the bag. The effects of frost formation on the bag were not included. The resulting conditions and calculations are summarized in Figure III-30b.

In comparison, the heat flux measured in test II-3A was 165 Btu/hr-ft^2 compared to a computed value of 250 Btu/hr-ft^2. The temperature distribution in the insulation system is presented in Figure III-23. Temperatures within the multi-layer are distributed linearly. The computed and measured temperatures of the purge bag at the tank side are in good agreement, i.e., 324°R experimental vs. 327°R for the measured value. The greater value of the computed flux is due possibly to the neglected affects of the frost which was observed to have formed on the bag during the test.

If hydrogen had replaced nitrogen in test II-3A, we estimate that the results would not have been greatly different. For example, as in the case of nitrogen, the bag surface would have remained above the condensation temperature of air (145°R). If the bag surface is assumed to be somewhat above this value at 185°R, we estimate a heat flow through the .4 inch purge space of 145 Btu/hr-ft^2. Data on the heat flow to a cryogenic surface at 185°R in a natural ground environment indicate that about 960 Btu/hr-ft^2 can be expected

initially with no frost on the surface. After a period of one hour, the presence of frost reduces the flux to about 480 Btu/hr-ft^2. This value is still considerably above 145 Btu/hr-ft^2. Thus, if the heat flux through the purge space is increased above 145 Btu/hr-ft^2, the bag surface temperature will rise above 185°R and away from the condensation temperature. We expect the bag to take on temperatures about 200°R, but probably less than the calculated and measured temperatures for the liquid nitrogen case.

Test II-3B

The pressure in the multi-layer insulation inside of the vacuum bag was approximately 125 mm Hg. As the bag leaked badly, the gas in the multi-layer was mainly air. The thermal conductivity of gases at this pressure level is relatively independent of pressure. The heat flux due to the presence of the gas can therefore be computed. The approximate bag outside temperature during the test was about 324°R. The differential temperature across the insulation is, therefore, 184°R. For a gas conductivity of 0.1 Btu-in/hr-ft^2-$^\circ$F, the computed heat flow is 142 Btu/hr-ft^2 based on an insulation thickness of .125 inches. This compares with 234 Btu/hr-ft^2 which is the value measured in test II-3B. The difference in these values, 92 Btu/hr-ft^2, should be representative of the solid conduction effect which results from compression of the insulation by the vacuum bag and/or water vapor and carbon dioxide which were pumped into the system and condensed. This also represents the value very near that which would have to be obtained if a sufficient vacuum had been achieved in the multi-layer.

The temperature distribution measured within the insulation system is shown in Figure III-23. It is to be noted that within the multi-layer, the shield temperatures have an anomolus distribution, i.e., shields 4 and 5 are lower in temperature than shields 2 and 3. We believe this condition is due to the shorting of the shields that results from the atmospheric pressure acting upon the bag. This shorting is quite probably a random phenomena both in terms of the shields affected and the location in the shields. The

thermocouples from which the data presented in Figure III-23 were obtained, were in the same general area at the side of the tank but were not precisely aligned. Therefore, each thermocouple is probably located in an area having different temperature gradients. Thus, when the thermocouple results are presented together, an impossible gradient is produced. Thus, the temperature distribution shown in the figure is not to be taken seriously.

e. Summary

The results of these tests may be summarized as follows: the 1/2 mil aluminum shields used in the five shield multi-layer resulted in a measured heat flux of .38 Btu/hr-ft^2. This value was less than predicted (.40 Btu/hr-ft^2) based upon measured shield emissivities and greater than the value obtained with the thermal conductivity apparatus (.22 Btu/hr-ft^2).

After undergoing tests at atmospheric conditions with helium purges and particularily the tests performed with a vacuum bag, the insulation heat flux in simulated space conditions was deteriorated by a factor of two to a value .83 Btu/hr-ft^2.

The thermal performance of the multi-layer was measured under conditions simulating ground hold. The helium purged shrouded tank resulted in a heat flux of 290 Btu/hr-ft^2. This was improved to a value of 165 Btu/hr-ft^2 by placing a helium purged bag around the insulation. The same bag evacuated to a pressure of about 125 mm Hg resulted in a flux of 234 Btu/hr-ft^2. We found it difficult to achieve lower pressures within the vacuum bag. The helium shroud and helium purge bag methods of handling the ground environment are practical and do not produce unreasonable values of heat flux.

FIGURE III-19 INSULATION SYSTEM NO. 4

FIGURE III-20 INSULATION SYSTEM NO. 4- BOTTOM

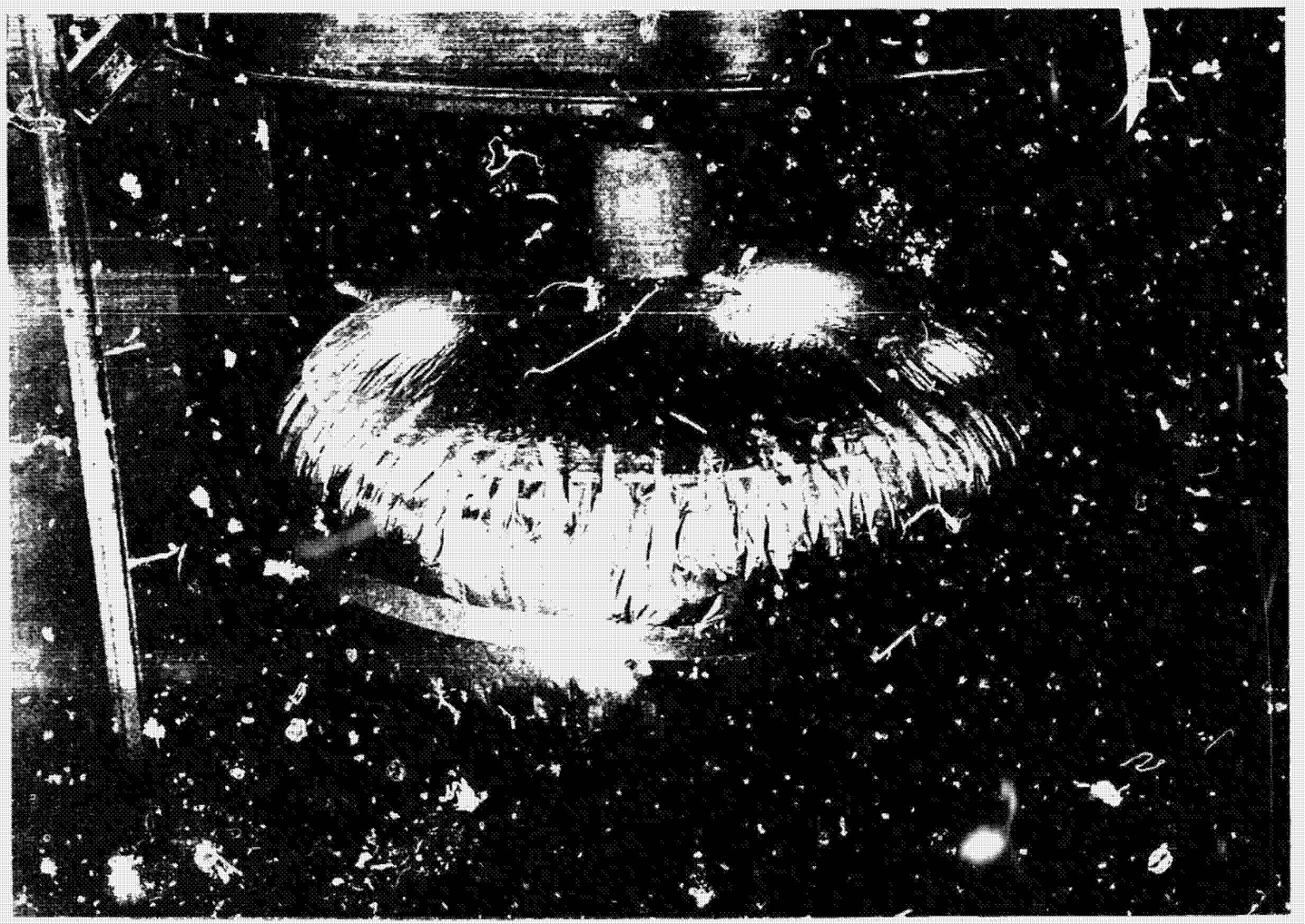

FICURE III-21 ALUMISEAL PURCE BAG, INFLATED ON CALORIMETER NO. 2

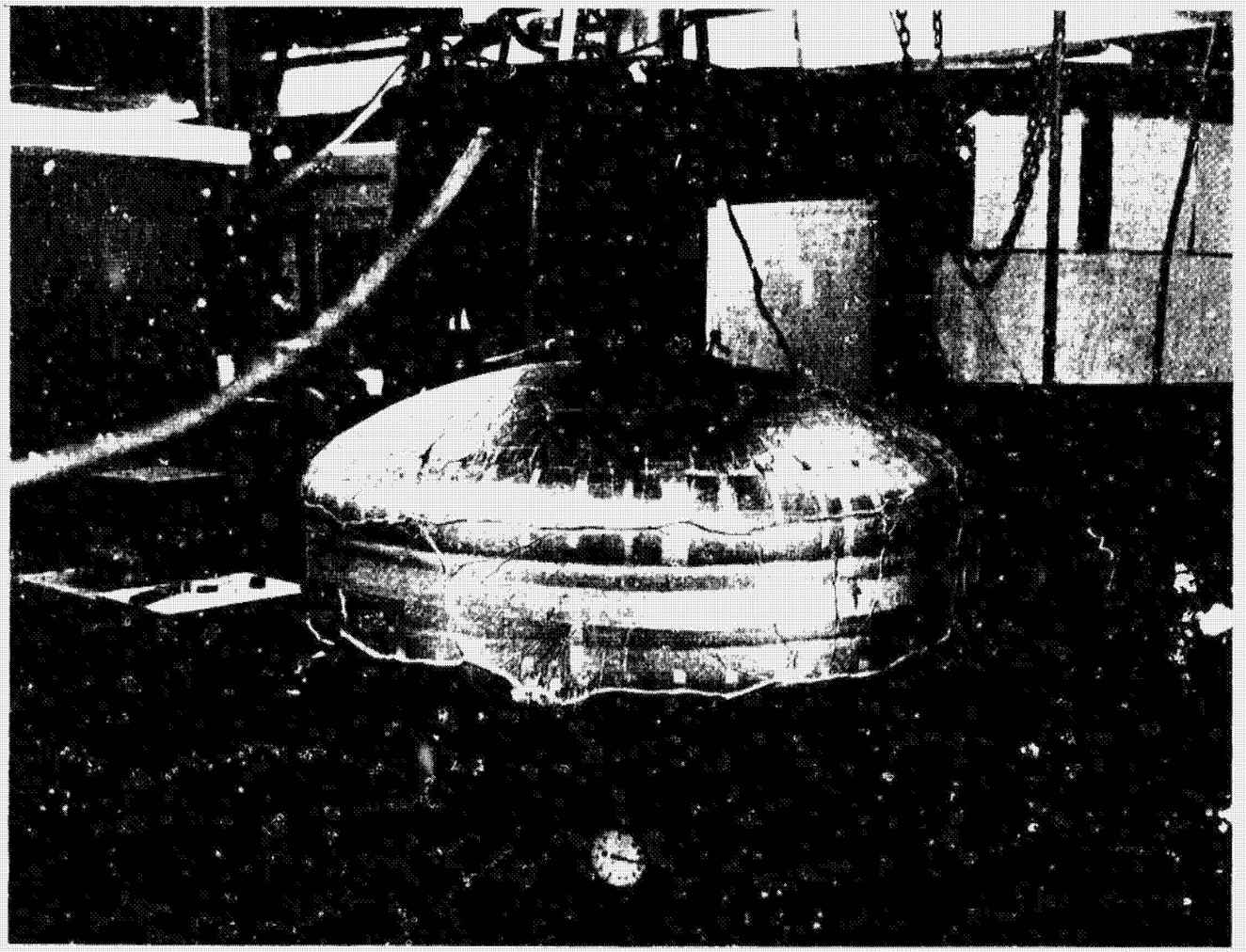

FIGURE III-22 ALUMISEAL PURGE BAG, EVACUATED ON CALORIMETER NO. 2

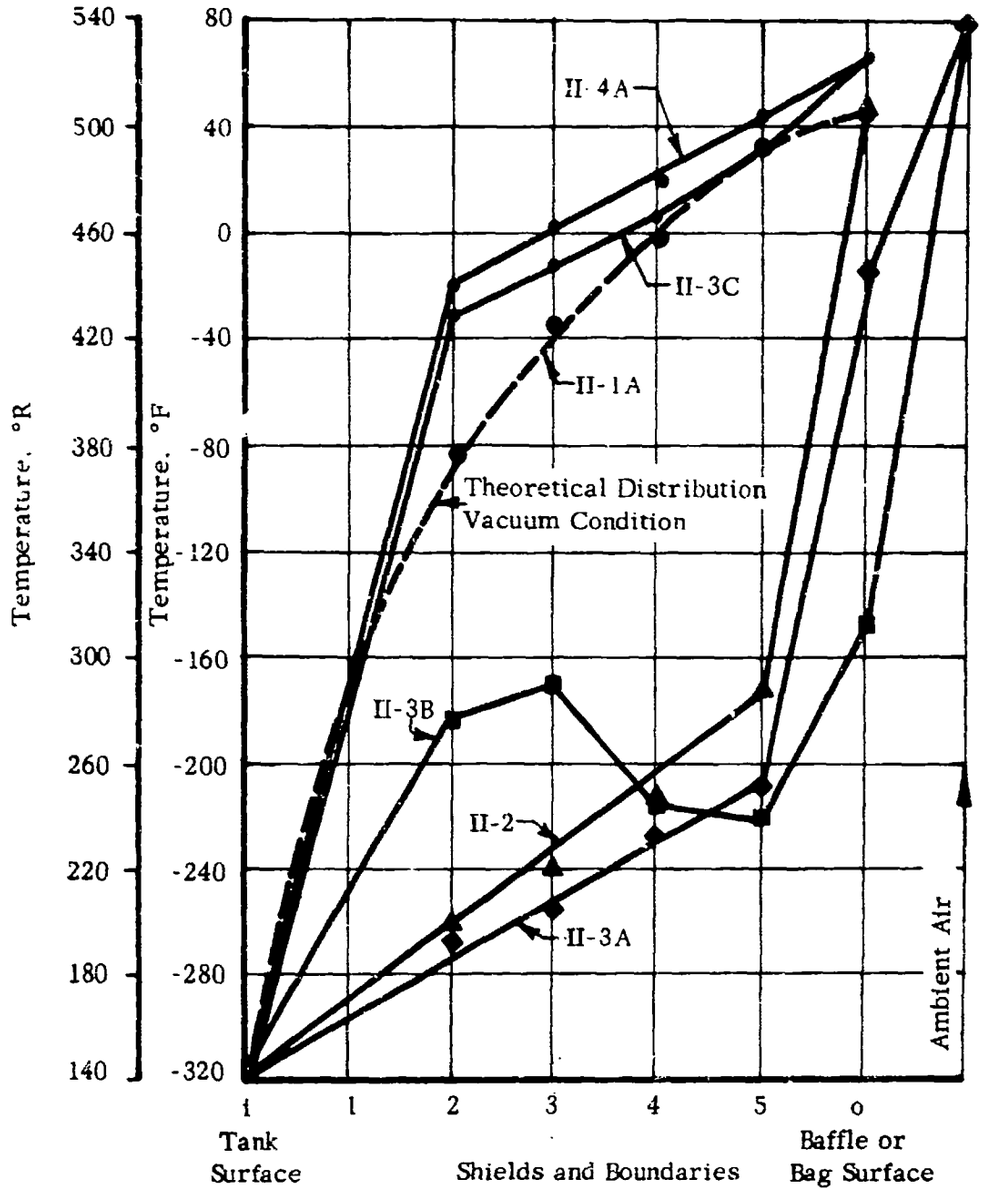

FIGURE III-23 TEMPERATURE DISTRIBUTION IN INSULATION SYSTEM NO. 4 FOR TESTS II-1, 2, 3 AND 4

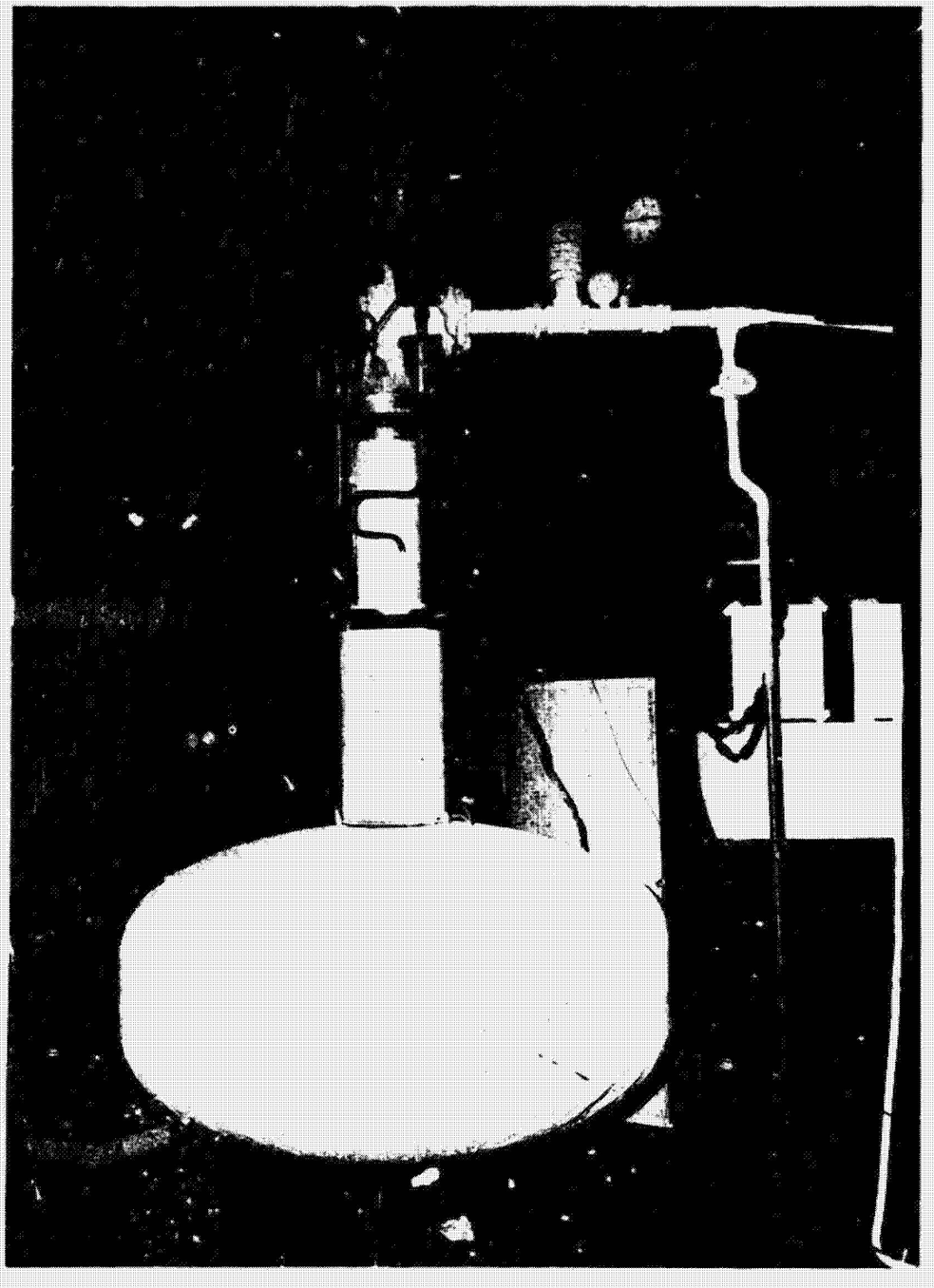

FIGURE III-24 INSULATION SYSTEM NO. 4 FROST FORMATION OVER PURGE BAG IN TEST II-3A

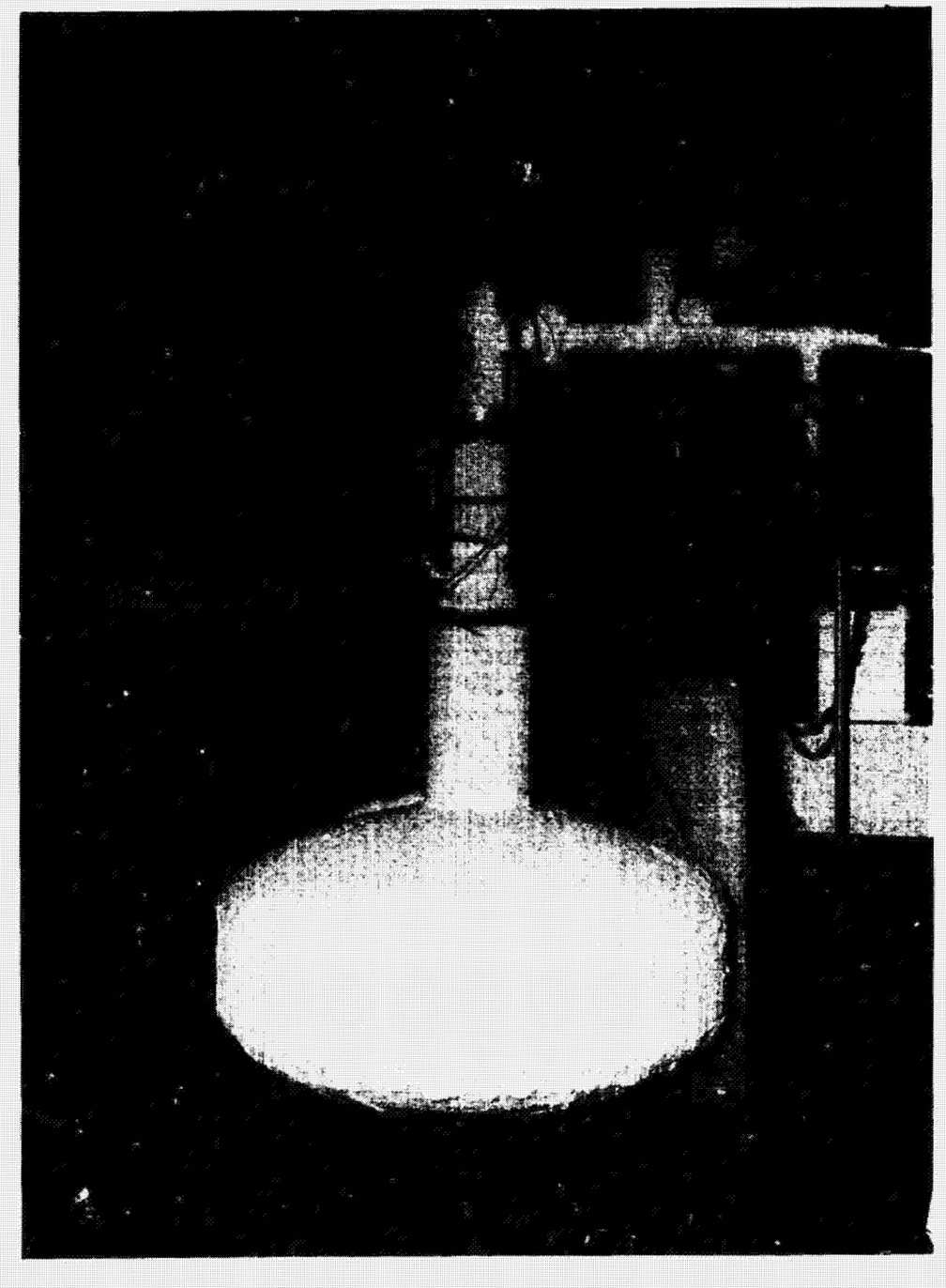

FIGURE III-25 INSULATION SYSTEM NO. 4 FROST FORMATION OVER VACUUM BAG IN TEST III-3B

FIGURE III-26 ALUMISEAL PURGE BAG - CLOSE-UP OF EVACUATED BAG

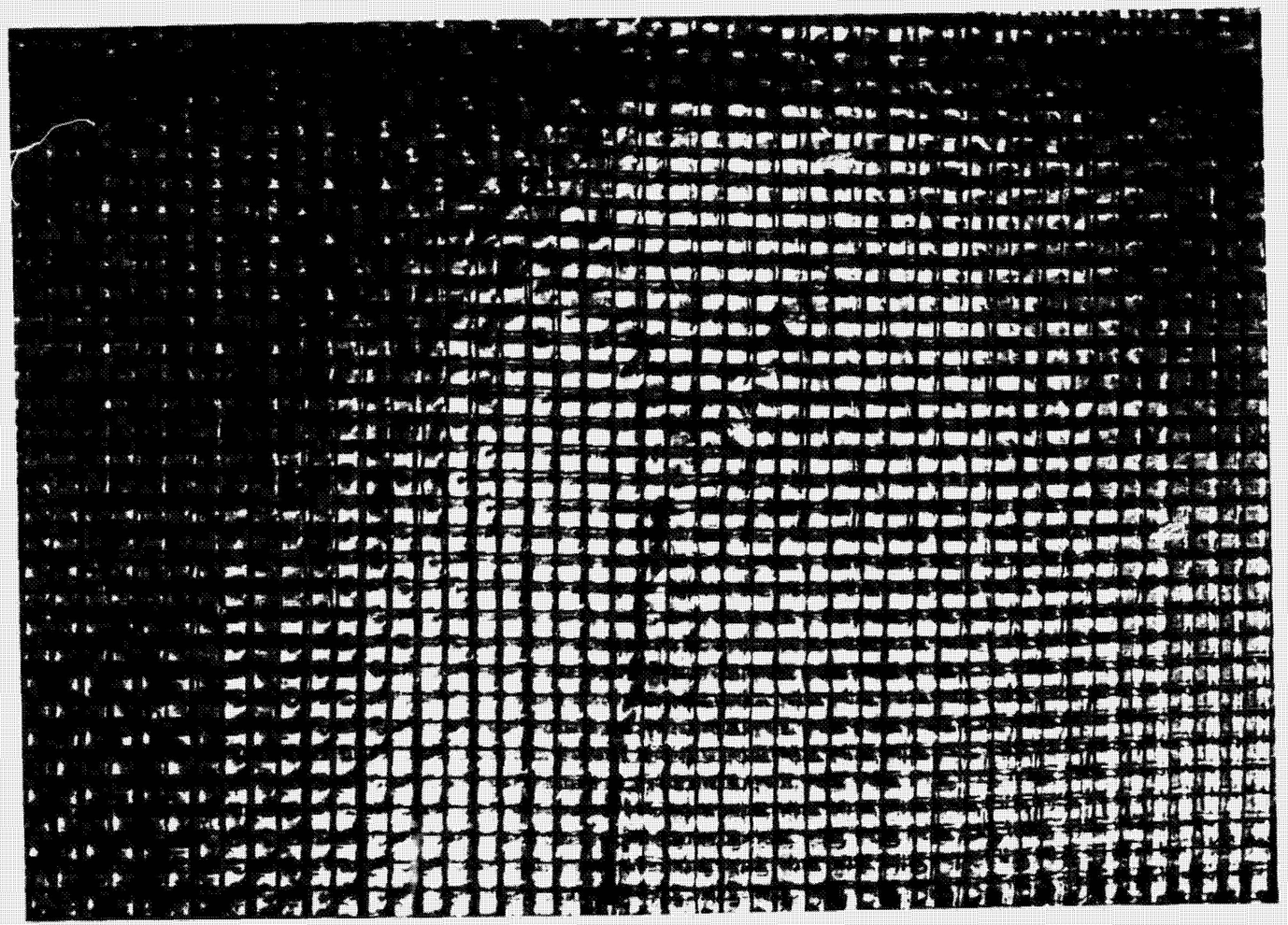

FIGURE III-27 INSULATION SYSTEM NO. 4-SHIELD EMBOSSING VISIBLE AFTER REMOVAL OF VACUUM BAG

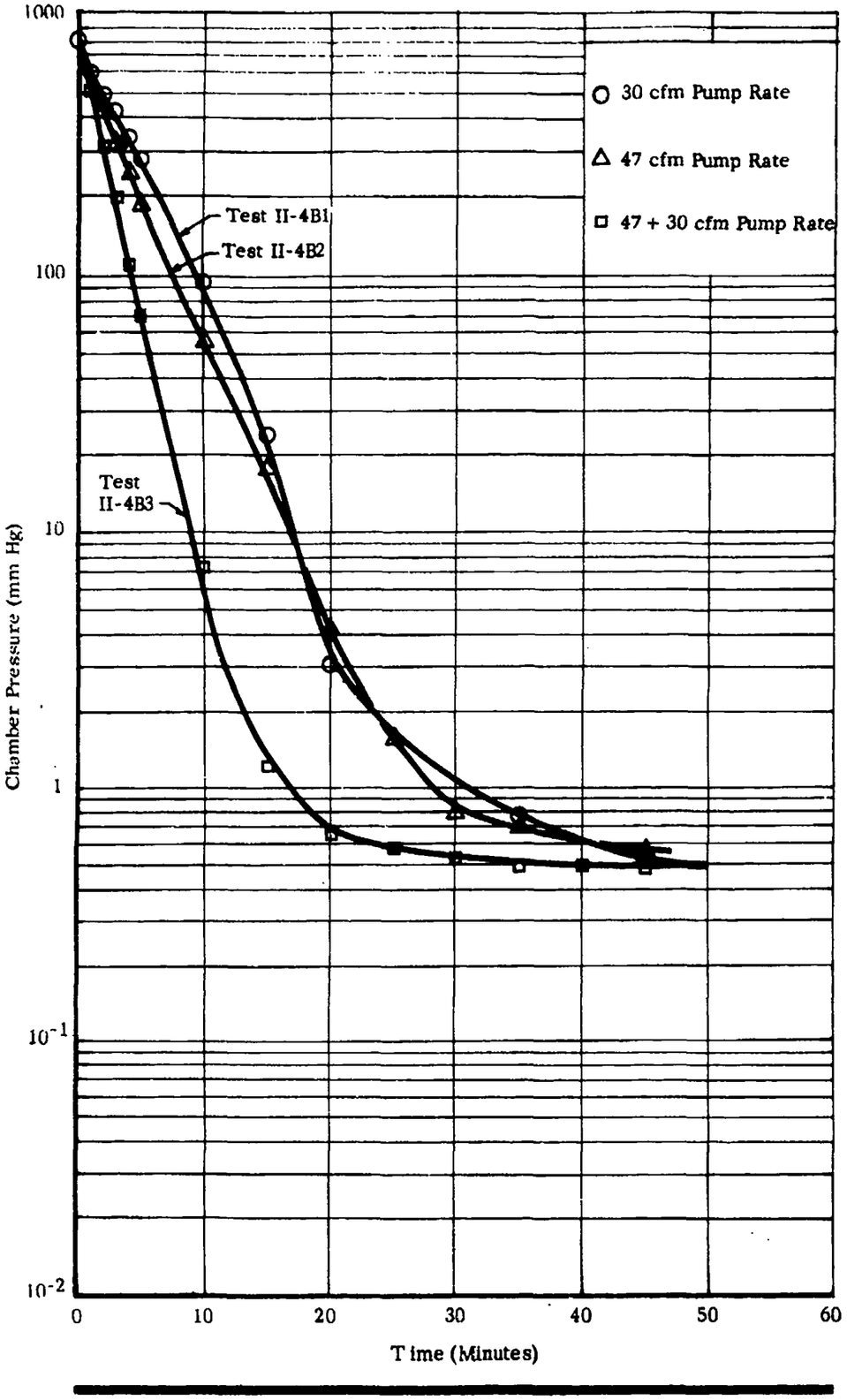

FIGURE III-28 TIME-PRESSURE TRANSIENT ADL CHAMBER
JUNE 3, 1964 TEST SERIES II-4B

FIGURE III-29 INSULATION SYSTEM NO. 4-FOLLOWING RAPID CHAMBER PUMP TEST

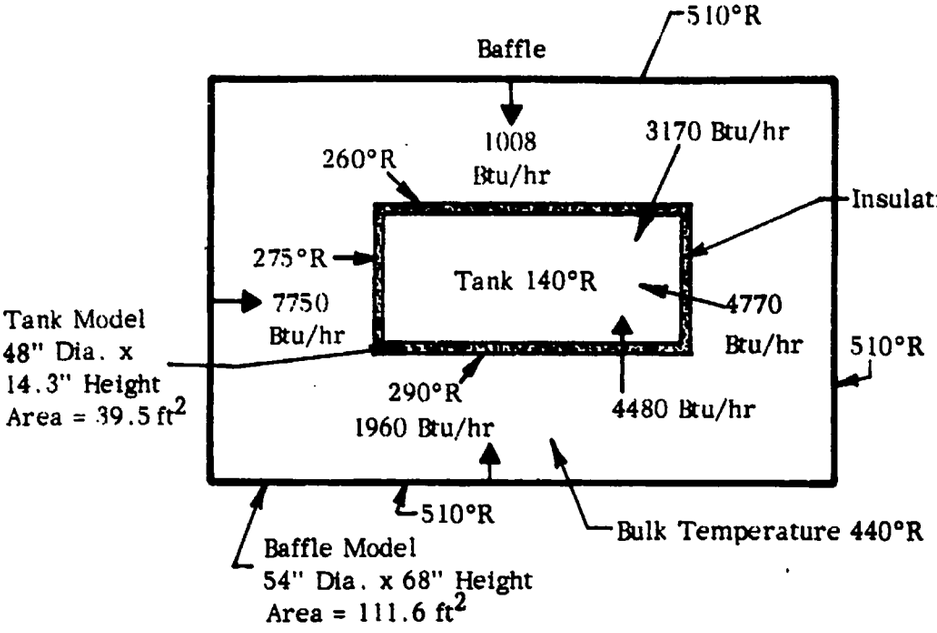

FIGURE III-30A TANK WITH HELIUM PURGED SHROUD

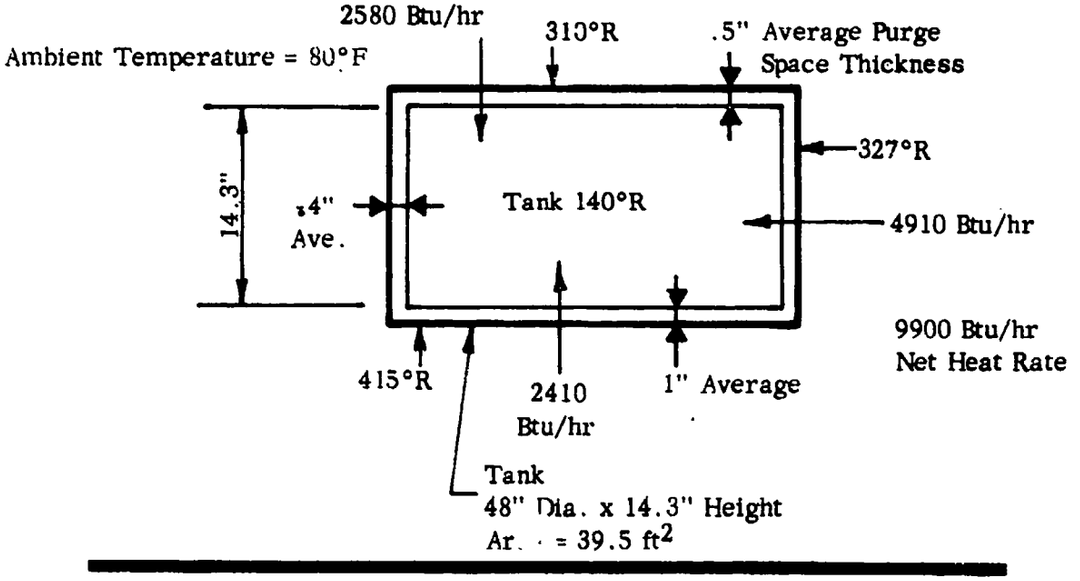

FIGURE III-30B TANK WITH HELIUM PURGE BAG

TABLE III-12

TANK INSULATION PROGRAM

TEST SUMMARY - INSULATION SYSTEM NO. 4 - CALORIMETER NO. 2 - TEST NO. II-1, 3C, 4A

SPACE ENVIRONMENT

Insulation System: Five aluminum radiation shields, .0005 inch thick spaced with six 1/8 x 1/8-inch mesh, vinyl coated, Fiberglas screen .020 inch thick.

Test Facility: ADL/Cambridge Test Facility

Penetration and/or gaps: None

Boundary Condition: Cold boundary and warm boundary are variable as shown below:

Emissivity: Not applicable

Tank Surface Area: 39.5 ft^2

Test Period No.	Tank Liquid	Data Period Date&Time	to Date&Time	Test Duration (hrs)	Ave. Vac. (mmHg)	Guard Liq/Temp (°F)	Total Heat Flow (Btu/hr)	Measured Heat Flux (Btu/hr-ft^2)	Ave. Baffle Temp (°F) Upper	Lower	Adjust.[1] Heat Flux[2] (Btu/hr-ft^2)
II-1A1[1]	LN_2	4/8/0800	4/9/0800	24	$1.0x10^{-6}$	-313	14.4	0.365	47	47	0.471
II-1A2[1]	LN_2	4/9/0800	4/10/0800	24	$.9x10^{-6}$	-313	14.6	0.371	48	48	0.474
II-1A3[1]	LN_2	4/10/0800	4/13/0800	72	$.6x10^{-6}$	-311	14.6	0.371	48	48	0.474
II-1B	LN_2	4/14/1300	4/15/0800	24	$.3x10^{-6}$	-309	8.0	0.400	-312	49	0.508
II-1C	LN_2	4/22/0800	4/24/0600	46	$.5x10^{-6}$	-312	11.2	0.573	55	-307	0.692
II-3C[2]	LN_2	5/22/1200	5/26/0800	92	$.7x10^{-6}$	-306	55.1	1.4	66	66	1.56
II-4A[3]	LN_2	5/29/1630	6/2/0830	88	$4.0x10^{-6}$	-306	32.7	0.83	69	69	0.91

Notes:

1. Tests performed prior to installation of bag.
2. Tests performed after vacuum bag tests, II-3B, but with bag still on calorimeter and in the vacuum chamber.
3. Test performed after removal of bag from calorimeter.

TABLE III-13

TANK INSULATION PROGRAM

TEST SUMMARY - INSULATION SYSTEM NO. 4 - CALORIMETER NO. 2 - TEST NO. II-2, 3A, 3B

ATMOSPHERIC ENVIRONMENT

Insulation System:	Five aluminum radiation shields, .005 inch thick spaced with six 1/8 x 1/8-inch mesh, vinyl coated, Fiberglas screen .020 inch thick.
Test Facility:	ADL/Cambridge Test Facility
Purging Medium:	Helium gas (tests II-2 and II-3A only)
Penetration and/or Gaps:	None
Boundary Condition:	Cold boundary and warm boundary are variable as shown below:
Emissivity:	Not applicable
Tank Surface Area:	39.5 ft^2

Test Period No.	Tank Liquid	Date&Time	to Date&Time	Test Duration (hrs)	Ave. Vac. (mm Hg)	Guard Liq/Temp (^oF)	Total Heat Flow (Btu/hr)	Heat Flux (Btu/hr-ft^2)	Ave. Baffle Temp (^oF) Upper	Lower	Ambient Temp. (^oF)
II-2[1]	LN_2	4/24/1215	4/24/1715	5	Atmos.	-185	11400	290	50	50	-
II-3A[2]	LN_2	5/7/1600	5/7/2400	8	Atmos	None Provided	6540	165	-	-	72
II-3B[3]	LN_2	5/13/1300	5/13/1800	5	125	None Provided	9270	234	-		67

1. Vacuum chamber and foils were purged with helium gas and maintained at atmospheric pressure throughout the test.

2. Purge bag was purged with helium gas and maintained at atmospheric pressure throughout the test. Test was performed in natural ground environment.

3. Test was performed in natural ground environment.

Insulation System No. 5

a. Introduction

The heat leak to a cryogenic propellant tank can be limited in a ground environment in several ways. In tests performed with insulation system No. 4 we demonstrated three methods, i.e., the use of a helium purged shroud, helium purge bag and vacuum bag. In these, the multi-layer system was used to perform both the space and ground insulating functions. One alternate approach to these methods is to provide two systems, one, a multi-layer to perform the insulating function in space, and the second to perform the insulating function in the ground environment.

In order for this second system to function effectively, it must isolate the tank surface, which is at liquid hydrogen temperatures, from the environment of the earth's atmosphere. Further, it must establish a second surface whose temperature is above the condensation point of air (about -315°F). This can be accomplished with a membrane spaced a small distance away from the hydrogen surface, provided that the volume between the two is either evacuated or purged with helium.

When the space between the membrane and the tank surface is evacuated, the atmosphere exerts a pressure on the membrane, tending to press it against the tank. If contact between the two is permitted, the membrane assumes the temperature of the tank, which in turn brings about condensation of air and other condensables on the outside of the membrane. For this reason, it must be supported at a distance from the tank by some structural media.

Also, the integrity of the membrane cannot be relied on completely, as small punctures would admit the atmosphere to the hydrogen-cooled surfaces, which could jeopardize the integrity of the vehicle. The effect of a failure in this membrane must be reduced by preventing communication between the failed region and the other spaces that lie between the tank surface and the membrane. This can be accomplished by using support media in the form of cells which communicate gas mass from one region to another at extremely small rates. Further, by bonding the support media to both the membrane

and tank surfaces, the effect of local failures cannot spread to other areas through the interface spaces. Thus, the combined membrane and support media offer a three-dimensional barrier to the passage of the condensable atmosphere to the tank surface. Therefore, the smaller the spaces where condensables can collect, and the smaller the passages between these spaces and the atmosphere, the smaller will be the probability that any failure in the system will become perpetuated.

This latter statement has served as the principal guide used in evolving the ground insulation component of Insulation System No. 5. It was the principal objective of this particular effort to develop and test this ground system by itself and in combination with a multilayer insulation.

b. Insulation System

(1) Ground System

(a) Selection

The heat leak to a hydrogen-filled vehicle tank in the ground environment should not exceed 100 BTU/hr/ft^2. Low-density rigid foams of the polyurethane and polystyrene variety have insulating performances that are suitable for meeting this requirement. For example, a 1/2-inch thickness of 5-lb/ft^3 density urethane foam can maintain this heat leak requirement.

Polyester honeycomb, cork board, and urethane foam systems were considered. Urethane foam was finally selected chiefly because it had a closed-cell structure and it could be foamed in place to any desired contour and shape while at the same time serving as its own bonding agent. Further, the urethane foams have a far greater latitude with regard to important properties such as mass density, cell size and surface control, than the other media.

Cutting foam from logs is a common technique for obtaining foam shapes to fit over curved surfaces. One advantage of this technique is that foam layers of uniform density can be obtained. However, the open cells at the cut surfaces absorb large quantities of adhesives when they are attached to the tank and membrane surfaces. This effect can be reduced considerably by foaming to the required

shape in molds. Thus, the foam surfaces are smooth and require a minimum quantity of bonding agent for attachment. The need for a bonding agent can be removed by foaming the required thickness to the tank surface.

(b) Structural Tests Approach

In the ground environment, the substrate insulation becomes the predominant thermal resistance restricting the heat flow to the propellant tanks. Thus the tank side of the insulation is at the stored propellant temperature, and the outer surface is at a temperature near that of the ambient environment. In the space environment, the multi-layer becomes the predominant thermal resistance; and, therefore, the temperature of the entire substrate material closely approaches the propellant temperature. The temperature gradients and transients introduce severe stresses into the foam, in addition to those resulting from the different thermal contractions taking place between the tank wall and foam. The differential contractions may cause shear and tensile type failures in the foam structure.

For initial testing of the foams a test procedure was developed by simulating the ground and space temperature enviornments in the test specimens. Specimen panels were foamed in place against a 12" x 6" sandblasted stainless steel plate to which a copper tubing coil had been soldered on the back side. The test specimen is chilled in air by circulating liquid nitrogen through the coil; this test simulated the ground environment. If the specimen did not delaminate from the plate, as shown in Figure III-31, or crack at the surface, as shown in Figure III-32, it was immersed in liquid nitrogen several times to produce severe thermal shock in the specimen and thereby simulate the space environment. If the foam withstood the initial immersion without cracking or delaminating, it was cycled several times between room temperature and liquid nitrogen temperature to test its endurance.

Several different types of polyurethane foams with a range of densities, were evaluated. All foams tested were found to be marginal or unsatisfactory unless reinforced with a fibrous filler, though there are substantial problems involved in mixing the fiber with

the components and placing this mixture in the mold before foaming starts. However, the improvement in the strength properties produced by the addition of glass fiber is substantial. Cyclic immersion and heating of the reinforced foam have failed to cause any degradation of the foam with 10% glass fiber added. If 7.5% glass fiber is added, there may be slight cracking of the higher density foams on cycling. At 5% glass fiber addition, an improvement is noted, but cracking occurs in the foams of higher density (5 to 8 pounds per cubic foot). Foams with a 2% glass fiber are only slightly better than the unreinforced foam. We have also worked with a glass scrim and a glass surfacing veil as reinforcements. These were held in place close to the metal test plate and the outer surface while the resin was foamed. Although both of these reinforcements produce some improvement, perhaps equivalent to the use of 5% glass fiber in the mix, neither approaches the effectiveness of the 10% glass fiber addition.

(c) Materials Tested and Results

We studied several different foam systems and the results achieved with them are summarized below:

Chempol 1325-1428 (Freeman Chemical Corporation)

This is a Freon blown polyester based foam. The density can be varied by varying the amount of Freon added to the components. This foam cracked and sheared from the test plate at all densities from two pounds up to eight pounds. The cracking was more severe at the higher densities. When 10% of chopped strand glass was added to this foam, it withstood immersion and cycling at all densities without cracking.

Chempol 1372-1407 (Freeman Chemical Corporation)

This is a CO_2 blown polyester based foam. It is formulated as supplied, to produce a two-pound density foam. This was the most promising foam that we tested prior to the start of the work on addition of glass fiber to the foams. This foam withstood immersion in liquid nitrogen without cracking or separating from the metal test plate. However, the foam consisted of widely varying cell sizes

and had very poor compressive strength. Further, because of the high viscosity of this foam, it is difficult to mix glass fibers with it and cause it to flow into the forms.

Nopco H-620N (Nopco Chemical Company)

This is a high-dimensional stability foam made by Nopco for use in refrigerator insulation. It is a Freon blown polyester based foam. Since the Freon had already been added to the components, it was possible to produce this foam only in a nominal two-pound density. At this density, the foam had some tendency to crack when immersed and was inferior to the Chempol 1372-1407 Foam. Because we could not adjust the density of this foam, we did attempt to add glass fiber to it.

Chempol 1320-1407 (Freeman Chemical Corporation)

This foam is a polyester based Freon blown foam which, according to Freeman, is very similar to the 1372-1407 system, except for the substitution of Freon as the blowing agent in place of internally generated CO_2. We have encountered some difficulty in getting good closed-cell structure with this foam. We have not worked extensively with it because the high viscosity of the components makes admixture with glass fibers difficult.

ADL Rigid Foam

This is a formulation based on a quadrol-triol mix that is combined with Mondur MR isocyanate. It is a Freon blown foam, and the density can be varied over a wide range. The performance of this foam at two-pound density was comparable with that of the 1372-1407 Chempol foam. However, it is somewhat lower in viscosity as mixed initially and is, therefore, easier to handle and pour in place. Because of this low viscosity, this foam is favored for use in glass fiber mixtures.

The formulation used for this urethane foam is as follows:

1.	Niax Triol LK-380	Union Carbide Corp.	85 parts by weight
2.	Niax Pentol LA-700		15 parts by weight
3.	Freon 11*	DUPont	20 parts by weight
4.	Dow Silicone 113	Dow Corning Corp.	1.0 parts by weight
5.	Mobay Catalysts C-16	Mobay Chemical Co.	0.5 parts by weight
6.	Mondur MR		109 parts by weight
7.	¼ inch chopped strand Fiber-glass X624 binder	Pittsburg Plate Glass Co.	10% on the weight of the entire formulation.

Items 1 through 5 in the formulation were premixed in a proper ratio in order to speed up the process of mixing when we were applying foam to the tank. Appropriate quantities of the premix, the glass fiber, and Mondur MR were placed in a mixing vessel and mixed rapidly for approximately 30 seconds. The mix was then placed in the cartridge of a Semco sealant gun manufactured by Semco, Inc. of Englewood, California. The sealant gun was used to inject the foam-fiber mix between the mold and the calorimeter tank.

Based upon strength tests performed with liquid nitrogen and on the ease of fabrication, it was decided to use the ADL Rigid foam. However, we considered it important to perform cold shock tests with liquid helium and liquid hydrogen prior to making the final selection. The samples to be placed in liquid helium consisted of a ½- inch foam thickness on a 1 x 10 inch metal backing plate. The samples to be placed in liquid hydrogen were cut from a flat plate calorimeter sample disc, 12 inches in diameter, which consisted of ½-inch thickness of foam applied to 1/8-inch thick aluminum plate. Three samples, about 4 inches wide, were cut from the disc. The helium tests were performed at A.D. Little, Inc., and the hydrogen tests were performed at Lewis

*"Equivalent materials are available from Allied Chemical under the name of Genetron 11 and from other suppliers".

Research Center. The minimum immersion time was about ten minutes for all tests. We could find no evidence of surface cracking or delamination of the foam from the metal backing plate after soaking in the liquid helium and liquid hydrogen environments. These results confirm those we obtained previously by immersion of the foam bonded to 6 x 12 and the larger 10 x 36 -inch sample plates in liquid nitrogen.

In addition to tests concerned with the mechanical performance of the selected foam, we measured its thermal and gas permeability performance. Thermal conductivities of 0.15 and 0.11 Btu in/hrft^2°F were measured in flat plate tests 1062a and 1062b, respectively. These values are characteristic of foam insulations.

The permeability of the foam was found to be extremely small; i.e., we measured a rate of 8.4×10^{-7} std cc of helium/sec. on a sample 7.95 cm^2 in area and 1.27 cm thick. This indicates that the foam acts very much like an impermeable membrane or gas barrier.

These final performance results indicated the suitability of the ADL Rigid Foam for use as the substrate of the composite insulation system. It was foamed in place in segments on the calorimeter tank to a thickness of 1/2 inch through the use of a plastic form as shown in Figures III-33 and 34. Both the tank and form were maintained at 120°F to assure uniform foam density throughout the layer. All joints were sealed with foam to form a gap-free layer around the tank. The neck was protected with foam.

(d) Vapor Barrier

A laminate of aluminum foil and polyester film was selected for use as the foam vapor barrier. This was based upon the high strength and tear resistance of such laminates as well as on their low permeability. Samples of a 2 mil thick laminate consisting of a 1 mil aluminum core and two 1/2 mil polyester films were checked with a helium mass spectrometer and found to have a zero permeability. While this performance quite probably cannot be totally achieved over large surface areas, the tests indicate that a sufficient gas barrier could be obtained.

The performance of the vapor barrier and of the adhesive used to bond it to the foam was determined from liquid nitrogen tests of the 6 x 12-inch plate mounted specimens. A urethane and a versamid-epoxy adhesive were both tested.

A proprietary polyurethane adhesive manufactured by Narmco Materials Division, Whitaker Corporation was used to bond the Alumiseal over the foam. This adhesive consists of Narmco Resin 7343 with curing agent 7139. It is a rather soft rubbery adhesive that is used in cryogenic applications because its bond strength actually increases as the temperature is lowered to liquid hydrogen temperature. For the work of bonding the Alumiseal to the tank it has the additional advantage that it goes through a tacky stage in which it is very similar to a pressure sensitive adhesive. This pressure sensitive stage can be used to form a tight bond and eliminate air entrapment under the Alumiseal.

In some of our experimental work we have also used an epoxy Versamid adhesive which consisted of equal parts by weight of Epon 828 manufactured by Shell Chemical Company and Versamid 140 manufactured by General Mills, Inc. This adhesive also has proven effective in cryogenic work and also has excellent room temperature pot life, but does not have the pronounced tacky stage that is characteristic of the Narmco polyurethane adhesive. It is therefore more difficult to use in bonding the Alumiseal to the foam or in other applications where the materials being bonded have sufficient stiffness that they may tend to pull apart after they are assembled.

The vapor barrier for the calorimeter tank was formed in a manner similar to that used to fabricate the shields in the previous multilayer systems fabricated. The barriers over the tank ends were pressure-formed into spherical segments. The side sheets were gored to fit over the tank knuckle radii. All joints in the three main sheets are of the butt type. Each joint was then sealed with vapor barrier tape containing pressure-sensitive adhesive. The adhesion properties of this tape were tested and found satisfactory at liquid nitrogen and liquid helium temperatures.

(2) Multi-layer Component

It had been our intent to apply a multi-layer system consisting of shields of ¼-mil polyester film coated on both sides with gold. Our supplier, however, had difficulty producing a uniformly-coated product with an acceptable coating thickness. It became necessary, therefore, to substitute aluminum coating for the gold coating. We procured polyester film which had been coated on both sides with vapor-deposited aluminum applied to a thickness of about 400 Å

During the fabrication of the multi-layer component, the surface emittance of the shields used in System No. 5 was measured on samples taken from material adjacent to that from which the tank side pieces were formed. These data and the measured apparent thickness of the vapor-deposited aluminum are presented in Table III-17. The average values are 421 Å and .035 for the apparent thickness and emissivity, respectively, with about 10% scatter in the data for each property. The theoretical heat flux for System No. 5 multi-layer component, based on the average measured emissivity, is .49 BTU/hr ft^2 for an 80° F source temperature. The thermal conductivity of the foam is so high with respect to that of the multi-layer that the foam has little effect on the total heat flux in the space environment.

The principal characteristics of the composite insulation system tested are presented in Table III-1. The completed substrate system, including the foam and vapor barrier, are shown in Figure III-35. The completed system with the multi-layer applied over the substrate is shown in Figure III-36. The neck configuration used is shown in Figure III-37A with the multi-layer.

c. Test Conditions

Six significant tests were performed with foam substrate, and ten additional tests were performed with the composite insulation system. The test conditions are summarized briefly in the following paragraphs, while a tabulated summary is presented in Table III-1.

(1) Foam Substrate Tests-J-4 Facility

Test II-5A (Nitrogen boil-off at atmospheric conditions)

The structural integrity and thermal performance of the foam substrate and vapor barrier applied to the tank calorimeter were tested

in actual ground conditions at the J-4 facility, Plum Brook Station. The calorimeter was filled with liquid nitrogen at the beginning of the test and then allowed to boil off freely until the contents were depleted. The test had a duration of about ten hours. The boil-off gases were measured continuously during this period; at the same time the insulation was under continual observation.

The entire insulation surface was above the freezing point of water, as evidenced by the presence of condensed moisture and the absence of frost or ice formation. There were no apparent breaks in the vapor barrier nor heaves or breaks in the foam.

Test II-5B1 and B2 (Liquid Hydrogen boil-off at atmospheric conditions)

These tests were performed in an identical manner to the previous test except that liquid hydrogen was used as the test fluid. Further, because of the short run times experienced with hydrogen, due to its low latent heat per unit volume compared to nitrogen, we performed two tests instead of a single test to obtain additional data.

Moisture condensed on the vapor barrier surface as in test II-5A during the performance of the boil-off test. In addition, a frost spot of about 2 inches in diameter developed on the upper head of the tank and a light frosting developed on a quadrant sector of the bottom head during the test. These areas were inspected after the hydrogen was removed from the tank, but no damage to the insulation system could be detected.

However, the vapor barrier on the neck insulation developed a gas bubble on one side representing almost 50% of the area. We attribute this to a lack of any bond between barrier and the foam and also to a poorly-formed foam structure which contained large voids that connected to the atmospheric environment. We believe that cryopumping of the atmosphere into the void occurred, which resulted subsequently in the large blister observed when the calorimeter was warmed.

Tests II-5C and II-5D (Foam cold shock at atmospheric conditions)

These tests were performed to check the structural integrity of the foam substrate under conditions of temperature prevailing in the

space envirorment. The actual tests were performed in a ground environment. In test II-5C, the tank was first filled with nitrogen. Next, a spray of liquid nitrogen was directed at the outside of the insulation at the top and bottom heads. The tank and spray nozzles were enclosed within a plastic bag to insure cool-down of tank surroundings to liquid nitrogen temperatures. The spray to the tank was maintained for a period of about one hours. Test II-5D was performed in a similar manner, except that hydrogen was used instead of nitrogen to fill the tank.

No deterioration of the foam or vapor barrier could be detected at the completion of test II-5C. However, at the completion of test II-5D we observed 18 blisters that had developed in the vapor barrier, ranging in size from 1½ inches in diameter to the largest on the tank side which measured 8 x 21 inches. A number of these blisters are shown in Figure III-38. A total of 15 per cent of the tank area was affected in this manner: Seventy-five per cent of the blistering was evidenced as a delamination of the vapor barrier; i.e., the inner polyester film laminate had delaminated from the aluminum and outer film layers, and an unidentified gas was present in the delaminated area. Only 25% of the blistering was due to failure of the adhesive which was used to bond the vapor barrier to the foam. It is important to note, however, that in almost half the number of blistered areas, both delamination and adhesive failure occurred together. The results of these observations are summarized in Table III-16.

After the calorimeter was returned to Cambridge, the blistered areas of the vapor barrier were cut away and new vapor barrier patches used to repair them. The patches were bonded to the foam as before with versamid-epoxy blanded adhesive. The edges of each patch were sealed with pressure-sensitive tape.

Test II-5E (Vaccum test of foam and vapor barrier)

This test was performed at the Arthur D. Little, Inc., facilities in Cambridge after repair of the vapor barrier was completed. In order to develop assurances that the vapor barrier would not blow off of the foam under vacuum condition and, thus, cause the multi-layer insulation system to fail, we subjected the foam and vapor barrier to vacuum in the micron

range. Initial tests were performed while the insulation was at approximately room temperature. These were followed by tests in which the entire insulation system was held at -320°F. This was accomplished by filling the calorimeter with liquid nitrogen and at the same time maintaining the chamber baffles at -320°F. No degrading effects resulted from these tests; and we, therefore, proceeded with the multi-layer application.

(2) Foam and Multi-layer Insulation Tests-J-3 Facility

The five-shield, multi-layer insulation, described previously, was applied to the calorimeter at the completion of test II-5E. The calorimeter was returned to the Plum Brook Station for testing with liquid hydrogen in the J-3 facility chamber. Based upon the emittance measurements performed with the emissimeter, we predicted a value for the heat flux of .49 BTU/hr ft^2 for insulation system.

Test II-6A1 (Liquid nitrogen-space environment)

The experimental heat flux of 1.54 BTU/hr ft^2 obtained in the test was approximately three times greater than this expected value. We attributed this result to the calorimeter neck shield, which had been altered to accommodate the foam insulation that was added to the tank to form the composite system. (See Figure III-37A) The heat flux data are summarized in Table III-17

Test II-6A2 (Liquid nitrogen-space environment)

Prior to this test, the neck shield was modified in the field to conform more closely to the design used in previous insulation systems. The modified configuration is shown in Figure III-37B. In every other respect the test conditions were a repeat of Test II-6A1, performed previously. The average heat flux of the insulation system was reduced to .850 BTU/hr ft^2 as a result of modification performed at the neck. However, the heat flux results were still higher than the expected values. The values are summarized in Table III-17.

Test II-6B (Liquid Hydrogen-space environment)

Whereas tests II-6A1 and II-6A2 were performed with liquid nitrogen in the calorimeter, test II-6B was performed with liquid hydrogen. The use of liquid hydrogen should result, theoretically, in a flux increase of no more than .01 BTU/hr ft^2. The experimental results show an increase

of about .06 BTU hr ft^2 to an average flux of .91 BTU/hr ft^2.

Test II-6C (Liquid nitrogen, space environment, warm bottom half)

The heat flux values obtained in tests II-6A2 and II-6B were still significantly higher than the expected heat flux of .49 Btu/hr ft^2. We, therefore, decided to isolate completely any influence the neck might have on the heat transfer to the calorimeter by reducing the heat flow to the upper half of the tank to nearly zero value. This was accomplished by maintaining the upper baffle of the chamber at -320°F through the use of liquid nitrogen circulated through the baffle coil. Under these circumstances, the heat flux measured for the bottom half of the tank insulation is .72 BTU/hr ft^2.

Test II-6D (Liquid nitrogen-helium shroud)

In this test we simulated the vehicle configuration in which the propellant tank is shrouded with the vehicle air-frame and the space between the two is purged with gaseous helium. The test was performed in the chamber at the J-3 facility. Test II-6D is similar to test II-2 performed with Insulation System No. 4 and similar also to test II-9B performed subsequently at the Arthur D. Little, Inc., facilities. The data are compared and presented in Table III-19.

In this test, the foam surface and outer shield temperatures were available. The data show that both of these surfaces are warmer at the top of the tank and get progressively cooler in the direction of the tank bottom. These gradients and how they vary with time during the progress of the test can be seen in Figure III-39. We ascribe these time variations to the fact that the cooling water was not used in the chamber baffles and jacket and the entire system, including the chamber, was cooling with time.

Substrate and Multi-layer Tests -A.D. Little, Facility

When the tank calorimeter was returned to Cambridge, the J-3 tests were re-run in the Arthur D. Little, Inc. chamber. Prior to these tests, however, an asbestos tape, placed there prior to test I-6A2, was removed from the lower end of the neck shield because it applied pressure to the multi-layer and provided also a weak thermal

short between the multi-layer and the neck shield. The results of these tests are summarized in Table III-18.

Test II-9A (Liquid nitrogen - space environment)

This test is a repetition of tests II-6A and II-6B performed at the J-3 facility. The insulation was placed in the simulated space environment to obtain heat flux measurements with both upper and lower baffles at about room temperature.

Test II-9A was divided into three periods as shown in the table. The average heat flux obtained in over 120 hours of test is .78 BTU hr ft^2. Compared to the similar test II-6A2 performed at J-3, this represents an 8% improvement (based on adjusted heat flux values), for which we believe the removal of the asbestos from the neck is at least partly responsible.

Test II-9C2 (Liquid nitrogen-warm bottom baffle)

This test is similar to test II-6C. The upper chamber baffle was held at liquid nitrogen temperature while the bottom baffle was held at near room temperature. The measured heat flux for the bottom half of the insulation is .65 BTU/hr ft^2. This represents a decrease of almost 17% from the total average value measured in test II-9A. It is interesting to note that a similar decrease occurred at J-3 facility between tests II-6A2 and II-6C. This indicates that the top half of the insulation has a higher heat flux than the bottom portion. To reconfirm this result, we performed test 1I-9D.

Test II-9D (Warm top baffle)

In test II-9D, the bottom baffle was held at -320°F and the upper baffle was held at near room temperature. The resulting heat flux, adjusted to 80°F baffle temperature, is 1.03 BTU/hr ft^2. This confirms the higher heat rate through the upper half previously anticipated from tests II-9A and I-9C2.

We believe that heat leak through the neck was reduced to a negligible amount when the shield was modified at our facilities. Further, it is our belief that the heat flux values for the upper half of the insulation are greater than those to the lower half, possibly as a result of the gravity settling of the upper shields and

spacers during shipment to and from Cambridge.

Test II-9B (Helium shroud)

As indicated earlier, the test conditions used in test II-9B are similar to those of II-6D. The vacuum chamber baffle was used for simulating the shroud once the calorimeter was installed in the chamber. We obtained an experimental heat flux of 85.6 BTU/hr ft^2, as noted in Table III-19.

In this test, the baffles in the chamber were maintained at $66^{\circ}F$ through the use of circulated water. The only remaining thermocouple on shield No. 5, location B, indicated an average temperature of $-3^{\circ}F$. The foam surface temperature was indicated to be about $-31^{\circ}F$; and, of course, the tank surface temperature was $-320^{\circ}F$.

Test II-10 (Helium purge bag)

A purge bag was placed around the composite insulation system, and heat flux measurements were made with the calorimeter in a ground environment.

The purge bag was fabricated from a polyester film, aluminum-foil laminate. We estimate that the average distance between the bag and the foam substrate was 0.3 inches. The space between the foam and bag contained the five-shield multi-layer system.

A heat flux of 92.2 BTU/hr ft^2 was obtained with this system, as noted in Table III-19. The foam thermal conductivity could not be accurately determined from the test, as the surface thermocouple readings were not available. However, by comparison with the results of Test II-5, performed at Plum Brook Station, the heat leaks for the two are comparable.

The principal temperature drop of the system occurs in the foam substrate. With an ambient temperature of $72^{\circ}F$, we measured typical bag temperatures of about $22^{\circ}F$. While the surface temperature of the foam substrate was not available, some temperatures measured on shield No. 3, which is displaced a small distance from the foam, indicate temperatures of about $0^{\circ}F$. From this, we estimate the foam temperature drop at about $320^{\circ}F$.

d. Results and Discussion

(1) Foam Insulation

(a) Thermal Performance

The thermal conductivities computed from the conditions established in the ground simulation tests show good agreement with the results obtained in the flat plate thermal conductivity apparatus and those reported by Haskins.[5] The results we obtained are summarized below. The temperature distribution within the system for tests II-6D and II-9B is shown in Figure III-41.

Test	Measured Heat Flux Btu/hr ft^2	Temp. (^{o}R) Tank	Vapor Barrier	ΔT (^{o}R)	Temp (^{o}R) Mean	Thermal Conductivity Btu-in / hr-ft^2-^{o}F
II-5A	97.0	140	522	382	331	.127
II-5B	93.2	40	503	473	272	.100
II-6D	69.1	140	400	260	270	.133
II-9B	85.6	140	429	289	285	.149
II-10	92.2	140	460	320	300	.144

In tests 1062 a and b with the K-apparatus, thermal conductivity values of .150 and .110 Btu-in/hr-ft^2-^{o}F, respectively, were obtained. Haskins reports a value of .110 Btu-in/hr-ft^2-^{o}F for a Freon-blown polyurethane foam with a 4.0 lb/ft^3 density at a mean temperature of about -175^o F (285^o R). The results obtained with the tank insulation range from .127 to .149 Btu-in/hr-ft^2-^{o}F, with liquid nitrogen on the cold side.

Haskins shows a correlation between thermal conductivity and mean insulation temperature. From our limited data it is not possible to show this correlation. Further, because of the large surface area of the tank-mounted foam, we experienced variations in the warm surface

temperature. The thermal conductivity was computed using the average of the measured temperature values.

Finally, the thermal performance of the foam system appeared unimpaired throughout the sixteen tests performed with the system. Equally important is the fact that the foam system stabilized the heat flux for the various ground conditions studied. The thermal resistance of the foam is about a factor of three greater than the total thermal resistance exterior to the foam. This can be established from the temperatures presented in the above tabulation. Thus, if the outside resistance is reduced to zero value, the heat flux will increase no more than about 35% to a value of 130 Btu/hour (based on average ambient of 80° F).

(b) Mechanical Performance

The foam system has undergone a series of sixteen tests under a variety of conditions simulating both space and ground environments. No significant deterioration occurred in the system except for failure of 15 per cent of the vapor barrier surface in Test II-5D. This latter condition, we believe, can be remedied through the use of a temperature-rated barrier material and by applying the barrier to the foam in small sections. On the other hand, the foam selected, the method used to strengthen the foam, and the method used to apply and attach the foam to the tank gave excellent performance. These materials and techniques should, therefore, be considered further with regard to insulating space vehicle tanks.

(2) Multi-Layer

The data we obtained in three tests strongly supports the contention that the new neck design used with the composite system was the major extraneous source contributing to the high heat rate to the calorimeter. The three tests are compared below. The temperature distributions in the system for tests II-6A2 and II-9A are shown in Figure III-40.

Test	Measured Flux Btu/hr ft^2	Adjusted Flux Btu/hr ft^2	Test Facility	Test Fluid
II-6A1	1.56	1.54	J-3	LN_2
II-6A2	.85	.85	J-3	LN_2
II-9A	.71	.78	ADL	LN_2

The first conversion towards the original neck design took place between tests II-6A1 and 6A2. The conversion was completed prior to test II-9A. The heat flux obtained in the latter test is taken as the actual thermal performanc of the multi-layer insulation.

In Test II-6B, in which liquid hydrogen was used as the test fluid, we obtained a higher flux than obtained in test II-6A2 with liquid nitrogen. These tests are compared below. The temperature distribution in the system obtained in test II-6B is shown in Figure III-40.

Boundary Temperature (^{o}F)			Measured Flux	Adjusted Flux		
Warm	Cold	Test	Btu/hr ft^2	Btu/hr ft^2	Test Facility	Test Fluid
80	-420	II-6B	.91	.91	J-3	LH_2
79	-320	II-6A2	.85	.85	J-3	LN_2

The difference in the two measured heat flux values may be due to solid conduction taking place within the multi-layer insulation. If solid conduction is present and is significant, the lowering of the sink temperature from -320^o F to -420^{o}F should produce a noticeable increase in heat transfer because there is a 26 per cent increase in the differential temperature from a value of 390^o F to 490^o F.

If all the heat transfer occurring in tests II-6A2 and II-6B were by radiation, then the two measured heat flux values should correspond to within ½ per cent. This can be demonstrated analytically for the low temperature levels of the sink and the constant source temperature taking place in the experiments.

If in both tests it is assumed that the radiative flux is .50 Btu/hr-ft^2 as calculated from a shield emittance value of .035, and if this flux is not altered by lowering the sink temperature from -320° F to -420° F, then, by subtraction of the radiation flux from the measured flux, we obtain an estimated solid conduction flux of .35 and .41 Btu/hr-ft^2 for tests II-6A2 and II-6B, respectively. This represents an increase of 17 per cent in the solid conduction flux between the two tests and corresponds to a 26 per cent increase in temperature. This correspondence infers the presence of a significant amount of solid conduction in the insulation system.

The higher than estimated heat flux (.50 Btu/hr-ft^2) could be assumed also to result from out-gassing of the foam insulation. However, this is not probable, since the flux obtained in II-6B would have been substantially lower than .85 Btu/hr-ft^2, instead of .91 Btu/hr-ft^2 as measured. In test II-6B, the entire foam-vapor barrier structure is at less than 50° R and very likely in an evacuated state. Thus, unless hydrogen or helium gas is present in the chamber space, cryopumping or condensation of the gases in the multi-layer rather than out-gassing is the more probable occurrence. This cryopumping effect would condense the interstitial gas and eliminate any significant heat transfer taking place by molecular conduction. The fact, therefore, that the heat flux increased between the two tests is a further confirmation of the presence of solid conduction in the multi-layer insulation.

A comparison was made between those tests in which the insulation received heat over the entire surface and those in which the insulation received heat only through the bottom half. This comparison is shown below:

Test	Measured Flux Btu/hr-ft^2	Adjusted Flux Btu/hr-ft^2	Remarks	Test Facility	Test Fluid
II-6A2	.85	.85	Entire Insulation	J-3	LN_2
II-6C	.71	.72	Bottom Half	J-3	LN_2
II-9A	.71	.78	Entire Insulation	ADL	LN_2
II-9C2	.60	.65	Bottom Half	ADL	LN_2

A comparison of the first two and the last two tests shows that the heat flux through the lower half of the insulation is less than the over-all average. Therefore, the heat flux through the upper half must be greater than the over-all average. This is confirmed when the heat flux is measured separately through each half of the insulation and compared, as is done below:

Test	Measured Flux Btu/hr-ft^2	Adjusted Flux Btu/hr-ft^2	Remarks	Test Fluid
II-9C2	.60	.65	Bottom Half	LN_2
II-9D	.93	1.03	Upper Half	LN_2

Further, the sum of the heat rates measured in these two tests is 30.30 Btu/hr, which compares with a heat rate of 28.3 Btu/hr obtained for the entire insulation in test II-9A (see Table III-18). The agreement of these values to within 10% establishes the validity of the individual measurements obtained in II-9C2 and II-9D.

It is reasonable to expect that the shields and spacers on the lower half of the calorimeter tank are not compressed because they hang freely. If, then, the average heat flux measured in the insulation system indicates the presence of solid conduction heat flux effects, the magnitude of this effect should be less for the lower half than for the upper half of the insulation system. The data obtained in tests II-9C2 and II-9D support this assumption and are further evidence of the presence of a significant amount of solid conduction heat flow.

From the foregoing, we conclude the following:

e. Summary

1. The expected heat flux was not achieved with the multi-layer insulation because of solid conduction effects taking place in the insulation, particularly in the upper half. The compacting takes place in the upper half of the insulation because of the normal orientation of the calorimeter and

because the lower portion of the insulation is supported from the upper part.

2. The foam did not out-gas to any observable degree in the simulated space environment or in any way affect the thermal performance of the multi-layer insulation component.

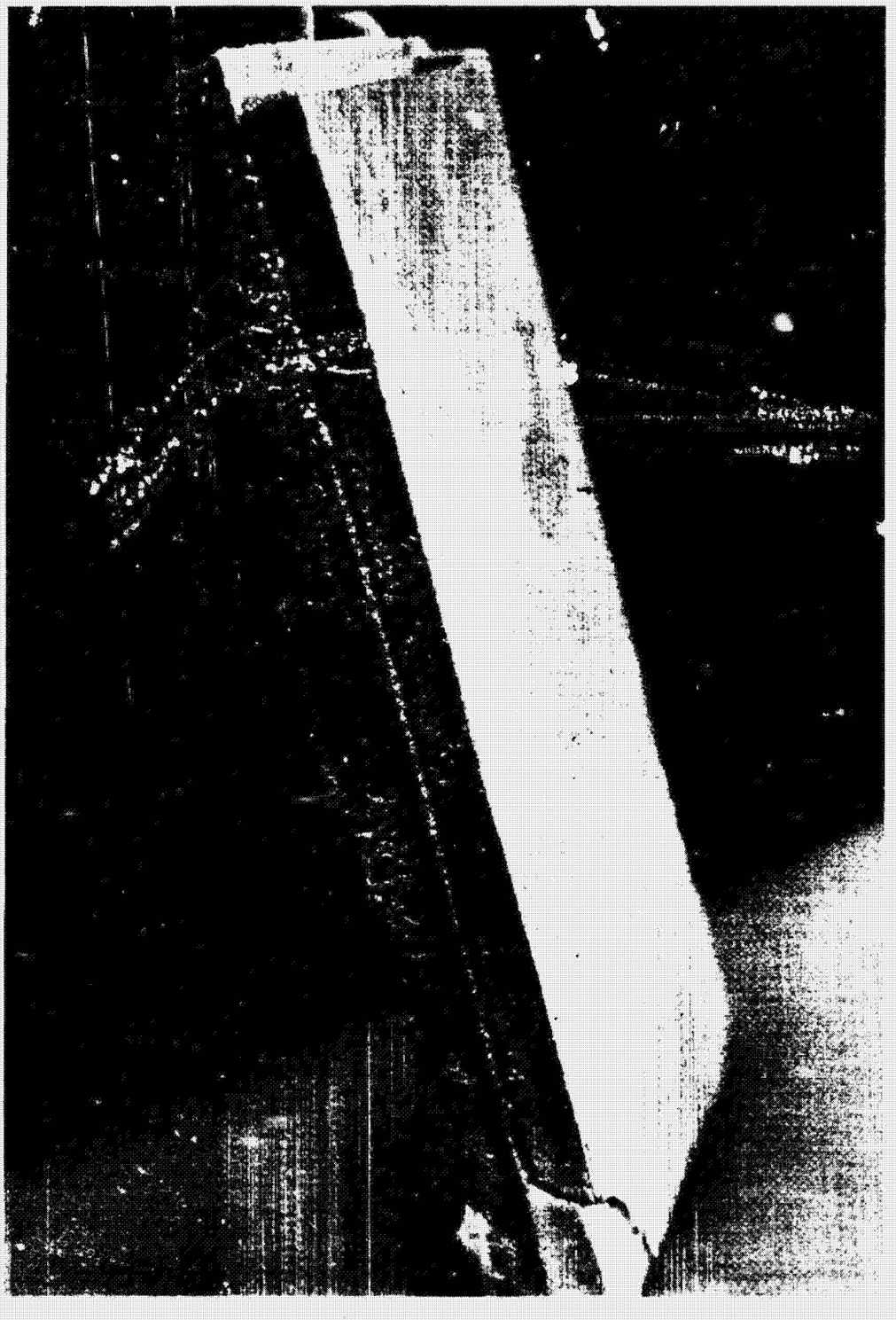

FIGURE III-31 COLD SHOCK OF FOAM INSULATION - FOAM TO METAL BOND SEPARATION

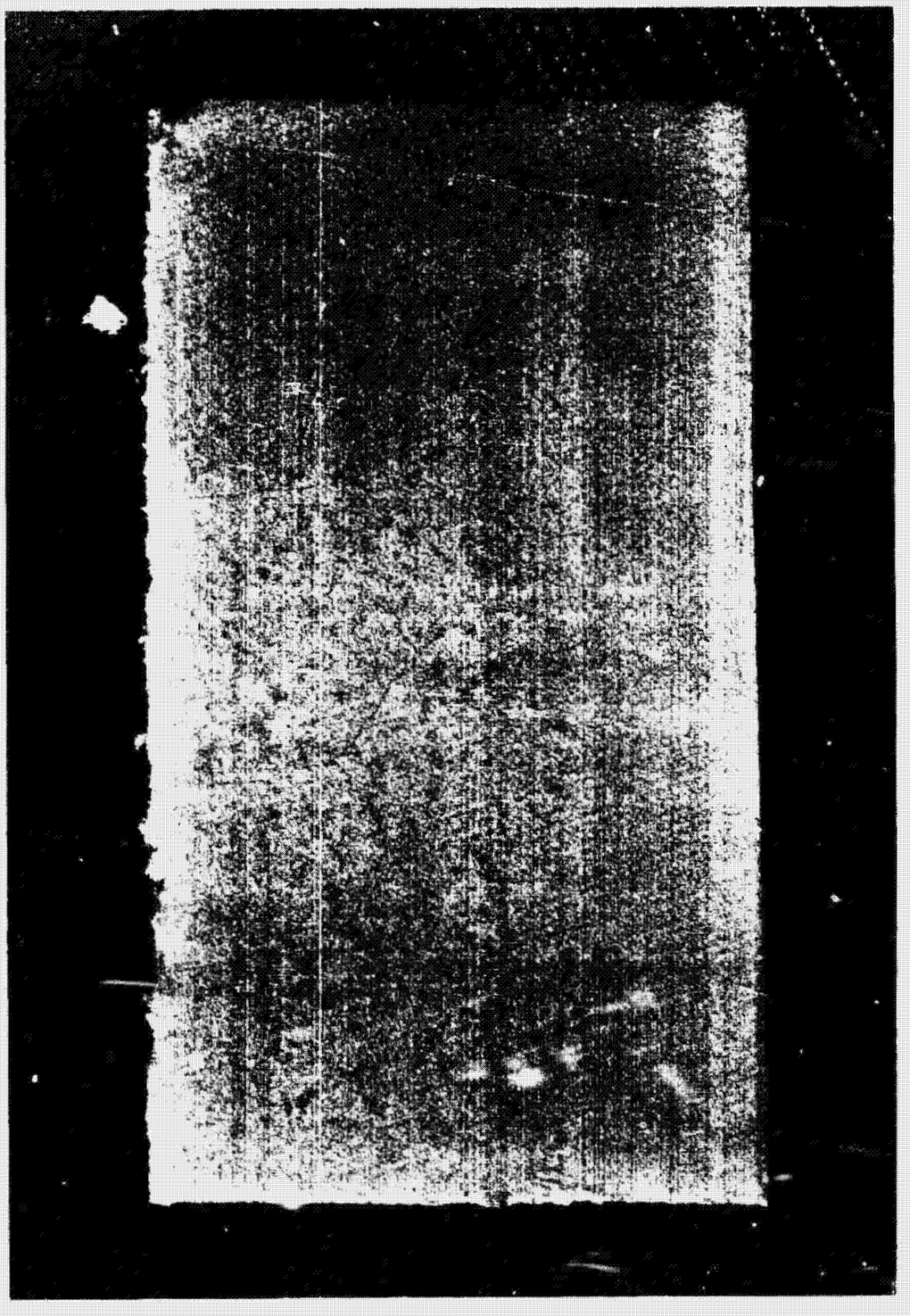

FIGURE III -32 COLD SHOCK OF FOAM INSULATION
SURFACE CRACKING

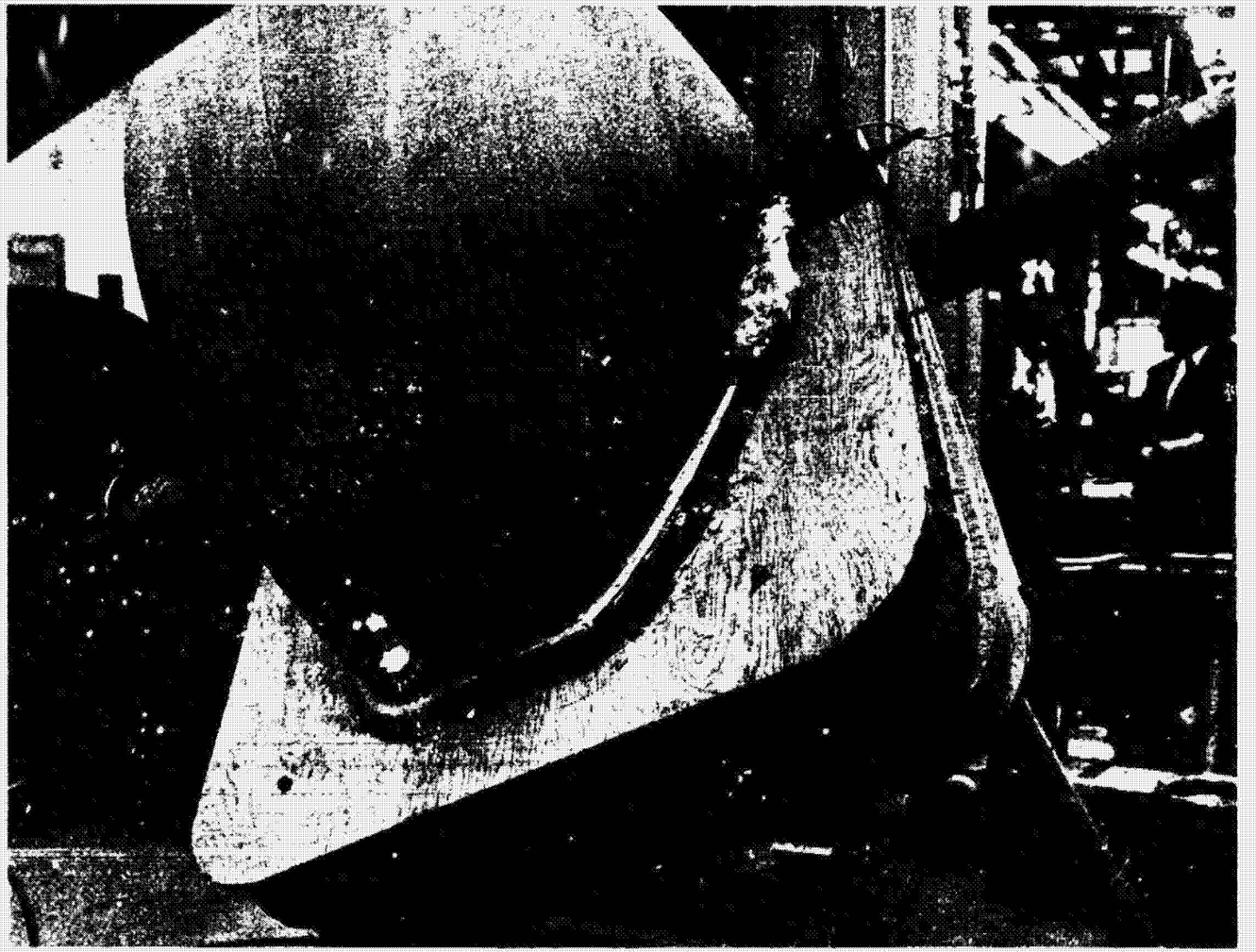

FIGURE III-33 FOAM INSULATION - FOAMING AND TRIMMING

FIGURE III-34 FOAM INSULATION-MOLDING DIE AND FIXTURE

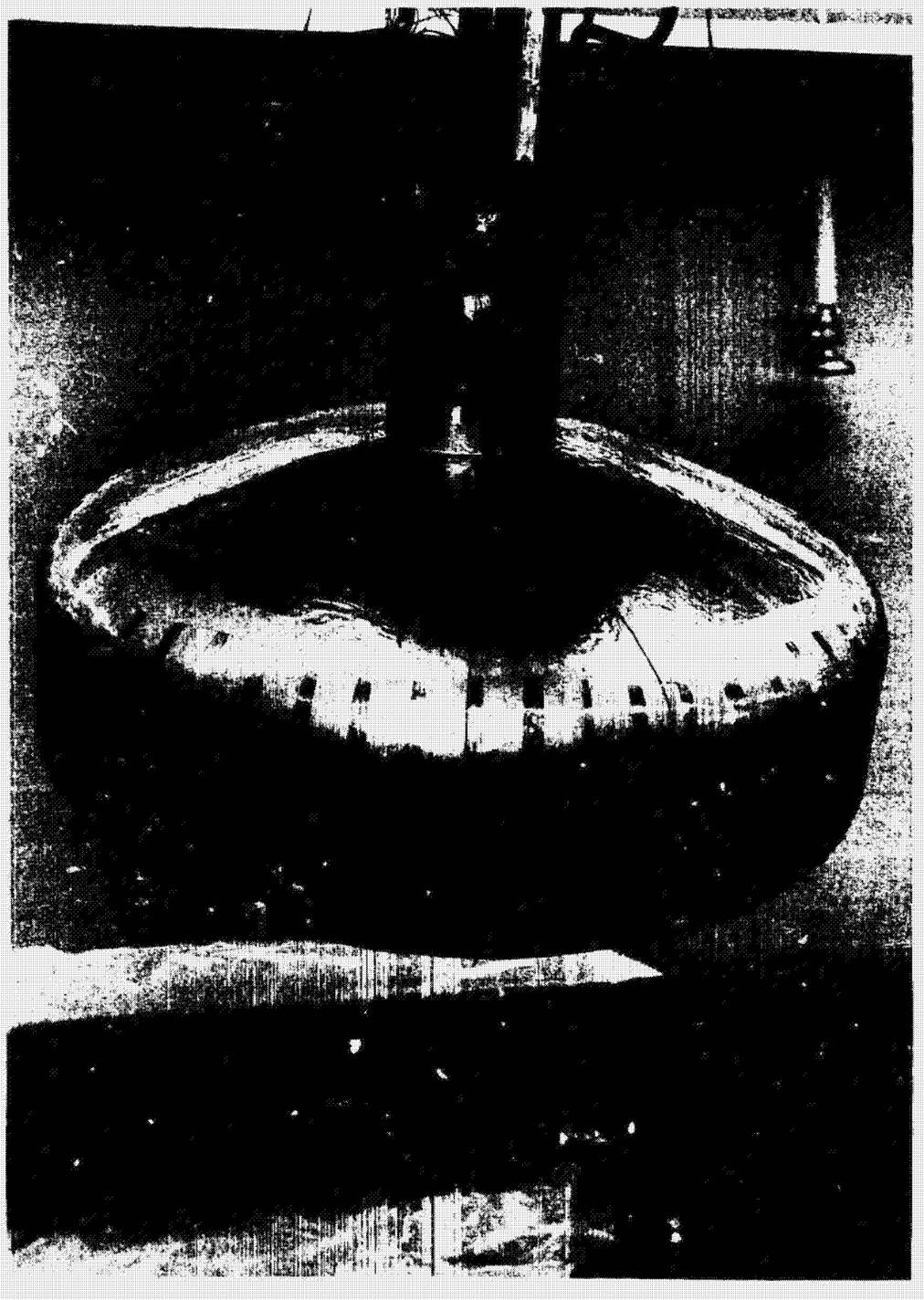

FIGURE III-35 INSULATION SYSTEM NO. 5-FOAM AND VAPOR BARRIER-BEFORE II-5 TEST SERIES

FIGURE III-36 INSULATION SYSTEM NO. 5-COMPLETE WITH MULTI-LAYER INSULATION

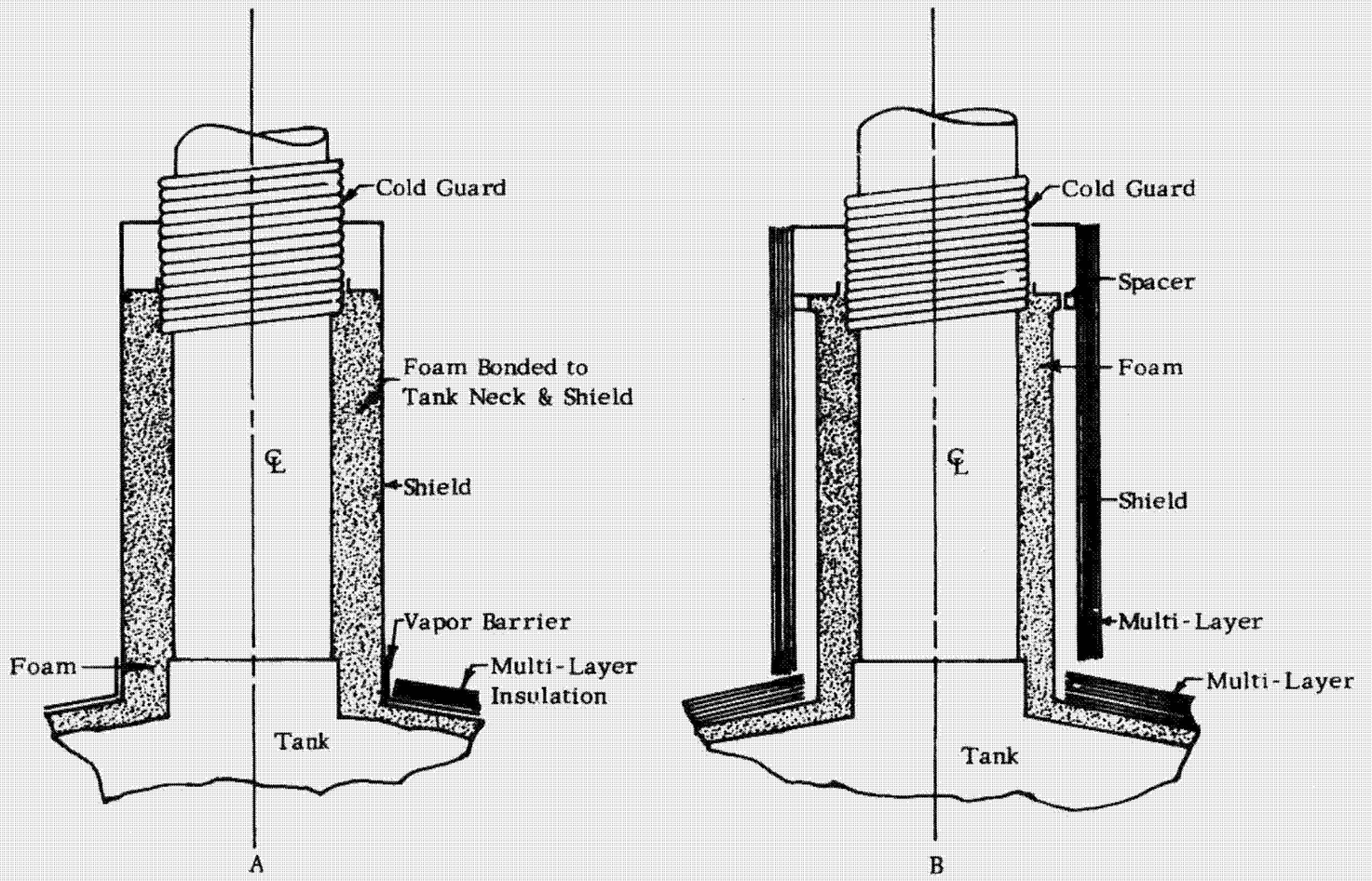

FIGURE III-37 INSULATION SYSTEM NO. 5 - NECK CONFIGURATION

FIGURE III-38 INSULATION SYSTEM NO. 5-VAPOR BARRIER BLISTERING-AFTER TEST II-5D

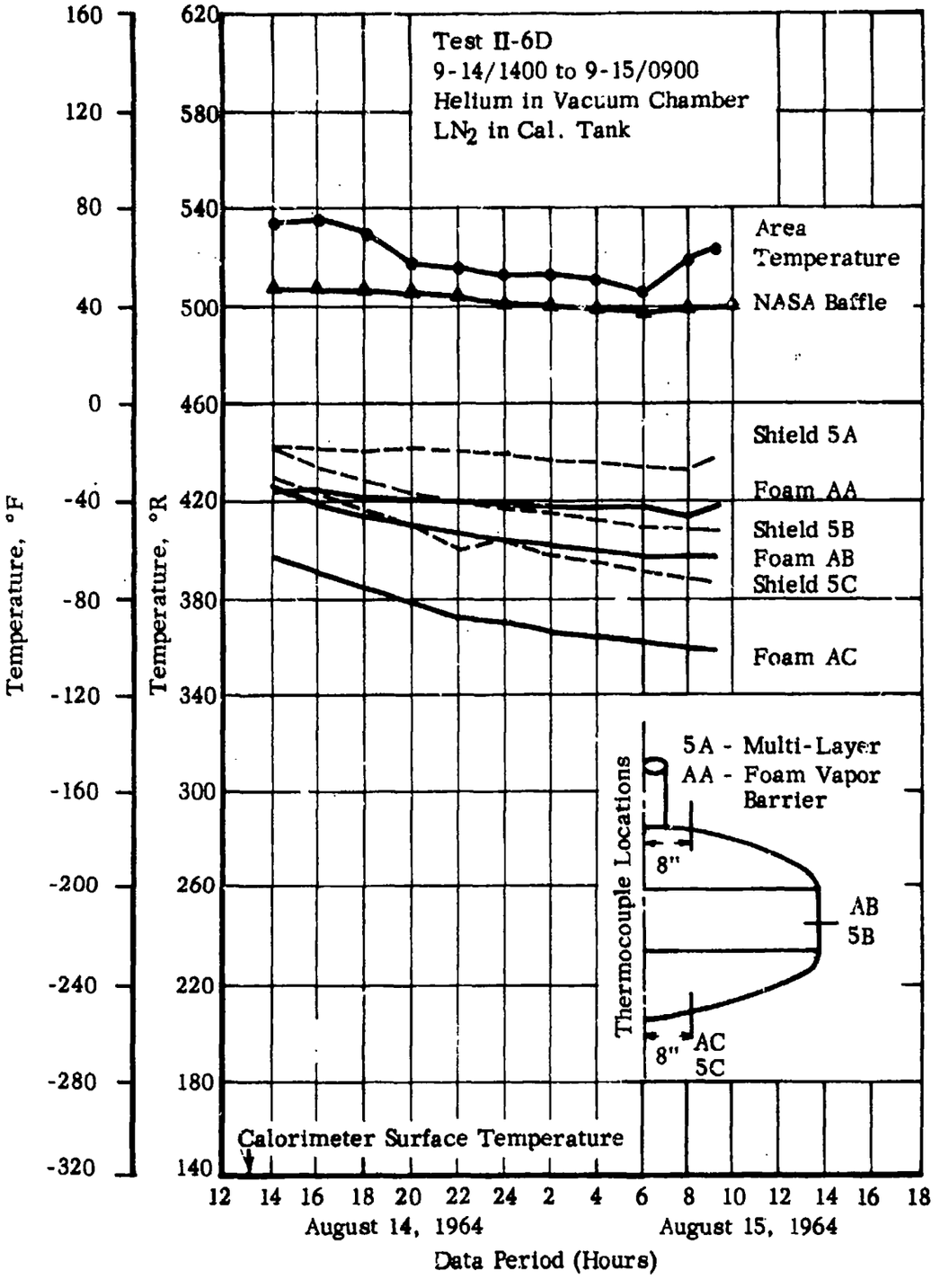

FIGURE III-39 INSULATION SYSTEM NO. 5, SYSTEM TEMPERATURE VARIATION WITH TIME

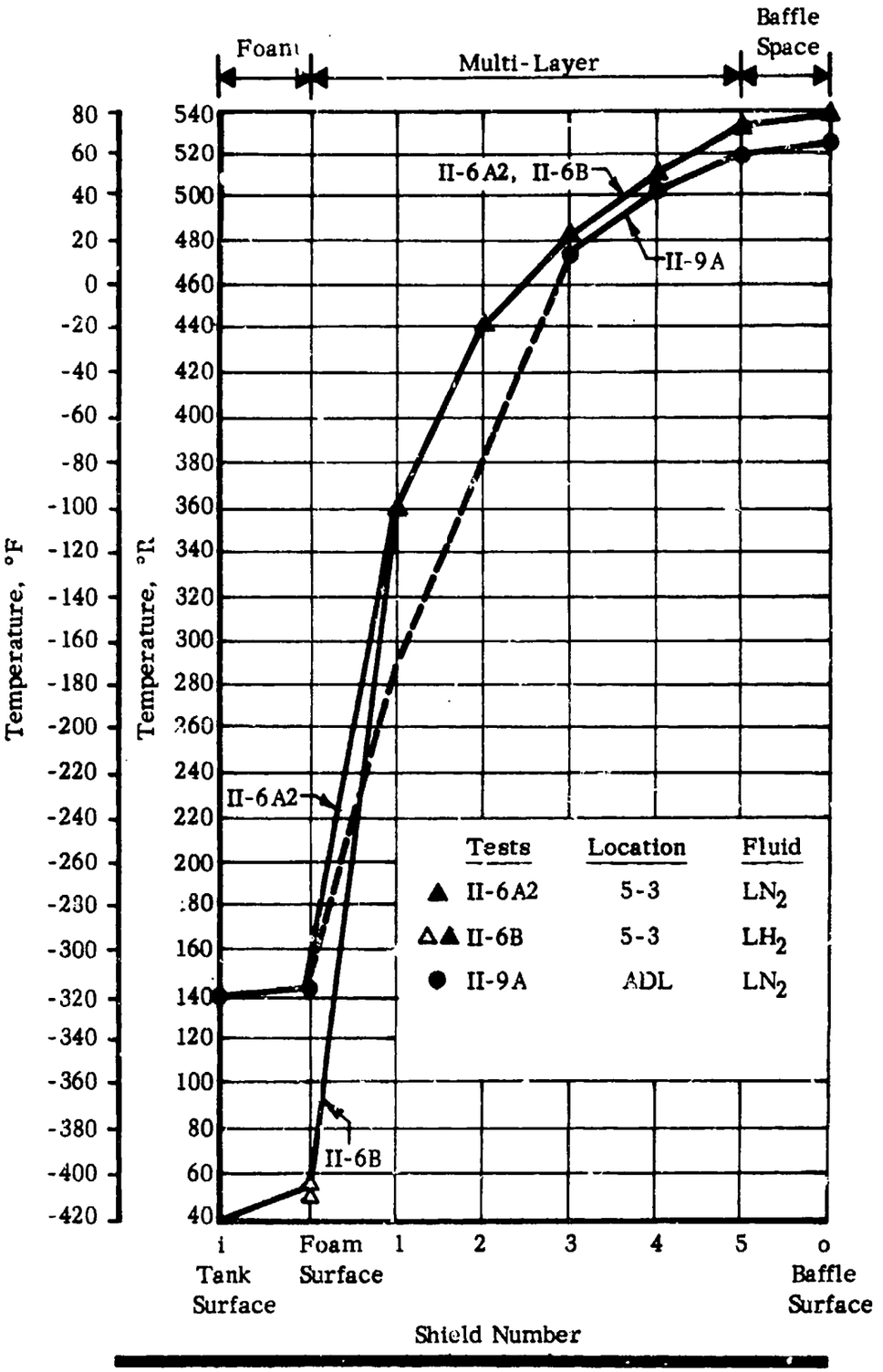

FIGURE III-40 INSULATION SYSTEM NO. 5, TEMPERATURE DISTRIBUTION, TESTS II-6A2, 6B, 9A

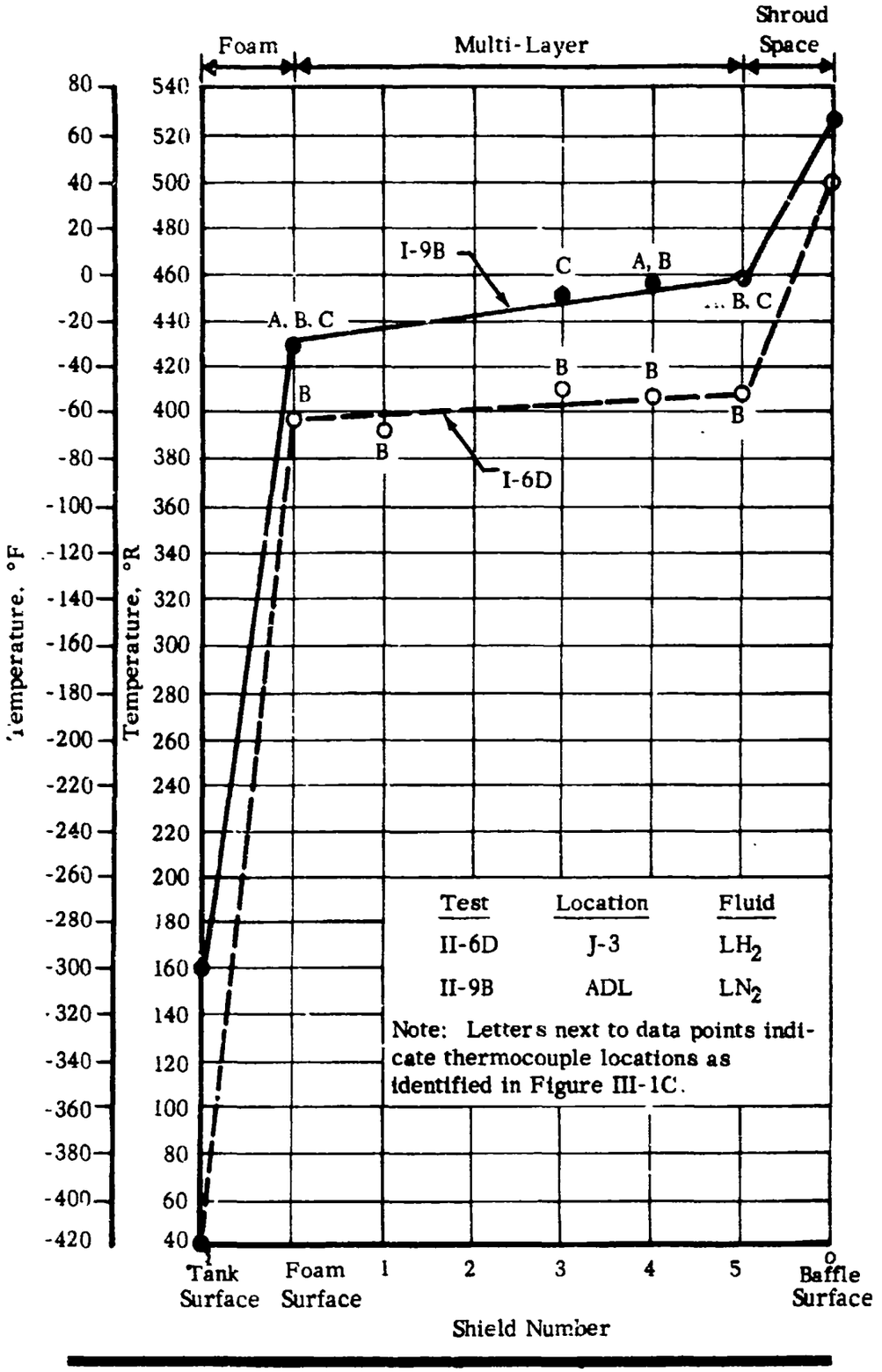

FIGURE III-41 INSULATION SYSTEM NO. 5, HELIUM PURGED SHROUD, TESTS II-6D, 9B

TABLE III-14

SHIELD EMISSIVITY DATA

INSULATION SYSTEM NO. 5

Shield No.	Surface Material	Shield Side	Resistance (ohm/square)	Computed Thickness (Å)[1]	Emittance[2]
1	Aluminum	A	.626	455	.0334
		B	.755	378	.0335
2	Aluminum	A	.630	453	.0335
		B	.723	395	.0378
3	Aluminum	A	.633	450	.0300
		B	.749	380	.0381
4	Aluminum	A	.633	450	.0369
		B	.714	400	.0358
5	Aluminum	A	.625	456	.0335
		B	.722	395	.0243

1. Resistivity of wrought aluminum, 2.85×10^{-6} ohm cm, used to compute vapor deposited layer thickness. Deposited metal assumed at wrought metal density.

2. Data taken with No. 2 Receiver disc in the emissometer.

TABLE III-15

TANK INSULATION PROGRAM

TEST SUMMARY - INSULATION SYSTEM NO. 5 - CALORIMETER NO. 1 - TEST NO. II-5

GROUND ENVIRONMENT

Insulation System:	ADL, Rigid Foam with 10 per cent chopped strand glass fiber. Insulation was foamed in place to 1/2 inch thickness. Surface of the foam was sealed with Alumiseal, Zero Perm, vapor barrier bonded to the foam with a versamid-epoxy blended adhesive.
Test Facility:	NASA/Plum Brook Station, J-4 facility; calorimeter was placed in natural atmospheric environment.
Penetrations or Gaps:	None
Boundary Condition:	As noted below
Tank Surface Area:	38.14 (tank surface area basis)

Test No.	Tank Liquid	Data Period Date&Time	to Date&Time	Test Duration (hrs)	Ave. Vac. (mm Hg)	Guard Liq/Temp (°F)	Total Heat Flow (Btu/hr)	Measured Heat Flux (Btu/hr ft^2)	Ave. Skin Temp (°F)	Ave. Ambient (°F)
II-5A	LN_2	6/9/1200	6/9/1900	7	Atmos	None	3670	97.0	62	89
II-5B-1	LH_2	6/10/1300	6/10/1430	1.5	Atmos	None	3540	93.0	51	76
II-5B-2	LH_2	6/10/1730	6/10/2015	2.75	Atmos	None	3550	93.3	34	58

TABLE III-16

SUMMARY VAPOR BARRIER BLISTER DAMAGE

	Tank	Neck
Alumiseal Surface Area (ft^2)	41	2.75
Blister Area (ft^2)	6	.84
Blister Area (per cent of total)	14.7	30
Blister Area Delaminated (per cent)	75	None
Blister Area Separated (per cent)	25	100

TABLE III-17

TANK INSULATION PROGRAM

TEST SUMMARY, INSULATION SYSTEM NO. 5, CALORIMETER NO. 1, TEST II-6

SPACE ENVIRONMENT

Insulation System: Composite insulation system consisting of a 1/2 inch thickness of foam substrate and five radiation shields of polyester film aluminized on both sides. Shields are separated with 1/8 x 1/8 inch mesh vinyl coated Fiberglas screen. Foam is reinforced with Fiberglas strands and sealed on the outside with a vapor barrier.

Test Facility: NASA/Plum Brook Station, J-3 facility

Penetrations or Gaps: None

Boundary Conditions: Tank surface at -320°F, see below for source temperature.

Surface Area: 39.80 ft^2 (area of the outer surface of the foam)

Test No.	Tank Liquid	Data Period Date&Time	to Date&Time	Test Duration (hrs)	Ave. Vac. (mm Hg)	Guard Liq/Temp (°F)	Total Heat Flow (Btu/hr)	Measured Heat Flux, $_2$ (Btu/hr ft^2)	Ave. Baffle Temp. (°F)	Adjusted[1] Heat Flux, $_2$ (Btu/hr ft^2)
II-6A-1	LN_2	7/27/2400	7/30/1200	60	1.0×10^{-6}	-304	62.3	1.56	82	1.54
II-6A-2	LN_2	8/1/2300	8/3/0900	34	2.5×10^{-6}	-309	33.7	.845	79	..850
II-6B	LH_2	8/4/1800	8/8/0800	86	3.5×10^{-7}	-416	36.5	.912	80	..907
II-6C	LN_2	8/12/0300	8/14/0900	54	3.0×10^{-7}		14.7	.712	79	..717

1. Measured heat flux adjusted to standard conditions for 80°F warm boundary and -320°F cold boundary.

TABLE III-18

TANK INSULATION PROGRAM

TEST SUMMARY, INSULATION SYSTEM NO. 5, CALORIMETER NO. 1, TEST II-9

SPACE ENVIRONMENT

Insulation System	Composite insulation system consisting of a 1/2 inch thickness of foam substrate and five radiation shields of polyester film aluminized on both sides. Shields are separated by 1/8 x 1/8-inch vinyl coated Fiberglas screen. Foam is reinforced with Fiberglas strands and sealed on the outside with a vapor barrier.
Test Facility:	ADL/Cambridge
Penetrations or Gaps:	None
Boundary Conditions:	Tank surface temperature at $140^{\circ}R$; source temperature as noted below.
Tank Surface Area:	39.80 ft^2 (area of the outer surface of the foam)

Test No.	Tank Liquid	Data Period Date&Time	to Date&Time	Test Duration (hrs)	Ave. Vac. (mm Hg)	Guard Liq/Temp ($^{\circ}F$)	Total Heat Flow (Btu/hr)	Measured Heat Flux (Btu/hr ft^2)	Ave. Baffle Temp. ($^{\circ}F$)	Adjusted[1] Heat Flux (Btu/hr ft^2)
II-9A1	LN_2	9/18/0830	9/21/0830	72	$.14 \times 10^{-5}$	-319	28.38	.712	67.5	.777
II-9A2	LN_2	9/21/0830	9/22/0830	24	$.95 \times 10^{-6}$	-319	27.84	.700	67.5	.771
II-9A3	LN_2	9/22/0830	9/23/0830	24	$.12 \times 10^{-5}$	-319	28.60	.720	67.0	.795
II-9C2	LN_2	9/30/1630	10/2/0830	40	$.58 \times 10^{-6}$	-318	12.12	.604	71.0	.651
II-9D	LN_2	10/2/1630	10/3/1630	24	$.63 \times 10^{-6}$	-315	18.20	.927	66.0	1.03

Notes:

1. Measured Heat flux adjusted to standard conditions for $80^{\circ}F$ warm boundary and $-320^{\circ}F$ cold boundary.

TABLE III-19

TANK INSULATION PROGRAM

TEST SUMMARY, INSULATION SYSTEM NO. 5, CALORIMETER NO. 1 - TESTS II-9, II-10

GROUND ENVIRONMENT

Insulation System: Composite insulation system consisting of 1/2 inch thickness of foam substrate and five shields of Mylar film aluminized on both sides. Shields are separated with 8 mesh vinyl coated Fiberglas screen.

Test Facility: A. D. Little, Inc., Cambridge and NASA/Plum Brook Station, J-3 facility as noted.

Penetrations or Gaps: None

Boundary Conditions: Calorimeter filled with liquid nitrogen is placed in ground environment.

Tank Surface Area: 39.8 ft^2 (area of the outer surface of the foam)

Test No.	Tank Liquid	Data Period Date&Time	to Date&Time	Test Duration (hrs)	Ave. Vac. (mm Hg)	Guard Liq/Temp (^oF)	Total Heat Flow (Btu/hr)	Measured Heat Flux (Btu/hr ft^2)	Ave. Warm Boundary Temp. (^oF)
II-10 [1]	LN_2	10/7/1420	10/7/2200	8.16	--	--	3670	92.2	72
II-9B [2]	LN_2	9/23/1030	9/23/2330	13.0	--	--	3400	85.6	66
II-6D [3]	LN_2	9/14/1400	9/15/0800	18.0	--	--	2750	69.1	30

Notes:

1. Insulation system surrounded with bag, purged with helium. Test performed in ground environment at A.D. Little, Inc. facilities.
2. Insulation system without bag in A. D. Little, Inc. chamber. Chamber purged with helium at 1 atmosphere.
3. Insulation system without bag in NASA/Plum Brook facility. Chamber purged with helium at 1 atmosphere.

Insulation System No. 6

a. Introduction

The improvement in the unit weight of the shield and spacer of a multi-layer is as important as the improvements achieved in the thermal performance of the shields. In Insulation Systems 2 through 5 the shield weight was improved compared to System No. 1 by the use of thinner foils and coated films. However, the same 1/8 x 1/8-inch mesh vinyl-coated Fiberglas spacer was used in all the systems. By comparison this spacer has a unit weight approximately 8 times that of 1/4 mil polyester film. It was expected that some improvement in the spacer weight could be achieved. The weight goal established for the lighter spacer materials was that equivalent to the unit weight of 1/4 mil polyester film. This was derived in the following manner: Coated 1/4 mil polyester film is very nearly the lightest weight shield material available (thinner films are available but not common). If the film is coated on one side only, then the shield can serve as its own spacer because of the low thermal conductivity present in the fiber and uncoated side. However, as discussed elsewhere, it appears that the uncoated side is not effective at all as a radiation shield. Thus, compared to a film coated on both sides, two single-sided shields are required to achieve the same thermal performance. However, the film coated on both sides requires a spacer to prevent shorting of the shields through the high conductivity coatings. From this, the equivalence between the spacer and singly-coated shield is thus established.

A preliminary investigation indicated that there are few materials that approach the unit weight by 1/4 mil polyester film. Two were found that appeared suitable as spacer materials, one a nylon net and the other a silk net. The former weighs .00271 lbs/ft^3 and is about 60 per cent heavier than the film, and the latter weighs .00121 lb/ft^3 and is about 30 per cent lighter than the film. Table III-20 is a comparison of some of the physical properties of multi-layer systems which might utilize these shields.

Although the nylon was the higher-weight spacer, the manner in which it was knit created pointed supports which we expected would lead

to a lower heat leak than the silk. We did not measure the performance of the silk net; however, the heat flux results obtained with the K-apparatus in tests 2039 and 2040 under zero load indicated that nylon was a good choice.

One disturbing factor about both the nylon and silk nettings, however, was their high coefficient of expansion. The value for nylon is presented in Table III-20. A rough comparative measurement was made with silk, and it appears to have as high a coefficient as nylon. The computed contraction for a 400° F change is almost 1-1/2 inches on the calorimeter tank circumference. This contraction was expected to affect the insulation system performance.

b. Insulation System

The insulation system selected consisted of 5 shields of polyester film aluminized on both sides, and six spacers of nylon netting. This system was applied to Calorimeter No. 2. As shown in Figure III-42, the netting side sheet was gored and attached to a top and bottom cap to hold it in place. The shields were applied in the same manner as those in insulation system No. 2 and No. 5. The completed system is shown in Figure III-43. A closer view of the insulation shown in Figure III-44 shows the netting and shields in greater detail. Additional details of and characteristics of the system are presented in Table III-1.

c. Results and Discussion

Heat fluxes to the insulation system were measured over a period of 140 hours. Average values of 1.11 Btu/hr ft^2 (adjusted to 80° F source temperature) were obtained (see Table III-21). This value was about twice the calculated value (.49 Btu/hr ft^2) and about three times results obtained with the thermal conductivity apparatus in test 2039. The calculated value is based on shield emissivities of .035 that were obtained with the ADL emissometer.

We measured the temperature distribution in the multi-layer system during the heat flux tests. Typical values of the shield temperatures are shown in Figure III-45. It was apparent from the almost linear variation in shield temperature that conductive heat transfer between the shields was taking place in addition to the radiative heat transfer.

We were able to compute approximate values for both of these components from the data and multi-layer system properties. The results are presented in Table III-22.

We conclude that the use of the nylon netting spacer in Insulation System No. 6 resulted in a high flux due to solid conduction. The probable cause is the thermal contraction of the spacer material which introduced normal loading pressures into the multi-layer.

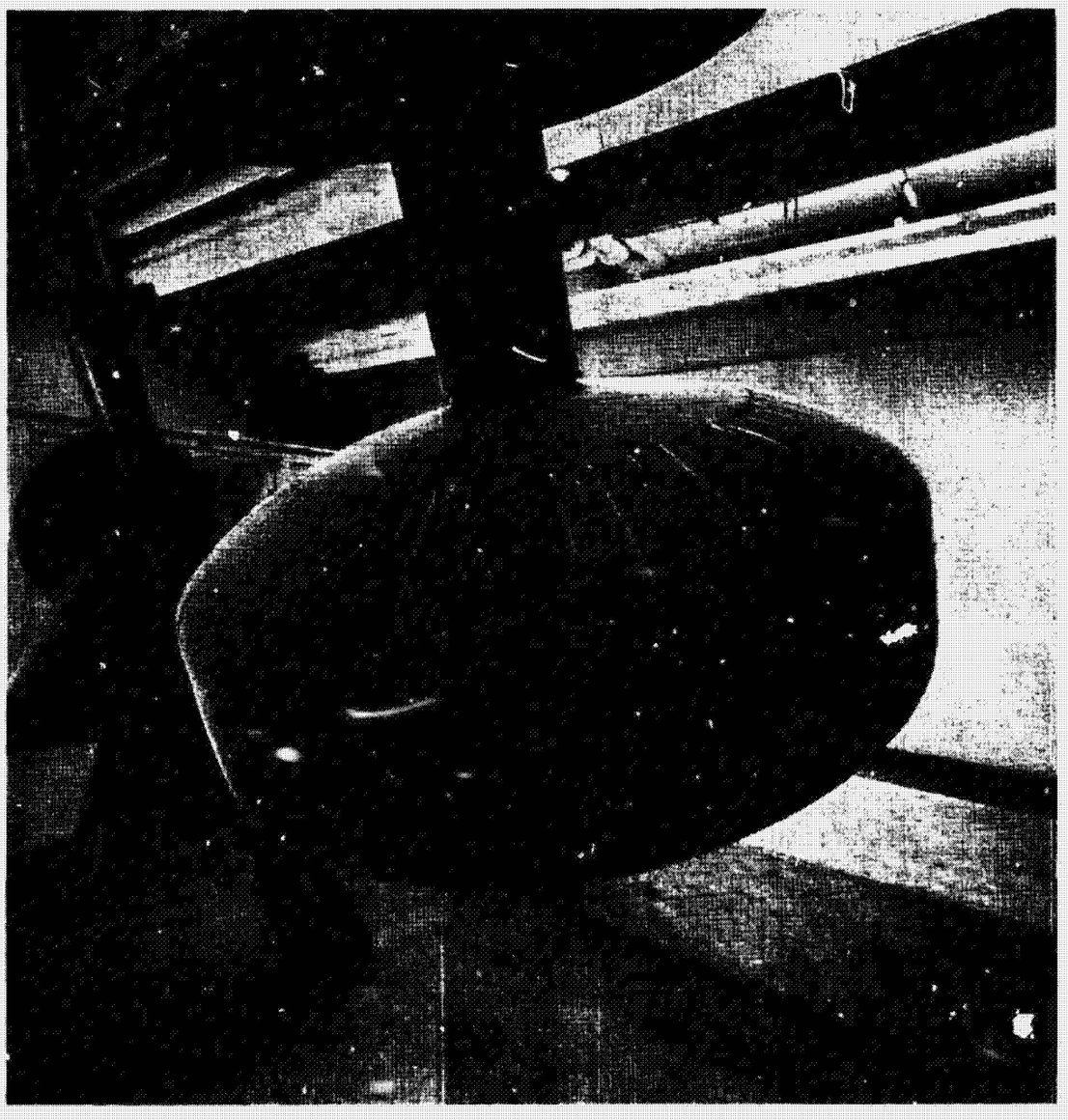

FIGURE III-42 INSULATION SYSTEM NO. 6-FIRST NYLON NETTING SPACER

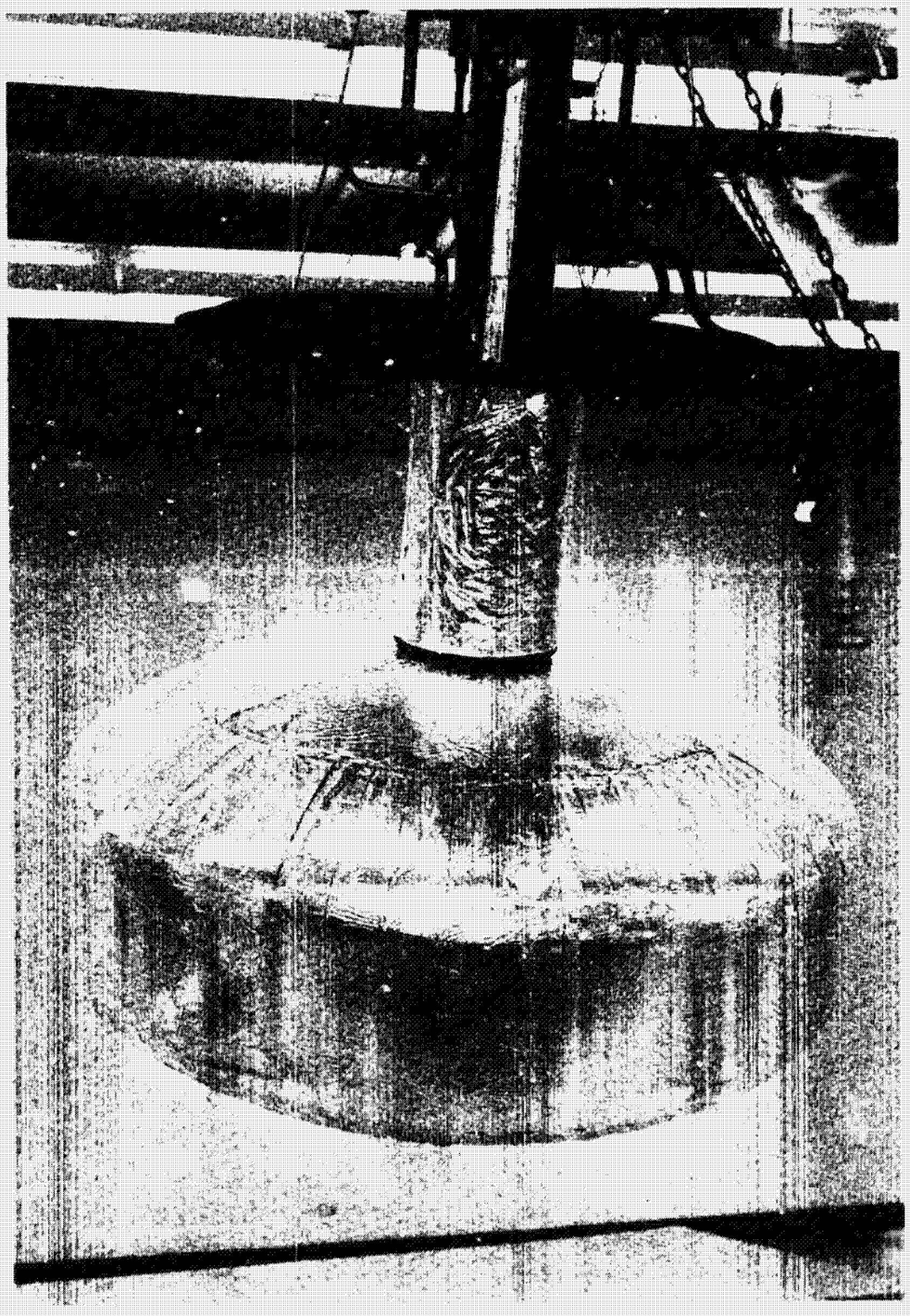

FIGURE III-43 INSULATION SYSTEM NO. 6

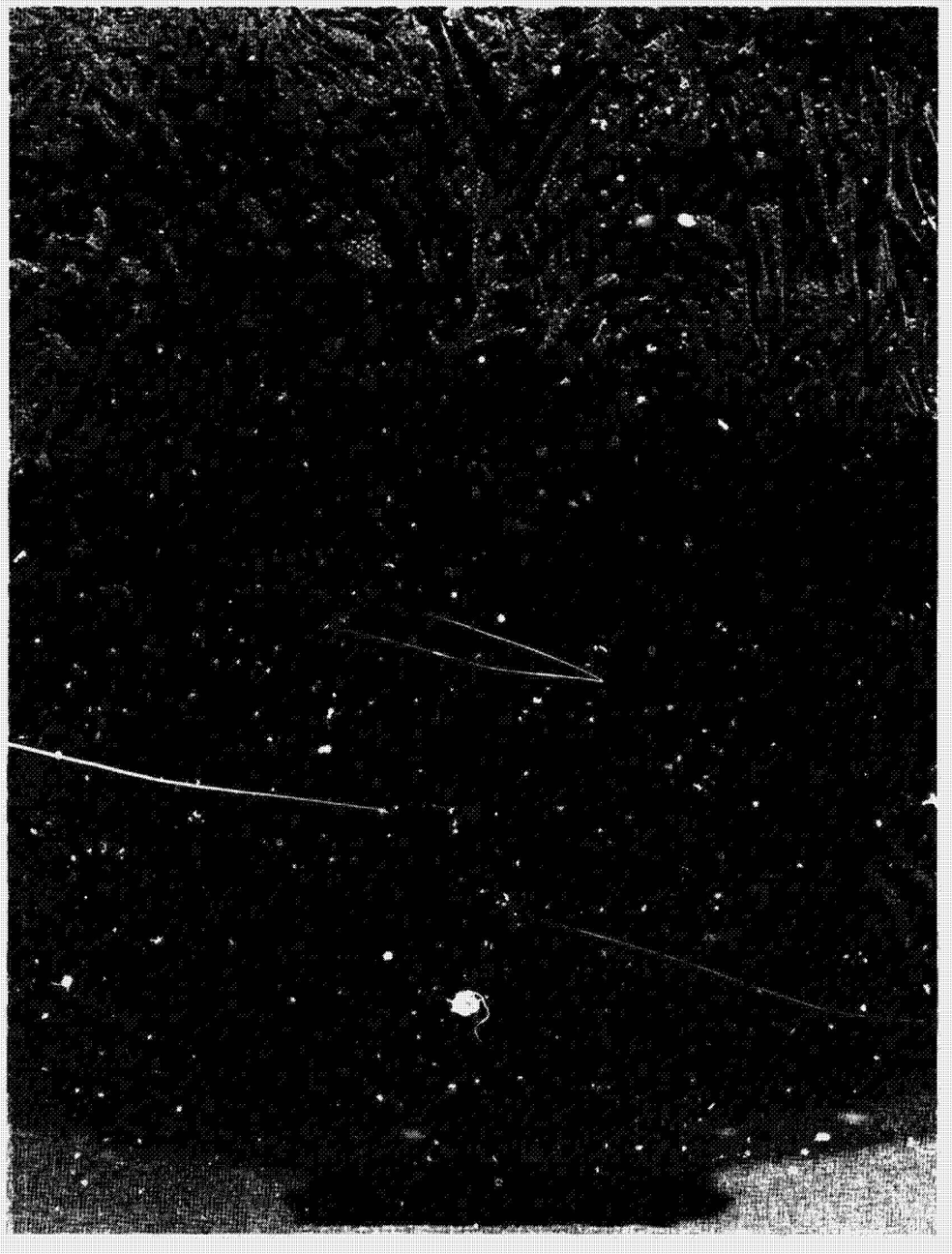

FIGURE III-44 INSULATION SYSTEM NO. 6-SECOND NYLON NETTING SPACER

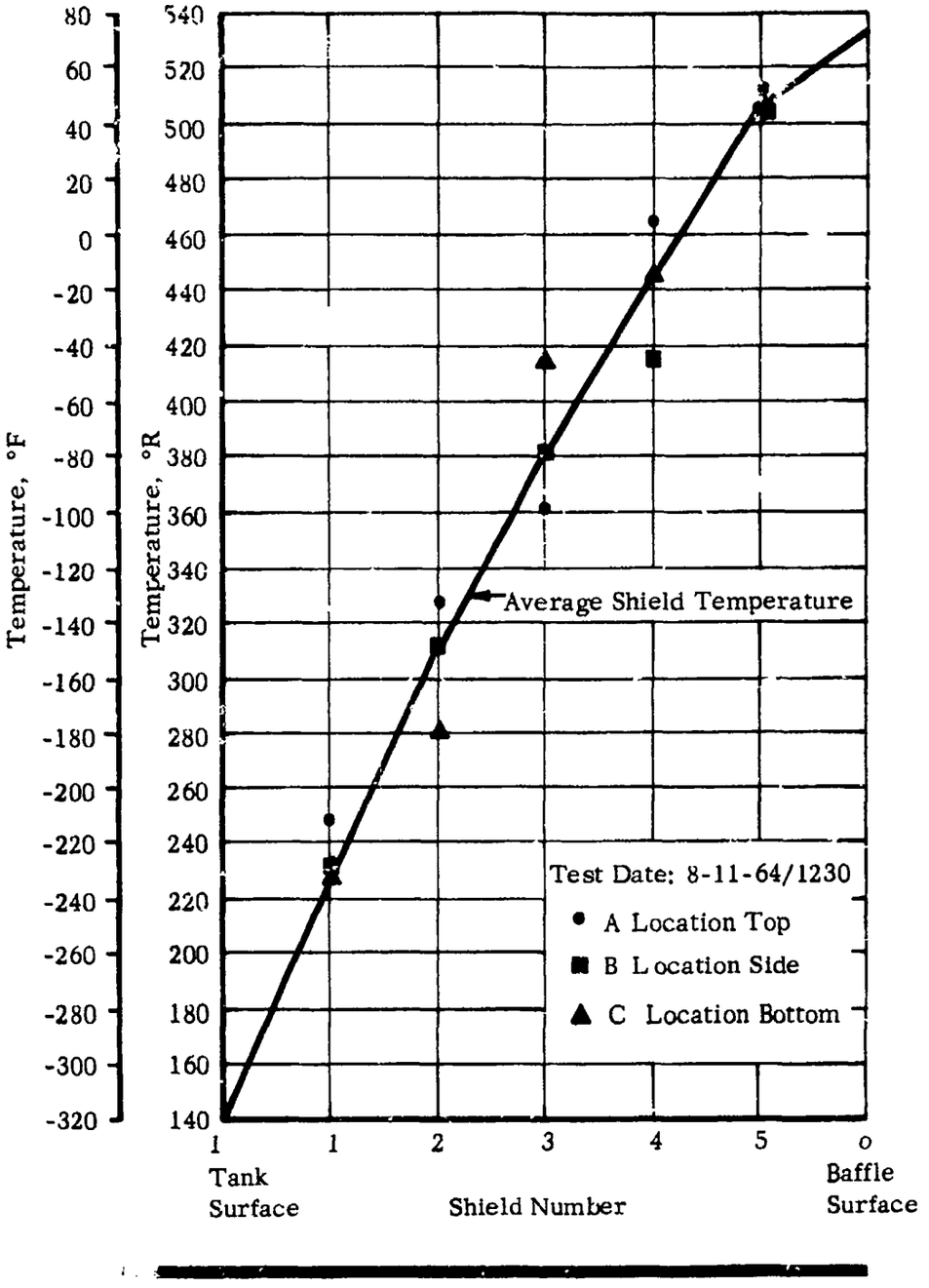

FIGURE III-45 INSULATION SYSTEM NO. 6, SHIELD TEMPERATURE DISTRIBUTION

TABLE III-20

COMPARISON OF THE PHYSICAL PROPERTIES OF MULTI-LAYER INSULATION WITH LIGHTWEIGHT SPACERS

	Sample A	Sample B (K-apparatus test 2039)	Sample C
elds			
umber	ten	ten	ten
aterial	aluminum 1100-0	aluminum coated mylar on two sides	aluminum coated mylar on two sides
eight	.007	0.00176	0.00176
hickness (in)	.0005	0.00025	0.00025
luminization thickness (Å)	---	375 ± 50	375 ± 50
missivity (average)	.035	.035	.035 (tentative)
cer			
umber	11	11	11
aterial	nylon net	nylon net	silk netting
eight (lb/ft^2)	.00271	.00271	0.00121
hickness (in)	.007	.007	0.0045
pen Area	80% (estimated)	80% (estimated)	84% (estimated)
ontraction	.014 inches/in (68 to -423° F)	.014 inches/in (68 to -423° F)	---
oretical Sample Thickness (in)	.082	.0795	0.052
ple Weight (lb/ft^2)	.0997	.0476	0.0309
oretical Density, (lb/ft^3)	14.2	7.2	7.5
oretical Shield Density	133 shields/in	138 shields/i	210 shields/in
ure of merit [1] (wt. basis)	2.75	1.27	0.85

1. Ratio of shield and spacer weight compared to weight of two 1/4 mil thicknesses of polyester film.

TABLE III-21

TANK INSULATION PROGRAM

TEST SUMMARY - INSULATION SYSTEM NO. 6 - CALORIMETER NO. 1 - TEST II-7

SPACE ENVIRONMENT

Insulation System: Five shields of 1/4 mil mylar film aluminized on both sides to an apparent metal thickness of 375° A. Shields are spaced with six nylon netting .007 inches thick.

Test Facility: ADL, Cambridge

Penetrations or Gaps: None

Boundary Conditions: As noted below

Tank Surface Area: 39.5 ft^2

Test No.	Tank Liquid	Data Period Date & Time	to Date & Time	Test Duration (hrs)	Ave. Vac. (mm Hg)	Guard Liq/Temp (°F)	Total Heat Flow (Btu/hr)	Measured Heat Flux (Btu/hr-ft^2)	Ave. Baffle Temp °F	Adjusted[1] Heat Flux (Btu/hr-ft^2)
II-7A1	LN_2	8/8/64/0800	8/9/64/2400	40	$.16 \times 10^{-5}$	-316	41.1	1.05	73	1.12
II-7A2	LN_2	8/10/64/1230	8/14/64/1630	100	$.10 \times 10^{-5}$	-317	40.7	1.03	75	1.10

Note: 1. Measured heat flux adjusted to standard conditions for 80° F warm boundary and -320° F cold boundary.

TABLE III-22

SUMMARY OF THE RADIATIVE AND CONDUCTIVE

HEAT TRANSFER COMPONENTS IN INSULATION SYSTEM NO. 6

Shield Space	Warm Surface Temp. (^{o}R)	Cold Surface Temp. (^{o}R)	Measured Flux Btu/hr ft^2	Computed Radiation Flux Btu/hr ft^2	Conduction Measured Minus Radiation Btu/hr ft^2
i-1	225	140	1.03	.13	.90
1-2	305	225	1.03	.18	.86
2-3	380	305	1.03	.38	.67
3-4	448	380	1.03	.57	.47
4-5	508	448	1.03	.66	.38
5-0	537	508	1.03	1.03	0

Insulation System No. 7

a. Introduction

The insulation system on a space vehicle is susceptible to damage when the vehicle is subjected to all the necessary static firings, checkout, and calibration tests as well as transportation and handling. Thus, it becomes very important in the case of damage that the repair to the insulation can be made quickly and effectively. In some cases, it may be necessary to remove the entire insulation in order to gain access to the tank surface, i.e., checking for leaks that develop in the tank after the insulation has been applied.

Multi-layer insulation systems 1 through 6 were applied to the calorimeter tank one shield at a time. The time required was reduced from one shield per week on the first system to about one per day on the last system. However, large tanks with 50 to 100 shields would still take months to insulate even though the techniques are refined and made more efficient. It is necessary, therefore, that new application techniques be developed that will result in a substantial improvement in the application time of multi-layer insulations. The approach we selected to be used in the initial trial was to pile spacers and shields together on a table and sew them together as in a quilted blanket. Once the shields and spacers are tied to each other in this manner, the pile would be cut to suit the tank contour, i.e., gores would be cut into the side sheet section so as to cover the tank sides and knuckle radii. The quilted blanket would provide the means of applying many shields simultaneously. Through appropriate fitting and cutting, this blanket could be applied possibly in the time required previously to apply a single shield. Further the blanket could be easily and quickly removed and reapplied when it is necessary to do so.

b. Insulation System

Insulation System No. 7 was applied to the calorimeter over the existing multilayer insulation, system No. 6. This was done to begin the exploration of multilayer on the calorimeter in increasing number of shields and to further confirm the thermal contractors effects of the nylon spacer on heat flux. Each is a five shield system in which the shields are 1/4 mil polyester film aluminized on both sides and the spacers are nylon net. The first five shields were applied one at a time, the second set was preassembled into the form of a quilted blanket and then applied to the tank. Added details are presented in Table III-1. The side sheet blanket for the tank is shown in Figure III-46. The completed insulation system is shown in Figures III-47 and 48.

c. Results and Discussion

The experimental heat fluxes produced with System No. 7 are presented in Table III-23. The average of the measured values was 0.78 Btu/hr ft^2. This compares with an expected value of 0.24 Btu/hr ft^2 which was computed for the radiation flux under the prevailing test conditions. Inasmuch as solid conduction effects were present in the original five shields (test series II-7) it was expected that these effects would be present possibly in a more pronounced fashion, in the 10 shield system.

The temperature distribution in the first multi-layer system which occurred during Test II-8 is shown in Figure III-49. These gradients show that:

1. The temperature distribution at top, bottom, and side is almost linear with respect to shield number and,

2. The temperature across the five shield system is about 60°F less at the side location than at the head locations.

The former indicated solid conduction heat transfer is taking place throughout the first five shields of No. 7 system; the latter indicates that the conduction effect is greater on the

cylinder portion of the tank than at the heads. Further, compared to the results obtained in Test II-7, the conductive heat leak, as a per cent of total heat leak, has increased.

These effects can be seen in the tabulations presented in Table III-24. The conduction component of heat transfer is established from the difference of the experimental average heat flux and the computed value of the radiation flux. The latter were determined from the experimental shield temperatures and the use of .033 for the value of the surface emissivities.

No thermocouples were placed in the five shields blanket insulation portion of No. 7 system except at the outer shield. However, from the temperature of the chamber baffles and temperatures on No. 5 shield, we computed radiation fluxes of .360 and .302 Btu/hr ft^2 for the tank sides and heads respectively using shield emissivity of .033. Thus, the difference of these values from the average heat flux indicates that heat transfer, possibly by conduction, radiation through the butt joints and from other sources is taking place.

The results obtained with the thermal conductivity apparatus for sample 2039 which consisted of ten shields and spacers identical to tank insulation system No. 7 result in a no load heat flux .14 Btu/hr ft^2. This flux would correspond to a shield emissivity of approximately .020. This apparent emissivity value is significantly lower than emissivity values obtained with the emissometer on similar samples of aluminum-coated mylar which average .033 about at 100°F. This latter emissivity value could correspond to a theoretical heat flux of .24 Btu/hr ft^2. Thus, the theoretical heat flux predicted from the emissometer results are about 65 percent higher than the values measured with the thermal conductivity apparatus. This discrepancy may be due in part to the influence of temperatures on shield emissivity; many of the shields in the thermal conductivity sample are at a significantly lower temperature than the emissometer sample.

Thus, from results obtained with the thermal conductivity apparatus, emissometer, and tank applied insulation, we believe that nylon netting spacer offers good thermal performance under no load conditions. However, where the netting is restrained over a curved surface as in its application on the tank, the thermal contraction of the netting spacers with temperature seriously degrades the thermal performance of the multilayer system by introducing a loading pressure on the shields.

FIGURE III-46 INSULATION SYSTEM NO. 7, FIVE SHIELD BLANKET, GORED SIDE SHEET

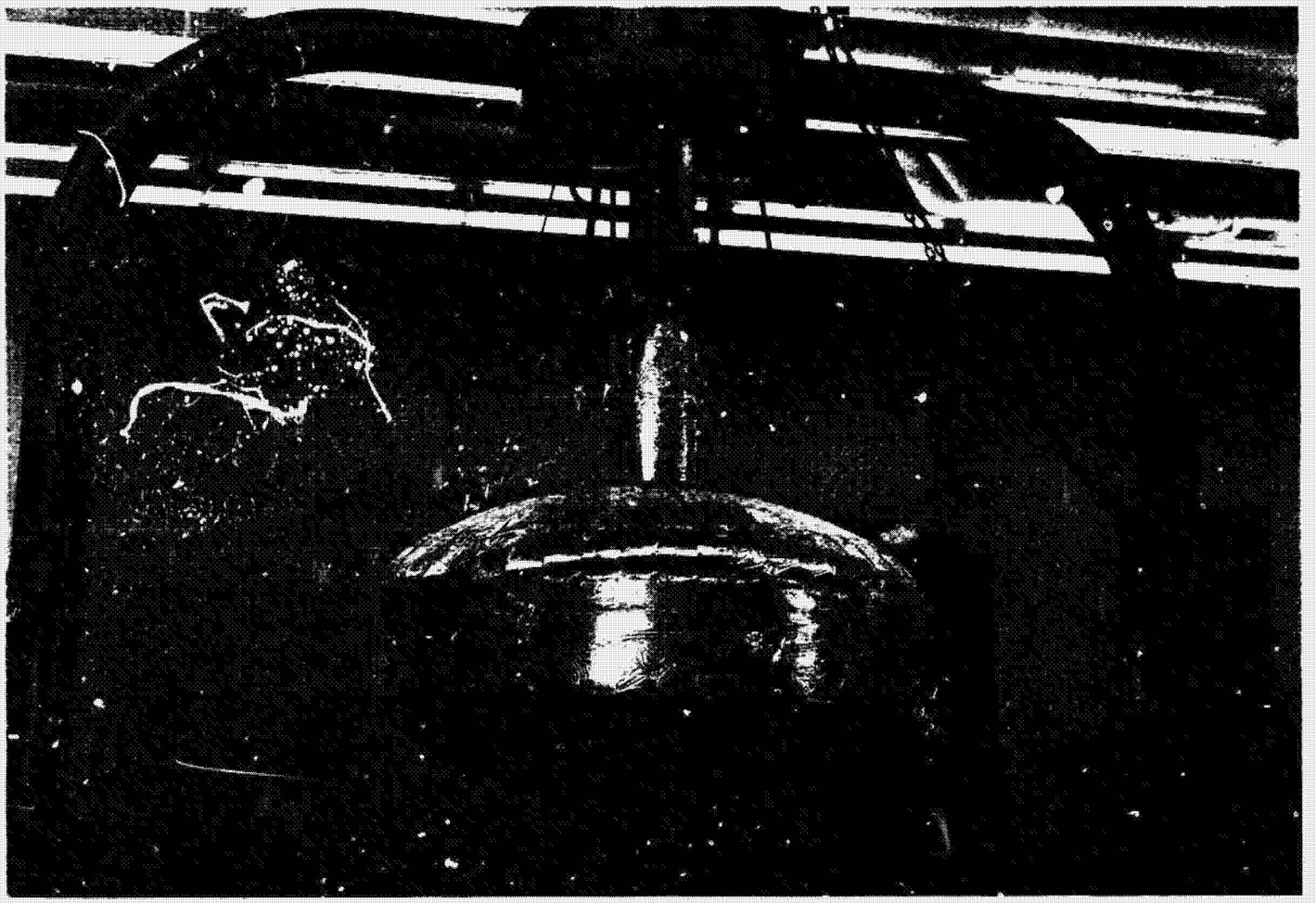

FIGURE III-47 INSULATION SYSTEM NO. 7 - SIDE

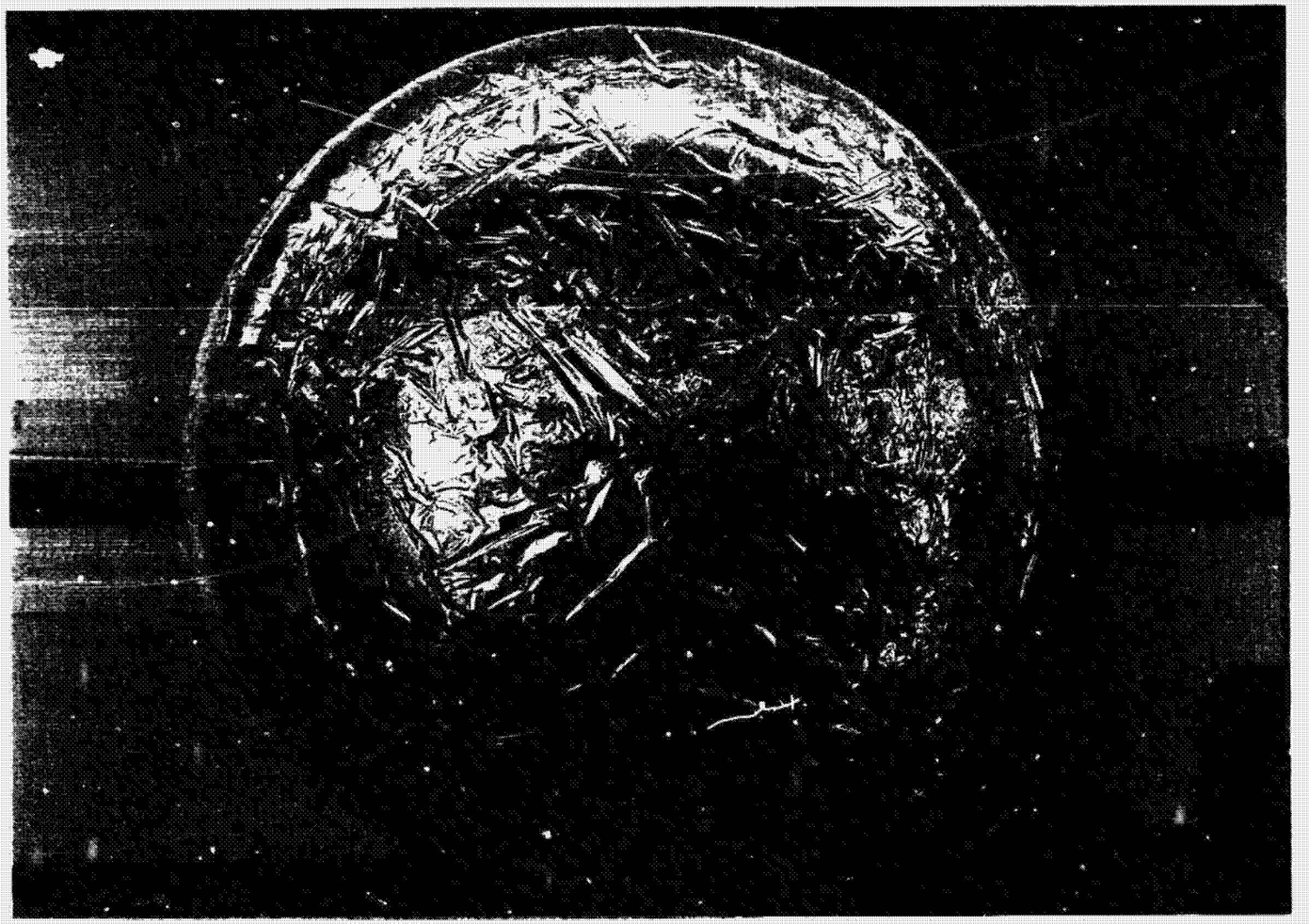

FIGURE III-48 INSULATION SYSTEM NO. 7, BOTTOM

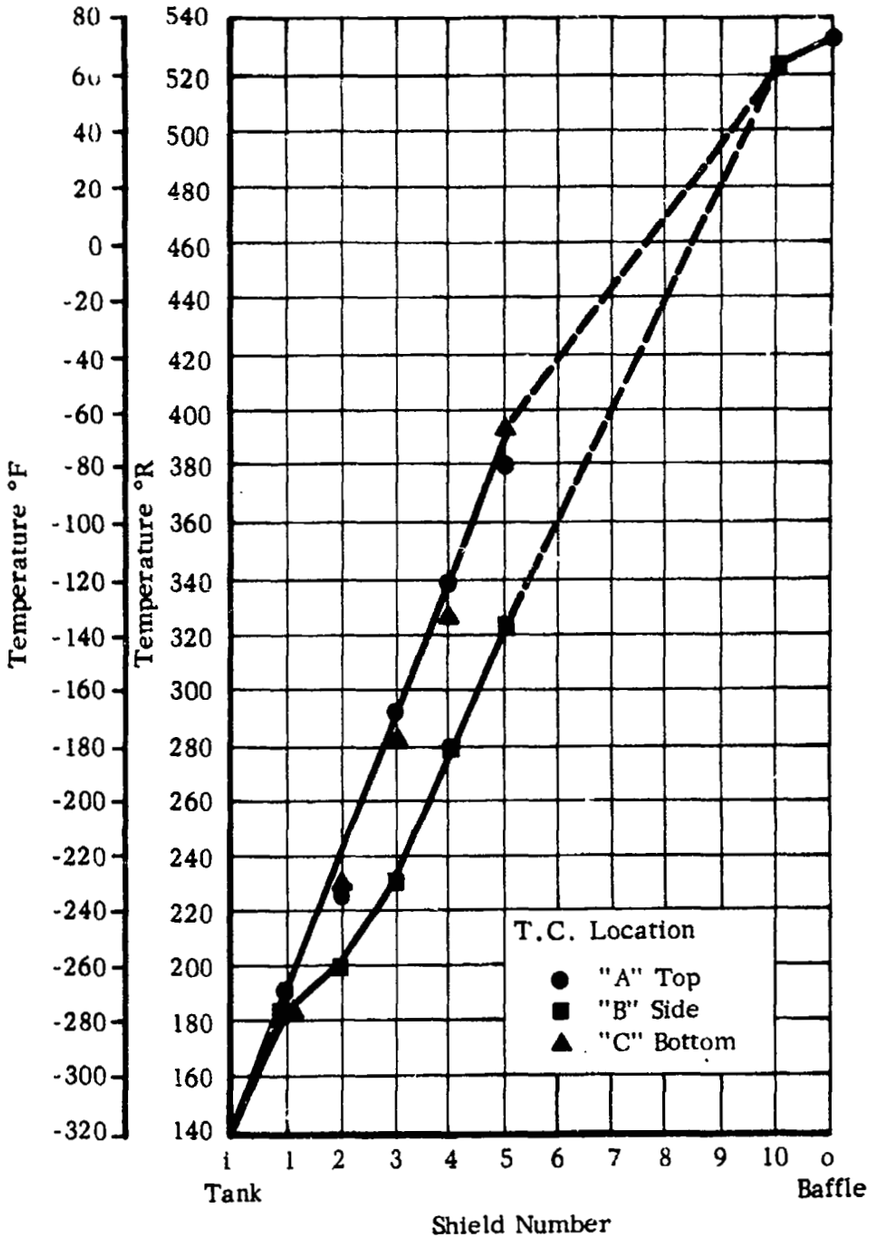

FIGURE III-49 INSULATION SYSTEM NO. 7. TEMPERATURE DISTRIBUTION

TABLE III-23

TANK INSULATION PROGRAM

TEST SUMMARY, INSULATION SYSTEM NO. 7, CALORIMETER NO. 2, TEST NO. II-8A

Insulation System: Ten, 1/4 mil Mylar film coated on both sides with vapor deposited aluminum to a thickness of about 375 A nylon netting, .007 inches thick was used as spacer. The first five shields are the original Insulation System No. 6. The second set of shields were preassembled into blanket form before application to the calorimeter.

Test Facility: ADL/Cambridge facility

Penetrations or Gaps: None

Boundary Conditions: Cold boundary at -320°F

Tank Surface Area: 39.5 ft^2

Test No.	Tank Liquid	Data Period Date&Time	to Date&Time	Test Duration (hrs)	Ave. Vac. (mm Hg)	Guard Liq/Temp (°F)	Total Heat Flow (Btu/hr)	Measured Heat Flux (Btu/hr ft^2)	Ave. Baffle Temp. (°F)	Adjusted[1] Heat Flux (Btu/hr ft^2)
II-8A1	LN_2	9/9/0830	9/10/1030	26	$.8 \times 10^{-6}$	-318	30.4	.771	69	.835
II-8A2	LN_2	9/10/1030	9/14/1230	98	$.6 \times 10^{-6}$	-138	30.9	.782	74	.821

1. Measured heat flux adjusted to standard conditions for 80°F warm boundary and -320°F cold boundary.

TABLE III-24

SUMMARY OF RADIATIVE AND CONDUCTIVE HEAT TRANSFER COMPONENTS IN FIRST FIVE SHIELDS OF INSULATION SYSTEM NO. 7

	Shield Space	Cold Surface Temp(^{o}R)	Warm Surface Temp(^{o}R)	Measured Flux (Btu/hr ft^2)	Computed Radiation Flux (Btu/hr ft^2)	Conduction Flux Measured Minus Radiation$_2$ (Btu/hr ft^2)
Tank Cylindrical Section	1-1	140	183	.78	.04	.74
	1-2	183	200	.78	.01	.77
	2-3	200	230	.78	.04	.73
	3-4	230	279	.78	.09	.69
	4-5	279	323	.78	.14	.64
Tank Top & Bottom Heads	1-1	140	190	.78	.05	.73
	1-2	190	227	.78	.04	.74
	2-3	227	287	.78	.12	.66
	3-4	287	333	.78	.16	.62
	4-5	333	386	.78	.30	.25

REFERENCES

(1) "Liquid Propellant Losses During Space Flight," Final Report, Report No. 65008-00-04, by Arthur D. Little, Inc., for National Aeronautics and Space Administration under Contract NASw-615, October 1963.

(2) Sopp, A. L. Jr., and J. L. Brandt, "Reflectivity and Emissivity of Bare and Coated Aluminum," Finishes Division, Alcoa Research Laboratories, February 1963.

(3) Scott, Russell B. Cryogenic Engineering. Princeton: D. Van Nostr nd Company, Inc., 1959, pg. 146.

(4) Bonneville, Jacques M., "Design and Optimization of Space Thermal Protection for Cryogens - Analytical Techniques and Results," Report No. 65008-02-01, Arthur D. Little, Inc. for National Aeronautics and Space Administration under Contract NAS3-4181, December 1964.

(5) Haskins, J. F. and J. Herts. Advances in Cryogenic Engineering. New York: Plenum Press, Inc. Volume 7, pg. 353.

APPENDIX III-E-1

THERMODYNAMIC INTERPRETATION OF THE EFFECT OF BAROMETRIC VARIATIONS ON CALORIMETER PERFORMANCE

A vented saturated liquid calorimeter whose performance is measured by the quantity of vented gas, is affected by changes in barometric pressure. Such changes are reflected in variations of saturation temperature, i.e., in the energy of the contents of the calorimeter. This brief analysis shows how such barometric changes may be taken into account by a general equation. The equation is rather complex, but in the cases of interest for this project, the rigorous equation reduces to a rather simple form. The simplification is justified with specific cases.

Statement of Problem and Basic Assumptions

A calorimeter of volume V^* containing a saturated liquid-vapor mixture of either hydrogen or nitrogen is subjected to a heat leak Q and gas is vented through a measuring instrument. The pressure inside the calorimeter is essentially equal to the ambient barometric value, P. This ambient pressure may vary during any given run depending upon local weather conditions or other factors.

In the calorimeter is shown schematically in the sketch below.

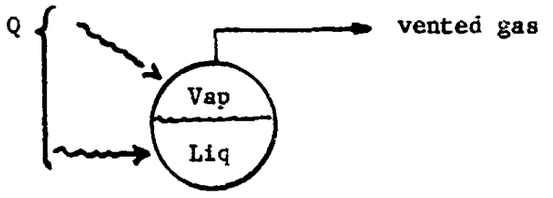

The mass of liquid in the calorimeter at any time is m^L and similarly m^V represents the the quantity of vapor; the total mass is $m^L + m^V = m^S$. During a run, these masses vary but it is assumed that <u>at all times</u> the liquid and vapor are in equilibrium with the existing value of barometric pressure at a temperature T; T varies, of course, with P. It is further assumed that the calorimeter metal is also at T at any time.

*A list of pertinent symbols is presented at the end of this appendix.

General Analysis

Three conservation equations are used in the analysis, i.e., conservation of mass, energy, and total volume. The remainder of the analysis is simply arithmetical manipulation to arrive at a convenient final result. In the analysis, superscripts c, L, V, and s are used to designate whether the quantity is container metal, liquid, vapor or the system of liquid and vapor. Subscripts 1 and 2 refer to the time the run is begun and ended; if no subscript is included, the time is anytime during the run. It will be shown that the final equation in Q contains a series of terms all but one of which is independent of how the barometric pressure varies with time, i.e., only the initial and final barometric pressures enter.

Energy Balance

The system is chosen as the calorimeter, including metal walls, liquid and vapor contents. In differential form,

$$\frac{dE^s}{dt} = Q - h^V \left(\frac{dm}{dt}\right)_{out} \tag{1}$$

Mass Balance

$$\frac{dm^s}{dt} = \frac{-dm}{dt}_{out} = \frac{dm^L}{dt} + \frac{dm^V}{dt} \tag{2}$$

Introduction of Specific Energy Terms

$$E^s = E^c + E^L + E^V = m^c e^c + m^L e^L + m^V e^V \tag{3}$$

and

$$\frac{dE^s}{dt} = m^c \frac{de^c}{dt} + m^L \frac{de^L}{dt} + e^L \frac{dm^L}{dt} + m^V \frac{de^V}{dt} + e^V \frac{dm^V}{dt} \tag{4}$$

In Eq. (4), the specific energies e refer, of course, to saturation values since it was assumed above that the liquid and vapor were always in equilibrium. Combining Eq. (1), (2), and (4),

$$Q = m^c \frac{de^c}{dt} + m^V \frac{de^V}{dt} + m^L \frac{de^L}{dt} - (h^V - e^V) \frac{dm^V}{dt} - (h^V - e^L) \frac{dm^L}{dt} \tag{5}$$

Introducing the definition

$$e = h - Pv \tag{6}$$

$$de = dh - Pdv - vdP \tag{7}$$

then $$h^V - e^V = Pv^V \tag{8}$$

$$h^V - e^L = (h^V - h^L) + Pv^L \tag{9}$$

Substituting Eqs. (6) through (9) into (5) and making use of the fact that since the calorimeter volume is constant,

$$V^S = V^L + V^V = m^L v^L + m^V v^V \tag{10}$$

$$dV^S = 0 = m^L dv^L + v^L dm^L + m^V dv^V + v^V dm^V \tag{11}$$

then

$$Q = m^c \frac{de^c}{dt} + m^V \frac{dh^V}{dt} + m^L \frac{dh^L}{dt} - (h^V - h^L) \frac{dm^L}{dt} - V^S \frac{dP}{dt} \tag{12}$$

To obtain an equation more suitable for integration, add and subtract $h^V dm^V$ from Eq. (12),

$$Q = m^c \frac{de^c}{dt} + \frac{d}{dt}(m^V h^V) + \frac{d}{dt}(m^L h^L) - h^V \frac{dm^S}{dt} - V^S \frac{dP}{dt} \tag{13}$$

Integrating Eq. (13) from the initial state (1) to the final state (2),

$$Q_t = \int_1^2 Q dt = m^c (e_2^c - e_1^c) + (m_2^V h_2^V - m_1^V h_1^V) + (m_2^L h_2^L - m_1^L h_1^L)$$

$$- \int_1^2 h^V dm^S - V^S (P_2 - P_1) \tag{14}$$

or in a more convenient form to use, add and subtract $h_1^V (m_2^S - m_1^S)$

from Eq. (14) and rearrange,

$$Q_T = m^c (e_2^c - e_1^c) + (h_2^V - h_1^V) m_2^V - \int_1^2 (h^V - h_1^V) dm^s - V^s (P_2 - P_1)$$

$$+ (h_1^V - h_1^L)(m_1^L - m_2^L) + m_2^L (h_2^L - h_1^L) \qquad (15)$$

Eq. (15) is the desired result.

Discussion of Terms

In Eq. (15), all terms except the one with the integral are functions only of the initial and end states. In particular, if these end states were identical, then independent of any pressure fluctuations during the run, Eq. (15) reduces to

$$\text{if} \quad P_2 = P_1, \; Q_T = (h^V - h^L)_{2 \text{ or } 1} (m_1^L - m_2^L) - \int_1^2 (h^V - h_1^V) dm^s \qquad (16)$$

In this simplified form, the first term is the enthalpy of vaporization times the mass vaporized; the second term accounts for the variation in enthalpy of the vented gas if the pressure varies during a run. It, of course, equals zero if the pressure is constant.

It will be shown below that of the terms in Eq. (15) only the last two are of any importance during a typical calorimeter test. The maximum barometric pressure change expected is about 2-in. mercury or 1 psi. The more reasonable change is probably about 2-in. mercury but the higher value is chosen here for illustrative purposes.

For this $\Delta P \tilde{=}$ 1 psi, (considered as an increase in the examples below) Δ T (nitrogen) $\sim 1^\circ R$ and Δ T (hydrogen) $\sim 0.4^\circ R$. The calorimeter volume is 19.25 ft^3 and holds about 968 lbs. of liquid nitrogen when full and 84.7 lbs. of hydrogen.

a. The term $m^c (e_2^c - e_1^c)$ amounts to about 23 Btu (nitrogen case) and 0.4 Btu (hydrogen case) when $\Delta P = 1$ psi. For the maximum effect, assume no evaporation (i.e., negligible running time). Then the important term in Eq. (15) is $m^L (h_2^L - h_1^L)$ which is about 475 Btu (nitrogen case) and 82 Btu (hydrogen case). The maximum contribution of the term is

then about 5% (nitrogen case) and 0.5% (hydrogen case). For more realistic cases, where evaporation occurs and $\Delta P < 1$ psi, the contribution becomes negligible.

b. The term $(h_2^V - h_1^V)\, m_2^V$ would be maximized if the final state were all vapor. In this case, the term has the values 0.5 Btu (nitrogen case) and 1.0 Btu (hydrogen case). These are quite small values and may be considered negligible, especially for the more realistic case when evaporation is not complete.

c. The term $V^S (P_2 - P_1)$ is equal to about 3.6 Btu. Again this number is small compared to the total of the last two terms in Eq.(15).

d. The term $\int_1^2 (h^V - h_1^L)\, dm^S$ is similar to the one discussed in (b) and the maximum value of this path-dependent function is of the same order (albeit slightly larger) than found in (b). They are, however, of opposite sign and tend to cancel and, in any case, both are small compared to the last two terms in Eq. (15).

Conclusion

Within experimental accuracy, the heat leak into the calorimeter may be calculated from Eq. (15) with the first four terms neglected, i.e.,

$$Q_T = (h_1^V - h_1^L)\,(m_1^L - m_2^L) + m_2^L\,(h_2^L - h_1^L) \tag{16}$$

and if $(m_1^L - m_2^L) \gg (m_2^V - m_1^V)$, then

$$Q_T = (h_1^V - h_1^L)\,(m_1^s - m_2^s) + m_2^L\,(h_2^L - h_1^L) \tag{17}$$

where the first term is simply the enthalpy of vaporization times the mass vented; the second term reflects the energy gain or loss due to a temperature change resulting from a barometric pressure variation. It is often closely approximated as $\bar{m}^L \bar{c}_{P_{sat}} \Delta T$, i.e.,

$$Q_T \approx (\Delta H_v)\ (\text{mass vented}) + \bar{m}^L \bar{c}_{P_{sat}} \Delta T \tag{18}$$

Note About Hydrogen Conversion, Para to-Ortho Form

Eq. (15) or (16) is also applicable if there should occur any substantial variation in orth-para composition for liquid hydrogen. The enthalpies in this case would then be a function both of temperature (or pressure) and composition. For the practical situation of liquid hydrogen near the atmospheric boiling point, small pressure fluctuations will not change the saturation temperature sufficiently to make such a correction necessary.

TABLE OF SYMBOLS

c	heat capacity, Btu/lb-^{o}R
e	specific internal energy, Btu/lb
E	total internal energy, Btu
h	specific enthalpy, Btu/lb
ΔH_v	enthalpy of vaporization, Btu/lb
m	mass, lbs
P	barometric or system pressure, psia
Q	heat leak rate, Btu/time
Q_T	total heat leak, Btu
t	time
T	temperature
v	specific volume, ft^3/lb
V	total calc.imeter volume, ft^3

subscripts

1	initial
2	final

superscripts

c	container
L	liquid
s	system of liquid and vapor
V	vapor

APPENDIX III-E-2

SHIELD TEMPERATURE DISTRIBUTION IN A MULTI-LAYER SYSTEM

It is often necessary to predict the temperature distribution in a multi-layer insulation when radiation is the sole heat transfer mode. The present analysis makes use of the Ohm's law analogy by expressing the emittance of the radiation shields as a radiation resistance. The use of the analogy contributes to a better understanding of the thermal properties of multi-layer insulations.

Statement of the Problems

A tank is covered with n radiation shields separated from each other with non-conducting spacers. The planes of the boundaries and shields are parallel to one another. All surfaces can have different emittances although the resulting relation is simplified if all shields have an equal emittance.

General Analysis

For any two parallel surfaces, the rate of heat transfer between them is determined by the Stefan-Boltzmann law as expressed by the following relation:

$$Q = \sigma A \left(T_o^4 - T_i^4 \right) \frac{1}{\frac{1}{e_o} + \frac{1}{e_i} - 1} \qquad (1)$$

where
- Q = heat flow, Btu/hr
- σ = Stefan-Boltzmann constant, 0.173×10^{-8} Btu/ft^2-hr-$^\circ$R^4
- A = surface area, ft^2
- T = surface temperature, $^\circ$R; T_o, temperature of warm surface; T_i, temperature of cold surface
- e = total hemispherical emissivity of the surface, dimensionless; e_o, emissivity of warm surface; e_i, emissivity of the cold surface

Equation (1) can be written in the form

$$\frac{Q}{A}(R_o + R_i - 1) = \sigma (T_o^4 \; T_i^4) \qquad (1a)$$

where R = Dimensionless radiation resistance, $\frac{1}{e}$

The radiation Equation (1a) now states that the product of the heat flux and sum of the radiation resistances is proportional to the difference of the fourth power temperature potentials.

If n shields are inserted between the warm and cold boundaries, then N + 1 spaces are formed. The resistance of each space can be expressed by Equation (1a) and the total resistance between the boundaries can be expressed as the sum of the individual resistances. This sum is carried out below and results in Equation (2) because the heat flux in all spaces has a single value due to series nature of the heat flow path.

$$(R_i + R_1 - 1) = \sigma \frac{(T_1^4 - T_i^4)}{(Q/A)_{i,1}}$$

$$(R_1 + R_2 - 1) = \sigma \frac{(T_2^4 - T_1^4)}{(Q/A)_{1,2}}$$

$$\cdots\cdots\cdots\cdots\cdots\cdots\cdots\cdots$$

$$(R_{n-1} + R_n - 1) = \sigma \frac{(T_n^4 - T_{n-1}^4)}{(Q/A)_{n-1,\,n}}$$

$$(R_n + R_o - 1) = \sigma \frac{(T_o^4 - T_n^4)}{(Q/A)_{n,o}}$$

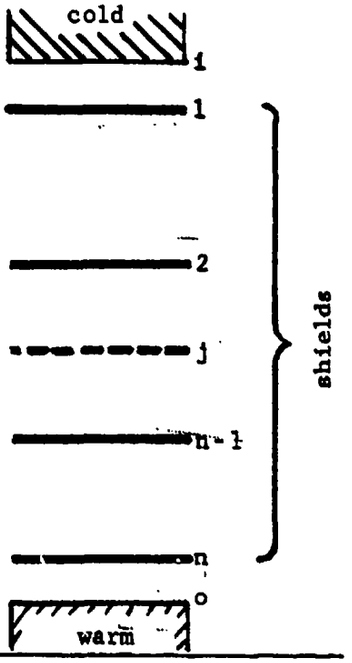

$$R_i + 2\sum_{j=1}^{n} R_j + R_o - (n+1) = \sigma \frac{(T_o^4 - T_i^4)}{(Q/A)_{i,o}} \qquad (2)$$

If all the shield surfaces have the same emissivity and, therefore, the same radiation resistance, Equation (2) can be simplified to,

$$R_T = \left[R_i + R_o + 2nR_s - (n+1) \right] = \frac{\sigma (T_o^4 - T_i^4)}{(Q/A)_{i,o}} \qquad (2a)$$

where R_s is the radiation resistance of each shield surface and R_T is the total resistance between the boundaries. When the boundary emissivities approach 1.0 ($R_i = R_o = 1$) and the shield emissivities are of the order of .05 ($R_s = 20$) or less the total radiation resistance between the boundaries is given to within 5 per cent by the relation

$$R_T = 2nR_s = \frac{\sigma (T_o^4 - T_i^4)}{(Q/A)_{i,o}} \qquad (2b)$$

These specialized conditions prevailed in most of the space simulation tests performed with the tank calorimeter. In the case of aluminum shields having surface emittances of .035, we obtained total system resistance of the order of 275 (no dimensions). For cold and warm boundary temperatures of 140 and 540°R respectively, we obtain a value for $\sigma (T_o^4 - T_i^4)$ of 145 Btu/hr ft^2. For a five shield system, Equation (2b) results in a calculated heat flux of .51 Btu/hr ft^2.

It is often of interest to know the temperature distribution that would prevail in a multi-layer system if radiation were the sole means of heat transfer. Since the heat flow in a given system is a constant, the following identity is valid:

$$(Q/A)_{i,o} = (Q/A)_{i,m} = \frac{(T_o^4 - T_i^4)}{R_{T_{i,o}}} = \frac{(T_m^4 - T_i^4)}{R_{T_{i,m}}} \qquad (3)$$

where $R_{T_{i,o}}$ = resistance between warm and cold boundaries for a system with n shields

$R_{T_{i,m}}$ = resistance cold boundary and shield m in a system with n shield

The resistance of m shields in a system with n shields is obtained by summing the individual resistances between shields as established by Equation (2).

Equation (2) can be written for the first m shields where the emissivity of each shield surface has the same value as

$$R_{T_{i,m}} = \left[R_i + 2R_1 + 2R_2 + \ldots + R_m - m\right] \tag{4}$$

Since $R_1 = R_2 = R_m$, Equation (4) can be simplified to

$$R_{T_{i,m}} = R_i + (2m-1)\, R_s - m \tag{4a}$$

For the conditions where the emissivity of the cold boundary approaches 1.0 ($R_i = R_o = 1$) and the shield emissivities are .05 ($R_s = 20$) or less, $R_{T_{i,m}}$ can be obtained with an accuracy of five per cent or better by elimination of the terms R_i and m from Equation (4) giving $R_{T_{i,m}} = (2m-1)R_s$

Equation (3) can be solved for the temperature of shield m and the appropriate simplifying values substituted for the partial and total resistance of the multi-layer system to give

$$T_m = \sqrt[4]{\frac{2m-1}{2n}\left(T_o^4 - T_i^4\right) + T_i^4} \tag{5}$$

For absolute temperatures, T_i, of the cold boundary less than 140°R and for all but very small values of the ratio 2m-1/2n, T_m can be obtained to good accuracy from

$$T_m = T_o \sqrt[4]{\frac{2m-1}{2n}} \tag{5a}$$

Thus, from this equation, it can be seen that the temperature of any shield m is a function only of the warm boundary temperature and the shield position.

The relation between the temperature of any shield and its position as expressed by Equation (5a) is shown in Figure III-50. The ordinate is the ratio of the temperature of shield m to the warm boundary temperature. This is plotted against the position of shield m in a system containing n shields expressed as a ratio of value less than 1.0. From this figure it is apparent, for example, that in any multi-layer system having a warm boundary of 80°F (540°R), approximately fifty per cent of the shields have a temperature greater than 0°F (460°R).

Notes:

1. Cold Boundary Less than 140°R
2. Shield Emittances Less than .05
3. Boundary Emittances Approaching 1.0
4. T_o = Warm Boundary Temperature
5. n = Total Number of Shields in System
6. T_m = Temperature of Shield m Counting from Cold Boundary

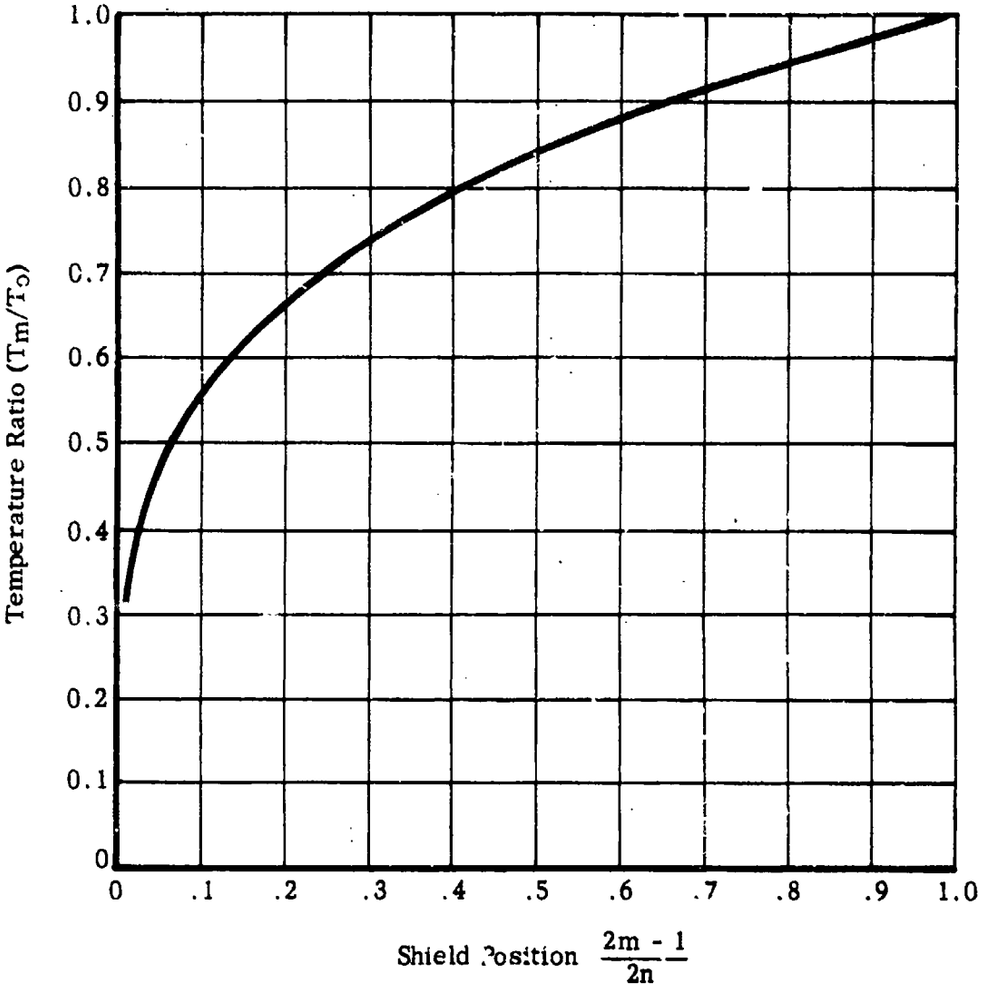

FIGURE III-50 TEMPERATURE DISTRIBUTION IN MULTI-LAYER INSULATION

APPENDIX III-E-3

K ρ PRODUCT

The product of the thermal conductivity and weight density of an insulation provides a measure of the insulations usefulness in space applications and a basis for comparing it with other systems. A relation is derived in which this product is expressed directly in the measured system properties which include the heat flux, number of shields, differential temperature, and unit weight of the multi-layer.

The apparent thermal conductivity of a multi-layer insulation is expressed by the relation for solid conduction by

$$K = \frac{Q}{A} \frac{x}{\Delta T} \tag{1}$$

where K = thermal conductivity, Btu-in/hr-ft^2-$^\circ$F

Q/A = heat flux, Btu/hr-ft^2

x = insulation thickness, inches

ΔT = temperature across the insulation, $^\circ$R

The insulation thickness can also be expressed in terms of the number of layers in the insulation, i.e., one shield and spacer per layer, and the measured thickness of the layer. Thus,

$$x = n\ t_L \tag{2}$$

where n = number of layers

t_L = layer thickness, inches

The insulation density in lbs/ft^3 can be expressed by

$$\rho = 12\ \frac{w_L}{t_L} \tag{3}$$

where w_L = unit weight of each layer, lb/ft^2-layer

From Equations 1, 2, and 3, the $K\rho$ product can be expressed by the following:

$$K\rho = \left(\frac{Q}{A}\right) \times \left(\frac{n}{\Delta T}\right) \quad 12\ w_L \tag{4}$$

Each term on the right is a measurable property and for a given system, three of the four terms may be constant.

Information regarding the weight per layer and number shields used in each system can be found in Table III-1. The measured heat flux and differential temperature across the insulation systems in the simulated space environments can be found in the detail tabulation results for each system.

PART IV

EMISSOMETER

IV. EMISSOMETER

LIST OF FIGURES

LIST OF TABLES

IV. EMISSOMETER

A. Summary

1. Purpose

It has been the purpose of this effort to measure at minimum cost, the total hemispherical emissivity (hereinafter referred to as emittance) of radiation shield materials, to screen them for use in multi-layer insulation and related systems and to provide added information for understanding the results obtained in the flat plate and tank insulation studies conducted in the contract.

2. Scope

As no commercial instrument is available for this purpose, it was necessary to design, fabricate and perfect the performance of a suitable device with which to perform the emittance measurements. The instrument is currently suited for performing measurements on surfaces at or near room temperature; extension of this capability to lower temperature is not now required but can be achieved through minor modification of the instrument. The instrument was used to measure the emittance of a wide variety of foils, plates, and coatings. This included materials having low emittance values suitable for use as radiation shields as well as materials with high emittance values used for other purposes related to space vehicles.

3. Conclusions

1) The measured average emittance of aluminum foils is about .035. Comparable results were obtained with about 400°A of aluminum vacuum deposited on polyester film.
2) The emittance of the uncoated surface of polyester film, ¼ mil thick, is approximately 10 times greater than when coated with 400°A of aluminum.
3) Compared to aluminum foil, improved emittances appear to be possible with polyester film coatings through the use of heavy gold coatings, gold coated over aluminum and protected silver coatings.

B. Introduction

The consideration of the emittance value of shield materials is of primary importance in the design of multi-layer insulations for application to space vehicles. The emittance value establishes the number of shields necessary to achieve a prescribed heat flow. The unit weight of the shield material is an important consideration also as the heat flow is the result of an optimization performed on the weight of the insulation, the mission characteristics, and the loss of propellant due to boil-off.

The emittance of a surface is a rather complex function of its material make up, smoothness, and temperature. The program described in this report has been an attempt to measure the emittance value at one temperature only and to relate this value to the material with a secondary emphasis placed on the smoothness of the surface and other surface conditions. Further, we investigated the metals such as aluminum, gold, and silver which in pure form have exceptionally low emittance values. Metals in the form of foils, chemical plating and vacuum deposited coatings have been investigated. In this work, we have also obtained information on high emittance surfaces which are involved in the equipment used for performing space simulation and involved also with the actual exterior surfaces of space vehicles.

The data obtained has been used primarily for developing a greater understanding of the measurements made with the multi-layer shields in the programs associated with the flat plate and tank calorimeter studies. This data will also serve in the future as a partial compendium of the emittance property shield materials.

C. Experimental Equipment

1. Principal of Operation

The emissometer instrument measures the total hemispherical emittance of samples of candidate radiation shield materials. It has been designed to permit fairly rapid measurements, i.e., about 2 hours per sample, and can be used for comparative measurements without extensive calibration.

The emissometer uses the receiver disc principle. A circular, thin-metal blackened disc, about 1.5 inches in diameter, is placed closely adjacent, and parallel, to a circular sample piece in an evacuated space. The back side of the receiver disc, (also blackened), is surrouned by a black cavity held at a temperature low with respect to the sample temperature. The receiver disc exchanges heat with the sample on one side and with the black cavity on the other side principally by radiative heat transfer. The geometry is such that the heat transfer between the sample and the receiver disc is essentially like that between two infinite parallel planes. Radiative transfer between the back side of the disc and the black cavity is essentially that between two black bodies. Hence, a heat balance on the disc yields the equation:

$$e_s \sigma (T_s^4 - T_d^4) = \sigma (T_d^4 - T_c^4)$$

or

$$e_s = \frac{T_d^4 - T_c^4}{T_s^4 - T_d^4}$$

Thus, if the sample temperature, the cavity temperature, and the disc temperature are measured, the emissivity of the sample can be determined. In our apparatus, the sample temperature is maintained constant at a value of [illegible]°F. The cavity temperature is maintained at the temperature of liquid nitrogen (77°K) and the receiver disc temperature is measured with a thermocouple.

2. Description of the Apparatus

An assembly drawing of the apparatus is shown in Figure IV-1. Only the vacuum vessel with internal parts is shown. The vacuum pumping system is shown schematically in Figure IV-2. A liquid nitrogen supply system, and instrumentation for controlling sample temperature and reading the thermocouple outputs are also required.

Referring to Figure IV-1, the sample is mounted on the lower surface of the sample holder block, part 9. Its temperature is maintained at a fixed level by means of a heater, part 28. A controller with thermistor sensing element monitors the temperature and controls

the heat input to maintain a present level within $\pm$ 0.25°F. The temperature of the sample holder is accurately measured by an imbedded copper-constantan thermocouple.

The receiver disc is immediately adjacent to the sample surface. The disc is blackened on both sides with 3M Brand Velvet Coating #9564 black, which has an emissivity of about 0.94.*

It is extremely important to insure that the major heat input to the disc is the radiative transfer from the sample and the major heat flow from the disc is due to its radiative interchange with the surrounding cold, black cavity. The construction places strong emphasis on minimizing extraneous heat inputs to or outputs from the disc. The disc is suspended by six 0.003 inch diameter stainless steel wires which pass radially outward to a mounting ring, part 6. A copper-constantan thermocouple made of 0.001 inch diameter wire is mounted on the rear surface of the receiver disc; the two leads pass downward and connect to heavier thermocouple leads, which then pass out through the vacuum shell.

For low emissivity samples, the radiative flux received by the disc is very low and the disc temperature approaches that of the cavity. The mounting ring, to which both the support wires and the thermocouple leads are connected (thermally, but not electrically, in the case of the thermocouple leads) is cooled to the same temperature as the cavity, i.e., 77°K. Conductive heat leaks from the disc, through the supports and thermocouple leads, are thereby minimized for low emissivity samples. Thus, even for low emissivity samples, the conductive heat leaks are small compared to the radiative transfer on which the measurement depends, and good accuracy is maintained.

The black cavity around the receiver disc is formed by a copper tube with a flat end piece, cooled by a flow of liquid nitrogen passing through tubes soldered to its exterior. The interior of the cavity is also blackened with the 3M paint. The geometrical arrangement of the

---

*Emissivity at room temperature, measured by Arthur D. Little, Inc. using a calorimeter technique.

cavity and mounting ring (with baffles) is such as to prevent radiation from the warm walls of the chamber from passing into the cavity and reaching the disc.

The sample holder can be moved axially in its mounting tube and is adjusted so the surface of the sample is in a plane established by four points on the end of the tube. The sample is placed on the sample holder and set in position with the sample holder sub-assembly, parts 1, 2 and 9, removed from the vacuum vessel. The sub-assembly is then inserted into the vessel; the construction insures that the sample face will be positioned, parallel to the receiver disc and at a fixed distance from it. In this way, samples with various thicknesses can be emplaced with the same axial space between the sample surface and the receiver disc surface, thereby eliminating variations in measurement due to change in geometry of the set-up.

The receiver disc and its mounting ring are incorporated in a second sub-assembly, consisting primarily of parts 13, 3, 4, 6, 7, 8 and 26, that can be removed from the vacuum vessel to facilitate inspection of the receiver disc, calibration of its thermocouples and alignment of the receiver disc with the sample surface.

The vacuum vessel and black cavity, principally parts 12, 14, 15, 30 and 31 comprise the third major sub-assembly. Part 32 is a port for connecting the roughing vacuum pump. The liquid nitrogen coolant tubes, part 17, pass into the chamber through pantleg arrangements, parts 16 and 18. Four penetrations are made, two inputs and two outputs. The two liquid nitrogen circuits will be connected in series external to the vacuum vessel so that only one liquid nitrogen input is required.

The vacuum pumping train, shown schematically in Figure 2, consists of a high vacuum valve connected to the flange on the vessel, a chevron baffle at room temperature, a 2" oil diffusion pump and a forepump, which also serves as a roughing pump. When the chamber is not under vacuum, the high vacuum valve will be kept closed and the diffusion pump running.

3. Operation

In a typical test, the sample will be mounted on the sample holder, by means of vacuum grease, and inserted into the emissometer. The system is then evacuated. First, with the foreline valve closed and the roughing valve open, the chamber is pumped down to about 200 microns. Then with the roughing valve closed and the foreline and high vacuum valves open, evacuation continues down to a level of about 10^{-6} torr. Just before the high vacuum valve is opened, the cylindrical cavity and receiver disc mounting ring will be cooled by passing liquid nitrogen through the cooling tubes. These cold surfaces protect the sample, the receiver disc and the interior of the cavity from oil backstreaming from the diffusion pump. The cavity cooldown and pumpdown to the 10^{-6} torr range takes about one hour. After the cavity is cooled, an additional hour is required for the receiver disc to reach its equilibrium temperature. During this time, the sample holder temperature, hence, the sample temperature is maintained constant by the heater-controller. Measurement of the steady-state temperature of the receiver disc and of the sample holder temperature is all that is required for the completion of the test, since the temperature of the cavity is known.

4. Accuracy of Measurement

A number of factors combine to introduce errors into the measurement of the emissivity of the sample. These include:

1) Uncertainty in measuring the receiver disc temperature.
2) Uncertainty in knowing the cavity temperature
3) Uncertainty in measuring the sample temperature.
4) Departure of the emissivity of the receiver disc from unity.
5) Departure of the absorptivity of the cavity from unity.
6) Conductive heat leaks from the receiver disc through supports and the thermocouple.
7) Deviations of the geometry from that assumed in calculating the sample emissivity.

We have carried out an error analysis to determine the effects of these factors on the accuracy of determination of the sample emissivity. We estimate that sample emissivities in the range 0.01 to 1.0

can be determined within ±10 per cent with very little calibration of the apparatus. Improved accuracy may be achieved by calibration.

After completion of the instrument, a number of runs were made to measure the emissivity of the sample holder face as a means of determining the reproducibility of results. Runs on four consecutive days showed values of 0.043, 0.042, 0.043, and 0.041. Hence, the measurement was reproducible within a spread between maximum and minimum values of about 5 per cent.

Measurements on two consecutive days were also made with a specially prepared sample of very low emissivity to establish the utility of the device for such samples. The sample is a 2.5 inch diameter x 1/8 inch thick fused quartz disc, polished optically flat on both surfaces and coated on one surface by vacuum deposition with a 1000°A thick aluminum film. This disc was stuck to the sample holder with two-sided adhesive tape, with the aluminum coated surface facing the receiver disc in the emissometer. Emissivity values determined from the two runs were both 0.022, demonstrating the capability of the apparatus for measuring very low emissivities.

A high emittance calibrating device for the instrument was also built. It fits in place of the sample holder and provides a black cavity which can be maintained at constant temperature. The cavity simulates a sample with an emittance very close to 1, and has been used as a periodic check on the instrument.

Data[1] on the emittance at low temperatures of the 3M Brand Velvet Coating #9564 suggests that the emittance of the coating drops from 0.94 at room temperature to about 0.8 at 200°K and remains constant at near that value down to about 90°K. If so, analysis shows that sample emittances indicated by the Emissometer would be higher than the actual values, particularly for low emittance samples. The possible error would be considerably larger than that from any other

source we have been able to identify (as high as about 30% for a sample with $\epsilon \leq 0.1$). However, it appears that the error would be relatively constant and always in the same direction, so that comparative measurements between samples would not be affected.

Both receiver discs No. 1 and No. 2 were made from 2 mil aluminum which was painted on both sides with 3M Velvet Black No. 9654. Disc No. 3 is made from 2 mil gold foil which is coated with platinum black. As noted in Table IV-1, the latter disc was used in better than 50 per cent of the measurements made.

D. Results

Approximately 160 emittance measurements were made with the emissometer. These results are presented in Table IV-1. The largest number of samples tested are vacuum deposited coatings on polyester film. Also, many aluminum foils and a number of gold plated specimens were tested. High emittance paints and coatings received some attention in this study.

With regards to coatings an attempt was made to establish some quantitative measure of the sample coating thicknesses. We have determined the electrical resistances of the films according to a method commonly used. Consideration of the equation for resistance shows that, for a square piece of coated material, the resistance from one edge to an opposite edge is given by

$$R = \frac{\rho}{\delta}$$

where

R = Resistance, ohms

ρ = Resistivity of metal coating, ohm-cms

δ = Thickness of metal coating, cms.

Resistance measurements were made for the various samples and the coating thicknesses calculated from the equation using a room temperature resistivity value for aluminum of 2.85×10^{-6} ohm-cm, for gold of 2.35×10^{-6} ohm-cm, and for silver of 1.60×10^{-6} ohm-cm.[2] The

sample size used in this measurement is 2 x 2 inches square. When the shield material was sufficiently large, at least two resistance specimens were taken in an area adjacent to that from which the emissometer specimen was taken.

E. Discussion of Results

1. Aluminum Foils

We have made approximately 25 measurements on aluminum foils. The emittance results range from 0.023 to as high as 0.103. About 50 per cent of the measured values are in the range from 0.030 to 0.040. As indicated previously, we consider the emissometer instrument to have an inherent accuracy better than 10 per cent based on theoretical considerations and calibration data. Thus, the observed scatter we feel is the result of either surface condition (not necessarily roughness) or metal purity which we have not studied in detail. The frequency distribution of the emittance values for aluminum is shown in Figure IV-3.

2. Aluminum Coated Polyester Film

Approximately 40 measurements were made on polyester film containing coated aluminum. The emittance values obtained vary from .0143 to .0773. About 50 per cent of the data are in a range from 0.030 to 0.040. See Figure IV-3. In one group of 10 tests performed with shield material used in Insulation System No. 5, we obtained emittance results in a range of $0.0345 \pm .044$ for coating thicknesses that were in the range $420 \pm 40^{\circ}A$.

3. Uncoated Polyester Film

In tests performed on May 5 and in test 225, the uncoated sides of an aluminum and gold coated polyester film respectively gave an emittance result of 0.36. This data is discussed in Part III Insulation System No. 2 with reference to spectrophotometer measurements made with polyester film. The emissometer and spectrophotometer measurements corroborate one another. Thus, it appears that if the uncoated side has an emittance of about one order of magnitude greater than the aluminum coated side, that two of these shields are required in order to achieve a thermal effectiveness equivalent to one aluminum foil shield.

4. Gold and Silver Coated Polyester Film

We have studied the variation in the emittance of gold coatings, vacuum deposited on polyester film, as a function of the coating thickness in the range from less than 1°A to 2350°A. The test results are presented in Table IV-1 and summarized in Figure IV-4. The numbers in brackets refer to test numbers given in Table IV-1. The data show a trend of decreasing emittance with increasing thickness as would be expected.

Test 221 performed with specimen coated with gold to a thickness of 2350°A gave an emissivity value of 0.020. This value compares with some of the best values reported for gold at or near room temperature. The data sampled are too few to support firm conclusions with regard to the smallest coating thickness that would correspond to the best surface emissivity. However, we suspect this apparent coating thickness for gold is about 2000°A.

Tests 210 and 211 were performed with specimens consisting of gold vacuum deposited on aluminum that is vacuum deposited on ¼ mil polyester film. The primary aluminum coating had a thickness of about 285°A. The gold coating on samples 210 and 211 was about 100°A and 200°A respectively. The results obtained show an improvement in the emittance compared to the average results obtained with the vacuum deposited aluminum coating alone.

Tests 222 and 223 were performed with specimens coated with silver on Mylar. Further, the silver on each film was protected with a light coating of silicone oxide. The average results obtained by us are comparable to those obtained with the gold specimen used in Test 221.

5. Limit of Reflectance of a Radiation Shield

In considering the various methods of improving multi-layer insulation systems, the question arises--what is the limiting performance that can be expected if the necessary engineering developments could be carried out? The factors that control the insulation system performance are the number of radiation shields and the manner in which

each shield emits and reflects thermal radiation. It is, therefore, of interest to examine the most favorable radiation performance which could be achieved with a radiation shield, assuming that the performance is limited only by the inherent properties of the shield.

a. Discussion

Let us assume that the shields can be separated so that radiation is the only mode of heat transfer between the shields and that the shields are optically smooth and chemically pure. The shield surface can then be made highly reflective, i.e., have as high a total hemispherical reflectance (ρ) as possible and as low a total hemispherical emittance* (ϵ) as possible. The two properties are not independent being directly related by:

$$1 = \epsilon + \rho \quad (3)$$

so that the determination of one property specifies the other.

Superconducting foils and surface layers of controlled spacing to correspond to integral multiples of a wavelength though superficially interesting do not provide the basis for workable insulation systems. The reasons why they are not applicable are discussed later.

Carefully prepared metallic surfaces are the most practical approach. To determine how reflective a metallic surface could possibly be made, assume that a single metallic crystal forms the surface. Surface crystals are ideal reflectors because they are pure, flat, have no internal boundaries, and thus have a minimum of scattering centers at the surface and within the body of the material.

The reflectance of infrared radiation at the surface is dependent on the condition of the electrons in the crystal as well as the wavelength of the impinging radiation. In metals, the long wavelength reflectivity is related to the d-c electrical conductivity

*Following Worthing, the terms emissivity and emittance are used to signify respectively the intrinsic property of the material (or the property which is equal of a pure optically flat sample) and the corresponding property of a nonpure, nonflat, real sample (emittance).

based on the Drude free electron model.[4] The Hagen-Rubens equation[4] assumes that this model is applicable to electrically conductive metals at the longer infrared wavelengths and is given by:

$$R = 1 - 2 (D/\sigma)^{1/2} \quad \text{or} \quad A = 2 (D/\sigma)^{1/2}$$

where

R = the normal spectral reflectivity
D = the frequency of the incident radiation
σ = the electrical conductivity
A = the normal spectral absorptivity
ϵ = the normal spectral emissivity

There are more refined models and equations in existence also based on electrical conductivity that attempt to take into account other effects; for example, the relaxation time of the electrons in the metal.[5]

Since electrical resistivity is directly related to temperature (conductivity is inversely proportional to temperature) and the material, the Hagen-Rubens equation can be expressed in terms of absolute temperature and as such predicts that the emissivity or absorptivity would approach zero (reflectance 100%) as temperature approaches zero. This effect is predicted quite aside from effects of superconductivity Thus, high purity copper, for example, is predicted to have an emissivity at the cryogenic temperatures of 10^{-5}.[6]

However, more recent theoretical derivations and experiments show that these predictions are not correct. At cryogenic temperatures the effect of anomalous skin depth begins to be important. The result of this effect is that electrical resistivity does not continue to drop as temperature is lowered but reaches a limiting value.

In the example of copper cited above, the emissivity will be several hundred times greater ($\epsilon = 10^{-2}$ to 10^{-3}) than predicted without taking account of the anomalous skin effect.

Since radiation shields operate at different temperatures depending on their position, the ideal reflectivity of a metal should be known at a given temperature in terms of the electrical resistivity. It appears possible to utilize theoretical models which have been shown to give good empirical results to take into account anomalous effects. These models could serve as a guide during engineering development of radiation shields and suggest in terms related to economic factors possible further increases in performance.

b. Phenomena Related to High Reflectivity

(1) Superconductivity

Zero electrical resistance will result in 100% reflectivity. Therefore, a superconductor would appear potentially capable of achieving 100% reflectance. However, it has been established that the phenomenon of superconductivity does not occur with electrons oscillating at frequencies above the microwave range. The reflectance of a superconducting metal to infrared is identical to its ordinary (nonsuperconducting) reflectance. There is, therefore, no apparent means by which superconductivity can be made the basis for a highly reflective insulating material.

(2) Controlled Layer Thickness and Spacing

Controlled layer thicknesses and spacings can be used to create barriers that exhibit very high impedance to radiative transfer through resonance phenomena. For example, two semi-reflective transparent films accurately spaced at a distance equal to one-half wavelength will very effectively impede the passage of monochromatic radiation through the barrier formed by the two films acting in effect like a nearly 100% reflecting foil. Difficulty arises in applying this phenonenon because thermal radiation covers a broad wavelength band while the controlled spacing layer is only effective in reflecting a narrow band, at most 20% of the total radiation represented by the Planck distribution.

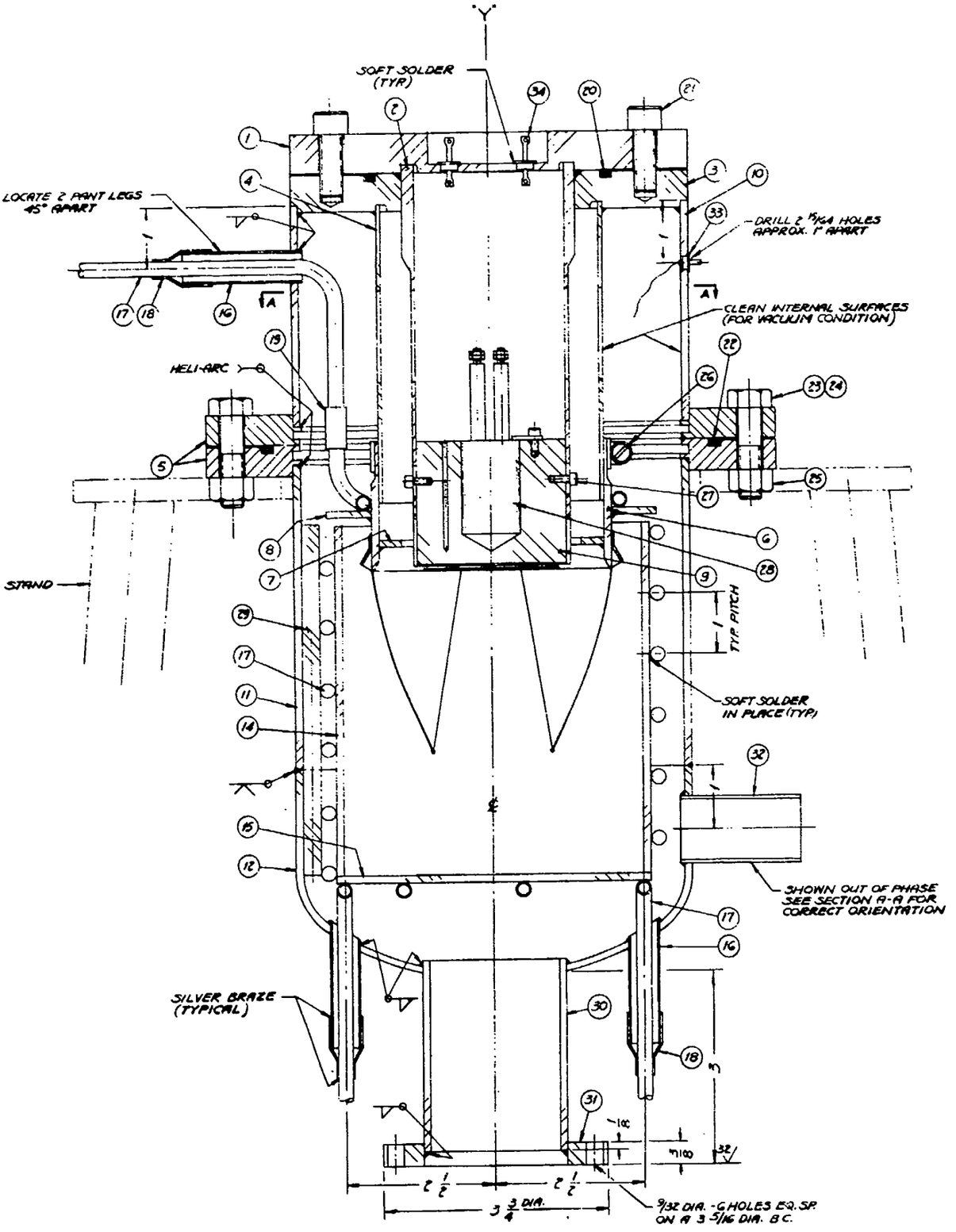

FIGURE IV-1 ASSEMBLY EMISSOMETER

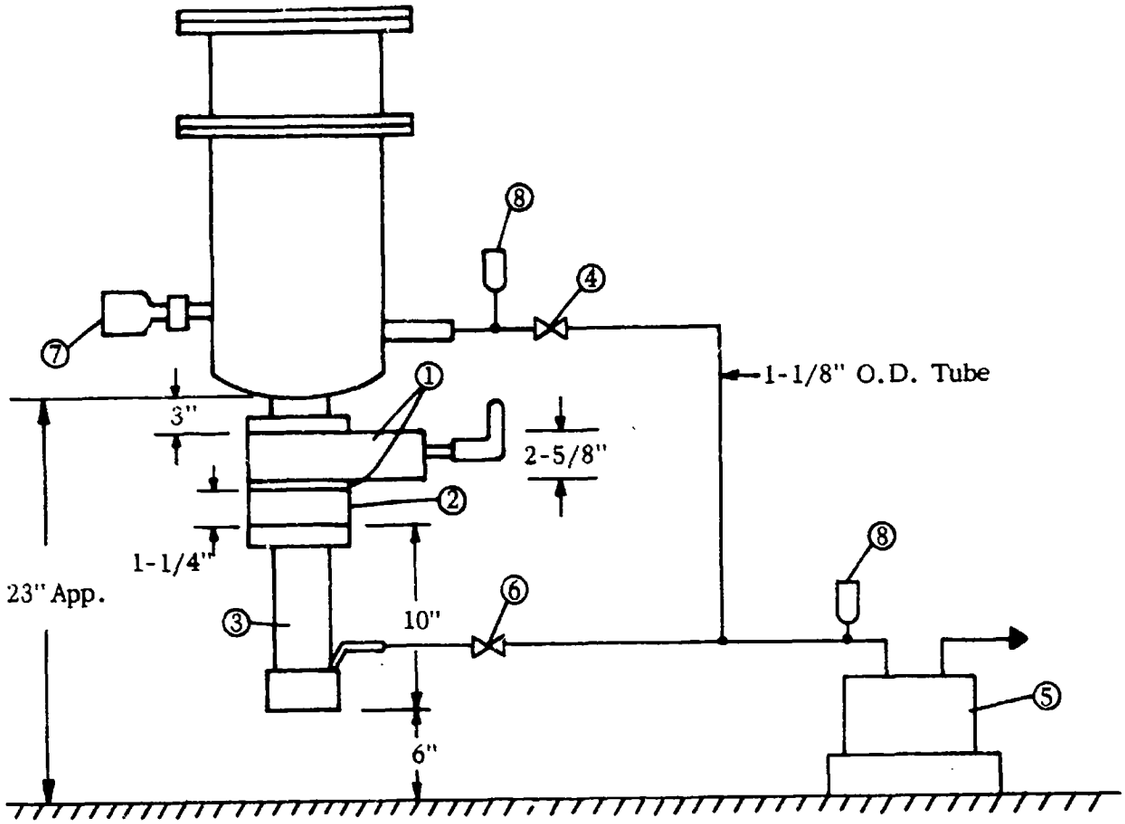

1	High Vacuum Gate Valve
2	Chevron Baffle
3	2" Diffusion Pump
4	Roughing Valve - Veeco Bellows Angle Type
5	5 CFM Roughing and Fore Pump
6	Foreline Valve
7	Ion Pressure Gage
8	Thermocouple Pressure Gage

FIGURE IV-2 SCHEMATIC DIAGRAM OF EMISSOMETER VACUUM SYSTEM

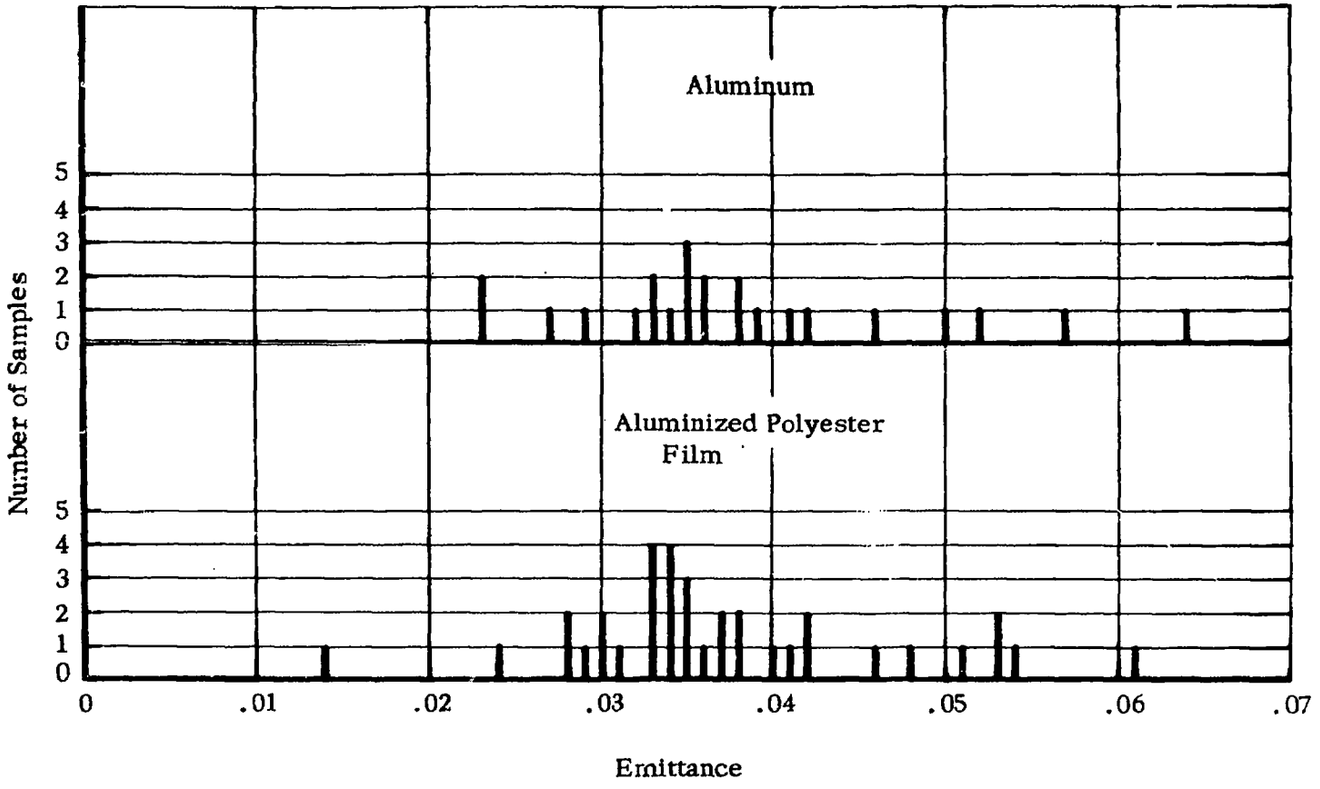

FIGURE IV-3 FREQUENCY DISTRIBUTION OF EMITTANCE VALUES OBTAINED WITH EMISSOMETER FOR ALUMINUM FOILS AND COATING

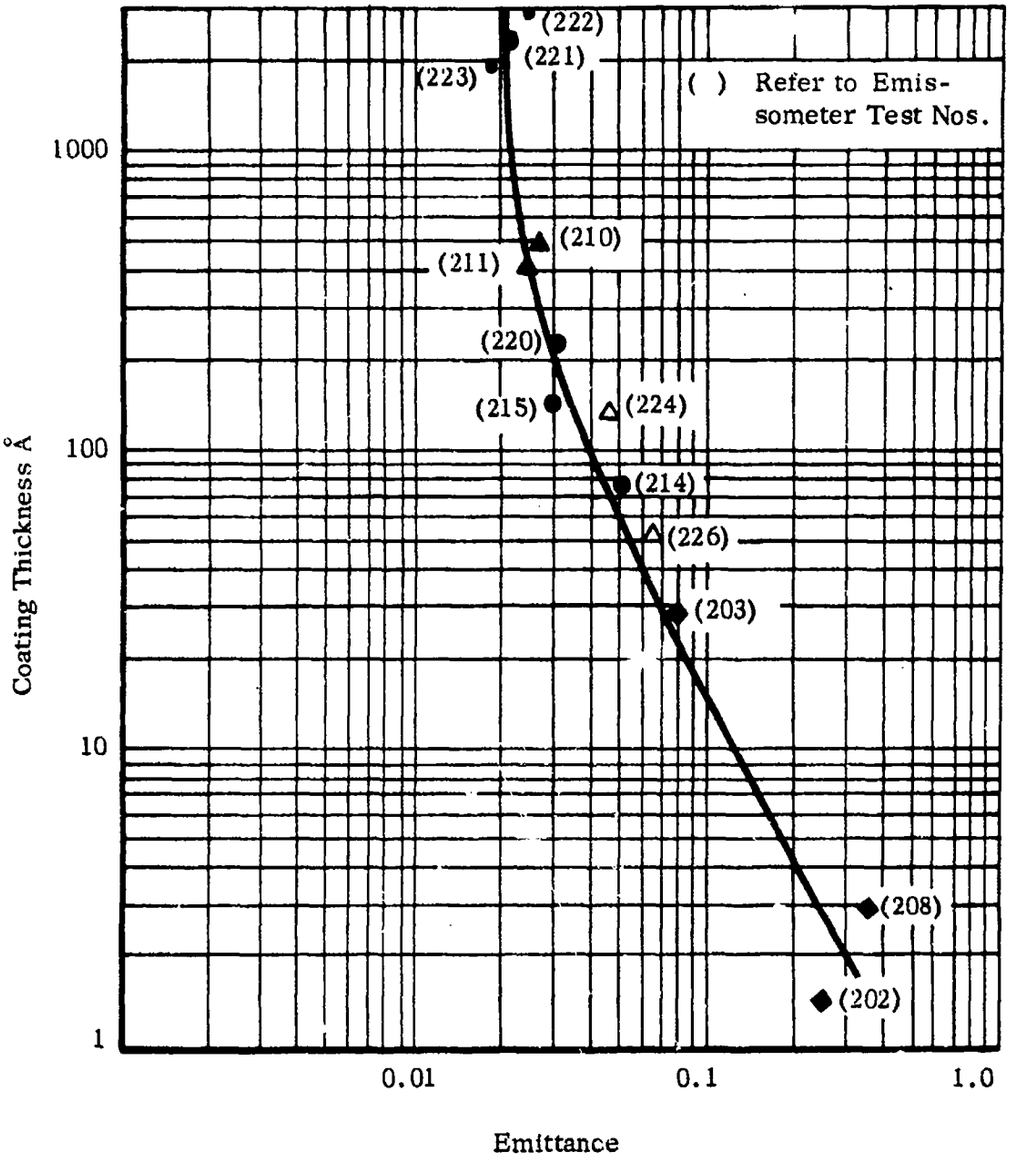

FIGURE IV-4 EMITTANCE OF GOLD AND SILVER COATINGS VERSUS COATING THICKNESS, VACUUM DEPOSITION ON MYLAR

TABLE IV-1

Summary of Emissometer Results

Surface Emittance

Date	Rec. Disc No.	Test No.	Sample Description	Side	Emittance	Coating Thickness
4/10	1		Aluminum coated quartz		0.0246	
4/21	1		Gold coated polyester film		0.043	900-1500°A
4/27	1		Aluminum coated polyester film	Coated	0.0143	
4/30	1		Gold coated polyester film	A	0.047	
4/30	1		Gold coated polyester film	B	0.048	
4/30	1		Aluminum coated polyester film	A or B	0.0543	
4/30	1		Aluminum coated polyester film	Coated	0.0613	
4/30	1		Same as above	Coated	0.0609	
5/1	1		Gold coated polyester film	Coated	0.0483	900-1500°A
5/4	1		Aluminum, System 1, Shield 1, 1100-0	Uncorroded	0.0501	
5/5	1		Aluminum coated polyester film	Coated side	0.0460	235
5/5	1		Aluminum coated polyester film	Polyester film	0.364	
5/5	1		Aluminum coated polyester film	Coated side	0.0476	
5/6	1		Sample holder face calibration		0.0401	
5/6	1		Aluminum coated mylar	A	0.0377	

TABLE IV-1 (cont'd)

Date	Rec. Disc No.	Test No.	Sample Description	Side	Emittance	Coating Thickness
5/6	1		Aluminum coated polyester film	B	0.0532	
5/7	1		Aluminum coated polyester film	A	0.0773	334
5/7	1		Aluminum coated polyester film	B	0.0513	248
5/12	1	1	Shield No. 5, Insulation System No. 1	Corroded	0.860	
5/12	1	2	Shield No. 5, Insulation System No. 1	Adj. to corr.	0.0355	
5/13	1	3	Aluminized scrim - reinforced polyester film	Scrim	0.669	
5/14	1	4	Aluminized scrim - reinforced polyester film		0.472	
5/14	1	5	Balloon Material		0.215	
5/4	1		Aluminum, System 1	Uncorroded	0.0459	
5/18	1	7	Gold coated polyester film	B	0.0382	
5/19	1	8	Aluminum disc coated with 3M optical black		0.94	
5/20	1	9	Same as sample in Test No. 8		0.926	
5/21	1	10	Copper oxide coating on 1/8" copper disc		0.832	
5/21	1	11	Quartz disc		0.0274	
5/28	1	12	Aluminum, 1145-H19, 2 mil	A	0.0346	

TABLE IV-1 (cont'd)

Date	Rec. Disc No.	Test No.	Sample Description	Side	Emmittance	Coating Thickness
5/28	1	13	Aluminum, 1100-0, 1/2 mil	Shiny	0.0348	
5/29	1	14	Same sample as in Test No. 12	B	0.0338	
5/29	1	15	Aluminum, 1100-0, 2 mil	Shiny	0.0362	
5/29	1	16	Repeat Test No. 2		0.0349	
6/1	1	17	Aluminum, Sys. No. 1, Shield No. 1		0.0379	
6/2	1	18	Sample holder face calibration		0.0408	
6/2	1	19	Aluminum Sys. No. 1, Shield No. 1	Outside	0.0470	
6/2	1	20	Repeat Test No. 2	Inside	0.0334	
6/4	1	21	Iron oxide coating on 1/8" tk copper		0.351	
6/4	1	22	Black nickel coating on 1/8" tk copper		0.384	
6/4	1	23	Aluminized quartz disc		0.0248	
6/29	1	24	Sample holder face calibration		0.0430	
7/1	1	25	Black nickel on 1/8" thick copper		0.369	
7/6	1	26	Aluminum, Insul. Sys. 4, Shield 5	Inside	0.0636	
7/8	1	27	Aluminum, Insul. Sys. 4, Shield 5	Inside	0.0569	
7/10	1	28	Aluminum, soft, 3/32" tk		0.0417	
7/10	1	29	Repeat Test 28		0.0389	
7/10	1	30	Aluminized polyester film, black chromium coating, Sample IE	1	0.0528	

TABLE IV-1 (cont'd)

Date	Rec. Disc No.	Test No.	Sample Description	Side	Emmittance	Coating Thickness
7/17	2	100	ETP Copper disc.		0.1605	
7/20	2	101	Aluminized polyester film, Sample 2E	1	0.0176	
7/21	2	102	Aluminized polyester film, Sample 2E	2	0.0410	
7/21	2	103	Aluminized polyester film, Sample 2E	1	0.0416	
7/21	2	104	Aluminized polyester film, Sample 1E	1	0.0422	
7/21	2	105	Aluminized polyester film, Sample 1E	2	0.0398	
7/22	2	106	Sample holder face calibration		0.0330	
7/22	2	107	Aluminum, chemically polished, soft 3 3/32 tk	A	0.0274	
7/22	2	108	Same as Test 107	B	0.0332	
7/22	2	109	Aluminized polyester film, Sample 1BE	A	0.0333	455°A
7/23	2	110	Aluminized polyester film, Sample 2BE	A	0.0334	453°A
7/23	2	111	Aluminized polyester film, Sample 3BE	A	0.0299	450°A
7/24	2	112	Aluminized polyester film, Sample 4BE	A	0.0369	450°A
7/24	2	113	Aluminized polyester film, Sample 5BE	A	0.0334	456°A
7/24	2	114	Aluminized polyester film, Sample 1BE	B	0.0335	378°A
7/24	2	115	Aluminized polyester film, Sample 2BE	B	0.0347	395°A
7/27	2	116	Black Chromium coating on 1/8" tk copper		0.603	

TABLE IV-1 (Cont'd)

Date	Rec. Disc No.	Test No.	Sample Description	Side	Emmittance	Coating Thickness
7/27	2	117	Aluminized polyester film, Sample 3BE	B	0.03810	380 Å
7/27	2	118	Aluminized polyester film, Sample 4BE	B	0.0358	400 Å
7/27	2	119	Aluminized polyester film, Sample 5BE	B	0.0244	395 Å
7/28	2	120	Dulite II black oxide coated on 1015 steel		0.520	
7/28	2	121	Test 120 Repeat		0.712	
7/28	2	122	Copper sulfide black on OFHC copper		0.676	
7/28	2	123	Test 122 Repeat		0.684	
7/30	2	124	3M optical black on copper		0.859	
7/30	2	125	Sample used in Tests 122, 123, machined surface		0.628	
7/30	2	126	Hard aluminum .005" tk	A	0.103	
7/31	2	127	.0003" gold plate on 304 S/S, XHV7		0.0397	
7/31	2	128	Sample holder face calibration		0.0460	
8/5	3	129	Aluminum, 1145-H19, 5 mil	A	0.0379	
8/5	3	130	3M optical black 9564, on copper		0.933	
8/5	3	131	Gold plate on 304 S/S XHV-5		0.1044	
8/5	3	132	Gold plate on ETP copper, XHV-3		0.0695	
8/7	3	133	Gold plate on 304 S/S, XHV-5		0.1057	
8/7	3	134	Gold plate on 304 S/S, XHV-8		0.0409	
8/7	3	135	Gold plate on 5 mil al. foil	B	0.362	

TABLE IV-1 (cont'd)

Date	Rec Disc No.	Test No.	Sample Description	Side	Emmittance	Coating Thickness
8/7	3	136	Gold plate on 5 mil al. foil	B	0.364	
8/7	3	137	Aluminum, hard, 5 mil, cleaned	A	0.0232	
8/14	3	138	Gold matte, .0003", on dull nickel			
8/15	3	139	Gold matte, .0003", on dull nickel			
8/14	3	140	Gold matte, .0003", on dull nickel		0.0829	
8/15	3	141	Aluminum, 1100-0, .001" foil	A	0.0295	
8/15	3	142	Aluminum, 1100-0, .001" foil	B	0.0401	
8/15	3	143	Sample holder face calibration		0.0358	
8/17	3	144	Gold plate, on ETP copper, XHV-6.		0.0608	
8/17	3	145	Gold plate on 304 S/S, XHV-4		0.0589	
8/17	3	146	Gold plate on 304 S/S, XHV-5		0.1050	
8/18	3	147	Gold plate, on 304 S/S, XHV-1		0.0366	
8/18	3	148	Gold plate on 304 S/S, XHV-2		0.0630	
8/18	3	149	Aluminum, 1100-H19, 1 mil	Bright	0.0517	
8/18	3	150	Aluminum, 1100-H19, 1 mil	Dull	0.0406	
9/8	3	151	Optical black on 1/8" tk copper disc		0.923	
9/10	3	152	Gold plated, 100%, .0003" thk., ETP copper		0.0757	
9/11	3	153	Optical black on 1/8" thk. copper disc			
9/15	3	154	Optical black on 1/8" thk. copper disc		0.910	

TABLE IV-1 (Cont'd)

Date	Rec Disc No.	Test No.	Sample Description	Side	Emmittance	Coating Thickness
9/16	3	155	Gold plated, 100% ETP copper 1/8" thk disc, Sample #XHV-6	Dull	0.0626	
9/16	3	156	1015 St. dulite coated, Cat-A-Lac Flat Black 463-3-8, LDA Sample #1		0.865	
9/16	3	157	1015 St. dulite coated, Cat-A-Lac Flat Black 463-3-8, LPJ Sample #1		0.865	
9/17	3	158	1015 St. dulite coated, Cat-A-Lac Flat Black 463-3-8, LDA Sample #2		0.900	
9/17	3	159	1015 St. dulite coated, Cat-A-Lac Flat Black 463-3-8, LPJ Sample #2		0.861	
9/17	3	160	1015 St. dulite coated, Cat-A-Lac Gloss White #443-1-500, LDA Sample #3		0.886	
9/18	3	161	1015 St. dulite coated, Cat-A-Lac Gloss White #443-1-500, LPJ Sample #3		0.886	
9/18	3	162	1015 St. dulite coated, Cat-A-Lac Gloss White #443-1-500, LDA Sample #4		0.869	
9/18	3	163	1015 St. dulite coated, Cat-A-Lac Gloss White #443-1-500, LPJ Sample #4		0.882	
9/21	3	164	3M Optical Black		0.906	
9/21	3	165	Gold plated 100% EXP copper, Sample XHV-6		0.0657	
9/21	3	166	Gold plated 100% EXP copper, Sample XHV-6		0.0558	

TABLE IV-1 (cont'd)

Date	Rec Misc No.	Test No.	Sample Description	Side	Emittance	Coating Thickness
9/21	3	167	1015 St. dulite coated, Vit-A-Var, P.V. 100 White #15966, LDA Sample #5		0.847	
9/22	3	168	1015 St. dulite coated, Vit-A-Var, P.V. 100 White #15966, LPJ Sample #5		0.852	
9/22	3	169	Gold plated 10%, ETP copper, Sample XHV-6		0.0553	
9/22	3	170	1015 St. dulite coated, Vit-A-Var, P.V. 100 White #15966, LDA Sample #6		0.852	
9/22	3	171	1015 St. dulite coated, Vit-A-Var, P.V. 100 White #15966, LPJ Sample #6		0.857	
9/22	3	172	1015 St. dulite coated, 4-B-2 Laminar X-500 Satin black poly, LDA Sample #7		0.871	
9/22	3	173	1015 St. dulite coated, 4-B-2 Laminar X-500 Satin black poly, LPJ Sample #7		0.857	
9/23	3	174	1015 St. dulite coated, 4-B-2 Laminar X-500 Satin black poly, LDA Sample #8		0.870	
9/23	3	175	1015 St. dulite coated, 4-B-2 Laminar X-500 Satin black poly, LPJ Sample #8		0.865	
9/23	3	176	1015 St. dulite coated Laminar X-4-83 Dark gray poly, LDA Sample #9		0.881	
9/23	3	177	1015 St. dulite coated Laminar X-4-83 Dark gray poly, LDA Sample #10		0.875	
9/24	3	178	1015 St. dulite coated Laminar X-4-83 Dark gray poly, LPJ Sample #9		0.894	

TABLE IV-1 (cont'd)

Date	Rec Disc No.	Test No.	Sample Description	Side	Emmittance	Coating Thickness
9/24	3	179	1015 St. dulite coated Laminar X-4-83 Dark gray poly, LPJ Sample #10		0.894	
9/24	3	180	2 mil aluminum - soft		0.0319	
9/24	3	181	Al. coated polyester film 1/4 mil thk Sample 1B2	B	0.0349	
9/25	3	182	Al. coated polyester film 1/4 mil thk. Sample 2B2	B		
9/25	3	183	Al. coated polyester film 1/4 mil thk. Sample 2B2	B	0.0337	
9/25	3	184	Gold plated 100%, ETP copper Sample XHV-6		0.0638	
9/25	3	185	Al. coated polyester film 1/4 mil thk. Sample 3B2	B	0.0350	
9/29	3	186	Gold plated 100%, ETP copper Sample XHV-6		0.0630	
9/29	3	187	Gold plated, polished ETP copper, 1/8" Disc Sample A		0.020	
9/29	3	188	Gold plated, not polished, ETP copper 1/8" disc, Sample C		0.0354	
9/29	3	189	Gold plated, polished, ETP copper, 1/8" disc Sample A		0.0200	
9/29	3	190	Gold plated, 100%, ETP copper, Sample XHV-6		0.0532	
9/30	3	191	Gold plated, polished, ETP copper, 1/8" disc, Sample B		0.0218	

TABLE IV-1 (cont'd)

Date	Rec Disc No.	Test No.	Sample Description	Side	Emmittance	Coating Thickness
9/30	3	192	Gold plated, unpolished, ETP copper, 1/8" disc, Sample D		0.0242	
9/25	3	193	Al. coated polyester film, 1/4 mil thk. Sample 4B2	B	0.0835	
9/30	3	194	Al. coated polyester film, 1/4 mil thk. Sample 5B2	B	0.0306	
9/30	3	195	Al. coated polyester film, 1/4 mil thk. Sample 1B2	A	0.0284	
9/30	3	196	Al. coated polyester film, 1/4 mil thk. Sample 2B2	A	0.0369	
10/1	3	197	Al. coated polyester film, 1/4 mil thk Sample 3B2	A	0.0275	
10/1	3	198	Al. coated polyester film, 1/4 mil thk Sample		0.0270	
10/1	3	199	Al. coated polyester film, 1/4 mil thk Sample		0.0289	
9/30	3	200	Aluminum - Soft		0.0226	
10/2	3	201	Gold plated, 100%, .0003" thk. ETP copper Sample XHV-6		0.0514	
10/2	3	202	Gold coated polyester film NRL #92264-1-E1 Mfr A		0.247	1.45°A
10/2	3	203	Gold coated polyester film NRL #92264-1-E1 Mfr A		0.0769	29.3°A

TABLE IV-1 (cont'd)

Date	Rec Disc No.	Test No.	Sample Description	Side	Emittance	Coating Thickness
10/2	3	204	Al. coated polyester film 1/4 mil. thk. test #1		0.0326	
10/2	3	205	Al. coated polyester film 1/4 mil thk. test #2		0.030	
10/2	3	206	Al. coated polyester film 1/4 mil thk. test #3		0.0337	
10/5	3	207	Gold coated polyester film, Mfr. A		0.857	1.0°A
10/5	3	208	Gold coated polyester film		0.356	2.94°A
10/5	3	209	Al. coated polyester film Mfr. A		0.0231	218°A
10/5	3	210	Gold coated, on aluminum on polyester film		0.0254	500°A
10/6	3	211	Gold coated, on aluminum on polyester film		0.0235	412°A
10/6	3	212	Aluminum on polyester film, Sample 9-1E Mfr. A		0.0722	30°A
10/6	3	213	Aluminum on polyester film, Sample 8-1E Mfr. A		0.0399	108°A
		214	Gold coated polyester film, Mfr. K, Sample 10664-1-1E		0.0485	78°A
		215	Gold coated polyester film, Mfr. K Sample 10664-2-1E		0.0287	147°A
10/7	3	216	Gold plated copper 1/8 thk, Sample XHV-6		0.0540	

TABLE IV-1 (cont'd)

Date	Rec Disc No.	Test No.	Sample Description	Side	Emmittance	Coating Thickness
10/8	3	217	Gold plated copper 1/8 thk, Sample XHV-6		0.0540	
10/9	3	218	Mfr. J, Std. optical black		--	
10/9	3	219	Mfr. J, Std. optical black		0.900	
10/9	3	220	Gold coated polyester film, Mfr. K, M0640 Sample 10664-3-1E		0.0302	224°A
10/13	3	221	Gold coated polyester film, Mfr. K, 645 Sample 10664-4-1E		0.020	2350°A
10/14	3	222	SiO_2 over silver on polyester film Mfr. K, 647, Sample 10864-1-1E		0.0227	2810°A
10/14	3	223	SiO_2 over silver on polyester film Mfr. K, 648, Sample 10864-2-1E		0.0175	2000°A
10/14	3	224	Gold-Vac. deposited on polyester film Mfr. A, 48 inch wide sheet, Sample 101469-1-1E		0.0443	135°A
10/14	3	225	Gold-Vac deposited on .25 mil polyester film Mfr. A, 48 inch wide sheet Sample 101464-1-2E	uncoated	0.365	
10/15	3	226	Gold-Vac. deposited on polyester film Mfr. A, 48 inch wide sheet, Sample No. 101464-2-1E		0.0633	52°A

REFERENCES

(1) Jenkins, R. S., C. ". Butler, and W. J. Parker, "Total Hemispherical Emittance Measurements Over the Temperature Range 77°K to 300°K," U. S. Naval Radiological Defense Laboratory Technical Report 663SS-TDR-62-189.

(2) Resistivities of pure bulk material. Condon, E. U. and Hugh Odishaw. Handbook of Physics. New York: Mc-Graw Hill. 1958.

(3) Givens, M. Parker. Solid State Physics. Academic Press. Volume 6, 1958.

(4) W. J. Parker and G. L. Abbott. "Total Emittance of Metals," preprint of paper presented at Symposium on Thermal Radiation of Solids, San Francisco, California, March 4, 5, & 6, 1964.

(5) Robert J. Corruccini. "Thermal Radiation Properties of Solids at Low Temperatures," paper presented at a symposium in Dayton, Ohio, September 5, 6, & 7, 1962, and published in the volume entitled, "Measurement of Thermal Radiation Properties of Solids," NASA OST I 1963.

(6) "Optical Properties of Satellite Surface Materials, Part III: Theory of Optical and Infrared Properties of Metals," Arthur D. Little, Inc., NASA Contract No. DA-19-020-ORD-4857.